

**ALMA MATER STUDIORUM
UNIVERSITÀ DI BOLOGNA**

**DIPARTIMENTO DI INGEGNERIA CIVILE, CHIMICA,
AMBIENTALE E DEI MATERIALI**

CORSO DI LAUREA MAGISTRALE IN INGEGNERIA CIVILE

TESI DI LAUREA

in

Dinamica delle Strutture M

**THE GALERKIN METHOD FOR VIBRATIONAL PROBLEM ON
STEPPED STRUCTURES**

CANDIDATO
Marco Amato

RELATORE
Chiar.mo Prof. Alessandro Marzani
CORRELATORE
Prof. Isaac Elishakoff

Anno Accademico 2019/2020

Sessione I

*To my family who
has always supported and
accompanied me to this goal*

Abstract

All physical phenomena studied in engineering are modeled by differential equations. In general, the obtained problem hardly finds a solution with classical analytical methods. This is why many scientists started searching some numerical approaches by which a generic differential equation can be solved in an approximate way. Most popular numerical approaches are: Finite Element Method, Finite Difference Method and Weighted Residual Method. The latter, in particular, is a family of methods, one member of which is the main topic of this thesis, namely the Galerkin method.

This work is dedicated to the vibrational problem of non-uniform and in-homogeneous structural elements. In particular, we investigate free vibrations in terms of natural frequencies of various structural elements and dynamic stability of elastic beam in a fluid flow. With the term *stepped structures*, we mean structures with one or more sections of discontinuity in both meanings: geometrical and material.

Galerkin method is a celebrated approximate technique suggested over a century ago. Reviews of this method are provided by numerous authors and many papers are dedicated to its application to elastic structures. In literature, it is possible to find several studies reporting Galerkin application on stepped structures. In these works, the Galerkin procedure is applied in naïve (or straightforward) form.

In this thesis, we deal with the vibrational problem on stepped structures, providing two versions of the Galerkin method. The first one, named naïve, consists in the integration along each step, where the rigidity and the mass remain constant. The second version, named rigorous, consists in representing the rigidity and the mass as generalized functions. This implementation utilizes unit step functions, as well as the Dirac delta function, and its derivative: the doublet function.

In order to verify the robustness of the method, we study different structural elements: bars, beams and plates in different constrain conditions. It emerges that the rigorous implementation leads to additional terms which do not appear in the naïve realization of the Galerkin method. Both versions of Galerkin method are compared with exact analytical solution. The obtained result is that, in contrast with the naïve version, the rigorous implementation tends to the exact solution through the increase in the terms in the expansion. This work demonstrates that great attention is required when implementing the Galerkin method for stepped structures because only rigorous implementation converges.

Keywords: Natural frequency, flutter, Galerkin method, Dirac delta function, doublet function, convergence, stepped structure, bar, beam, plate.

Contents

Abstract	v
Keywords	vii
1 Introduction	5
2 Weighted Residual Method	9
2.1 Weighted Residual Method	9
2.2 Point collocation method	13
2.3 Subdomain collocation method	15
2.4 Least-squares method	17
2.5 The Galerkin method	18
3 Bar	21
3.1 Basic Equations	21
3.1.1 Two-stepped bar free at both ends	24
3.1.2 Two-stepped bar clamped at both ends	25
3.1.3 Two-stepped bar clamped at one end and free at the other	27
3.2 Evaluation of exact solutions	28
3.3 Comparison functions for Galerkin method	30
3.4 Naïve Galerkin method	33
3.5 Rigorous Galerkin method	34
3.6 Numerical example	36
3.6.1 Exact solution	37
3.6.2 Galerkin method with trigonometric comparison function	39
3.6.3 Galerkin method with polynomial comparison function	45
3.7 Conclusion	50
4 Beam	53
4.1 Basic Equations	53
4.2 Krylov Functions	56
4.3 Exact solution	56
4.4 Naïve Galerkin method	58
4.5 Rigorous Galerkin method	60
4.6 Comparison functions for Galerkin method	62
4.6.1 Beam simply supported at both ends	63
4.6.2 Cantilever beam	64
4.6.3 Beam clamped at one end and simply supported at the other	64
4.6.4 Beam clamped at both ends	65

4.7	Numerical example	65
4.7.1	Exact solution	66
4.7.2	Naïve Galerkin method	69
4.7.3	Rigorous Galerkin method	72
4.8	Conclusion	78
5	Beam: Jaworsky and Dowell case	79
5.1	Jaworsky and Dowell study	79
5.2	Comparison function	81
5.3	Numerical results	82
5.3.1	Exact solution	82
5.3.2	Naïve Galerkin method	83
5.3.3	Rigorous Galerkin method	85
5.3.4	Comparison of results	87
5.4	Conclusion	90
6	Plate	91
6.1	Basic Equations	91
6.2	Exact solution	96
6.3	Naïve Galerkin method	97
6.4	Rigorous Galerkin method	99
6.5	Comparison functions for Galerkin method	102
6.6	Numerical example	102
6.6.1	Exact solution	103
6.6.2	Naïve Galerkin method	107
6.6.3	Rigorous Galerkin method	118
6.6.4	Finite Element Method solution	129
6.7	Conclusion	140
7	Flutter of a Bernoulli-Euler beam	141
7.1	Free vibrations	141
7.1.1	Numerical example	142
7.2	Dynamic stability	154
7.2.1	Piston theory	154
7.2.2	Governing differential equation	154
7.2.3	Exact solution	155
7.2.4	Finite Element Method	158
7.2.5	Naïve Galerkin method	165
7.2.6	Rigorous Galerkin method	167
7.2.7	Numerical example	169
7.3	Conclusion	177
8	Conclusion	179
Appendices		181

A Flutter of a Timoshenko-Ehrenfest beam	183
A.1 Introduction	183
A.2 Free vibrations	184
A.2.1 Governing differential equation for original theory	184
A.2.2 Governing differential equation for consistent theory	186
A.2.3 Exact solution for original theory	187
A.2.4 Exact solution for consistent theory	191
A.2.5 Numerical example	194
A.3 Dynamic Stability	199
A.3.1 Governing differential equation for original Timoshenko-Ehrenfest beam in gas flow	199
A.3.2 Governing differential equation for consistent Timoshenko-Ehrenfest beam in gas flow	201
A.3.3 Galerkin method	203
A.3.4 Numerical example	204
A.4 Conclusion	214
Bibliography	215

1. Introduction

All physical phenomena studied in engineering are modeled by differential equations. In general, the obtained problem hardly finds a solution with classical analytical methods. This is why many scientists started searching some numerical approaches by which a generic differential equation can be solved in an approximate way. Most popular numerical approaches are: Finite Element Method, Finite Difference Method and Weighted Residual Method (see Ref. [1]). The latter, in particular, is a family of methods and this work is dedicated to one member of this family: the Galerkin method. A brief presentation of the weighted residual method will be provided in the next chapter.

This work deals with the vibrational problem of non-uniform and in-homogeneous structural elements. In particular, we investigate free vibrations in terms of natural frequencies of various structural elements and dynamic stability of elastic beam in a fluid flow. With the term *stepped structures*, we mean structures with one or more sections of discontinuity in both meanings: geometrical and material. In general, a stepped structure can be made of one same material but with n different cross-sections or it can be a unique cross-section but with n material discontinuity points or both. In Fig. 1.1, we have an example of non-uniformity: a steel shaft with eight cross-sectional changes which define the points of geometrical discontinuities and in Fig. 1.2, we have an example of in-homogeneity: a golf-club shaft with a material discontinuity because it is made of graphite and steel.



Figure 1.1: Stepped shaft



Figure 1.2: Golf-club shaft

The studies of stepped structures took the attention of many researchers. Considering the beam element, many structures can be modeled as beams: aircraft wings, helicopter rotor blade, spacecraft antennae, robot arms and many others. Free vibration of beams is a classic subject originated around 1735 when Daniel Bernoulli and Leonhard Euler investigated the vibration of some uniform beams. After that, the topic has been developed and the beams with discontinuous cross-sectional areas, our stepped beams, have also been investigated through different approaches. For example, Cauchy iteration method was applied by Taleb and Suppiger (1961) [2]; a decomposition method was used by Buckens (1963) [3]; variational component method with Lagrange multipliers to satisfy geometric continuity conditions between different steps was employed by Klein (1974) [4] and finally Rayleigh-Ritz energy approach was used by Yuan and Dickinson (1993) [5] and also by Maurizi and Belles (1993) [6]. All of these are approximate methods. Exact solution instead, was furnished by Levinson (1993) [7] for a single-stepped beam simply supported at both ends. Naguleswaran (2002) [8] dealt with beams with up to three steps, whereas Duan and Wang (2013) [9], Lu et al. (2009) [10], Mao (2011) [11] and Wang X-W and Wang Y-L (2013) [12] dealt with the case of multiple-stepped beams.

Considering now bi-dimensional structural elements, we deal with plates. Plates with variable thickness are frequently used in order to save materials or to make the element lighter, specially when used in wings for high-performance aircrafts. In literature, it is possible to find many researches about vibration of non-uniform thickness of rectangular plate. It is interesting to see that researchers investigated various forms of thickness variation such as a linear function along one direction (W.H. Wittrick and C.H. Ellen (1962) [13] and M. Ohga, T. Shigematsu and K. Kawaguchi (1995) [14]) or a piecewise constant step function in both directions (F. Ju, H.P. Lee and K.H. Lee (1995) [15] and Y.K. Cheung, F.T.K. Au and D.Y. Zheng (2000) [16]). In general, it is difficult to obtain the exact solution dealing with non-uniform structures; this is why many of the above mentioned researches used numerical method. In order to study the convergence, validity and accuracy of numerical method, it is necessary to have exact solution as benchmarks. The exact vibration solution of stepped rectangular plate based on Kirchhoff-Love theory (thin plates) has been derived for the only case of plates simply supported on all edges.

Galerkin method is a celebrated approximate technique suggested over a century ago (Galerkin (1915) [17]). Reviews of this method are provided by numerous authors. Interested readers can consult the paper by Leipholz (1976) [18], Gander and Wanner (2012) [19], Repin (2017) [20]

as well as the book by Mikhlin (1971) [21]. There are numerous papers dedicated to its application to elastic structures. We are particularly interested in the application of this method to structures with discontinuities, and especially to stepped structures. Several studies deal with this topic. Interested readers can consult papers by Chehil and Jategaonkar (1987) [22], Maurini, Porfiri and Pouget (2006) [23], Soheylian and Ahmadian (2007) [24], Al-said (2008) [25], Borneman, Hashemi and Alighanbari (2009) [26], Pirmoradian, Keshmiri and Karimpour (2015) [27], to name a few examples. In the above-mentioned works, the Galerkin procedure is applied in the naïve (or straightforward) form.

In this thesis, we deal with free vibrations on stepped structures, providing two versions of the Galerkin method. The first one, named *naïve* or *straightforward*, consists in the integration along each step, where the rigidity and the mass remain constant. The second version, named *rigorous*, consists in representing the rigidity and the mass as generalized functions. This implementation utilizes unit step functions, as well as the Dirac delta function and its derivative: the doublet function. In order to verify the robustness of the method, we study different structural elements: bars, beams and plates in different constrain conditions. It emerges that the rigorous implementation leads to additional terms which do not appear in the naïve realization of the Galerkin method. Both versions of the Galerkin method are compared with exact analytical solution. The obtained result is that, in contrast with the naïve version, the rigorous implementation tends to the exact solution through the increase in the terms in the expansion. This work demonstrates that particular attention is required when implementing the Galerkin method for stepped structures because only rigorous implementation converges.

2. Weighted Residual Method

Weighted residual method is a group of methods mainly used in applied mathematics for solving differential equations. The common and basic idea is that the solution of a generic differential equation can be approximated with a finite sum of test functions Ψ_i with a negligible error. In this case, the weighted residual method is applied in order to find the value for each coefficient for each corresponding test function. The aim is to minimize the error between the linear combination of test functions and the exact solution.

2.1 Weighted Residual Method

We consider the following one-dimension differential equation applicable in the interval $a \leq x \leq b$:

$$Lu + g = 0; \quad a \leq x \leq b \quad (2.1.1)$$

where $u(x)$ is the unknown function and $g(x)$ is a known function; L denotes a differential operator. We use this format in order to write a more general discussion because through the choice of L , we can specify the actual form of the differential equation given by (2.1.1). For example, when L is defined as $L = d/dx$, it implies that (2.1.1) takes the form $du/dx + g = 0$. A different example can be for $L = d^2/dx^2 + 1$, (2.1.1) implies the differential equation $d^2u/dx^2 + u + g = 0$.

We represent the boundary conditions for (2.1.1) with the following notation:

$$u(a) = u_a; \quad u(b) = u_b \quad (2.1.2)$$

where u_a and u_b are known quantities. In this case, we have imposed two boundary conditions; this means that the differential equation (2.1.1) is of second order.

In general, a differential equation (2.1.1) with boundary conditions (2.1.2) can only be solved analytically in terms of an exact closed-form solution for a few simple expressions for the differential operator L and the function g . The method we are looking for is one that allows us to solve for arbitrary expressions of L and g (2.1.1) subject to (2.1.2). The benefit in terms of generality results in the approximation of our searched solution.

To this end, we first slightly modify (2.1.1). We multiply (2.1.1) by the arbitrary weight function $v(x)$, to get:

$$v(Lu + g) = 0 \quad (2.1.3)$$

and we integrate this expression from a to b ,

$$\int_a^b v(Lu + g)dx = 0 \quad (2.1.4)$$

Obviously, (2.1.1) implies (2.1.4) and since v represents any function, it is easy to prove that (2.1.4) implies (2.1.1); in other words the two forms are equivalent. To prove that (2.1.4) implies (2.1.1), we set the arbitrary weight function v as $v = Lu + g$, so (2.1.4) becomes:

$$\int_a^b (Lu + g)^2 dx = 0 \quad (2.1.5)$$

This expression is true only if (2.1.1) is satisfied. Therefore, we prove that (2.1.1) and (2.1.3) are equivalent. Obviously, this discussion has much in common with the weak formulation of the one-dimensional problem. In any case, we have to specify that the formulation (2.1.3) is not a weak one. In order to obtain a weak formulation, an integration by parts must be performed to reduce the differential order of the unknown function at the cost of the differentiation of the weight function.

With these considerations in mind, we return to the formulation given by (2.1.3). When we look for a numerical solution, we must choose an approximate expression for the unknown function u . Generally, we make the following suppositions, assuming that the boundary conditions (2.1.2) are satisfied:

$$u^{app} = \Psi_1 a_1 + \Psi_2 a_2 + \dots + \Psi_n a_n \quad (2.1.6)$$

where $a_1 \dots a_n$ are unknown parameters and $\Psi_1 \dots \Psi_n$ are functions of x , which we specify in advance. These functions are known as trial, basis or comparison functions. When we can define the parameters $a_1 \dots a_n$, our approximate solution is given by (2.1.6), so the task is to find a value for the parameters $a_1 \dots a_n$. You can choose the trial function at will, but it is obvious that some knowledge about physical problems can help you choose the appropriate trial function. However, (2.1.6) can be used as any approximation, which is why $\Psi_1 \dots \Psi_n$ are called trial functions.

Using a vector notation, approximation (2.1.6) can be represented as follows:

$$u^{app} = \mathbf{\Psi} \mathbf{a} \quad (2.1.7)$$

where:

$$\mathbf{\Psi} = \begin{bmatrix} \Psi_1 & \Psi_2 & \dots & \Psi_n \end{bmatrix}; \quad \mathbf{a} = \begin{bmatrix} a_1 \\ a_2 \\ \vdots \\ a_n \end{bmatrix} \quad (2.1.8)$$

We can replace u in (2.1.3) by u^{app} and require that:

$$\int_a^b v(Lu^{app} + g)dx = 0 \quad (2.1.9)$$

Similarly, in differential equation (2.1.1), u can be replaced with u^{app} , and since u^{app} will not fully satisfy the equation, we get:

$$Lu^{app} + g = e \quad (2.1.10)$$

where $e(x)$ is an error. This term is named residual. Using (2.1.9), (2.1.10) can be written as:

$$\int_a^b ve \, dx = 0 \quad (2.1.11)$$

Since the residual e , due to (2.1.10) and (2.1.7), is in function of the unknown \mathbf{a} , (2.1.11) in terms of components depends on the parameter $a_1 \dots a_n$. The purpose is to select the weight function v , as a result these parameters can be determined and, as a consequence, the approximate solution (2.1.7) is found.

Eq. (2.1.11) may be explained as follows: the residual, $e(x)$, is associated with a certain weight, $v(x)$, and the integral of this weighted residual, $v(x)e(x)$, must be zero into a specific interval. We have different weighted residual methods depending on how the weight function v is selected. Clearly, the selection of the weight function affects the values of the unknown parameters $a_1 \dots a_n$. One more property also connected to (2.1.11) is the orthogonality. The orthogonality condition for two column vectors \mathbf{a} and \mathbf{b} is represented by $\mathbf{a}^T \mathbf{b} = 0$. In terms of functions, we can say that function $v(x)$ is orthogonal to the function $e(x)$ in the interval $a \leq x \leq b$ if (2.1.11) is verified.

Eq. (2.1.11) is used as a tool to determine the unknowns $a_1 \dots a_n$, which is \mathbf{a} . In order to understand how to achieve this, we generally write arbitrary weight functions as:

$$v = V_1 c_1 + V_2 c_2 + \dots + V_n c_n \quad (2.1.12)$$

where $V_1 \dots V_n$ are known functions of our pre-specified x , and $c_1 \dots c_n$ are some parameters. We note that the number of components in (2.1.12) is the same as the number of terms in (2.1.6). Thanks to the definitions:

$$\mathbf{V} = [V_1 \ V_2 \ \dots \ V_n] ; \quad \mathbf{c} = \begin{bmatrix} c_1 \\ c_2 \\ \vdots \\ c_n \end{bmatrix} \quad (2.1.13)$$

(2.1.12) can be expressed as:

$$v = \mathbf{V}\mathbf{c} \quad (2.1.14)$$

Since the weight function is arbitrary and since V is known, we achieve that the parameters $c_1 \dots c_n$, or in a different notation \mathbf{c} , are arbitrary. In addition, since v is a number and since the transpose of a number is equal to the number itself, that is $v = v^T$, we can state (2.1.14) as:

$$v = \mathbf{c}^T \mathbf{V}^T \quad (2.1.15)$$

If we insert (2.1.15) into (2.1.11) and observe that \mathbf{c}^T is not in function of the coordinate x , we have:

$$\mathbf{c}^T \int_a^b \mathbf{V}^T e \, dx = 0 \quad (2.1.16)$$

Since this expression should be applicable to any \mathbf{c}^T -matrix, we can reach the following conclusion:

$$\int_a^b \mathbf{V}^T e \, dx = 0 \quad (2.1.17)$$

It is important to understand that since the column matrix \mathbf{V}^T has the dimensions $n \times 1$, Eq. (2.1.16) actually contains n equations. In other words, (2.1.16) can be written as:

$$\begin{aligned} \int_a^b V_1 e \, dx &= 0 \\ \int_a^b V_2 e \, dx &= 0 \\ &\vdots \\ \int_a^b V_n e \, dx &= 0 \end{aligned} \quad (2.1.18)$$

(2.1.18) derives from (2.1.11) and (2.1.14), and bases on the fact that the weight function v is arbitrary; as a result, also \mathbf{c} is arbitrary. Through a different approach, in (2.1.11) we can directly select n arbitrary weight functions v and select first $v = V_1$, then $v = V_2$ and so forth. Obviously, the result of this method is again given by (2.1.18). The method based on (2.1.14) is preferred here because it facilitates a short notation, but the equivalence of the two methods leading to (2.1.18) should be noted.

Back to (2.1.18), the key point is that the residual e depends on the n unknowns $a_1 \dots a_n$. Therefore (2.1.18) can be used as a system of equations to evaluate these n unknowns. To see this in a clearer way, we insert (2.1.7) into (2.1.10) to provide:

$$e = L(\Psi \mathbf{a}) + g \quad (2.1.19)$$

The \mathbf{a} -matrix is not in function of the coordinate x , namely:

$$e = L(\Psi) \mathbf{a} + g \quad (2.1.20)$$

Differentiation of a matrix means that each component is differentiated, so from (2.1.8) we obtain:

$$L(\Psi) = [L(\Psi_1) \ L(\Psi_2) \ \dots \ L(\Psi_n)] \quad (2.1.21)$$

proving that $L(\Psi)$ is a matrix with dimension $1 \times n$. Using (2.1.20) in (2.1.17) it means that:

$$\left(\int_a^b \mathbf{V}^T L(\Psi) \, dx \right) \mathbf{a} = - \int_a^b \mathbf{V}^T g \, dx \quad (2.1.22)$$

where \mathbf{a} is independent of x . Defining:

$$\mathbf{K} = \left(\int_a^b \mathbf{V}^T L(\Psi) dx \right); \quad \mathbf{f} = - \int_a^b \mathbf{V}^T g dx \quad (2.1.23)$$

where both \mathbf{K} and \mathbf{f} are independent of \mathbf{a} (2.1.22), we can write the system of linear equations in the following form:

$$\mathbf{Ka} = \mathbf{f} \quad (2.1.24)$$

Since the dimension of \mathbf{V}^T is $n \times 1$ and the dimension $L(\Psi)$ is $n \times 1$, we can express \mathbf{K} and \mathbf{f} as:

$$\mathbf{K} = \begin{bmatrix} \int_a^b V_1 L(\Psi_1) dx & \int_a^b V_1 L(\Psi_2) dx & \dots & \int_a^b V_1 L(\Psi_n) dx \\ \int_a^b V_2 L(\Psi_1) dx & \int_a^b V_2 L(\Psi_2) dx & \dots & \int_a^b V_2 L(\Psi_n) dx \\ \vdots & \vdots & & \vdots \\ \int_a^b V_n L(\Psi_1) dx & \int_a^b V_n L(\Psi_2) dx & \dots & \int_a^b V_n L(\Psi_n) dx \end{bmatrix}; \quad \mathbf{f} = - \begin{bmatrix} \int_a^b V_1 g dx \\ \int_a^b V_2 g dx \\ \vdots \\ \int_a^b V_n g dx \end{bmatrix} \quad (2.1.25)$$

proving that \mathbf{K} is a square matrix of size $n \times n$. That is to say, (2.1.24) is composed of n linear equations from which you can get the n unknowns $a_1 \dots a_n$, included into \mathbf{a} . After obtaining \mathbf{a} from (2.1.24) using (2.1.7), the required approximate solution is finally known.

The above process is applicable to all weighted residual methods. According to our choice of the weight function v , or the choice of vector \mathbf{V} , a variety of specific weighted residual methods can be obtained. Some commonly used weighted residual methods are: point collocation method, subdomain collocation method, least-squares method and Galerkin method.

2.2 Point collocation method

In this method, the weight function v is selected based on *Dirac delta function* $\delta(x - x_i)$ which is defined as:

$$\delta(x - x_i) = \begin{cases} \infty & \text{if } x = x_i \\ 0 & \text{otherwise} \end{cases} \quad (2.2.1)$$

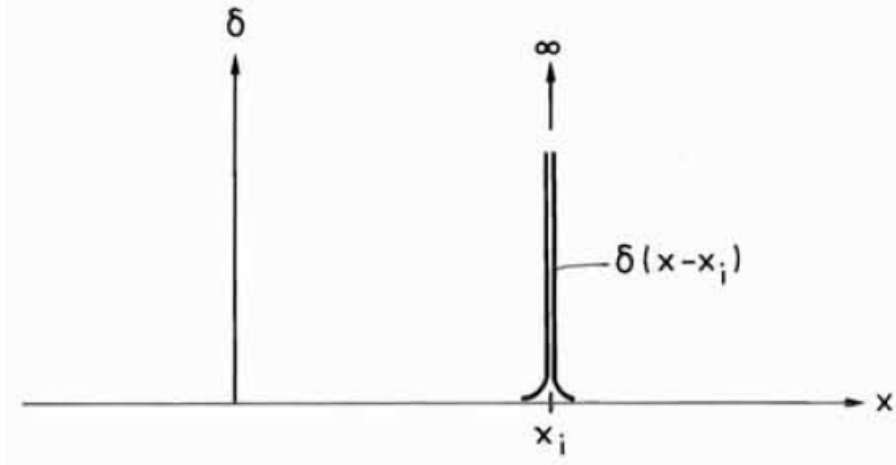


Figure 2.1: Dirac delta function

and:

$$\int_{-\infty}^{\infty} \delta(x - x_i) dx = 1 \quad (2.2.2)$$

where x_i is a given fixed value. Or, because of (2.2.1), we can express (2.2.2) as:

$$\int_{x_i^-}^{x_i^+} \delta(x - x_i) dx = 1 \quad (2.2.3)$$

where x_i^+ and x_i^- represent the values of x which are slightly greater than and lesser than x_i , respectively. According to these definitions, Dirac delta function is represented in Fig. 2.1.

In the *point collocation method*, the weight function v in (2.1.14) is selected as:

$$\mathbf{V} = [\delta(x - x_1) \ \delta(x - x_2) \ \dots \ \delta(x - x_n)] \quad (2.2.4)$$

Into the interval $a \leq x \leq b$ we arbitrarily select the fixed points $x_1 \dots x_n$ and we call them *collocation points*. To illustrate the results of selection of this weight function, we evaluate (2.1.18), leading to:

$$\int_b^a V_i e(x) dx = \int_b^a \delta(x - x_i) e(x) dx = 0; \quad i = 1, \dots, n \quad (2.2.5)$$

Since Dirac delta function is zero unless $x = x_i$ (see (2.2.1)) we obtain:

$$\int_b^a \delta(x - x_i) e(x) dx = \int_{x_i^-}^{x_i^+} \delta(x - x_i) e(x) dx = e(x_i) \int_{x_i^-}^{x_i^+} \delta(x - x_i) dx = e(x_i) \quad (2.2.6)$$

where (2.2.3) has been used. From (2.2.5) and (2.2.6), we have:

$$\int_b^a V_i e(x) dx = e(x_i) = 0; \quad i = 1, \dots, n \quad (2.2.7)$$

In other words, the point collocation method forces the residual $e(x)$ to be zero at the collocation points, as shown in Fig. 2.2.

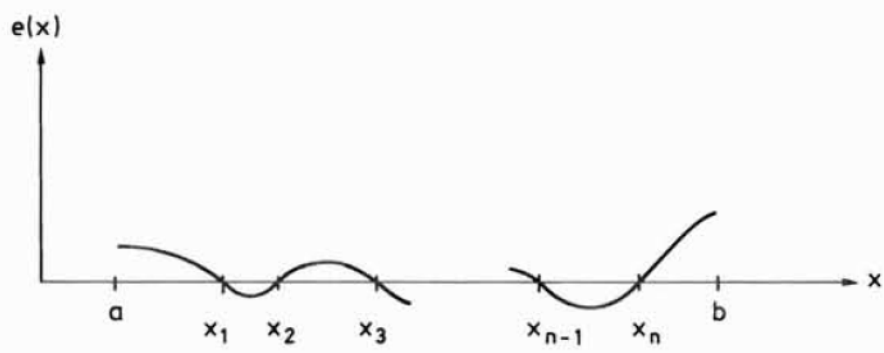


Figure 2.2: Point collocation method

Representing it in matrix manner, we have:

$$\mathbf{K} = \begin{bmatrix} L(\Psi_1(x_1)) & L(\Psi_2(x_1))dx & \dots & L(\Psi_n(x_1)) \\ L(\Psi_1(x_2)) & L(\Psi_2(x_2))dx & \dots & L(\Psi_n(x_2)) \\ \vdots & \vdots & & \vdots \\ L(\Psi_1(x_n)) & L(\Psi_2(x_n))dx & \dots & L(\Psi_n(x_n)) \end{bmatrix}; \mathbf{f} = -\begin{bmatrix} g(x_1) \\ g(x_2) \\ \vdots \\ g(x_n) \end{bmatrix} \quad (2.2.8)$$

The differentiation represented by the operator L , in example $L(\Psi_1(x_2))$, should be understood as follows: first the differentiation of the function $\Psi_1(x)$ is performed and then the specific x -value, $x = x_2$, is executed.

2.3 Subdomain collocation method

In the point collocation method n points are selected. In the *subdomain collocation method*, instead, the interval of interest is divided into n sub-intervals. Each of these sub-intervals is defined by $x_i \leq x \leq x_{i+1}$ where $1 \leq i \leq n$ and both x_i and x_{i+1} are located in the region $a \leq x \leq b$. The choice of the matrix \mathbf{V} , which defines the weight function, is made as follows:

$$V_i = \begin{cases} 1 & \text{if } x_i \leq x \leq x_{i+1} \\ 0 & \text{otherwise} \end{cases} \quad i = 1, \dots, n \quad (2.3.1)$$

as we can see in Fig. 2.3.

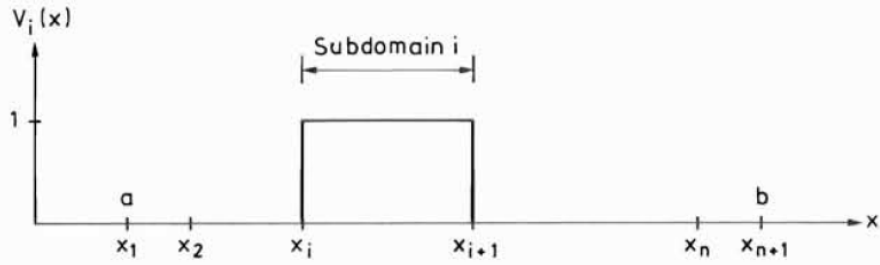


Figure 2.3: Weight function in subdomain collocation method

This means that (2.1.18) becomes:

$$\int_b^a V_i e(x) dx = \int_{x_i}^{x_{i+1}} e(x) dx = 0; \quad i = 1, \dots, n \quad (2.3.2)$$

In other words, the subdomain collocation method leads the average of the residual on each subdomain to be equal to zero, as shown in Fig. (2.4).

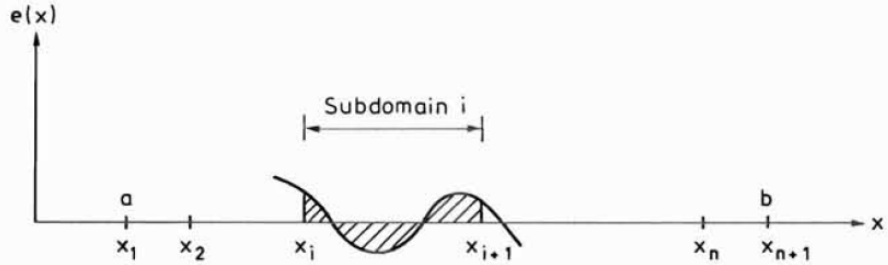


Figure 2.4: Subdomain collocation method

With (2.3.1) and thanks to (2.1.25), the coefficient matrix \mathbf{K} and the vector \mathbf{f} of (2.1.24) take the following forms:

$$\mathbf{K} = \begin{bmatrix} \int_{x_1}^{x_2} L(\Psi_1) dx & \int_{x_1}^{x_2} L(\Psi_2) dx & \dots & \int_{x_1}^{x_2} L(\Psi_n) dx \\ \int_{x_2}^{x_3} L(\Psi_1) dx & \int_{x_2}^{x_3} L(\Psi_2) dx & \dots & \int_{x_2}^{x_3} L(\Psi_n) dx \\ \vdots & \vdots & & \vdots \\ \int_{x_n}^{x_{n+1}} L(\Psi_1) dx & \int_{x_n}^{x_{n+1}} L(\Psi_2) dx & \dots & \int_{x_n}^{x_{n+1}} L(\Psi_n) dx \end{bmatrix}; \mathbf{f} = - \begin{bmatrix} \int_{x_1}^{x_2} g dx \\ \int_{x_2}^{x_3} g dx \\ \vdots \\ \int_{x_n}^{x_{n+1}} g dx \end{bmatrix} \quad (2.3.3)$$

2.4 Least-squares method

Because of (2.1.20), we observe that the residual e is in function of x and of the parameters $a_1 \dots a_n$, namely:

$$e = e(x, a_1, \dots, a_n) \quad (2.4.1)$$

In the *least-squares method*, a classic component of the matrix \mathbf{V} given by (2.1.13) is selected as:

$$V_i = \frac{\partial e}{\partial a_i}; \quad i = 1, \dots, n \quad (2.4.2)$$

This means that (2.1.18) is expressed as:

$$\int_a^b \frac{\partial e}{\partial a_i} e dx = 0; \quad i = 1, \dots, n \quad (2.4.3)$$

In order to evaluate this choice, we define the quantity I as follows:

$$I = \int_a^b e^2(x, a_1, \dots, a_n) dx \quad (2.4.4)$$

Since we integrate with respect to the only variable x , it is concluded that the quantity I depends only on the parameters $a_1 \dots a_n$, which means $I = I(a_1 \dots a_n)$. From (2.4.4), we state that:

$$\frac{\partial I}{\partial a_i} = 2 \int_a^b e \frac{\partial e}{\partial a_i} dx; \quad i = 1, \dots, n \quad (2.4.5)$$

An evaluation of (2.4.4) demonstrates that I is the square of the error, that means the residual integrated on the interval of interest. Comparing (2.4.3) and (2.4.5), we can find:

$$\frac{\partial I}{\partial a_i} = 0; \quad i = 1, \dots, n \quad (2.4.6)$$

In other words, our choice of the weight function given by (2.4.2) means that I is stationary. Since the residual e can be arbitrarily large, and thus the amount I can also be made arbitrarily large, we conclude that the stationarity of I represented by (2.4.6) is minimum. Therefore, the choice of the weight function given by (2.4.2) implies that the square of the error is minimum. This is why it is called least-squares method.

In order to find the coefficient matrix \mathbf{K} and the vector \mathbf{f} when using the least-squares method (2.1.24), we first insert (2.1.20) into (2.4.2) to obtain:

$$V_i = L(\Psi_i); \quad i = 1, \dots, n \quad (2.4.7)$$

That is, (2.1.25) yields:

$$\mathbf{K} = \begin{bmatrix} \int_a^b L(\Psi_1)L(\Psi_1) dx & \int_a^b L(\Psi_1)L(\Psi_2) dx & \dots & \int_a^b L(\Psi_1)L(\Psi_n) dx \\ \int_a^b L(\Psi_2)L(\Psi_1) dx & \int_a^b L(\Psi_2)L(\Psi_2) dx & \dots & \int_a^b L(\Psi_2)L(\Psi_n) dx \\ \vdots & \vdots & & \vdots \\ \int_a^b L(\Psi_n)L(\Psi_1) dx & \int_a^b L(\Psi_n)L(\Psi_2) dx & \dots & \int_a^b L(\Psi_n)L(\Psi_n) dx \end{bmatrix} \quad (2.4.8)$$

$$\mathbf{f} = - \begin{bmatrix} \int_a^b L(\Psi_1)g dx \\ \int_a^b L(\Psi_2)g dx \\ \vdots \\ \int_a^b L(\Psi_n)g dx \end{bmatrix}$$

which shows that the coefficient matrix \mathbf{K} is symmetric.

2.5 The Galerkin method



Figure 2.5: Boris Galerkin

In the *Galerkin method* (1915), the components of the matrix \mathbf{V} given by (2.1.13) are selected according to:

$$V_i = \Psi_i; \quad i = 1, \dots, n \quad (2.5.1)$$

This means that each component V_i is equal to the trial function Ψ_i . In other words, we express this concept stating that:

$$\text{weight functions} = \text{trial functions} \quad (2.5.2)$$

With (2.5.1) and (2.1.18), we obtain:

$$\int_a^b \Psi_i e \, dx = 0; \quad i = 1, \dots, n \quad (2.5.3)$$

Considering the discussion about (2.1.11), it can be concluded that in the Galerkin method, the trial function is orthogonal to the residual. In order to clearly define the coefficient matrix \mathbf{K} and the vector \mathbf{f} of the system of equations (2.1.24), we insert (2.5.1) into (2.1.25) to obtain:

$$\mathbf{K} = \begin{bmatrix} \int_a^b \Psi_1 L(\Psi_1) \, dx & \int_a^b \Psi_1 L(\Psi_2) \, dx & \dots & \int_a^b \Psi_1 L(\Psi_n) \, dx \\ \int_a^b \Psi_2 L(\Psi_1) \, dx & \int_a^b \Psi_2 L(\Psi_2) \, dx & \dots & \int_a^b \Psi_2 L(\Psi_n) \, dx \\ \vdots & \vdots & & \vdots \\ \int_a^b \Psi_n L(\Psi_1) \, dx & \int_a^b \Psi_n L(\Psi_2) \, dx & \dots & \int_a^b \Psi_n L(\Psi_n) \, dx \end{bmatrix}; \mathbf{f} = - \begin{bmatrix} \int_a^b \Psi_1 g \, dx \\ \int_a^b \Psi_2 g \, dx \\ \vdots \\ \int_a^b \Psi_n g \, dx \end{bmatrix} \quad (2.5.4)$$

3. Bar

In this chapter, we analyze the axial free vibration of one-stepped rod, which is mathematically characterized by one-dimension second order differential equation. The bar object of study is composed of two elements with different cross-sections and made of two different materials which have one section in common.

We solve this problem through three different approaches which are the theoretical exact solution obtained from the classical theory and the two versions of Galerkin method: naïve and rigorous. In particular, for the Galerkin method, we use two different strategies for the comparison functions, implementing both trigonometric and polynomial comparison functions. For a more convincing argument, we solve this problem in three different constrain conditions, and we compare the obtained results in terms of relative error.

3.1 Basic Equations

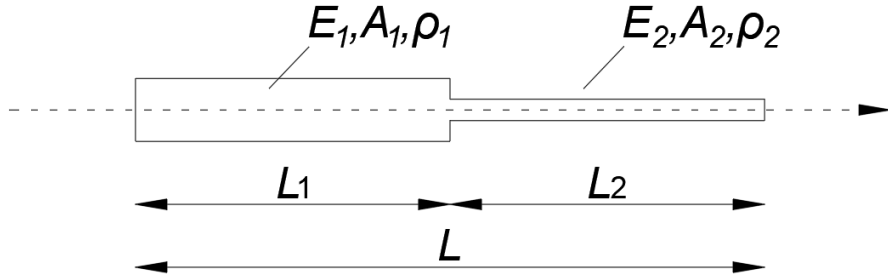


Figure 3.1: A stepped bar of length L

We consider the stepped bar, as shown in Fig. 3.1. The modulus of elasticity of the material of the bar's first step is denoted as E_1 , whereas second step's elastic modulus equals E_2 . Their cross-sectional areas are denoted as A_1 and A_2 , respectively. The material density of the first step's material equals ρ_1 , whereas second step has material density ρ_2 . The lengths of each step equal L_1 and L_2 , respectively.

We derive the governing differential equation of in-homogeneous and non-uniform bar. We consider the dynamic equilibrium of the differential element of rod represented in Fig. 3.2:

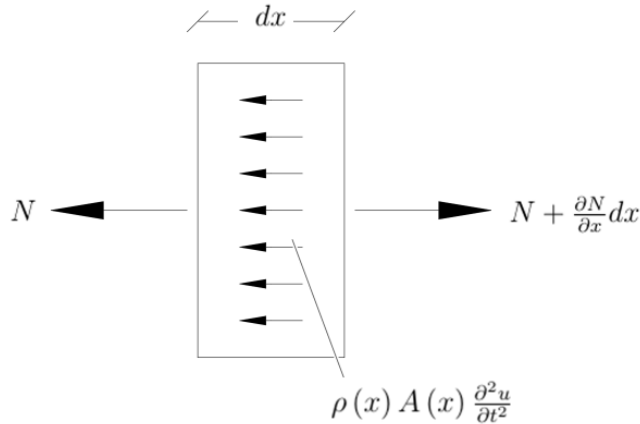


Figure 3.2: A differential element of rod

$$-N + \left(N + \frac{\partial N}{\partial x} dx\right) = \rho(x)A(x)\frac{\partial^2 u}{\partial t^2}dx \quad (3.1.1)$$

$$\frac{\partial N}{\partial x} = \rho(x)A(x)\frac{\partial^2 u}{\partial t^2} \quad (3.1.2)$$

We have to remember that:

$$N = \sigma A \quad (3.1.3)$$

$$\sigma = E\varepsilon \quad (3.1.4)$$

$$\varepsilon = \frac{\partial u}{\partial x} \quad (3.1.5)$$

Then:

$$\frac{\partial}{\partial x} \left(E(x)A(x)\frac{\partial u}{\partial x} \right) = \rho(x)A(x)\frac{\partial^2 u}{\partial t^2} \quad (3.1.6)$$

where $u(x, t)$ is the displacement in longitudinal direction.

Specifically, for the stepped bar, with piecewise constants E , A and ρ , we can write:

$$\frac{E_1}{\rho_1} \frac{\partial^2 u_1}{\partial x^2} = \frac{\partial^2 u_1}{\partial t^2} \quad 0 \leq x \leq L_1 \quad (3.1.7)$$

$$\frac{E_2}{\rho_2} \frac{\partial^2 u_2}{\partial x^2} = \frac{\partial^2 u_2}{\partial t^2} \quad L_1 \leq x \leq L \quad (3.1.8)$$

or:

$$c_1^2 \frac{\partial^2 u_1}{\partial x^2} = \frac{\partial^2 u_1}{\partial t^2} \quad 0 \leq x \leq L_1 \quad (3.1.9)$$

$$c_2^2 \frac{\partial^2 u_2}{\partial x^2} = \frac{\partial^2 u_2}{\partial t^2} \quad L_1 \leq x \leq L \quad (3.1.10)$$

where $L = L_1 + L_2$ is the total length of the two-stepped bar, $u_1(x, t)$ denotes the axial displacement of the first bar, whereas $u_2(x, t)$ denotes the axial displacement of the second bar; c_j are defined as follows:

$$c_1 = \sqrt{\frac{E_1}{\rho_1}} \quad (3.1.11)$$

$$c_2 = \sqrt{\frac{E_2}{\rho_2}} \quad (3.1.12)$$

where c_j ($j = 1, 2$) is the propagation speed of longitudinal waves in the bar if it is made solely of material j , with homogeneous properties.

We now consider three cases of boundary conditions: (a) bar is free at each end, $x = 0, x = L$; (b) bar is clamped at each end; (c) bar is clamped at $x = 0$ and free at $x = L$. For free end, the boundary condition demands axial force to vanish, i.e.:

$$EA \frac{\partial u}{\partial x} = 0 \quad (3.1.13)$$

For clamped end, the constraint is:

$$u = 0 \quad (3.1.14)$$

The continuity conditions for all three cases are:

$$u_1 = u_2 \quad (3.1.15a)$$

$$E_1 A_1 \frac{\partial u}{\partial x} = E_2 A_2 \frac{\partial u}{\partial x} \quad (3.1.15b)$$

Eq. (3.1.15a) demands continuity in displacement, whereas Eq. (3.1.15b) requires continuity in the axial force.

We consider now harmonic vibrations:

$$u_1(x, t) = U_1(x) \sin(\omega t) \quad (3.1.16)$$

$$u_2(x, t) = U_2(x) \sin(\omega t) \quad (3.1.17)$$

where $U_1(x)$ and $U_2(x)$ constitute mode shapes of the first and second steps, respectively, ω is the sought natural frequency. Eq. (3.1.9) and (3.1.10) become:

$$c_1^2 \frac{d^2 U_1}{dx^2} + \omega^2 U_1 = 0 \quad (3.1.18)$$

$$c_2^2 \frac{d^2 U_2}{dx^2} + \omega^2 U_2 = 0 \quad (3.1.19)$$

Solutions of Eq. (3.1.18) and (3.1.19) read, respectively:

$$U_1 = D_1 \sin \beta_1 x + D_2 \cos \beta_1 x \quad (3.1.20)$$

$$U_2 = D_3 \sin \beta_2 x + D_4 \cos \beta_2 x \quad (3.1.21)$$

where:

$$\beta_1 = \frac{\omega}{c_1}, \quad \beta_2 = \frac{\omega}{c_2} \quad (3.1.22)$$

Hereinafter we deal with three distinct cases of boundary conditions at bar's ends.

3.1.1 Two-stepped bar free at both ends

We consider the case (a), free-free bar. Condition (3.1.13) applied at $x = 0$ yields:

$$\beta_1 D_1 = 0 \quad (3.1.23)$$

Condition (3.1.13) applied at $x = L$ results in:

$$\beta_2 \left(D_3 \cos(\beta_2 L) - D_4 \sin(\beta_2 L) \right) = 0 \quad (3.1.24)$$

Condition (3.1.15a) leads to:

$$D_1 \sin(\beta_1 L_1) + D_2 \cos(\beta_2 L_2) - D_3 \sin(\beta_1 L_1) + D_4 \cos(\beta_2 L_1) = 0 \quad (3.1.25)$$

Implementing condition (3.1.15b), we get:

$$E_1 A_1 \beta_1 D_1 \cos(\beta_1 L_1) - E_1 A_1 \beta_1 D_2 \sin(\beta_1 L_1) - E_2 A_2 \beta_2 D_3 \cos(\beta_2 L_1) + E_2 A_2 \beta_2 D_4 \sin(\beta_2 L_1) = 0 \quad (3.1.26)$$

From Eq. (3.1.23), we see that either $\beta_1 = 0$ or $D_1 = 0$. The condition:

$$\beta_1 = 0 \quad (3.1.27)$$

leads to the conclusion that the natural frequency vanishes, namely $\omega = 0$. We will check later if the free-free bar possesses a zero natural frequency. For now, we assume that $\beta \neq 0$, which means that $D_1 = 0$.

Demanding non-triviality of the solution for integration, constants D_2 , D_3 and D_4 lead to the following determinant to vanish:

$$\det \begin{bmatrix} \cos(\beta_1 L_1) & -\sin(\beta_2 L_1) & -\cos(\beta_2 L_1) \\ -E_1 A_1 \beta_1 \sin(\beta_1 L_1) & -E_2 A_2 \beta_2 \cos(\beta_2 L_1) & E_2 A_2 \beta_2 \sin(\beta_2 L_1) \\ 0 & \beta_2 \cos(\beta_2 L) & -\beta_2 \sin(\beta_2 L) \end{bmatrix} = 0 \quad (3.1.28)$$

Expanding this condition leads to the characteristic equation:

$$\begin{aligned} & E_2 A_2 \beta_2^2 \left[\cos(\beta_1 L_1) \cos(\beta_2 L_1) \sin(\beta_2 L) - \cos(\beta_1 L_1) \sin(\beta_2 L_1) \cos(\beta_2 L) \right] \\ & + E_1 A_1 \beta_1 \beta_2 \left[\sin(\beta_1 L_1) \sin(\beta_2 L_1) \sin(\beta_2 L) + \sin(\beta_1 L_1) \cos(\beta_2 L) \cos(\beta_2 L_1) \right] = 0 \end{aligned} \quad (3.1.29)$$

We note that one of the solutions of Eq. (3.1.29) is $\beta_2 = 0$. This equation:

$$\beta_2 = 0 \quad (3.1.30)$$

just like Eq. (3.1.27) implies possible presence of zero natural frequency. We now investigate if the free-free stepped bar indeed possesses the zero natural frequency. We substitute $\omega = 0$ into Eq. (3.1.18) and (3.1.19) to obtain:

$$\frac{\partial^2 U_1}{\partial x^2} = 0, \quad \frac{\partial^2 U_2}{\partial x^2} = 0 \quad (3.1.31)$$

Hence, if the zero natural frequency exists, the mode shape corresponding to it is represented by the following expressions:

$$U_1 = M_1 x + M_2 \quad (3.1.32)$$

$$U_2 = N_1 x + N_2 \quad (3.1.33)$$

where M_1 , M_2 , N_1 and N_2 are the constants of integration.

Satisfaction of the boundary condition (3.1.13) at $x = 0$ leads to:

$$\frac{dU_1(0)}{dx} = M_1 = 0 \quad (3.1.34)$$

The boundary condition (3.1.13) applied at $x = L$ results in:

$$\frac{dU_2(L)}{dx} = N_1 = 0 \quad (3.1.35)$$

Application of the continuity condition (3.1.15a) yields:

$$M_2 = N_2 \quad (3.1.36)$$

whereas continuity condition (3.1.15b) is identically satisfied.

We are left with the solutions:

$$U_1 = M_2, \quad U_2 = N_2 = M_2 \quad (3.1.37)$$

which satisfy all conditions, with M_2 being an arbitrary constant, i.e., the mode shape does not vanish identically. This demonstrates that the free-free stepped bar possesses zero frequency, with corresponding constant displacement $V_1 = V_2 = \text{constant}$ in axial direction, as a rigid body. It should be noted that Graff's (1975) characteristic equation given by his Eq. (2.3.15) does not account for this possibility (Ref. [28]).

3.1.2 Two-stepped bar clamped at both ends

We consider the case (b), clamped-clamped bar. Condition (3.1.14) applied at $x = 0$ yields:

$$D_2 = 0 \quad (3.1.38)$$

Condition (3.1.14) applied at $x = L$ yields:

$$D_3 \sin \beta_2 L + D_4 \cos \beta_2 L = 0 \quad (3.1.39)$$

Condition (3.1.15a) leads to:

$$D_1 \sin \beta_1 L_1 + D_2 \cos \beta_1 L_1 - D_3 \sin \beta_2 L_1 - D_4 \cos \beta_2 L_1 = 0 \quad (3.1.40)$$

Condition (3.1.15b) results in:

$$E_1 A_1 \beta_1 D_1 \cos \beta_1 L_1 - E_1 A_1 \beta_1 D_2 \sin \beta_1 L_1 - E_2 A_2 \beta_2 D_3 \cos \beta_2 L_1 + E_2 A_2 \beta_2 D_4 \sin \beta_2 L_1 = 0 \quad (3.1.41)$$

Demanding non-triviality of the solution for integration, constants D_1 , D_3 and D_4 lead to the following determinant to vanish:

$$\det \begin{bmatrix} \sin(\beta_1 L_1) & -\sin(\beta_2 L_1) & -\cos(\beta_2 L_1) \\ E_1 A_1 \beta_1 \cos(\beta_1 L_1) & -E_2 A_2 \beta_2 \cos(\beta_2 L_1) & E_2 A_2 \beta_2 \sin(\beta_2 L_1) \\ 0 & \sin(\beta_2 L) & \cos(\beta_2 L) \end{bmatrix} = 0 \quad (3.1.42)$$

Thus, we obtain the following characteristic equation:

$$\begin{aligned} & -E_2 A_2 \beta_2 \left[\sin(\beta_1 L_1) \cos(\beta_2 L_1) \cos(\beta_2 L) + \sin(\beta_1 L_1) \sin(\beta_2 L_1) \sin(\beta_2 L) \right] \\ & - E_1 A_1 \beta_1 \left[\cos(\beta_1 L_1) \cos(\beta_2 L_1) \sin(\beta_2 L) - \sin(\beta_2 L_1) \cos(\beta_2 L) \cos(\beta_1 L_1) \right] = 0 \end{aligned} \quad (3.1.43)$$

We can immediately observe that $\beta_1 = \beta_2 = 0$ is one of the solutions of this equation. Therefore, the question arises if the clamped-clamped stepped bar possesses zero frequency. To investigate this question, we substitute $\omega = 0$ into Eq. (3.1.18) and (3.1.19), leading, respectively to Eq. (3.1.31). The solution is given by Eq. (3.1.32) and (3.1.33). Satisfaction of the boundary condition (3.1.14) at $x = 0$ leads to:

$$U_1(0) = M_2 = 0 \quad (3.1.44)$$

The boundary condition (3.1.14) applied at $x = L$ results in:

$$U_2(L) = N_1 L + N_2 = 0 \quad (3.1.45)$$

Application of the continuity condition (3.1.15a) yields:

$$M_1 L_1 - N_1 L_1 - N_2 = 0 \quad (3.1.46)$$

whereas continuity condition (3.1.15b) results in:

$$E_1 A_1 M_1 - E_2 A_2 N_1 = 0 \quad (3.1.47)$$

Demanding non-triviality of the solution for integration, constants M_1 , N_1 and N_2 lead to the following determinantal equation:

$$\det \begin{bmatrix} L_1 & -L_1 & -1 \\ E_1 A_1 & -E_2 A_2 & 0 \\ 0 & L & 1 \end{bmatrix} = 0 \quad (3.1.48)$$

We observe that the left-hand side of this equation differs from zero:

$$-E_2 A_2 L_1 - E_1 A_1 L_1 \neq 0 \quad (3.1.49)$$

leading to the conclusion that Eq. (3.1.48) cannot take place. We conclude that there exists no non-trivial mode shape associated with zero frequency, therefore clamped-clamped stepped bar does not entertain zero frequency.

3.1.3 Two-stepped bar clamped at one end and free at the other

We consider the case (c), clamped-free bar. Condition (3.1.14) applied at $x = 0$ yields:

$$D_2 = 0 \quad (3.1.50)$$

Condition (3.1.13) applied at $x = L$ yields:

$$\beta_2(D_3\cos\beta_2L - D_4\sin\beta_2L) = 0 \quad (3.1.51)$$

Condition (3.1.15a) leads to:

$$D_1\sin\beta_1L_1 + D_2\cos\beta_1L_1 - D_3\sin\beta_2L_1 - D_4\cos\beta_2L_1 = 0 \quad (3.1.52)$$

Condition (3.1.13) results in:

$$E_1A_1\beta_1D_1\cos\beta_1L_1 - E_1A_1\beta_1D_2\sin\beta_1L_1 - E_2A_2\beta_2D_3\cos\beta_2L_1 + E_2A_2\beta_2D_4\sin\beta_2L_1 = 0 \quad (3.1.53)$$

Demanding non-triviality of the solution for integration, constants D_1 , D_3 and D_4 lead to the following determinant to be equal zero:

$$\det \begin{bmatrix} \sin(\beta_1L_1) & -\sin(\beta_2L_1) & -\cos(\beta_2L_1) \\ E_1A_1\beta_1\cos(\beta_1L_1) & -E_2A_2\beta_2\cos(\beta_2L_1) & E_2A_2\beta_2\sin(\beta_2L_1) \\ 0 & \beta_2\cos(\beta_2L) & -\beta_2\sin(\beta_2L) \end{bmatrix} = 0 \quad (3.1.54)$$

Expanding this equation leads to the characteristic equation:

$$\begin{aligned} & E_2A_2\beta_2^2 \left[\sin(\beta_1L_1)\cos(\beta_2L_1)\sin(\beta_2L) - \sin(\beta_1L_1)\sin(\beta_2L_1)\cos(\beta_2L) \right] \\ & - E_1A_1\beta_1\beta_2 \left[\cos(\beta_1L_1)\sin(\beta_2L_1)\sin(\beta_2L) + \cos(\beta_1L_1)\cos(\beta_2L_1)\cos(\beta_2L) \right] = 0 \end{aligned} \quad (3.1.55)$$

We can immediately observe that $\beta_1 = \beta_2 = 0$ is one of the solutions of this equation. Again, the question arises if the clamped-free stepped bar possesses zero frequency. Therefore, we substitute $\omega = 0$ into Eq. (3.1.18) and (3.1.19). The solution is given by Eq. (3.1.32) and (3.1.33). Satisfaction of the boundary condition (3.1.14) at $x = 0$ leads to:

$$U_1(0) = M_2 = 0 \quad (3.1.56)$$

The boundary condition (3.1.13) applied at $x = L$ results in:

$$\frac{dU_2(L)}{dx} = N_1 = 0 \quad (3.1.57)$$

Application of the continuity condition (3.1.15a) yields:

$$M_1L_1 - N_2 = 0 \quad (3.1.58)$$

whereas continuity condition (3.1.15b) results in:

$$E_1A_1M_1 = 0 \quad (3.1.59)$$

From Eq. (3.1.59), we deduce that $M_1 = 0$. From Eq. (3.1.58), we conclude that $N_2 = 0$. Thus, there is no non-trivial mode shape associated with the supposed zero frequency, and hence we conclude that clamped-free stepped bar does not entertain zero frequency.

3.2 Evaluation of exact solutions

We introduce the following parameter which contains the sought frequency ω :

$$z = \beta_1 L_1 = \frac{\omega L_1}{c_1} \quad (3.2.1)$$

Then:

$$\beta_2 L_1 = z \frac{c_1}{c_2} = z \sqrt{\frac{E_1 \rho_2}{E_2 \rho_1}} \quad (3.2.2)$$

$$\beta_1 L = z \frac{L}{L_1} = z \left(1 + \frac{L_2}{L_1}\right) \quad (3.2.3)$$

$$\beta_2 L = z \frac{c_1}{c_2} \frac{L}{L_1} = z \frac{c_1}{c_2} \left(1 + \frac{L_2}{L_1}\right) \quad (3.2.4)$$

Eq. (3.1.29) of the free-free bar can be rewritten as:

$$\begin{aligned} \phi_{F-F}(z) &= \frac{E_2}{E_1} \frac{A_2}{A_1} \frac{c_1}{c_2} \left[\cos(z) \cos\left(z \sqrt{\frac{E_1 \rho_2}{E_2 \rho_1}}\right) \sin\left(z \frac{c_1}{c_2} \left(1 + \frac{L_2}{L_1}\right)\right) \right. \\ &\quad \left. - \cos(z) \sin\left(z \sqrt{\frac{E_1 \rho_2}{E_2 \rho_1}}\right) \cos\left(z \frac{c_1}{c_2} \left(1 + \frac{L_2}{L_1}\right)\right) \right] \\ &\quad + \left[\sin(z) \sin\left(z \sqrt{\frac{E_1 \rho_2}{E_2 \rho_1}}\right) \sin\left(z \frac{c_1}{c_2} \left(1 + \frac{L_2}{L_1}\right)\right) \right. \\ &\quad \left. + \sin(z) \cos\left(z \sqrt{\frac{E_1 \rho_2}{E_2 \rho_1}}\right) \cos\left(z \frac{c_1}{c_2} \left(1 + \frac{L_2}{L_1}\right)\right) \right] \\ &= 0 \end{aligned} \quad (3.2.5)$$

This is a transcendental equation with respect to z . Likewise, for clamped-clamped bar Eq. (3.1.43) is rewritten as:

$$\begin{aligned} \phi_{C-C}(z) &= \frac{E_2}{E_1} \frac{A_2}{A_1} \frac{c_1}{c_2} \left[\sin(z) \sin\left(z \sqrt{\frac{E_1 \rho_2}{E_2 \rho_1}}\right) \sin\left(z \frac{c_1}{c_2} \left(1 + \frac{L_2}{L_1}\right)\right) \right. \\ &\quad \left. + \sin(z) \cos\left(z \sqrt{\frac{E_1 \rho_2}{E_2 \rho_1}}\right) \cos\left(z \frac{c_1}{c_2} \left(1 + \frac{L_2}{L_1}\right)\right) \right] \\ &\quad + \left[\cos(z) \cos\left(z \sqrt{\frac{E_1 \rho_2}{E_2 \rho_1}}\right) \sin\left(z \frac{c_1}{c_2} \left(1 + \frac{L_2}{L_1}\right)\right) \right. \\ &\quad \left. - \cos(z) \sin\left(z \sqrt{\frac{E_1 \rho_2}{E_2 \rho_1}}\right) \cos\left(z \frac{c_1}{c_2} \left(1 + \frac{L_2}{L_1}\right)\right) \right] \\ &= 0 \end{aligned} \quad (3.2.6)$$

For clamped-free bar, Eq. (3.1.55) is rewritten as:

$$\begin{aligned}
\phi_{C-F}(z) &= \frac{E_2}{E_1} \frac{A_2}{A_1} \frac{c_1}{c_2} \left[\sin(z) \cos\left(z \sqrt{\frac{E_1 \rho_2}{E_2 \rho_1}}\right) \sin\left(z \frac{c_1}{c_2} \left(1 + \frac{L_2}{L_1}\right)\right) \right. \\
&\quad \left. - \sin(z) \sin\left(z \sqrt{\frac{E_1 \rho_2}{E_2 \rho_1}}\right) \cos\left(z \frac{c_1}{c_2} \left(1 + \frac{L_2}{L_1}\right)\right) \right] \\
&\quad - \left[\cos(z) \sin\left(z \sqrt{\frac{E_1 \rho_2}{E_2 \rho_1}}\right) \sin\left(z \frac{c_1}{c_2} \left(1 + \frac{L_2}{L_1}\right)\right) \right. \\
&\quad \left. + \cos(z) \cos\left(z \sqrt{\frac{E_1 \rho_2}{E_2 \rho_1}}\right) \cos\left(z \frac{c_1}{c_2} \left(1 + \frac{L_2}{L_1}\right)\right) \right] \\
&= 0
\end{aligned} \tag{3.2.7}$$

We introduce the following notations:

$$M_c = \frac{E_2}{E_1} \frac{A_2}{A_1} \frac{c_1}{c_2} \tag{3.2.8}$$

$$\begin{aligned}
A\left(z, \frac{E_2}{E_1}, \frac{\rho_2}{\rho_1}, \frac{L_2}{L_1}\right) &= \left[\cos(z) \cos\left(z \sqrt{\frac{E_1 \rho_2}{E_2 \rho_1}}\right) \sin\left(z \frac{c_1}{c_2} \left(1 + \frac{L_2}{L_1}\right)\right) \right. \\
&\quad \left. - \cos(z) \sin\left(z \sqrt{\frac{E_1 \rho_2}{E_2 \rho_1}}\right) \cos\left(z \frac{c_1}{c_2} \left(1 + \frac{L_2}{L_1}\right)\right) \right]
\end{aligned} \tag{3.2.9}$$

$$\begin{aligned}
B\left(z \frac{E_2}{E_1}, \frac{\rho_2}{\rho_1}, \frac{L_2}{L_1}\right) &= \left[\sin(z) \sin\left(z \sqrt{\frac{E_1 \rho_2}{E_2 \rho_1}}\right) \sin\left(z \frac{c_1}{c_2} \left(1 + \frac{L_2}{L_1}\right)\right) \right. \\
&\quad \left. + \sin(z) \cos\left(z \sqrt{\frac{E_1 \rho_2}{E_2 \rho_1}}\right) \cos\left(z \frac{c_1}{c_2} \left(1 + \frac{L_2}{L_1}\right)\right) \right]
\end{aligned} \tag{3.2.10}$$

$$\begin{aligned}
C\left(z, \frac{E_2}{E_1}, \frac{\rho_2}{\rho_1}, \frac{L_2}{L_1}\right) &= \left[\sin(z) \cos\left(z \sqrt{\frac{E_1 \rho_2}{E_2 \rho_1}}\right) \sin\left(z \frac{c_1}{c_2} \left(1 + \frac{L_2}{L_1}\right)\right) \right. \\
&\quad \left. - \sin(z) \sin\left(z \sqrt{\frac{E_1 \rho_2}{E_2 \rho_1}}\right) \cos\left(z \frac{c_1}{c_2} \left(1 + \frac{L_2}{L_1}\right)\right) \right]
\end{aligned} \tag{3.2.11}$$

$$\begin{aligned}
D\left(z, \frac{E_2}{E_1}, \frac{\rho_2}{\rho_1}, \frac{L_2}{L_1}\right) &= \left[\cos(z) \sin\left(z \sqrt{\frac{E_1 \rho_2}{E_2 \rho_1}}\right) \sin\left(z \frac{c_1}{c_2} \left(1 + \frac{L_2}{L_1}\right)\right) \right. \\
&\quad \left. + \cos(z) \cos\left(z \sqrt{\frac{E_1 \rho_2}{E_2 \rho_1}}\right) \cos\left(z \frac{c_1}{c_2} \left(1 + \frac{L_2}{L_1}\right)\right) \right]
\end{aligned} \tag{3.2.12}$$

We rewrite the expressions of functions ϕ as follows:

$$\phi_{F-F}(z) = M_c A(z) + B(z) \quad (3.2.13)$$

$$\phi_{C-C}(z) = M_c B(z) + C(z) \quad (3.2.14)$$

$$\phi_{C-F}(z) = M_c C(z) + D(z) \quad (3.2.15)$$

In this form, we can immediately observe that if we have a homogeneous bar, the characteristic equations for free-free bar and clamped-clamped bar are the same, except that the free-free bar possesses the additional zero frequency.

3.3 Comparison functions for Galerkin method

A comparison function for Galerkin method is a function which is supposed to well represent the solution of the differential equation. For the Galerkin method, in order to be considered “comparison function”, a function must satisfy all the boundary conditions: geometrical condition, i.e. horizontal displacement, and force condition, i.e. axial force.

It appears instructive to use both trigonometric and polynomial functions as comparison functions, in view to contrast the results. The trigonometric comparison functions that satisfy all boundary conditions are denoted, for three respective sets of boundary conditions, respectively as F-F, C-C and C-F:

$$\psi_{j,F-F}(\xi) = \cos[(j-1)\pi\xi] \quad (3.3.1)$$

$$\psi_{j,C-C}(\xi) = \sin(j\pi\xi) \quad (3.3.2)$$

$$\psi_{j,C-F}(\xi) = \sin\left[\frac{(2(j-1)+1)\pi\xi}{2}\right] \quad (3.3.3)$$

where $j = 1, 2, 3, \dots, n$ is a serial number of the mode and $\xi = x/L$ is the non-dimensional axial coordinate.

The polynomial comparison functions are constructed with the following criterion in mind. The imposition is that the polynomial must cross the x -axis j times to imitate the presence of number j of nodal points. For simplicity, the nodes are placed equidistantly. In the clamped-clamped case, the boundary conditions coincide with the crossing x -axis conditions at the bar ends. We satisfy the above condition by multiplying the expression with the non-dimensional axial coordinate minus the numerical value, where the crossing of the ξ -axis is required:

$$\psi_{j,C-C}(\xi) = \prod_{i=1}^{j+1} \left(\xi - \frac{i-1}{j} \right) \quad (3.3.4)$$

The second case is the clamped-free bar. The clamped boundary condition at $x = 0$ means that the axial displacement must be zero, which coincides with a crossing requirement of x -axis condition (at $x = 0$) for polynomial representation of the axial displacement. The free end boundary condition at $x = L$ means that the axial force must vanish. The latter condition coincides with the demand that the first derivative equals zero for polynomial representation

of the axial displacement. This means that the function passes at the point of interest with the horizontal tangent (in our case at $\xi = 1$). This condition can be interpreted as a condition of symmetry if we treat the cross-section of interest as an axis of symmetry ($\xi = 1$). We construct a polynomial just like for a clamped-clamped bar whose length is the double of that of a clamped-free bar:

$$\psi_{j,C-F}(\xi) = \prod_{i=1}^{2j-1} \left[\xi - \frac{2(i-1)}{2j-1} \right] \quad (3.3.5)$$

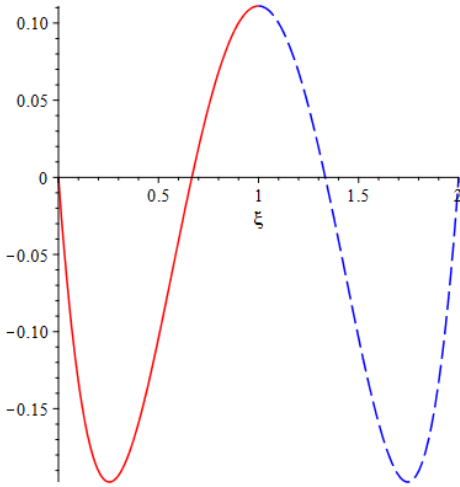


Figure 3.3: Example of symmetric function extending over the region $0 \leq \xi \leq 2$ with symmetry axis $\xi = 1$; the red color indicates the actual comparison function; the blue color is its symmetric image

For the free-free bar, the construction of the polynomial comparison function is slightly different. We first represent the displacement as a generic polynomial:

$$\psi_{j,F-F}(\xi) = \sum_{i=0}^{j+1} b_i \xi^i \quad (3.3.6)$$

Starting from this polynomial comparison function, we calculate the first derivative to satisfy the boundary conditions. The first derivative evaluated at $\xi = 0$ leads to condition $b_1 = 0$. The first derivative evaluated in $\xi = 1$ leads to an equation in the form:

$$\psi'_{j,F-F}(1) = \sum_{i=0}^{j+1} i b_i \quad (3.3.7)$$

The conditions of crossing x -axis are satisfied evaluating the polynomial at the inner points but not at $\xi = 0$ or at $\xi = 1$, since these two conditions are already satisfied. This is because at $\xi = 0$ and at $\xi = 1$ we do not need the polynomial to be equal to zero and thus we do not need the polynomial to cross the x -axis at these points. In this way, we derive j equations for $j + 1$ unknowns. The problem has infinite number of solutions. Then, we incorporate the additional arbitrary equation $b_0 \xi^0 = b_0 = 1$ to obtain an unique solution. This procedure can be written as a system of equations in the form:

$$\mathbf{A}\mathbf{x} = \mathbf{b} \quad (3.3.8)$$

where \mathbf{A} is $(j+1) \times (j+1)$ order matrix and \mathbf{b} is a $j+1$ order vector. The vector \mathbf{b} is composed of zeros with last component equal to 1. The first row of the matrix \mathbf{A} comprises the decreasing numbers starting from the order of the matrix to zero. The last row coincides with transposed vector \mathbf{b} . The other $j-2$ central rows are progressively starting with $\left(\frac{i}{j}\right)^p$ where j is the number of the comparison function under study, i is the number of the central rows taken into consideration and p is an exponent equal to the same number of the corresponding component of the first row. The final step is deleting column “ j ” because it corresponds to b_1 and is equal to zero, and row “ j ” that leads to $\psi_{j,F-F}(1) = 0$ since this condition should be not repeated.

The first comparison function is obviously constant. Dealing with the second comparison function, the matrix $\hat{\mathbf{A}}$ for determination of the second comparison function, that is the matrix \mathbf{A} before deleting row and column j , reads:

$$\hat{\mathbf{A}} = \begin{bmatrix} 3 & 2 & 1 & 0 \\ \left(\frac{1}{2}\right)^3 & \left(\frac{1}{2}\right)^2 & \left(\frac{1}{2}\right)^1 & \left(\frac{1}{2}\right)^0 \\ \left(\frac{2}{2}\right)^3 & \left(\frac{2}{2}\right)^2 & \left(\frac{2}{2}\right)^1 & \left(\frac{2}{2}\right)^0 \\ 0 & 0 & 0 & 1 \end{bmatrix} \quad (3.3.9)$$

When the j row and the j column are deleted, we obtain the matrix \mathbf{A} to evaluate $\psi_{2,F-F}(\xi)$:

$$\mathbf{A} = \begin{bmatrix} 3 & 2 & 0 \\ \left(\frac{1}{2}\right)^3 & \left(\frac{1}{2}\right)^2 & \left(\frac{1}{2}\right)^0 \\ \left(\frac{2}{2}\right)^3 & \left(\frac{2}{2}\right)^2 & \left(\frac{2}{2}\right)^0 \\ 0 & 0 & 1 \end{bmatrix} \quad (3.3.10)$$

The transposed vector \mathbf{b}^T to evaluate $\psi_{2,F-F}(\xi)$ reads:

$$\mathbf{b}^T = [0 \ 0 \ 1] \quad (3.3.11)$$

The solution \mathbf{x} of the system $\mathbf{A}\mathbf{x} = \mathbf{b}$ is:

$$\mathbf{b}^T = [4 \ -6 \ 1] \quad (3.3.12)$$

Finally, the second polynomial comparison function is obtained:

$$\psi_{2,F-F}(\xi) = 4\xi^3 - 6\xi^2 + 1 \quad (3.3.13)$$

Dealing with the third comparison function the matrix $\hat{\mathbf{A}}$ gets the following form:

$$\hat{\mathbf{A}} = \begin{bmatrix} 4 & 3 & 2 & 1 & 0 \\ \left(\frac{1}{3}\right)^4 & \left(\frac{1}{3}\right)^3 & \left(\frac{1}{3}\right)^2 & \left(\frac{1}{3}\right)^1 & \left(\frac{1}{3}\right)^0 \\ \left(\frac{2}{3}\right)^4 & \left(\frac{2}{3}\right)^3 & \left(\frac{2}{3}\right)^2 & \left(\frac{2}{3}\right)^1 & \left(\frac{2}{3}\right)^0 \\ \left(\frac{3}{3}\right)^4 & \left(\frac{3}{3}\right)^3 & \left(\frac{3}{3}\right)^2 & \left(\frac{3}{3}\right)^1 & \left(\frac{3}{3}\right)^0 \\ 0 & 0 & 0 & 0 & 1 \end{bmatrix} \quad (3.3.14)$$

When the j row and the j column are deleted, we obtain the matrix \mathbf{A} to evaluate $\psi_{3,F-F}(\xi)$:

$$\mathbf{A} = \begin{bmatrix} 4 & 3 & 2 & 0 \\ \left(\frac{1}{3}\right)^4 & \left(\frac{1}{3}\right)^3 & \left(\frac{1}{3}\right)^2 & \left(\frac{1}{3}\right)^0 \\ \left(\frac{2}{3}\right)^4 & \left(\frac{2}{3}\right)^3 & \left(\frac{2}{3}\right)^2 & \left(\frac{2}{3}\right)^0 \\ \left(\frac{3}{3}\right)^4 & \left(\frac{3}{3}\right)^3 & \left(\frac{3}{3}\right)^2 & \left(\frac{3}{3}\right)^0 \\ 0 & 0 & 0 & 1 \end{bmatrix} \quad (3.3.15)$$

The transposed vector \mathbf{b}^T to evaluate $\psi_{3,F-F}(\xi)$:

$$\mathbf{b}^T = [0 \ 0 \ 0 \ 1] \quad (3.3.16)$$

The solution of the system \mathbf{x}^T is:

$$\mathbf{b}^T = \left[-\frac{81}{4} \ \frac{81}{2} \ -\frac{81}{4} \ 1 \right] \quad (3.3.17)$$

Finally, the polynomial comparison function is obtained:

$$\psi_{3,F-F}(\xi) = -\frac{81}{4}\xi^4 + \frac{81}{2}\xi^3 - \frac{81}{4}\xi^2 + 1 \quad (3.3.18)$$

The first five polynomial comparison functions for the free-free bar are:

$$\psi_{1,F-F}(\xi) = 1 \quad (3.3.19)$$

$$\psi_{2,F-F}(\xi) = 4\xi^3 - 6\xi^2 + 1 \quad (3.3.20)$$

$$\psi_{3,F-F}(\xi) = -\frac{81}{4}\xi^4 + \frac{81}{2}\xi^3 - \frac{81}{4}\xi^2 + 1 \quad (3.3.21)$$

$$\psi_{4,F-F}(\xi) = \frac{704}{9}\xi^5 - \frac{1760}{9}\xi^4 + \frac{1444}{9}\xi^3 - \frac{406}{9}\xi^2 + 1 \quad (3.3.22)$$

$$\psi_{5,F-F}(\xi) = -\frac{78125}{288}\xi^6 + \frac{78125}{96}\xi^5 - \frac{258125}{288}\xi^4 + \frac{41875}{96}\xi^3 - \frac{11875}{144}\xi^2 + 1 \quad (3.3.23)$$

3.4 Naïve Galerkin method

In order to apply the Galerkin method, we express the axial deflection as a series in terms of comparison functions:

$$U(\xi) = \sum_{j=1}^n a_j \psi_j(\xi) \quad (3.4.1)$$

We substitute this expansion into Eq. (3.1.18) and (3.1.19); then we multiply each result by $\psi_k(\xi)$, integrate the result from zero to ξ_1 for Eq. (3.1.18), and from ξ_1 to 1 for Eq. (3.1.19), and sum the results. We get:

$$\begin{aligned} & \int_0^{\xi_1} \left[c_1^2 \frac{d^2}{d\xi^2} \sum_{j=1}^n a_j \psi_j(\xi) + \omega^2 L^2 \sum_{j=1}^n a_j \psi_j(\xi) \right] \psi_k(\xi) d\xi \\ & + \int_{\xi_1}^1 \left[c_2^2 \frac{d^2}{d\xi^2} \sum_{j=1}^n a_j \psi_j(\xi) + \omega^2 L^2 \sum_{j=1}^n a_j \psi_j(\xi) \right] \psi_k(\xi) d\xi = 0 \end{aligned} \quad (3.4.2)$$

where $k = 1, 2, 3, \dots, n$ is a positive integer, $\xi_1 = L_1/L$. Eq. (3.4.2) can be rewritten in the following form:

$$\sum_{j=1}^n (P_{jk} + \omega^2 Q_{jk}) a_j = 0 \quad (3.4.3)$$

where:

$$P_{jk} = \int_0^{\xi_1} c_1^2 \frac{d^2 \psi_j}{d\xi^2} \psi_k(\xi) d\xi + \int_{\xi_1}^1 c_2^2 \frac{d^2 \psi_j}{d\xi^2} \psi_k(\xi) d\xi \quad (3.4.4)$$

$$Q_{jk} = \int_0^{\xi_1} L^2 \psi_j(\xi) \psi_k(\xi) d\xi + \int_{\xi_1}^1 L^2 \psi_j(\xi) \psi_k(\xi) d\xi \quad (3.4.5)$$

or in matrix notation as:

$$(\mathbf{P} + \omega^2 \mathbf{Q}) \mathbf{a} = \mathbf{0} \quad (3.4.6)$$

which is a homogeneous linear system in the unknown \mathbf{a} . Eq. (3.4.6) has non-trivial solutions only when the determinant of the coefficient matrix is equal to zero. That lead us to the following eigenvalue problem where the eigenvalue is the sought frequency ω^2 :

$$\det(\mathbf{P} + \omega^2 \mathbf{Q}) = 0 \quad (3.4.7)$$

3.5 Rigorous Galerkin method

Within rigorous implementation, we represent the axial rigidity and the mass using a generalized function as follows:

$$D(x) = E(x) A(x) = D_1 H(x) + (D_2 - D_1) H(x - L_1) \quad (3.5.1)$$

$$M(x) = \rho(x) A(x) = M_1 H(x) + (M_2 - M_1) H(x - L_1) \quad (3.5.2)$$

where $H(x)$ is the unit step function or Heaviside function which has the following properties:

$$H(x - \alpha) = \begin{cases} 1, & \text{if } x > \alpha \\ 0, & \text{otherwise} \end{cases} \quad (3.5.3)$$

$$\frac{d}{dx} H(x - \alpha) = \delta(x - \alpha) \quad (3.5.4)$$

where $\delta(x)$ is the Dirac delta function.

Now, we rewrite (3.1.6) with these considerations:

$$\frac{d}{dx} \left[(D_1 H(x) + (D_2 - D_1) H(x - L_1)) \frac{du}{dx} \right] = [M_1 H(x) + (M_2 - M_1) H(x - L_1)] \frac{d^2 u}{dt^2} \quad (3.5.5)$$

Calculating derivatives lead to:

$$\begin{aligned} & [D_1 \delta(x) + (D_2 - D_1) \delta(x - L_1)] \frac{du}{dx} + [D_1 H(x) + (D_2 - D_1) H(x - L_1)] \frac{d^2 u}{dx^2} \\ &= [M_1 H(x) + (M_2 - M_1) H(x - L_1)] \frac{d^2 u}{dt^2} \end{aligned} \quad (3.5.6)$$

Substituting (3.1.16) and (3.1.17), we obtain:

$$\begin{aligned} & [D_1 \delta(x) + (D_2 - D_1) \delta(x - L_1)] \frac{dU(x)}{dx} + [D_1 H(x) + (D_2 - D_1) H(x - L_1)] \frac{d^2 U(x)}{dx^2} \\ &+ [M_1 H(x) + (M_2 - M_1) H(x - L_1)] \omega^2 U(x) = 0 \end{aligned} \quad (3.5.7)$$

We introduce the non-dimensional axial coordinate $\xi = \frac{x}{L}$. Using (3.4.1), we obtain:

$$\begin{aligned} & [D_1 \delta(\xi) + (D_2 - D_1) \delta(\xi - \xi_1)] \frac{d}{d\xi} \left(\sum_{j=1}^n a_j \psi_j(\xi) \right) \\ &+ [D_1 H(\xi) + (D_2 - D_1) H(\xi - \xi_1)] \frac{d^2}{d\xi^2} \left(\sum_{j=1}^n a_j \psi_j(\xi) \right) \\ &+ [M_1 H(\xi) + (M_2 - M_1) H(\xi - \xi_1)] \omega^2 L^2 \sum_{j=1}^n a_j \psi_j(\xi) = 0 \end{aligned} \quad (3.5.8)$$

We perform the Galerkin procedure:

$$\begin{aligned} & \int_0^1 [D_1 \delta(\xi) + (D_2 - D_1) \delta(\xi - \xi_1)] \frac{d}{d\xi} \sum_{j=1}^n a_j \psi_j(\xi) \psi_k(\xi) d\xi \\ &+ \int_0^1 [D_1 H(\xi) + (D_2 - D_1) H(\xi - \xi_1)] \frac{d^2}{d\xi^2} \sum_{j=1}^n a_j \psi_j(\xi) \psi_k(\xi) d\xi \\ &+ \int_0^1 [M_1 H(\xi) + (M_2 - M_1) H(\xi - \xi_1)] \omega^2 L^2 \sum_{j=1}^n a_j \psi_j(\xi) \psi_k(\xi) d\xi = 0 \end{aligned} \quad (3.5.9)$$

This equation can be rewritten in the following form:

$$\sum_{j=1}^n (N_{jk} + P_{jk} + \omega^2 Q_{jk}) a_j = 0 \quad (3.5.10)$$

where:

$$N_{jk} = \int_0^1 [D_1 \delta(\xi) + (D_2 - D_1) \delta(\xi - \xi_1)] \frac{d\psi_j(\xi)}{d\xi} \psi_k(\xi) d\xi \quad (3.5.11)$$

$$P_{jk} = \int_0^1 [D_1 H(\xi) + (D_2 - D_1) H(\xi - \xi_1)] \frac{d^2 \psi_j(\xi)}{d\xi^2} \psi_k(\xi) d\xi \quad (3.5.12)$$

$$Q_{jk} = \int_0^1 [M_1 H(\xi) + (M_2 - M_1) H(\xi - \xi_1)] L^2 \psi_j(\xi) \psi_k(\xi) d\xi \quad (3.5.13)$$

Introducing matrix notation, we have:

$$(\mathbf{N} + \mathbf{P} + \omega^2 \mathbf{Q}) \mathbf{a} = \mathbf{0} \quad (3.5.14)$$

Non trivial solutions of Eq. (3.5.14) can be found by solving the following eigenvalue problem in the eigenfrequency ω^2 :

$$\det(\mathbf{N} + \mathbf{P} + \omega^2 \mathbf{Q}) = 0 \quad (3.5.15)$$

We observe that if we delete the matrix \mathbf{N} , we obtain the naïve Galerkin method. The full expression of this matrix \mathbf{N} contains the terms N_{jk} appearing in the rigorous Galerkin method, but missing in the naïve version. Thus, utilization of the naïve Galerkin method is incorrect.

3.6 Numerical example

We consider a concrete steel bar, like in Fig. 3.4:

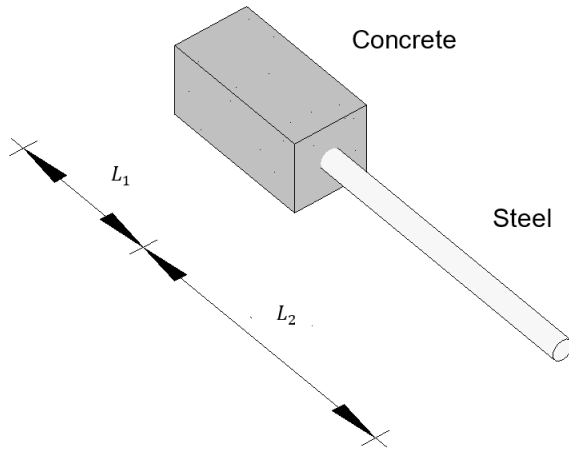


Figure 3.4: A concrete-steel stepped bar

We fix parameters at the following values:

Concrete		Steel	
E	$3.096 \cdot 10^{10}$ Pa	E	$3.096 \cdot 10^{10}$ Pa
ρ	$2.4 \cdot 10^3$ kg/m ³	ρ	$7.87 \cdot 10^3$ kg/m ³
b	0.5 m	ϕ	0.14 m
h	0.5 m	A	$1.49 \cdot 10^{-2}$ m ²
A	0.25 m ²		

Table 3.1: Parameters of each segment

We set $L_1 = 1m$ and $L_2 = 2m$, so $L = 3m$. The ratios:

$$\frac{E_2}{E_1} = 6.46, \quad \frac{\rho_2}{\rho_1} = 3.28, \quad \frac{L_2}{L_1} = 2, \quad \frac{A_2}{A_1} = 0.06 \quad (3.6.1)$$

3.6.1 Exact solution

Considering a free-free bar, the characteristic Eq. (3.2.5) left-hand side is depicted in Fig. 3.5:

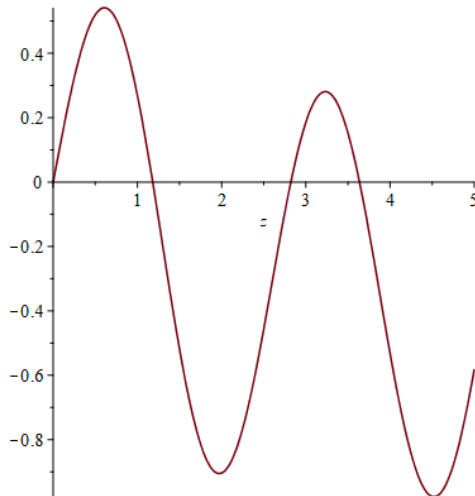


Figure 3.5: Characteristic equation for two-stepped free-free bar

The first four roots are:

$$z_1 = 0, \quad z_2 = 1.1811, \quad z_3 = 2.8217, \quad z_4 = 3.6368 \quad (3.6.2)$$

For a clamped-clamped bar, the characteristic Eq. (3.2.6) left-hand side is depicted in Fig. 3.6:

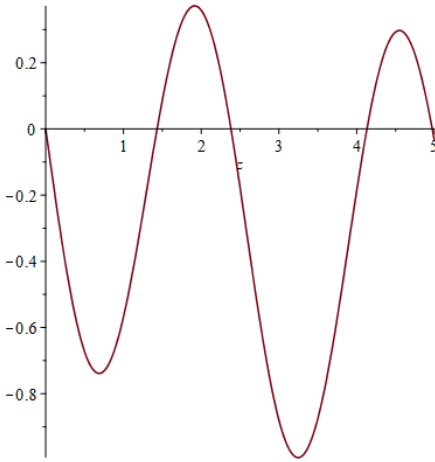


Figure 3.6: Characteristic equation for two-stepped clamped-clamped bar

The first four roots are:

$$z_1 = 1.4323, \quad z_2 = 2.3832, \quad z_3 = 4.1316, \quad z_4 = 4.9720 \quad (3.6.3)$$

In conclusion, for a clamped-free bar, the characteristic Eq. (3.2.7) left-hand side is depicted in Fig. 3.7:

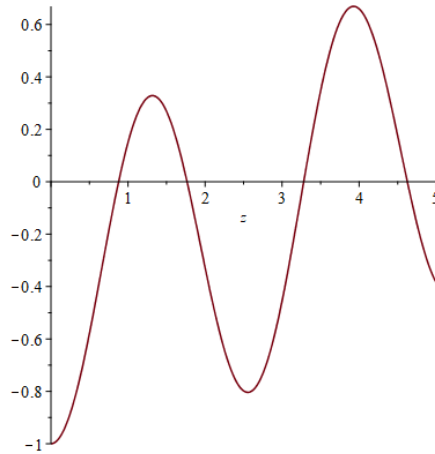


Figure 3.7: Characteristic equation for two-stepped clamped-free bar

The first four roots are:

$$z_1 = 0.8782, \quad z_2 = 1.7661, \quad z_3 = 3.2802, \quad z_4 = 4.6254 \quad (3.6.4)$$

Since we define z as $\beta_1 L_1$, in order to obtain the frequency ω , we need to multiply z by $\frac{c_1}{L_1}$.

Mode	Exact solution [rad/s]		
	Free-Free	Clamped-Clamped	Clamped-Free
1	0.0000	5 144.3235	3 154.3958
2	4 242.0721	8 559.5002	6 343.4155
3	10 134.5946	14 839.2830	11 781.4496
4	13 062.2902	17 857.6076	16 612.9061

Table 3.2: Exact solution for the stepped bar under consideration in three different constrain conditions

3.6.2 Galerkin method with trigonometric comparison function

Naïve Galerkin method with trigonometric comparison function drives us to the following results, shown in Tables 3.3, 3.4 and 3.5:

Mode	Naïve Galerkin method							
	Free-Free							
	Trigonometric comparison function							
Mode	Frequencies [rad/s]							
	1 Term	2 Terms	3 Terms	4 Terms	5 Terms	6 Terms	7 Terms	8 Terms
	1	0.0000	0.0000	0.0000	0.0000	0.0000	0.0000	0.0000
	2	4 626.3482	4 544.5625	4 531.8821	4 531.8758	4 529.6628	4 528.7348	4 528.6991
	3		9 884.8591	9 744.6600	9 635.3395	9 593.0143	9 592.4352	9 582.2433
	4			14 577.9632	14 091.5728	13 830.9121	13 788.7980	13 785.8068

Table 3.3: Frequencies obtained with naïve Galerkin method using trigonometric comparison functions on free-free bar

Naïve Galerkin method								
Clamped-Clamped								
Trigonometric comparison function								
Mode	Frequencies [rad/s]							
	1 Term	2 Terms	3 Terms	4 Terms	5 Terms	6 Terms	7 Terms	8 Terms
1	5 018.5420	4 930.1558	4 851.9846	4 834.2335	4 833.2432	4 820.9782	4 815.1357	4 814.9866
2		9 501.2833	9 215.2323	9 123.8169	9 119.5767	9 113.0776	9 104.2562	9 103.8069
3			14 689.0584	14 452.8971	14 318.3124	14 262.0080	14 257.8150	14 252.7848
4				19 723.2563	19 141.3765	18 692.1093	18 546.0617	18 544.4815

Table 3.4: Frequencies obtained with naïve Galerkin method using trigonometric comparison functions on clamped-clamped bar

Naïve Galerkin method								
Clamped-Free								
Trigonometric comparison function								
Mode	Frequencies [rad/s]							
	1 Term	2 Terms	3 Terms	4 Terms	5 Terms	6 Terms	7 Terms	8 Terms
1	2 601.7829	2 593.3054	2 580.4292	2 574.1105	2 573.9825	2 572.4638	2 570.5318	2 570.3954
2		7 242.6867	7 005.0234	6 885.1881	6 874.8656	6 867.0935	6 848.9891	6 846.1636
3			12 013.1027	11 775.7960	11 698.0334	11 686.0032	11 685.9176	11 682.9359
4				17 300.8328	16 944.5027	16 647.2233	16 513.9127	16 507.5007

Table 3.5: Frequencies obtained with naïve Galerkin method using trigonometric comparison functions on clamped-free bar

The relative error ε is defined as:

$$\varepsilon = \frac{\omega_{Galerkin} - \omega_{exact}}{\omega_{exact}} \times 100 \quad (3.6.5)$$

The relative errors are listed in Tables 3.6, 3.7 and 3.8:

Mode	Naïve Galerkin method							
	Free-Free							
	Trigonometric comparison function							
Mode	Relative error [%]							
	1 Term	2 Terms	3 Terms	4 Terms	5 Terms	6 Terms	7 Terms	8 Terms
1	N/A	N/A	N/A	N/A	N/A	N/A	N/A	N/A
2		9.06%	7.13%	6.83%	6.83%	6.78%	6.76%	6.76%
3			-2.46%	-3.85%	-4.93%	-5.34%	-5.35%	-5.45%
4				11.60%	7.88%	5.88%	5.56%	5.54%

Table 3.6: Relative error between naïve Galerkin method using trigonometric comparison functions and exact solution on free-free bar

Mode	Naïve Galerkin method							
	Clamped-Clamped							
	Trigonometric comparison function							
Mode	Relative error [%]							
	1 Term	2 Terms	3 Terms	4 Terms	5 Terms	6 Terms	7 Terms	8 Terms
1	-2.45%	-4.16%	-5.68%	-6.03%	-6.05%	-6.29%	-6.40%	-6.40%
2		11.00%	7.66%	6.59%	6.54%	6.47%	6.36%	6.36%
3			-1.01%	-2.60%	-3.51%	-3.89%	-3.92%	-3.95%
4				10.45%	7.19%	4.67%	3.86%	3.85%

Table 3.7: Relative error between naïve Galerkin method using trigonometric comparison functions and exact solution on clamped-clamped bar

Mode	Naïve Galerkin method							
	Clamped-Free							
	Trigonometric comparison function							
Mode	Relative error [%]							
	1 Term	2 Terms	3 Terms	4 Terms	5 Terms	6 Terms	7 Terms	8 Terms
1	-17.52%	-17.79%	-18.20%	-18.40%	-18.40%	-18.45%	-18.51%	-18.51%
2		14.18%	10.43%	8.54%	8.38%	8.26%	7.97%	7.93%
3			1.97%	-0.05%	-0.71%	-0.81%	-0.81%	-0.84%
4				4.14%	2.00%	0.21%	-0.60%	-0.63%

Table 3.8: Relative error between naïve Galerkin method using trigonometric comparison functions and exact solution on clamped-free bar

Rigorous Galerkin method with trigonometric comparison function leads us to the following results, shown in Tables 3.9 - 3.14:

Rigorous Galerkin method								
Mode	Free-Free							
	Trigonometric comparison function							
Frequencies [rad/s]								
Mode	1 Term	2 Terms	3 Terms	4 Terms	5 Terms	6 Terms	7 Terms	8 Terms
1	0.0000	0.0000	0.0000	0.0000	0.0000	0.0000	0.0000	0.0000
2		4 441.4719	4 369.1330	4 315.4440	4 315.2436	4 297.7796	4 285.2637	4 285.2544
3			10 284.1392	10 273.5637	10 225.7789	10 185.0023	10 178.2480	10 175.8876
4				13 377.3274	13 157.0018	13 156.8288	13 134.1756	13 131.6688

Table 3.9: Frequencies obtained with rigorous Galerkin method using trigonometric comparison functions on free-free bar

Rigorous Galerkin method								
Mode	Clamped-Clamped							
	Trigonometric comparison function							
Frequencies [rad/s]								
Mode	1 Term	2 Terms	3 Terms	4 Terms	5 Terms	6 Terms	7 Terms	8 Terms
1	5 202.1240	5 180.7197	5 158.3163	5 152.1139	5 152.1106	5 150.2015	5 148.6875	5 148.6688
2		8 712.2687	8 708.2820	8 663.7780	8 648.6380	8 644.2586	8 624.4633	8 620.1693
3			15 034.5161	15 033.8675	15 022.7849	14 971.2199	14 937.3245	14 936.5568
4				18 635.3520	18 008.0035	17 904.6285	17 903.9560	17 890.8099

Table 3.10: Frequencies obtained with rigorous Galerkin method using trigonometric comparison functions on clamped-clamped bar

Mode	Trigonometric comparison function							
	Frequencies [rad/s]							
	1 Term	2 Terms	3 Terms	4 Terms	5 Terms	6 Terms	7 Terms	8 Terms
1	3 332.7865	3 224.9983	3 224.8897	3 200.0409	3 187.1622	3 187.1012	3 179.9328	3 175.6501
2		6 448.0147	6 362.2911	6 362.2909	6 355.5801	6 354.3501	6 353.3065	6 351.1151
3			11 992.9007	11 975.6930	11 937.3957	11 937.1283	11 905.1234	11 884.6590
4				17 178.5257	16 883.8308	16 679.9085	16 636.1462	16 636.2359

Table 3.11: Frequencies obtained with rigorous Galerkin method using trigonometric comparison functions on clamped-free bar

Mode	Trigonometric comparison function							
	Relative error [%]							
	1 Term	2 Terms	3 Terms	4 Terms	5 Terms	6 Terms	7 Terms	8 Terms
1	N/A	N/A	N/A	N/A	N/A	N/A	N/A	N/A
2		4.70%	3.00%	1.73%	1.72%	1.31%	1.02%	1.02%
3			1.48%	1.37%	0.90%	0.50%	0.43%	0.41%
4				2.41%	0.73%	0.72%	0.55%	0.53%

Table 3.12: Relative error between rigorous Galerkin method using trigonometric comparison functions and exact solution on free-free bar

Mode	Trigonometric comparison function							
	Relative error [%]							
	1 Term	2 Terms	3 Terms	4 Terms	5 Terms	6 Terms	7 Terms	8 Terms
1	1.12%	0.71%	0.27%	0.15%	0.15%	0.11%	0.08%	0.08%
2		1.78%	1.74%	1.22%	1.04%	0.99%	0.76%	0.71%
3			1.32%	1.31%	1.24%	0.89%	0.66%	0.66%
4				4.36%	0.84%	0.26%	0.26%	0.19%

Table 3.13: Relative error between rigorous Galerkin method using trigonometric comparison functions and exact solution on clamped-clamped bar

Rigorous Galerkin method Clamped-Free Trigonometric comparison function								
Mode	Relative error [%]							
	1 Term	2 Terms	3 Terms	4 Terms	5 Terms	6 Terms	7 Terms	8 Terms
1	5.66%	2.24%	2.23%	1.45%	1.04%	1.04%	0.81%	0.67%
2		1.65%	0.30%	0.30%	0.19%	0.17%	0.16%	0.12%
3			1.79%	1.65%	1.32%	1.32%	1.05%	0.88%
4				3.40%	1.63%	0.40%	0.14%	0.14%

Table 3.14: Relative error between rigorous Galerkin method using trigonometric comparison functions and exact solution on clamped-free bar

In Fig. 3.8 and 3.9, we have the trend of the relative error between naïve and rigorous Galerkin method and the exact solution with the number of terms in Galerkin method implementation:

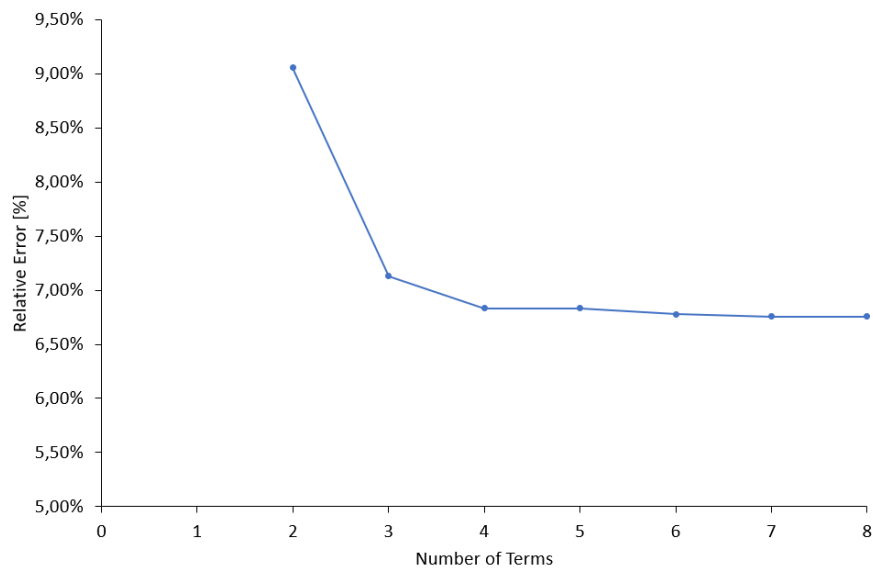


Figure 3.8: Trend of relative error of second natural frequency obtained with naïve Galerkin method using trigonometric comparison functions on free-free bar

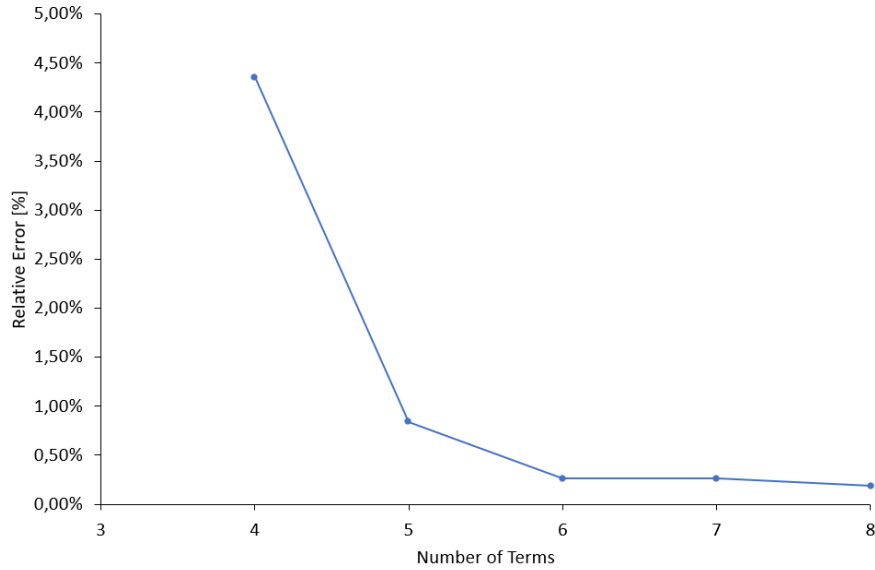


Figure 3.9: Trend of relative error of fourth natural frequency obtained with rigorous Galerkin method using trigonometric comparison functions on clamped-clamped bar

We see that rigorous implementation of Galerkin method tends to the exact solution. This trend is clear in Fig. 3.8 and Fig. 3.9. From Fig. 3.9, we can see that with four terms of approximation, we have 4.36% of relative error and with eight terms the relative error collapses at 0.19%. On the other side, from the naïve implementation of Galerkin method shown in Fig. 3.8, we have 9.06% of relative error with two terms of approximation and it arrives at 6.76% with eight terms. The benefit that we can have increasing the number of terms leads us to the conclusion that the naïve implementation does not tend to the exact solution.

3.6.3 Galerkin method with polynomial comparison function

We get similar results using polynomial comparison functions, as given in Tables 3.15 - 3.26:

Mode	Naïve Galerkin method							
	Free-Free							
	Polynomial comparison function							
Frequencies [rad/s]								
Mode	1 Term	2 Terms	3 Terms	4 Terms	5 Terms	6 Terms	7 Terms	8 Terms
1	0.0000	0.0000	0.0000	0.0000	0.0000	0.0000	0.0000	0.0000
2		4 620.1242	4 533.4977	4 536.9259	4 534.6363	4 530.6500	4 530.5517	4 529.4783
3			9 838.8894	9 607.8869	9 626.1519	9 628.9511	9 611.4205	9 591.0033
4				14 628.5096	13 887.5011	13 920.7158	13 873.4799	13 809.0809

Table 3.15: Frequencies obtained with naïve Galerkin method using polynomial comparison functions on free-free bar

Mode	Naïve Galerkin method							
	Clamped-Clamped							
	Polynomial comparison function							
Mode	Frequencies [rad/s]							
	1 Term	2 Terms	3 Terms	4 Terms	5 Terms	6 Terms	7 Terms	8 Terms
1	4 963.0702	4 830.4326	4 866.4668	4 867.5934	4 844.8277	4 834.1571	4 832.7925	4 822.3899
2		9 655.0031	9 237.1946	9 208.2668	9 147.2801	9 124.9379	9 125.3742	9 114.5656
3			15 415.7142	14 625.9675	14 385.8784	14 290.8509	14 279.0735	14 274.0455
4				21 551.9203	19 753.7976	19 141.2271	18 686.0089	18 628.9023

Table 3.16: Frequencies obtained with naïve Galerkin method using polynomial comparison functions on clamped-clamped bar

Mode	Naïve Galerkin method							
	Clamped-Free							
	Polynomial comparison function							
Mode	Frequencies [rad/s]							
	1 Term	2 Terms	3 Terms	4 Terms	5 Terms	6 Terms	7 Terms	8 Terms
1	2 558.1671	2 583.8280	2 580.1218	2 576.1399	2 574.3626	2 572.6140	2 571.8758	2 570.7230
2		6 862.5363	6 937.5857	6 913.3831	6 883.1668	6 870.0049	6 859.4084	6 851.3591
3			12 402.0206	11 677.5815	11 699.1617	11 694.9823	11 685.5640	11 684.8559
4				18 664.3564	16 542.1701	16 600.4071	16 589.3786	16 511.5465

Table 3.17: Frequencies obtained with naïve Galerkin method using polynomial comparison functions on clamped-free bar

Mode	Naïve Galerkin method							
	Free-Free							
	Polynomial comparison function							
Mode	Relative error [%]							
	1 Term	2 Terms	3 Terms	4 Terms	5 Terms	6 Terms	7 Terms	8 Terms
1	N/A	N/A	N/A	N/A	N/A	N/A	N/A	N/A
2		8.91%	6.87%	6.95%	6.90%	6.80%	6.80%	6.78%
3			-2.92%	-5.20%	-5.02%	-4.99%	-5.16%	-5.36%
4				11.99%	6.32%	6.57%	6.21%	5.72%

Table 3.18: Relative error between naïve Galerkin method using polynomial comparison functions and exact solution on free-free bar

Mode	Naïve Galerkin method							
	Clamped-Clamped							
	Polynomial comparison function							
Mode	Relative error [%]							
	1 Term	2 Terms	3 Terms	4 Terms	5 Terms	6 Terms	7 Terms	8 Terms
1	-3.52%	-6.10%	-5.40%	-5.38%	-5.82%	-6.03%	-6.06%	-6.26%
2		12.80%	7.92%	7.58%	6.87%	6.61%	6.61%	6.48%
3			3.88%	-1.44%	-3.06%	-3.70%	-3.78%	-3.81%
4				20.69%	10.62%	7.19%	4.64%	4.32%

Table 3.19: Relative error between naïve Galerkin method using polynomial comparison functions and exact solution on clamped-clamped bar

Mode	Naïve Galerkin method							
	Clamped-Free							
	Polynomial comparison function							
Mode	Relative error [%]							
	1 Term	2 Terms	3 Terms	4 Terms	5 Terms	6 Terms	7 Terms	8 Terms
1	-18.90%	-18.09%	-18.21%	-18.33%	-18.39%	-18.44%	-18.47%	-18.50%
2		8.18%	9.37%	8.99%	8.51%	8.30%	8.13%	8.01%
3			5.27%	-0.88%	-0.70%	-0.73%	-0.81%	-0.82%
4				12.35%	-0.43%	-0.08%	-0.14%	-0.61%

Table 3.20: Relative error between naïve Galerkin method using polynomial comparison functions and exact solution on clamped-free bar

Mode	Rigorous Galerkin method							
	Free-Free							
	Polynomial comparison function							
Mode	Frequencies [rad/s]							
	1 Term	2 Terms	3 Terms	4 Terms	5 Terms	6 Terms	7 Terms	8 Terms
1	0.0000	0.0000	0.0000	0.0000	0.0000	0.0000	0.0000	0.0000
2		4,474.7447	4,393.5396	4,335.0171	4,331.1123	4,305.2814	4,303.4683	4,294.4495
3			10,231.4611	10,211.1155	10,210.4630	10,203.1847	10,199.6844	10,182.0485
4				13,683.8093	13,550.7478	13,231.1408	13,168.6233	13,160.8169

Table 3.21: Frequencies obtained with rigorous Galerkin method using polynomial comparison functions on free-free bar

Rigorous Galerkin method Clamped-Clamped Polynomial comparison function								
Mode	Frequencies [rad/s]							
	1 Term	2 Terms	3 Terms	4 Terms	5 Terms	6 Terms	7 Terms	8 Terms
1	5,176.7471	5,163.0237	5,160.5259	5,160.4144	5,155.2704	5,152.3873	5,152.2694	5,150.2498
2		9,177.7155	9,176.3380	8,713.2303	8,712.2139	8,665.3025	8,657.2906	8,647.4597
3			15,705.9435	15,648.9100	14,998.2211	14,997.9510	14,994.2634	14,967.7172
4				20,594.8436	20,088.3807	18,328.6049	18,002.8785	17,985.6168

Table 3.22: Frequencies obtained with rigorous Galerkin method using polynomial comparison functions on clamped-clamped bar

Rigorous Galerkin method Clamped-Free Polynomial comparison function								
Mode	Frequencies [rad/s]							
	1 Term	2 Terms	3 Terms	4 Terms	5 Terms	6 Terms	7 Terms	8 Terms
1	3,406.3293	3,281.0026	3,212.3615	3,212.1483	3,191.8126	3,191.5861	3,182.3582	3,181.4120
2		6,716.8460	6,376.1722	6,365.9791	6,359.2035	6,357.5515	6,353.8069	6,353.7629
3			14,248.9052	12,362.1368	11,962.7219	11,953.0542	11,916.4697	11,911.4715
4				19,785.6030	16,690.8711	16,666.6926	16,666.4726	16,636.0693

Table 3.23: Frequencies obtained with rigorous Galerkin method using polynomial comparison functions on clamped-free bar

Rigorous Galerkin method Free-Free Polynomial comparison function								
Mode	Relative error [%]							
	1 Term	2 Terms	3 Terms	4 Terms	5 Terms	6 Terms	7 Terms	8 Terms
1	N/A	N/A	N/A	N/A	N/A	N/A	N/A	N/A
2		5.48%	3.57%	2.19%	2.10%	1.49%	1.45%	1.23%
3			0.96%	0.76%	0.75%	0.68%	0.64%	0.47%
4				4.76%	3.74%	1.29%	0.81%	0.75%

Table 3.24: Relative error between rigorous Galerkin method using polynomial comparison functions and exact solution on free-free bar

Rigorous Galerkin method Clamped-Clamped Polynomial comparison function								
Mode	Relative error [%]							
	1 Term	2 Terms	3 Terms	4 Terms	5 Terms	6 Terms	7 Terms	8 Terms
1	0.63%	0.36%	0.31%	0.31%	0.21%	0.16%	0.15%	0.12%
2		7.22%	7.21%	1.80%	1.78%	1.24%	1.14%	1.03%
3			5.84%	5.46%	1.07%	1.07%	1.04%	0.87%
4				15.33%	12.49%	2.64%	0.81%	0.72%

Table 3.25: Relative error between rigorous Galerkin method using polynomial comparison functions and exact solution on clamped-clamped bar

Rigorous Galerkin method Clamped-Free Polynomial comparison function								
Mode	Relative error [%]							
	1 Term	2 Terms	3 Terms	4 Terms	5 Terms	6 Terms	7 Terms	8 Terms
1	7.99%	4.01%	1.84%	1.83%	1.19%	1.18%	0.89%	0.86%
2		5.89%	0.52%	0.36%	0.25%	0.22%	0.16%	0.16%
3			20.94%	4.93%	1.54%	1.46%	1.15%	1.10%
4				19.10%	0.47%	0.32%	0.32%	0.14%

Table 3.26: Relative error between rigorous Galerkin method using polynomial comparison functions and exact solution on clamped-free bar

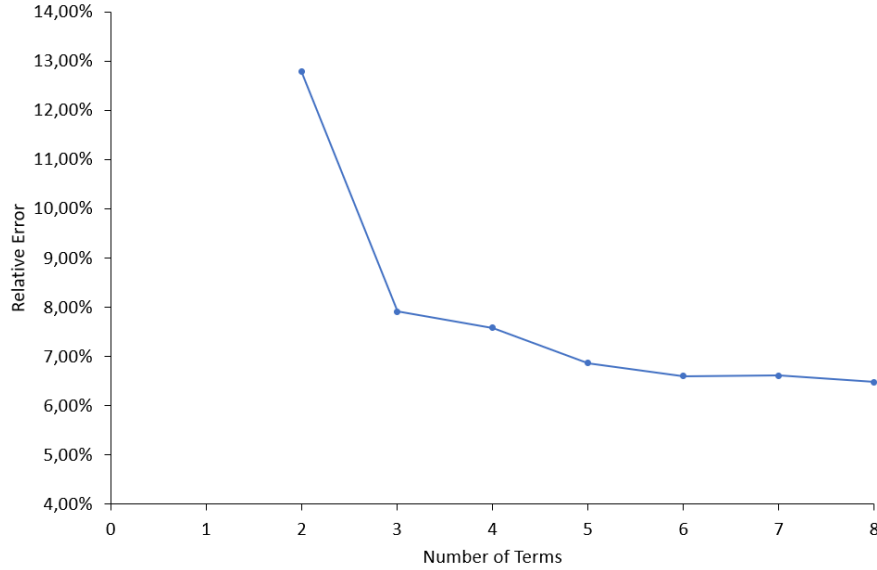


Figure 3.10: Trend of relative error of second natural frequency obtained with naïve Galerkin method using polynomial comparison functions on clamped-clamped bar

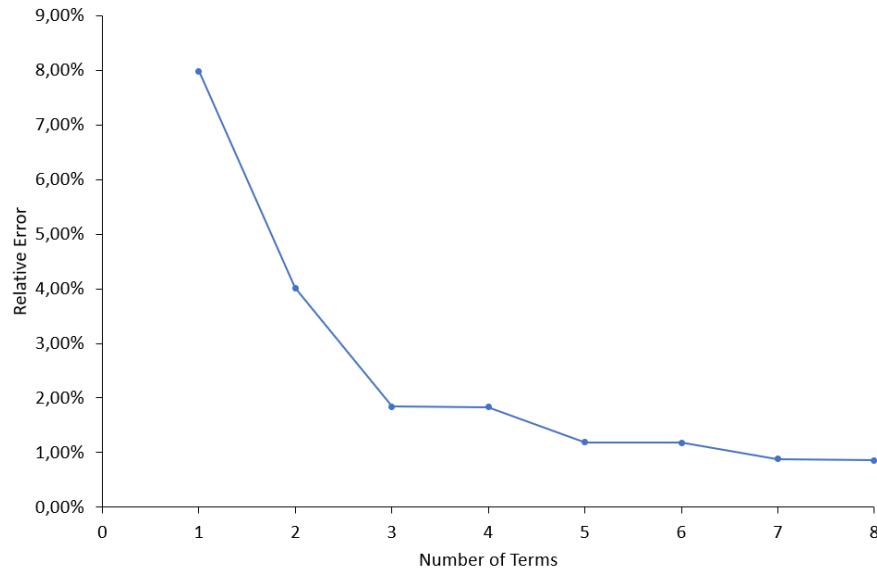


Figure 3.11: Trend of relative error of first natural frequency obtained with rigorous Galerkin method using polynomial comparison functions on clamped-free bar

3.7 Conclusion

Theoretical and numerical results derived in this study show that the naïve implementation of Galerkin method does not tend to the exact solution for stepped bars, whereas the rigorous version leads to the exact solution. In contrast with the naïve version, rigorous Galerkin method has one additional term. This term provides more precision and, most importantly, leads to the convergence to the exact solution. This study demonstrates that straightforward,

naïve Galerkin method should be abandoned altogether for stepped bars, and rigorous Galerkin method should be adopted.

4. Beam

In this chapter, we analyze the bending free vibration of stepped beams, which is mathematically characterized by one-dimension fourth order differential equation. We investigate five-step beams in four different boundary conditions: simply supported at both ends, clamped-free, clamped-simply supported and clamped at both ends.

Similarly to the previous chapter, firstly, we derive the exact solution for thin beams using the Bernoulli-Euler theory, secondly, we implement the two versions of Galerkin method and we compare the obtained results in terms of relative error. In this case, the comparison function is derived starting from the deflection associated with a static load condition.

4.1 Basic Equations

We are interested in solving the problem shown in Fig. 4.1: a stepped beam composed of five different elements.

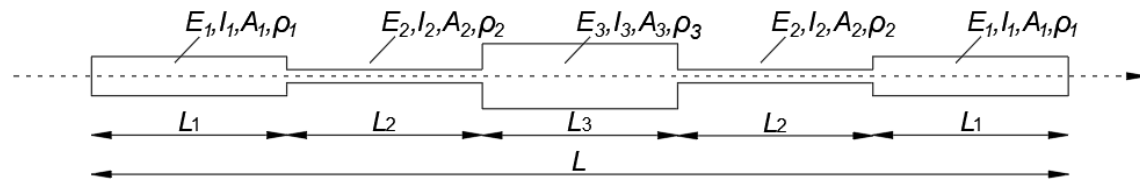


Figure 4.1: A multi-stepped beam of length L

In Fig. 4.1, E_1 , E_2 and E_3 denote the elastic modulus of the related element; I_1 , I_2 and I_3 denote the associated moments of inertia of the cross section; A_1 , A_2 and A_3 denote the cross-sectional areas of the span; ρ_1 , ρ_2 and ρ_3 denote the mass density of the span material and L_1 , L_2 and L_3 denote the lengths of the relevant portion.

Considering the dynamic equilibrium on a differential element of Bernoulli-Euler beam, as shown in Fig. 4.2:

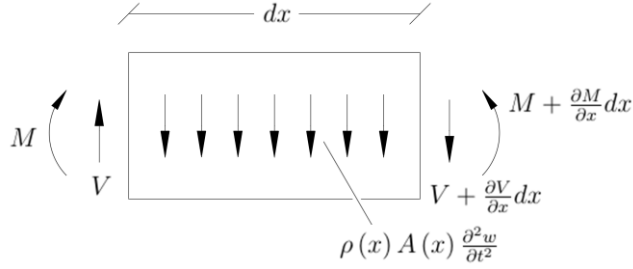


Figure 4.2: A differential element of beam

The equilibrium in vertical direction leads us to:

$$\frac{\partial V}{\partial x} = -\rho(x)A(x)\frac{\partial^2 w}{\partial t^2} \quad (4.1.1)$$

The equilibrium of bending moment yields to:

$$\frac{\partial M}{\partial x} = V \quad (4.1.2)$$

Remembering that:

$$M = \chi EI \quad (4.1.3)$$

$$\chi = \frac{d^2 w}{dx^2} \quad (4.1.4)$$

Finally, assembling (4.1.4), (4.1.3), (4.1.2) and (4.1.1), we obtain:

$$\frac{\partial^2}{\partial x^2} \left(E(x)I(x)\frac{\partial^2 w}{\partial x^2} \right) + \rho(x)A(x)\frac{\partial^2 w}{\partial t^2} = 0 \quad (4.1.5)$$

where $w(x, t)$ is the transverse displacement, x the axial coordinate and t is the time.

Specifically, for each component, with piecewise constants E, I, ρ and A , we can write:

$$E_j I_j \frac{\partial^4 w}{\partial x^4} + \rho_j A_j \frac{\partial^2 w}{\partial t^2} = 0 \quad (4.1.6)$$

where j is a serial number identifying the component.

Now we can separate the variables by supposing that the vertical displacement is described as follows:

$$w(x, t) = W(x) \sin(\omega t) \quad (4.1.7)$$

where ω is the sought natural frequency of the system.

Substituting Eq. (4.1.7) in the differential equation (4.1.5), we obtain:

$$\left[E_j I_j \frac{d^4 W}{dx^4} - \rho_j A_j \omega^2 W \right] \sin(\omega t) = 0 \quad (4.1.8)$$

Since Eq. (4.1.8) is valid for any value of the time instant t , the expression between square brackets must vanish yielding:

$$E_j I_j \frac{d^4 W}{dx^4} - \rho_j A_j \omega^2 W = 0 \quad (4.1.9)$$

Dividing by $E_j I_j$, we obtain:

$$\frac{d^4 W}{dx^4} - \frac{\rho_j A_j \omega^2}{E_j I_j} W = 0 \quad (4.1.10)$$

Introducing the parameter α_j :

$$\alpha_j = \sqrt[4]{\frac{\rho_j A_j \omega^2}{E_j I_j}} \quad (4.1.11)$$

we obtain:

$$\frac{d^4 W}{dx^4} - \alpha_j^4 W = 0 \quad (4.1.12)$$

Now we substitute for $W(x)$:

$$W(x) = C e^{rx} \quad (4.1.13)$$

where r is a characteristic exponent and C is the constant. Eq. (4.1.12) yields:

$$(r^4 - \alpha_j^4) C e^{rx} = 0 \quad (4.1.14)$$

We are not interested in the trivial solution $C = 0$. Assuming $C \neq 0$, we get:

$$r^4 - \alpha_j^4 = 0 \quad (4.1.15)$$

Or:

$$(r^2 - \alpha_j^2)(r^2 + \alpha_j^2) = 0 \quad (4.1.16)$$

Leading to:

$$r_{1,2} = \pm i\alpha_j, \quad r_{3,4} = \pm \alpha_j \quad (4.1.17)$$

The expression of $W(x)$ becomes:

$$W_j(x) = C_{1,j} e^{i\alpha_j x} + C_{2,j} e^{-i\alpha_j x} + C_{3,j} e^{\alpha_j x} + C_{4,j} e^{-\alpha_j x} \quad (4.1.18)$$

Remembering Euler's formulas:

$$e^{i\alpha_j x} = \cos(\alpha_j x) + i \sin(\alpha_j x) \quad (4.1.19a)$$

$$e^{-i\alpha_j x} = \cos(\alpha_j x) - i \sin(\alpha_j x) \quad (4.1.19b)$$

we arrive at:

$$W_j(x) = C_{1,j} [\cos(\alpha_j x) + i \sin(\alpha_j x)] + C_{2,j} [\cos(\alpha_j x) - i \sin(\alpha_j x)] + C_{3,j} e^{\alpha_j x} + C_{4,j} e^{-\alpha_j x} \quad (4.1.20)$$

or:

$$W_j(x) = (iC_{1,j} - iC_{2,j}) \sin(\alpha_j x) + (C_{1,j} + C_{2,j}) \cos(\alpha_j x) + C_{3,j} e^{\alpha_j x} + C_{4,j} e^{-\alpha_j x} \quad (4.1.21)$$

or:

$$W_j(x) = D_{1,j} \sin(\alpha_j x) + D_{2,j} \cos(\alpha_j x) + C_{3,j} e^{\alpha_j x} + C_{4,j} e^{-\alpha_j x} \quad (4.1.22)$$

Using the definition of the hyperbolic functions, we obtain:

$$W_j(x) = D_{1,j} \sin(\alpha_j x) + D_{2,j} \cos(\alpha_j x) + D_{3,j} \cosh(\alpha_j x) + D_{4,j} \sinh(\alpha_j x) \quad (4.1.23)$$

4.2 Krylov Functions

Krylov functions are four functions defined as follows:

$$K_1(\alpha x) = \frac{1}{2} [\cosh(\alpha x) + \cos(\alpha x)] \quad (4.2.1a)$$

$$K_2(\alpha x) = \frac{1}{2} [\sinh(\alpha x) + \sin(\alpha x)] \quad (4.2.1b)$$

$$K_3(\alpha x) = \frac{1}{2} [\cosh(\alpha x) - \cos(\alpha x)] \quad (4.2.1c)$$

$$K_4(\alpha x) = \frac{1}{2} [\sinh(\alpha x) - \sin(\alpha x)] \quad (4.2.1d)$$

We can note that:

$$K_1(0) = 1 \quad (4.2.2a)$$

$$K_2(0) = 0 \quad (4.2.2b)$$

$$K_3(0) = 0 \quad (4.2.2c)$$

$$K_4(0) = 0 \quad (4.2.2d)$$

The second property is that the first derivative of K_i is equal to K_{i-1} :

Krylov Function	$K_1(x)$	$K_1(x)$	$K_1(x)$	$K_1(x)$
First derivative	$K_4(x)$	$K_1(x)$	$K_2(x)$	$K_3(x)$
Second derivative	$K_3(x)$	$K_4(x)$	$K_1(x)$	$K_2(x)$
Third derivative	$K_2(x)$	$K_3(x)$	$K_4(x)$	$K_1(x)$

Table 4.1: Derivative of Krylov functions

We can use these functions into Eq. (4.1.23) in order to simplify the representation of the boundary conditions. This will lead us to the following equation:

$$W_j(x) = M_{1,j}K_1(\alpha_j x) + M_{2,j}K_2(\alpha_j x) + M_{3,j}K_3(\alpha_j x) + M_{4,j}K_4(\alpha_j x) \quad (4.2.3)$$

where $M_{i,j}$ are constants of integration.

4.3 Exact solution

The evaluation of the exact solution consists in the demand that not all four coefficients $M_{i,j}$ for each component vanish simultaneously. In our study case, we have 5 different elements for the multi-step beam resulting in a total of 20 unknowns. As a result, we need 20 equations to solve the problem. The solution should satisfy continuity conditions between the components and the boundary conditions for the first and the last components.

The continuity conditions are: continuity of vertical displacement, continuity of slope, continuity of bending moment and continuity of shear force. We have 4 continuity conditions for each cross-section of discontinuity. In our study case, we have 5 elements with 4 cross-sections of discontinuity. In total, we have 16 equations of compatibility. They read:

$$W_j(x = L_j) = W_{j+1}(x = L_{j+1}) \quad (4.3.1a)$$

$$\frac{dW_j}{dx}(x = L_j) = \frac{dW_{j+1}}{dx}(x = L_{j+1}) \quad (4.3.1b)$$

$$E_j I_j \frac{d^2 W_j}{dx^2}(x = L_j) = E_{j+1} I_{j+1} \frac{d^2 W_{j+1}}{dx^2}(x = L_{j+1}) \quad (4.3.1c)$$

$$E_j I_j \frac{d^3 W_j}{dx^3}(x = L_j) = E_{j+1} I_{j+1} \frac{d^3 W_{j+1}}{dx^3}(x = L_{j+1}) \quad (4.3.1d)$$

The boundary conditions are two for each end, in total 4 equations. Adding the compatibility conditions to the boundary conditions, we obtain 20 equations yielding 20 equations for 20 unknowns.

In this chapter, we study four cases of different boundary conditions: (a) simply supported at both ends beam, (b) the cantilever beam, (c) the clamped-simply supported beam and (d) the clamped-clamped beam. These boundary conditions are summarized in the following table:

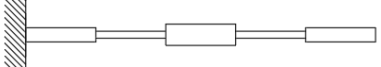
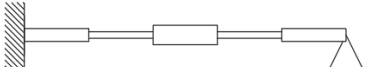
Constrain conditions	$x = 0$	$x = L$
 Simply supported at both ends	$W_1 = 0$ $E_1 I_1 \frac{d^2 W_1}{dx^2} = 0$	$W_5 = 0$ $E_5 I_5 \frac{d^2 W_5}{dx^2} = 0$
 Cantilever	$W_1 = 0$ $\frac{dW_1}{dx} = 0$	$E_5 I_5 \frac{d^2 W_5}{dx^2} = 0$ $E_5 I_5 \frac{d^3 W_5}{dx^3} = 0$
 Clamped-Simply supported	$W_1 = 0$ $\frac{dW_1}{dx} = 0$	$W_5 = 0$ $E_5 I_5 \frac{d^2 W_5}{dx^2} = 0$
 Clamped-Clamped	$W_1 = 0$ $\frac{dW_1}{dx} = 0$	$W_5 = 0$ $\frac{dW_5}{dx} = 0$

Table 4.2: Boundary conditions analyzed in this study

This system of equations is in the following form:

$$\mathbf{A}\mathbf{x} = \mathbf{0} \quad (4.3.2)$$

where \mathbf{A} is the coefficient matrix, \mathbf{x} the vector of unknowns and $\mathbf{0}$ the zero vector. This is a homogeneous system and has non-trivial solution only if the determinant of coefficients matrix \mathbf{A} vanishes. The solution of vibrational problem consists in finding the value of the natural frequencies ω that correspond to vanishing the determinant.

The coefficient matrix \mathbf{A} is a sparse matrix where the non-zero terms appear around the main diagonal. The structure of the matrix is represented in Fig. 4.3:

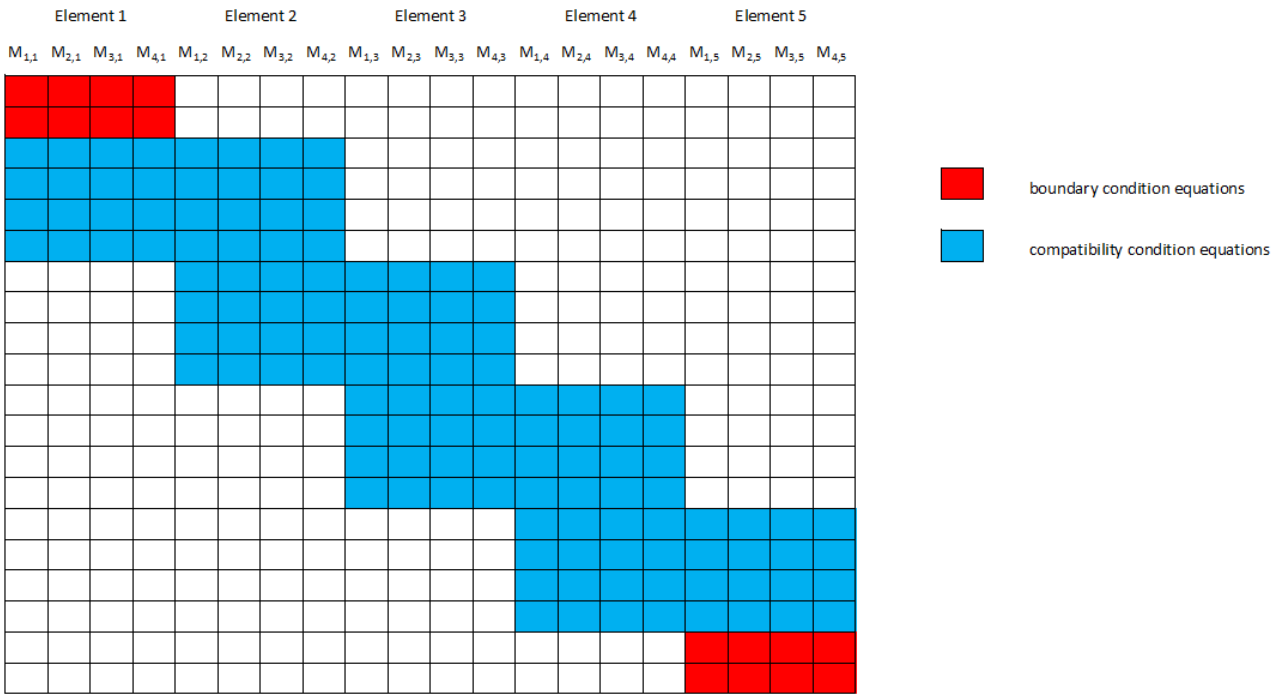


Figure 4.3: Matrix structure for exact solution

4.4 Naïve Galerkin method

The Galerkin method, as previously explained in Chapter 2, is a numerical method which solves the differential equations in an approximate way. The differential equation we are interested in solving is given by Eq. (4.1.9):

$$E_j I_j \frac{d^4 W}{dx^4} - \rho_j A_j \omega^2 W = 0 \quad x_{j-1} < x < x_j \quad (4.4.1)$$

Representing the axial coordinate in non-dimensional form:

$$E_j I_j \frac{d^4 W}{d\xi^4} - \rho_j A_j \omega^2 L^4 W = 0 \quad \xi_{j-1} < \xi < \xi_j \quad (4.4.2)$$

In order to apply the naïve Galerkin method, we have to express the vertical displacement in series in terms of comparison functions:

$$W(\xi) = \sum_{p=1}^n a_p \psi_p(\xi) \quad (4.4.3)$$

where a_p is an unknown constant and $\psi_p(\xi)$ is a comparison function.

Now we substitute the expression of $W(\xi)$ in the differential equation obtaining an error $\varepsilon_j(\xi)$ since $\psi_p(\xi)$ does not necessarily satisfy the differential equation:

$$E_j I_j \sum_{p=1}^n a_p \frac{d^4 \psi_p(\xi)}{d\xi^4} - \rho_j A_j \omega^2 L^4 \sum_{p=1}^n a_p \psi_p(\xi) = \varepsilon_j(\xi) \quad \xi_{j-1} < \xi < \xi_j \quad (4.4.4)$$

Now we multiply the error $\varepsilon_j(\xi)$ by $\psi_q(\xi)$, we sum it up for all the components and we integrate within j^{th} span:

$$\int_0^1 \sum_{j=1}^5 \left(E_j I_j \sum_{p=1}^n a_p \frac{d^4 \psi_p(\xi)}{d\xi^4} \psi_q(\xi) - \rho_j A_j \omega^2 L^4 \sum_{p=1}^n a_p \psi_p(\xi) \psi_q(\xi) \right) d\xi = 0 \quad (4.4.5)$$

After some algebra, we obtain:

$$\sum_{p=1}^n \left[\sum_{j=1}^5 \left(\int_{\xi_j}^{\xi_{j+1}} E_j I_j \frac{d^4 \psi_p(\xi)}{d\xi^4} \psi_q(\xi) d\xi \right) - \omega^2 \sum_{j=1}^5 \left(\int_{\xi_j}^{\xi_{j+1}} \rho_j A_j L^4 \psi_p(\xi) \psi_q(\xi) d\xi \right) \right] a_p = 0 \quad (4.4.6)$$

Defining:

$$K_{pq} = \sum_{j=1}^5 \left(\int_{\xi_j}^{\xi_{j+1}} E_j I_j \frac{d^4 \psi_p(\xi)}{d\xi^4} \psi_q(\xi) d\xi \right) \quad (4.4.7a)$$

$$M_{pq} = \sum_{j=1}^5 \left(\int_{\xi_j}^{\xi_{j+1}} \rho_j A_j L^4 \psi_p(\xi) \psi_q(\xi) d\xi \right) \quad (4.4.7b)$$

We obtain:

$$\sum_{p=1}^n (K_{pq} - \omega^2 M_{pq}) a_p = 0 \quad (4.4.8)$$

Using matrix expression:

$$(\mathbf{K} - \omega^2 \mathbf{M}) \mathbf{a} = \mathbf{0} \quad (4.4.9)$$

where \mathbf{K} represents the stiffness matrix of the beam, \mathbf{M} the mass matrix of the beam and \mathbf{a} the vector of the unknown scale factor.

This is a homogeneous system and has non-trivial solution only if the determinant of the coefficient matrix is equal to zero. It is an eigenvalue problem. We have to find the eigenvalues ω^2 of the problem.

4.5 Rigorous Galerkin method

Starting from Eq. (4.1.5), we apply consideration (4.1.7) on it obtaining:

$$\frac{\partial^2}{\partial x^2} \left(E(x) I(x) \frac{\partial^2 W}{\partial x^2} \right) \sin(\omega t) - \omega^2 \rho(x) A(x) W(x) \sin(\omega t) = 0 \quad (4.5.1)$$

We are interested in a solution which is true for any value of time. Thus we obtain:

$$\frac{\partial^2}{\partial x^2} \left(E(x) I(x) \frac{\partial^2 W}{\partial x^2} \right) - \omega^2 \rho(x) A(x) W(x) = 0 \quad (4.5.2)$$

or, with non-dimensional axial coordinate ξ :

$$\frac{\partial^2}{\partial \xi^2} \left(E(\xi) I(\xi) \frac{\partial^2 W}{\partial \xi^2} \right) - \omega^2 L^4 \rho(\xi) A(\xi) W(\xi) = 0 \quad (4.5.3)$$

In order to implement the rigorous Galerkin method, we represent the flexural rigidity and the mass of the system as a generalized function:

$$D(\xi) = E(\xi) I(\xi) = D_1 H(\xi) + \sum_{j=1}^4 [(D_{j+1} - D_j) H(\xi - \xi_j)] \quad (4.5.4)$$

$$M(\xi) = \rho(\xi) A(\xi) = M_1 H(\xi) + \sum_{j=1}^4 [(M_{j+1} - M_j) H(\xi - \xi_j)] \quad (4.5.5)$$

where $H(\xi)$ is the unit step function or Heaviside function which has the following properties:

$$H(\xi - \alpha) = \begin{cases} 1, & \text{if } \xi > \alpha \\ 0, & \text{otherwise} \end{cases} \quad (4.5.6)$$

$$\frac{d}{d\xi} H(\xi - \alpha) = \delta(\xi - \alpha) \quad (4.5.7)$$

$$\frac{d}{d\xi} \delta(\xi - \alpha) = \delta'(\xi - \alpha) \quad (4.5.8)$$

where $\delta(\xi)$ is the Dirac delta function and $\delta'(\xi)$ is the doublet function.

Now, rewriting the Eq. (4.5.3) with these considerations, we obtain:

$$\frac{\partial^2}{\partial \xi^2} \left(D(\xi) \frac{\partial^2 W}{\partial \xi^2} \right) - \omega^2 L^4 M(\xi) W(\xi) = 0 \quad (4.5.9)$$

We evaluate the derivatives to get:

$$D(\xi) \frac{d^4 W}{d\xi^4} + 2 \frac{d}{d\xi} D(\xi) \frac{d^3 W}{d\xi^3} + \frac{d^2}{d\xi^2} D(\xi) \frac{d^2 W}{d\xi^2} - \omega^2 L^4 M(\xi) W(\xi) = 0 \quad (4.5.10)$$

We substitute the approximation in series of $W(\xi)$ (Eq. (4.4.3)) arriving at:

$$\sum_{p=1}^n \left[D(\xi) \frac{d^4\psi_p(\xi)}{d\xi^4} + 2 \frac{d}{d\xi} D(\xi) \frac{d^3\psi_p(\xi)}{d\xi^3} + \frac{d^2}{d\xi^2} D(\xi) \frac{d^2\psi_p(\xi)}{d\xi^2} - \omega^2 L^4 M(\xi) \psi_p(\xi) \right] a_p = \varepsilon(\xi) \quad (4.5.11)$$

We multiply the differential equation by $\psi_q(\xi)$ and we integrate it from zero to one, to get:

$$\begin{aligned} & \sum_{p=1}^n \left[\int_0^1 D(\xi) \frac{d^4\psi_p(\xi)}{d\xi^4} \psi_q(\xi) d\xi + \int_0^1 2 \frac{d}{d\xi} D(\xi) \frac{d^3\psi_p(\xi)}{d\xi^3} \psi_q(\xi) d\xi \right. \\ & \quad \left. + \int_0^1 \frac{d^2}{d\xi^2} D(\xi) \frac{d^2\psi_p(\xi)}{d\xi^2} \psi_q(\xi) d\xi - \omega^2 \int_0^1 L^4 M(\xi) \psi_p(\xi) \psi_q(\xi) d\xi \right] a_p = 0 \end{aligned} \quad (4.5.12)$$

Defining:

$$K_{1,pq} = \int_0^1 D(\xi) \frac{d^4\psi_p(\xi)}{d\xi^4} \psi_q(\xi) d\xi \quad (4.5.13a)$$

$$K_{2,pq} = \int_0^1 2 \frac{d}{d\xi} D(\xi) \frac{d^3\psi_p(\xi)}{d\xi^3} \psi_q(\xi) d\xi \quad (4.5.13b)$$

$$K_{3,pq} = \int_0^1 \frac{d^2}{d\xi^2} D(\xi) \frac{d^2\psi_p(\xi)}{d\xi^2} \psi_q(\xi) d\xi \quad (4.5.13c)$$

$$M_{pq} = \int_0^1 L^4 M(\xi) \psi_p(\xi) \psi_q(\xi) d\xi \quad (4.5.13d)$$

We obtain:

$$\sum_{p=1}^n (K_{1,pq} + K_{2,pq} + K_{3,pq} - \omega^2 M_{pq}) a_p = 0 \quad (4.5.14)$$

Using matrix expression:

$$(\mathbf{K}_1 + \mathbf{K}_2 + \mathbf{K}_3 - \omega^2 \mathbf{M}) \mathbf{a} = \mathbf{0} \quad (4.5.15)$$

Defining:

$$\mathbf{K} = \mathbf{K}_1 + \mathbf{K}_2 + \mathbf{K}_3 \quad (4.5.16)$$

We obtain:

$$(\mathbf{K} - \omega^2 \mathbf{M}) \mathbf{a} = \mathbf{0} \quad (4.5.17)$$

where \mathbf{K} represents the stiffness matrix of the beam, \mathbf{M} the mass matrix of the beam and \mathbf{a} the vector of the unknown scale factor.

This is a homogeneous system and has non-trivial solution only if the determinant of the coefficient matrix is equal to zero. It is an eigenvalue problem. We have to find the eigenvalues ω^2 of the problem. We observe that the rigorous implementation of Galerkin method leads us to a more detailed stiffness matrix \mathbf{K} which is composed of three sub-stiffness matrices \mathbf{K}_1 , \mathbf{K}_2 and \mathbf{K}_3 . We also observe that \mathbf{K}_1 is exactly \mathbf{K} for the naïve implementation, so \mathbf{K}_2 and \mathbf{K}_3 represent the additional terms which give more precision to the method.

4.6 Comparison functions for Galerkin method

A comparison function for Galerkin method, as already illustrated in Chapter 3, is a function which is supposed to well represent the solution of the differential equation. For the beam case, the boundary conditions that the function must satisfy are: geometrical condition, i.e. displacement and slope, and force condition, i.e. shear force and bending moment.

In our case, we are looking for the natural frequencies associated with the mode shape of the beam. Since we already know the deformed shape of the beam, we have to find out a way to create a function which can be a good candidate to properly represent the solution of the differential equation. We start from a static condition. We know the deformed shape associated with the n^{th} mode shape. We statically load the beam in order to generate a similar deformed shape. In Fig. 4.4, we show the first four mode shapes and the relative static load pattern for the simply supported at both ends case.

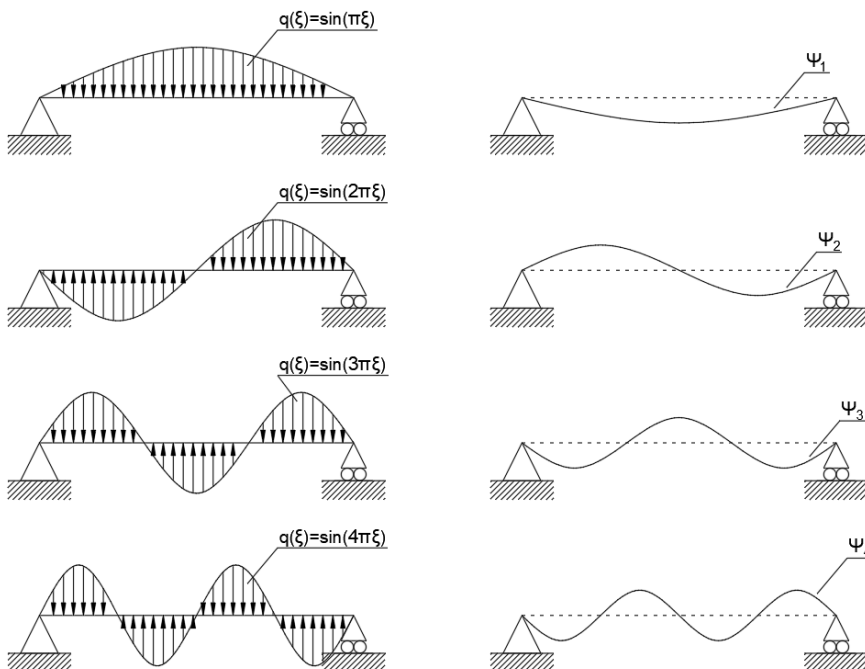


Figure 4.4: Trigonometrically distributed loads and respective deformed shapes

The latter satisfies all the boundary conditions, so it can serve as comparison function.

Mathematically, we can represent this load using the sinusoidal function:

$$q(\xi) = \sin(m\pi\xi) \quad (4.6.1)$$

In Eq. (4.6.1), m is a serial number $m = 1, 2, \dots, n$ which represents the sequential number of the mode shape.

Starting from the differential equation of the Bernoulli-Euler's homogeneous, uniform and elastic beam subject to a distributed load and represented with non-dimensional axial coordinate, we have:

$$\frac{EI}{L^4} \frac{d^4\psi(\xi)}{d\xi^4} = q(\xi) \quad (4.6.2)$$

We are looking for the function $\psi(\xi)$; the constant EI/L^4 acts as a scale factor; we can set it as unity obtaining:

$$\frac{d^4\psi(\xi)}{d\xi^4} = q(\xi) \quad (4.6.3)$$

Now we integrate four times with respect to the non-dimensional axial coordinate ξ to find out the expression of $\psi(\xi)$:

$$\frac{d^4\psi(\xi)}{d\xi^4} = \sin(m\pi\xi) \quad (4.6.4a)$$

$$\frac{d^3\psi(\xi)}{d\xi^3} = -\frac{\cos(m\pi\xi)}{m\pi} + A \quad (4.6.4b)$$

$$\frac{d^2\psi(\xi)}{d\xi^2} = -\frac{\sin(m\pi\xi)}{m^2\pi^2} + A\xi + B \quad (4.6.4c)$$

$$\frac{d\psi(\xi)}{d\xi} = \frac{\cos(m\pi\xi)}{m^3\pi^3} + \frac{A\xi^2}{2} + B\xi + C \quad (4.6.4d)$$

$$\psi(\xi) = \frac{\sin(m\pi\xi)}{m^4\pi^4} + \frac{A\xi^3}{6} + \frac{B\xi^2}{2} + C\xi + D \quad (4.6.4e)$$

The attribution of the boundary condition lets us find out the value of the four constants of integration A, B, C and D .

4.6.1 Beam simply supported at both ends

According to the boundary conditions, the system leads to:

$$\left\{ \begin{array}{l} D = 0 \\ B = 0 \\ \frac{A}{6} + \frac{B}{2} + C + D = 0 \\ A + B = 0 \end{array} \right. \quad (4.6.5)$$

or:

$$\left\{ \begin{array}{l} D = 0 \\ B = 0 \\ C = 0 \\ A = 0 \end{array} \right. \quad (4.6.6)$$

we obtain:

$$\psi(\xi) = \frac{\sin(m\pi\xi)}{m^4\pi^4} \quad (4.6.7)$$

We can simplify the expression multiplying by $m^4\pi^4$, obtaining:

$$\psi(\xi) = \sin(m\pi\xi) \quad (4.6.8)$$

4.6.2 Cantilever beam

According to the boundary conditions, the system leads to:

$$\begin{cases} D = 0 \\ \frac{1}{m^3\pi^3} + C = 0 \\ A + B = 0 \\ \frac{(-1)^3}{m\pi} + A = 0 \end{cases} \quad (4.6.9)$$

or:

$$\begin{cases} D = 0 \\ B = -\frac{(-1)^m}{m\pi} \\ C = -\frac{1}{m^3\pi^3} \\ A = \frac{(-1)^m}{m\pi} \end{cases} \quad (4.6.10)$$

we obtain:

$$\psi(\xi) = \frac{(-1)^m}{6m\pi}\xi^3 - \frac{(-1)^m}{2m\pi}\xi^2 - \frac{1}{m^3\pi^3}\xi + \frac{\sin(m\pi\xi)}{m^4\xi^4} \quad (4.6.11)$$

We can simplify the expression multiplying by $m^4\pi^4$, obtaining:

$$\psi(\xi) = \frac{(-1)^m m^3 \pi^3}{6} \xi^3 - \frac{(-1)^m m^3 \pi^3}{2} \xi^2 - m\pi\xi + \sin(m\pi\xi) \quad (4.6.12)$$

4.6.3 Beam clamped at one end and simply supported at the other

According to the boundary conditions, the system leads to:

$$\begin{cases} D = 0 \\ \frac{1}{m^3\pi^3} + C = 0 \\ C + \frac{B}{2} + \frac{A}{6} + D = 0 \\ A + B = 0 \end{cases} \quad (4.6.13)$$

or:

$$\begin{cases} D = 0 \\ C = -\frac{1}{m^3\pi^3} \\ B = \frac{3}{m^3\pi^3} \\ A = -\frac{3}{m^3\pi^3} \end{cases} \quad (4.6.14)$$

we obtain:

$$\psi(\xi) = -\frac{1}{2m^3\pi^3}\xi^3 + \frac{3}{2m^3\pi^3}\xi^2 - \frac{1}{m^3\pi^3}\xi + \frac{\sin(m\pi\xi)}{m^4\pi^4} \quad (4.6.15)$$

We can simplify the expression multiplying by $m^4\pi^4$, obtaining:

$$\psi(\xi) = -\frac{m\pi}{2}\xi^3 + \frac{3m\pi}{2}\xi^2 - m\pi\xi + \sin(m\pi\xi) \quad (4.6.16)$$

4.6.4 Beam clamped at both ends

According to the boundary conditions, the system leads to:

$$\left\{ \begin{array}{l} D = 0 \\ \frac{1}{m^3\pi^3} + C = 0 \\ C + \frac{B}{2} + \frac{A}{6} + D = 0 \\ B + \frac{A}{2} + \frac{(-1)^m}{m^3\pi^3} + C = 0 \end{array} \right. \quad (4.6.17)$$

or:

$$\left\{ \begin{array}{l} D = 0 \\ C = -\frac{1}{m^3\pi^3} \\ B = \frac{4}{m^3\pi^3} + \frac{2(-1)^m}{m^3\pi^3} \\ A = -\frac{6}{m^3\pi^3} - \frac{6(-1)^m}{m^3\pi^3} \end{array} \right. \quad (4.6.18)$$

we obtain:

$$\psi(\xi) = -\frac{(1 + (-1)^m)}{m^3\pi^3}\xi^3 + \frac{(2 + (-1)^m)}{m^3\pi^3}\xi^2 - \frac{1}{m^3\pi^3}\xi + \frac{\sin(m\pi\xi)}{m^4\pi^4} \quad (4.6.19)$$

We can simplify the expression multiplying by $m^4\pi^4$, obtaining:

$$\psi(\xi) = -m\pi(1 + (-1)^m)\xi^3 + m\pi(2 + (-1)^m)\xi^2 - m\pi\xi + \sin(m\pi\xi) \quad (4.6.20)$$

4.7 Numerical example

We consider the beam in Fig. 4.5:

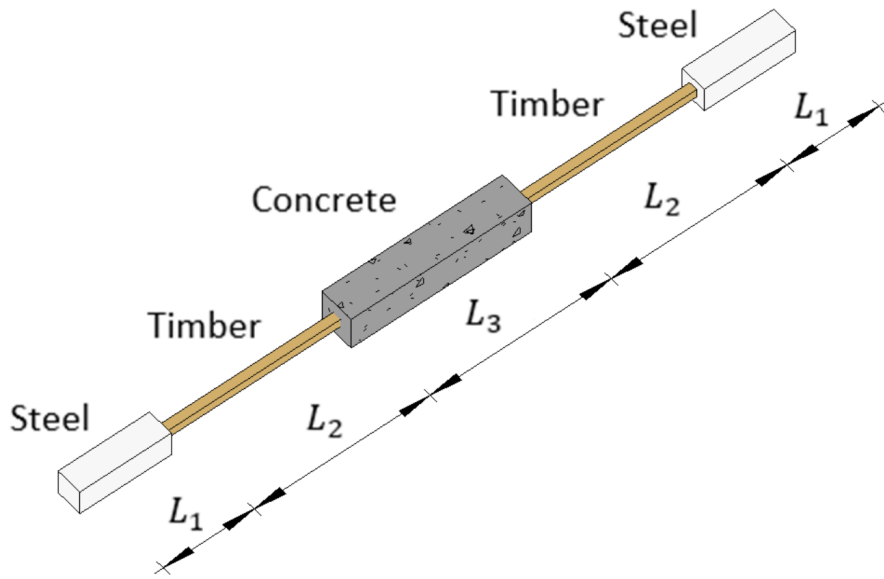


Figure 4.5: The multi-step beam under consideration

We fix parameters at the following values:

Steel		Timber Mahogany		Concrete	
E	$2.0 \cdot 10^{11} \text{ Pa}$	E	$1.6 \cdot 10^{10} \text{ Pa}$	E	$3.8 \cdot 10^{10} \text{ Pa}$
ρ	$7.87 \cdot 10^3 \text{ kg/m}^3$	ρ	$9.5 \cdot 10^2 \text{ kg/m}^3$	ρ	$2.4 \cdot 10^3 \text{ kg/m}^3$
b	0.3 m	b	0.1 m	b	0.4 m
h	0.3 m	h	0.1 m	h	0.4 m
A	$9 \cdot 10^{-2} \text{ m}^2$	A	$1 \cdot 10^{-2} \text{ m}^2$	A	$1.6 \cdot 10^{-1} \text{ m}^2$
I	$6.75 \cdot 10^{-4} \text{ m}^4$	I	$8.33 \cdot 10^{-6} \text{ m}^4$	I	$2.13 \cdot 10^{-3} \text{ m}^4$

Table 4.3: Parameters of each segment

We also set $L_1 = 1\text{m}$, $L_2 = 2\text{m}$, $L_3 = 2\text{m}$, $L_4 = 2\text{m}$ and $L_5 = 1\text{m}$.

4.7.1 Exact solution

Simply supported at both ends beam

Considering a simply supported at both ends beam, the plot of the characteristic equation is:

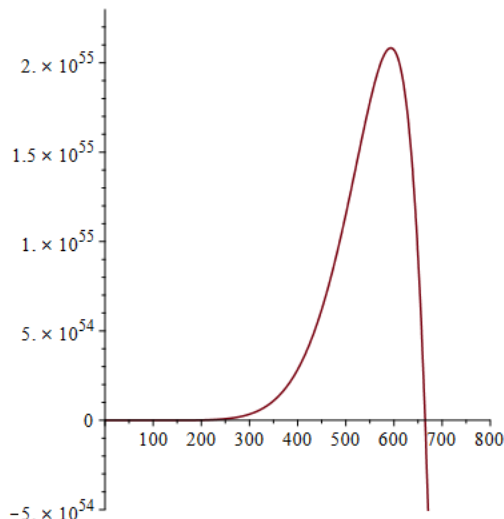


Figure 4.6: Characteristic equation for simply supported at both ends beam

The first two roots are:

$$\begin{aligned}\omega_1 &= 5.8599 \text{ rad/s} \\ \omega_2 &= 25.7812 \text{ rad/s}\end{aligned}\tag{4.7.1}$$

Cantilever beam

Considering a cantilever beam, the plot of the characteristic equation is:

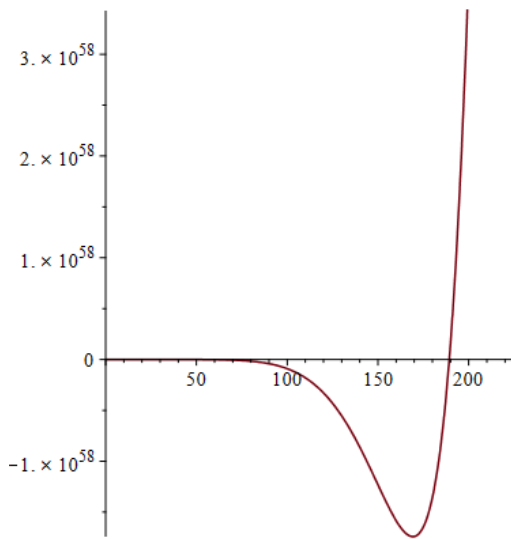


Figure 4.7: Characteristic equation for cantilever beam

The first two roots are:

$$\begin{aligned}\omega_1 &= 1.5661 \text{ rad/s} \\ \omega_2 &= 13.7573 \text{ rad/s}\end{aligned}\tag{4.7.2}$$

Clamped - Simply supported beam

Considering a beam with a clamped end and the other simply supported, the plot of the characteristic equation is:

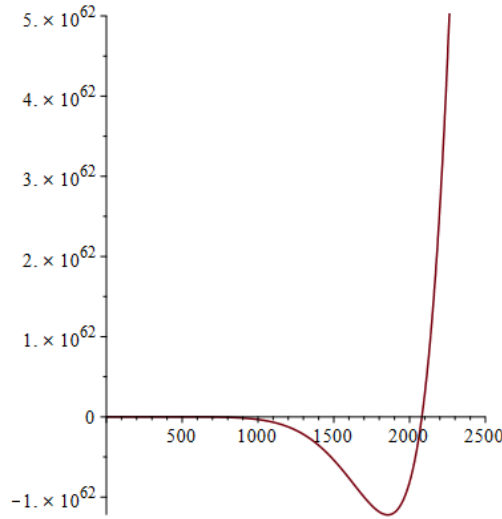


Figure 4.8: Characteristic equation for clamped-simply supported beam

The first two roots are:

$$\begin{aligned}\omega_1 &= 10.8343 \text{ rad/s} \\ \omega_2 &= 45.6172 \text{ rad/s}\end{aligned}\tag{4.7.3}$$

Clamped at both ends

Considering a beam clamped at both ends, the plot of the characteristic equation is:

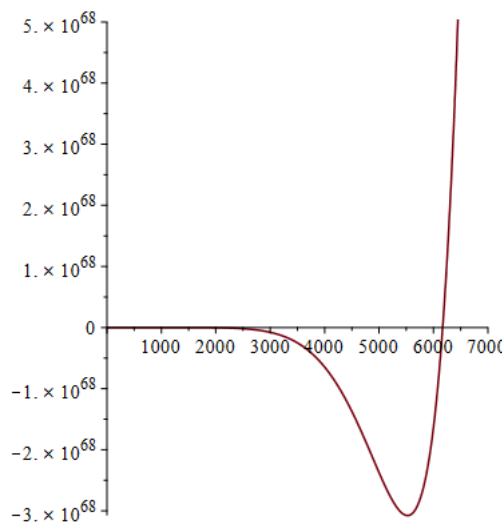


Figure 4.9: Characteristic equation for clamped at both ends beam

The first two roots are:

$$\begin{aligned}\omega_1 &= 22.5265 \text{ rad/s} \\ \omega_2 &= 78.5389 \text{ rad/s}\end{aligned}\quad (4.7.4)$$

Collecting these results into a table, we get:

Mode	Exact solution [rad/s]			
	Simply supported	Cantilever	Clamped - Simply supported	Clamped - Clamped
1	5.8559	1.5661	10.8343	22.5265
2	25.7812	13.7573	45.6172	78.5389

Table 4.4: Exact solution for the stepped beam under consideration in four different constrain conditions

4.7.2 Naïve Galerkin method

Naïve Galerkin method with 250 terms leads us to the following results:

Simply supported at both ends beam

Mode	Naïve Galerkin method						
	Simply supported at both ends						
	Frequencies [rad/s]						
Mode	1 Term	2 Terms	50 Terms	100 Terms	150 Terms	200 Terms	250 Terms
1	69.7841	69.7841	26.1460	25.5488	25.3482	25.2497	25.1921
2		264.9281	82.7603	81.3558	80.9320	80.7212	80.5863

Table 4.5: Frequencies obtained with naïve Galerkin method for simply supported at both ends beam

We evaluate the relative error between the obtained natural frequencies and the exact solution with the following formula:

$$\varepsilon = \frac{\omega_{\text{Galerkin}} - \omega_{\text{exact}}}{\omega_{\text{exact}}} \times 100 \quad (4.7.5)$$

Naïve Galerkin method							
Simply supported at both ends							
Mode	Relative error [%]						
	1 Term	2 Terms	50 Terms	100 Terms	150 Terms	200 Terms	250 Terms
1	1091.69%	1091.69%	346.49%	336.29%	332.87%	331.18%	330.20%
2		927.60%	221.60%	215.56%	213.92%	213.10%	212.58%

Table 4.6: Relative error between naïve Galerkin method and theoretical results for simply supported at both ends beam

Cantilever beam

Naïve Galerkin method							
Cantilever							
Mode	Frequencies [rad/s]						
	1 Term	2 Terms	50 Terms	100 Terms	150 Terms	200 Terms	250 Terms
1	19.4550	17.8500	9.7640	11.9201	<i>inf</i>	10.4199	67.7784
2		139.6066	76.0174	138.0787	<i>inf</i>	126.5773	<i>inf</i>

Table 4.7: Frequencies obtained with naïve Galerkin method for cantilever beam

Naïve Galerkin method							
Cantilever							
Mode	Relative error [%]						
	1 Term	2 Terms	50 Terms	100 Terms	150 Terms	200 Terms	250 Terms
1	1142.26%	1039.78%	523.46%	661.13%	<i>inf</i>	565.34%	4227.84%
2		914.78%	452.56%	903.68%	<i>inf</i>	820.07%	<i>inf</i>

Table 4.8: Relative error between naïve Galerkin method and theoretical results for cantilever beam

Clamped - Simply supported beam

Naïve Galerkin method							
Clamped - Simply supported							
Mode	Frequencies [rad/s]						
	1 Term	2 Terms	50 Terms	100 Terms	150 Terms	200 Terms	250 Terms
1	109.1045	107.8100	41.1672	40.2221	39.9049	39.7488	39.6578
2		334.5226	109.1193	107.1716	106.5734	106.2759	106.0905

Table 4.9: Frequencies obtained with naïve Galerkin method for clamped-simply supported beam

Naïve Galerkin method							
Clamped - Simply supported							
Mode	Relative error [%]						
	1 Term	2 Terms	50 Terms	100 Terms	150 Terms	200 Terms	250 Terms
1	906.20%	895.08%	279.97%	271.25%	268.32%	266.88%	266.04%
2		633.33%	139.21%	134.94%	133.63%	132.97%	132.57%

Table 4.10: Relative error between naïve Galerkin method and theoretical results for clamped-simply supported beam

Clamped at both ends beam

Naïve Galerkin method							
Clamped at both ends							
Mode	Frequencies [rad/s]						
	1 Term	2 Terms	50 Terms	100 Terms	150 Terms	200 Terms	250 Terms
1	154.3909	154.3909	63.8401	62.2381	61.6905	61.4234	61.2706
2		433.5928	127.6828	125.6799	125.0855	124.7908	124.6009

Table 4.11: Frequencies obtained with naïve Galerkin method for clamped at both ends beam

Mode	Naïve Galerkin method							
	Clamped at both ends							
	Relative error [%]							
Mode	1 Term	2 Terms	50 Terms	100 Terms	150 Terms	200 Terms	250 Terms	
1	585.37%	585.37%	183.40%	176.29%	173.87%	172.67%	171.99%	
2		425.07%	62.57%	60.02%	59.27%	58.89%	58.65%	

Table 4.12: Relative error between naïve Galerkin method and theoretical results for clamped at both ends beam

4.7.3 Rigorous Galerkin method

Rigorous Galerkin method with 250 terms leads us to the following results:

Simply supported at both ends beam

Mode	Rigorous Galerkin method							
	Simply supported at both ends							
	Frequencies [rad/s]							
Mode	1 Term	2 Terms	50 Terms	100 Terms	150 Terms	200 Terms	250 Terms	
1	69.7841	69.7841	6.2127	6.0328	5.9724	5.9429	5.9269	
2		264.9281	27.2340	26.4813	26.2488	26.1311	26.0562	

Table 4.13: Frequencies obtained with rigorous Galerkin method for simply supported at both ends beam

Rigorous Galerkin method

Simply supported at both ends

Relative error [%]

Mode	1 Term	2 Terms	50 Terms	100 Terms	150 Terms	200 Terms	250 Terms
1	1091.69%	1091.69%	6.09%	3.02%	1.99%	1.49%	1.21%
2		927.60%	5.64%	2.72%	1.81%	1.36%	1.07%

Table 4.14: Relative error between rigorous Galerkin method and theoretical results for simply supported at both ends beam

Cantilever beam

Rigorous Galerkin method

Cantilever

Frequencies [rad/s]

Mode	1 Term	2 Terms	50 Terms	100 Terms	150 Terms	200 Terms	250 Terms
1	26.4086	20.2374	1.6608	1.6119	1.4904	2.2984	1.9146
2		204.3019	15.0447	14.3781	10.5561	27.0037	8.4139

Table 4.15: Frequencies obtained with rigorous Galerkin method for cantilever beam

Rigorous Galerkin method

Cantilever

Relative error [%]

Mode	1 Term	2 Terms	50 Terms	100 Terms	150 Terms	200 Terms	250 Terms
1	1586.26%	1192.21%	6.04%	2.92%	-4.83%	46.76%	22.25%
2		1385.04%	9.36%	4.51%	-23.27%	96.29%	-38.84%

Table 4.16: Relative error between rigorous Galerkin method and theoretical results for cantilever beam

Clamped - Simply supported beam

Rigorous Galerkin method							
Clamped - Simply supported							
Mode	Frequencies [rad/s]						
	1 Term	2 Terms	50 Terms	100 Terms	150 Terms	200 Terms	250 Terms
1	141.7013	110.4095	11.7264	11.2661	11.1212	11.0467	11.0038
2		514.2851	53.1112	48.9311	47.7939	47.2050	46.8803

Table 4.17: Frequencies obtained with rigorous Galerkin method for clamped-simply supported beam

Rigorous Galerkin method							
Clamped - Simply supported							
Mode	Relative error [%]						
	1 Term	2 Terms	50 Terms	100 Terms	150 Terms	200 Terms	250 Terms
1	1207.90%	919.07%	8.23%	3.99%	2.65%	1.96%	1.56%
2		1027.39%	16.43%	7.26%	4.77%	3.48%	2.77%

Table 4.18: Relative error between rigorous Galerkin method and theoretical results for clamped-simply supported beam

Clamped at both ends beam

Rigorous Galerkin method							
Clamped at both ends							
Mode	Frequencies [rad/s]						
	1 Term	2 Terms	50 Terms	100 Terms	150 Terms	200 Terms	250 Terms
1	230.4128	230.4128	26.8820	24.4690	23.7977	23.4515	23.2651
2		830.4342	92.3904	84.5443	82.5794	81.4841	80.8980

Table 4.19: Frequencies obtained with rigorous Galerkin method for clamped at both ends beam

Rigorous Galerkin method							
Clamped at both ends							
Mode	Relative error [%]						
	1 Term	2 Terms	50 Terms	100 Terms	150 Terms	200 Terms	250 Terms
1	922.85%	922.85%	19.34%	8.62%	5.64%	4.11%	3.28%
2		957.35%	17.64%	7.65%	5.14%	3.75%	3.00%

Table 4.20: Relative error between rigorous Galerkin method and theoretical results for clamped at both ends beam

The previous tables show that the rigorous Galerkin method, in general, starts with a greatest error in comparison with the naïve version (e.g. for 1 term of approximation for the first natural frequencies in clamped-clamped boundary condition, we have 922.85% of error for the rigorous version and 585.37% for the naïve one). However, with the increase in the terms, the rigorous implementation is able to reduce the error reaching the convergence despite the naïve implementation, which still has a considerable error (considering the example of the second natural frequencies in simply supported case, we obtain 212.58% for the naïve version and 1.07% for the rigorous one).

For the mentioned examples, we also provide the charts reporting the trend of the relative error in function of the number of approximation terms (Fig. 4.10, 4.11, 4.12, 4.13 and 4.14).

In addition, it is interesting to observe the clamped-free case. In this case, it seems that the method does not converge. If we depict the trend of the relative error in function of Galerkin number of terms, we see that from the first to one hundredth the trend is exactly what we

expected: it tends to zero; but starting from one hundred we have some noise. This may be due to the comparison function: only in the clamped-free case, we obtain a power of the number of Galerkin terms in the function, in this case the cube, so it becomes a high value and it could create numerical instability.

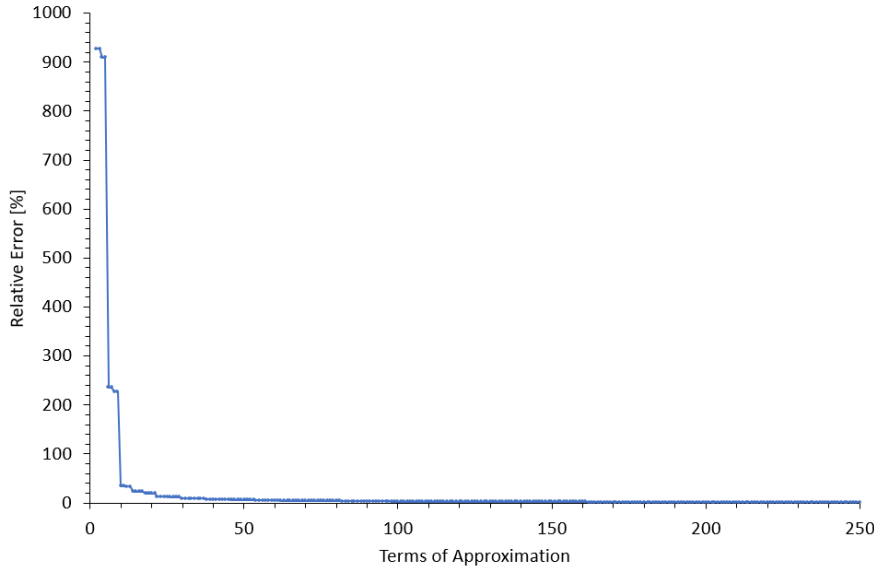


Figure 4.10: Trend of relative error of second natural frequencies obtained with rigorous Galerkin method in simply supported at both ends boundary condition

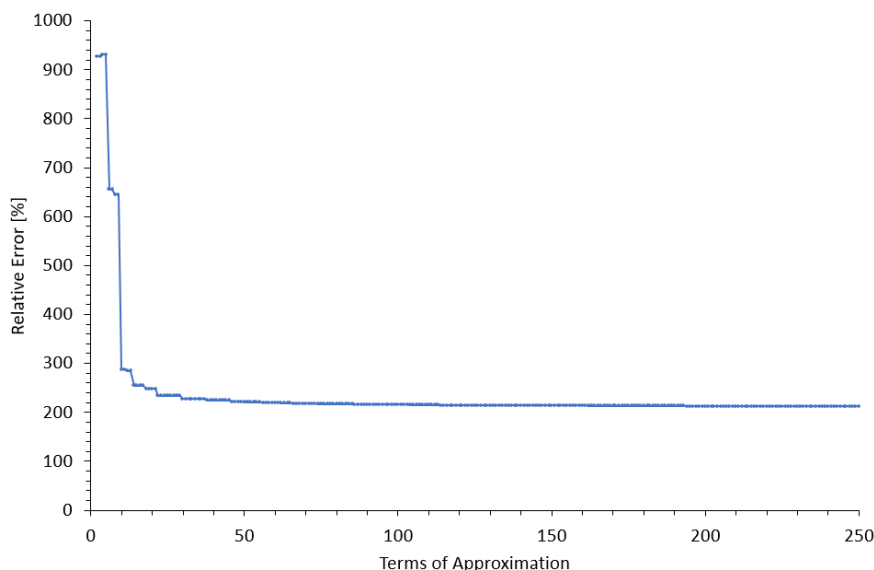


Figure 4.11: Trend of relative error of second natural frequencies obtained with naïve Galerkin method in simply supported at both ends boundary condition

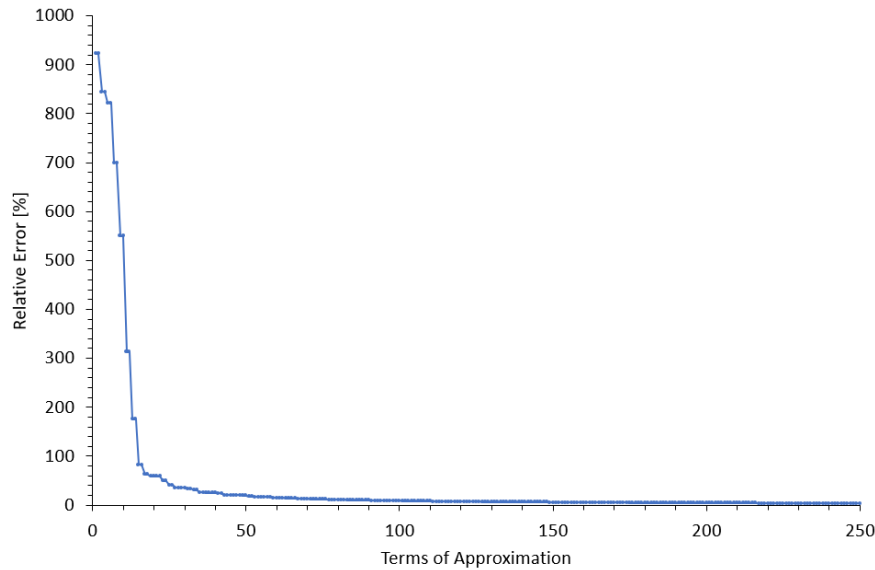


Figure 4.12: Trend of relative error of first natural frequencies obtained with rigorous Galerkin method in clamped-clamped boundary condition

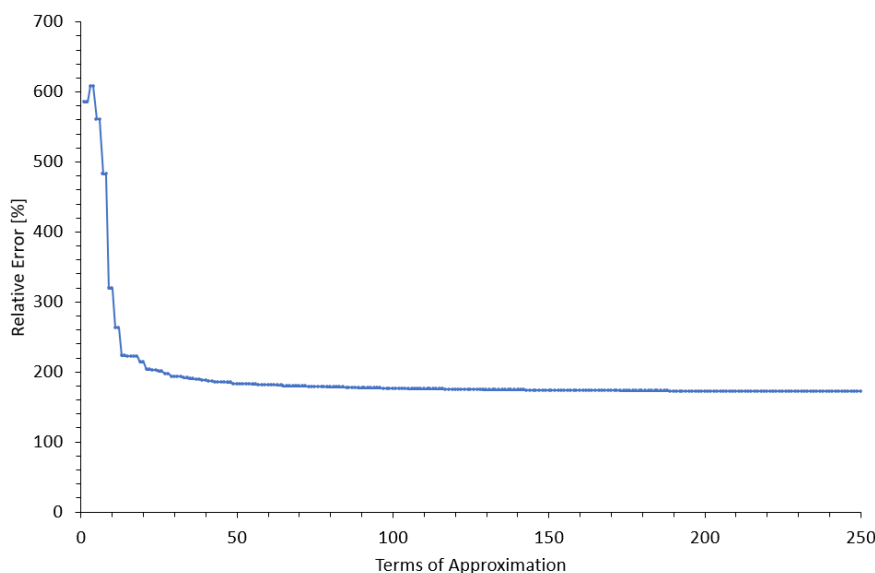


Figure 4.13: Trend of relative error of first natural frequencies obtained with naïve Galerkin method in clamped-clamped boundary condition

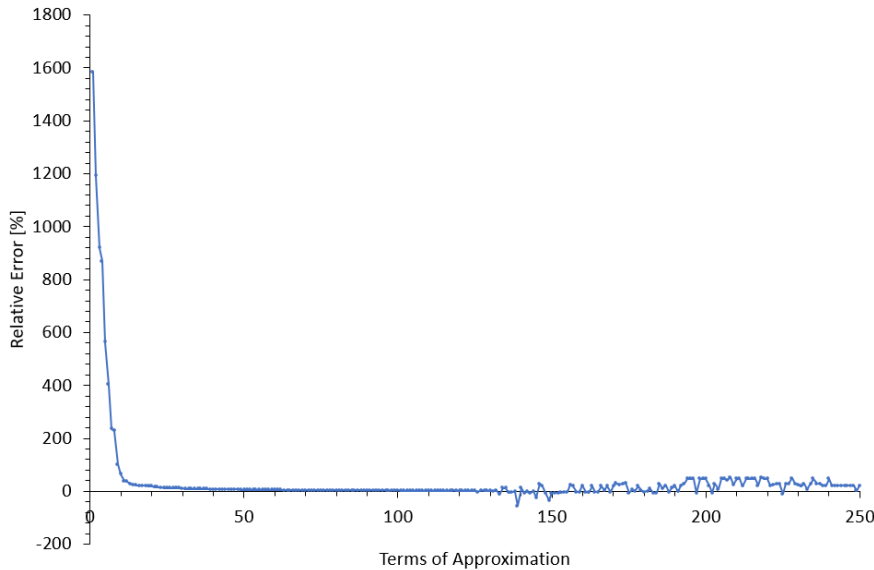


Figure 4.14: Trend of relative error of first natural frequencies obtained with rigorous Galerkin method in clamped-free boundary condition

4.8 Conclusion

In this study, we analyze the free vibration of an in-homogeneous and non-uniform beam. We compare two different implementations of Galerkin method: the rigorous version and the straightforward one. The study shows that the rigorous implementation reaches the convergence, on the other hand the naïve version does not. We also have to pay attention to the choice of the comparison function: it is not enough to prove that it respects the boundary conditions. Indeed, we demonstrate that building the comparison function starting from static load condition and imposing the respect of the boundary conditions is not a general method since it works with simply supported, clamped-clamped and clamped-simply supported beams, but not for clamped-free beam in which case we face some noise probably due to numerical instability.

5. Beam: Jaworsky and Dowell case

In Chapter 4, we show that the cantilever case does not reach the convergence. Analyzing the plot of the relative error in function of the Galerkin terms, we obtain an expected trend from zero to almost one hundred but for the second half of the plot we face some noise. Probably, this behavior is due to the comparison function where it contains the third power of the number of Galerkin terms, which at high levels becomes huge causing numerical instability. For this reason, in this chapter, we investigate the cantilever case. We choose in particular to study the Jaworsky and Dowell paper in Ref. [29], proposing a different comparison function, already applied by them in an another approximate method, i.e. Rayleigh–Ritz method.

Jaworsky and Dowell took a multi-stepped beam made of aluminum and analyzed the natural frequency in the vertical and horizontal plane through multiple methods: experimental, Rayleigh-Ritz method, component modal analysis and the FEM package ANSYS with different elements: BEAM4, BEAM188, SHELL93 and SOLID45.

In this analysis, we evaluate natural frequencies applying the same procedure, i.e. exact solution, naïve Galerkin method and rigorous Galerkin method, and we compare them with the results obtained by Jaworsky and Dowell through Rayleigh–Ritz method.

5.1 Jaworsky and Dowell study

The beam object of study is an aluminum multi-stepped cantilever beam as reported in Fig. 5.1. We are interested in evaluating the natural frequencies in both directions, namely planes $x - y$ and $x - z$. We report the scheme of the system in Fig. 5.2.

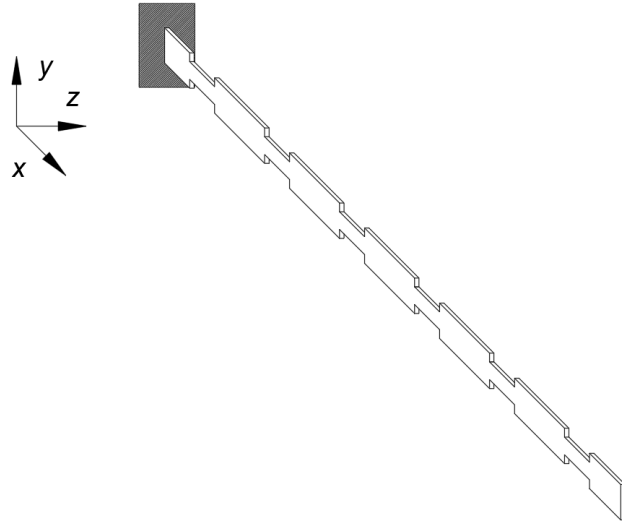


Figure 5.1: Jaworsky and Dowell cantilever beam

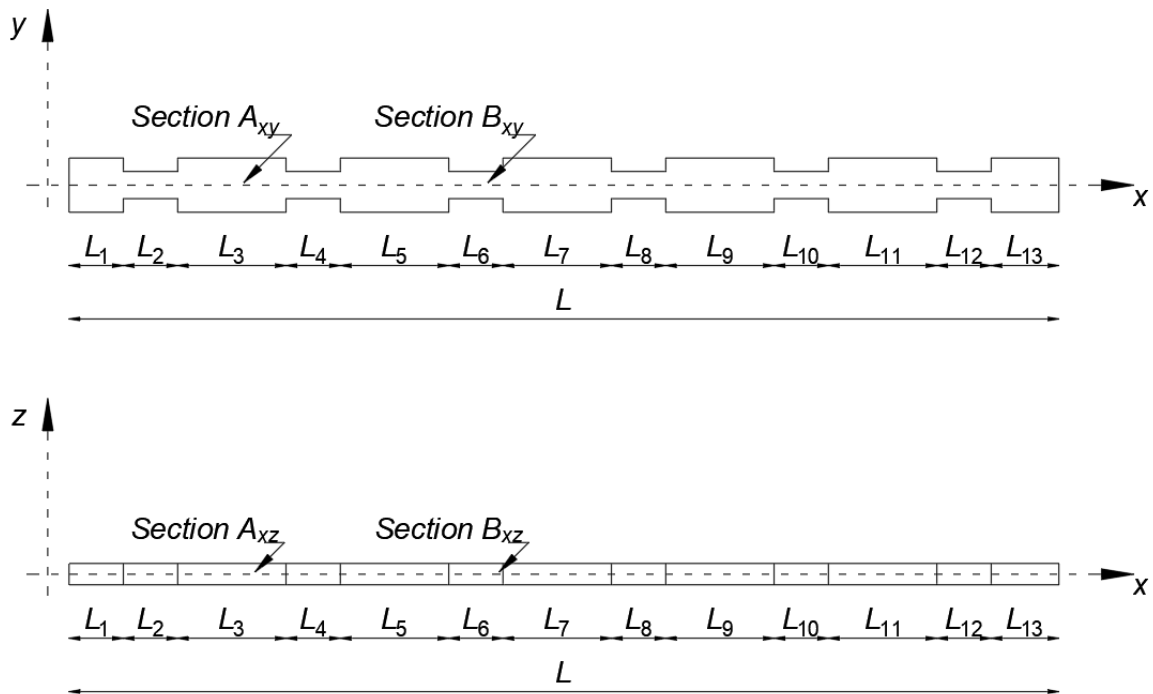


Figure 5.2: Scheme of the system

The data of the beam are reported in the following table:

Aluminum				
Section	A_{xy}	B_{xy}	A_{xz}	B_{xz}
E	$6.06 \cdot 10^{10}$ Pa	$6.06 \cdot 10^{10}$ Pa	$6.06 \cdot 10^{10}$ Pa	$6.06 \cdot 10^{10}$ Pa
ρ	2664 kg/m^3	2664 kg/m^3	2664 kg/m^3	2664 kg/m^3
b	3.175 mm	3.175 mm	25.4 mm	12.7 mm
h	25.4 mm	12.7 mm	3.175 mm	3.175 mm
A	$8.06 \cdot 10^{-5} \text{ mm}^2$	$4.03 \cdot 10^{-5} \text{ mm}^2$	$8.06 \cdot 10^{-5} \text{ mm}^2$	$4.03 \cdot 10^{-5} \text{ mm}^2$
I	$4.34 \cdot 10^{-9} \text{ mm}^4$	$5.42 \cdot 10^{-11} \text{ mm}^4$	$6.77 \cdot 10^{-11} \text{ mm}^4$	$3.39 \cdot 10^{-11} \text{ mm}^4$

Table 5.1: Parameters of each segment

They obtained the following results:

Jaworsky and Dowell results [Hz]								
Plane	Mode	Rayleigh–Ritz	Component		ANSYS		Experiment	
			Modal Analysis		Euler	Euler	Timoshenko	2D Shell
$x - y$	ω_1	54.795	54.985	54.469	54.429	49.62	49.83	49.38
$x - z$	ω_1	10.752	10.816	10.745	10.745	10.44	10.46	10.63
	ω_2	67.429	67.463	67.469	67.456	65.54	65.70	66.75

Table 5.2: Jaworsky and Dowell results with different approaches expressed in Hertz

5.2 Comparison function

As explicated in Chapter 4, a comparison function is a function which is supposed to well represent the solution of the differential equation and for the Galerkin method, the demand is that a function must satisfy all the boundary conditions, in order to be considered a comparison function.

According to Jaworsky and Dowell [29], among the various comparison functions, the mode shape equation for homogeneous cantilever beam resulted effective in the Rayleigh–Ritz method. Thus, to conduct our study we select the same comparison function.

The said equation reads as follows:

$$W_m(\xi) = \left(\frac{\sin(\alpha_m) - \sinh(\alpha_m)}{\cos(\alpha_m) + \cosh(\alpha_m)} \right) (\sinh(\alpha_m \xi) - \sin(\alpha_m \xi)) + (\cosh(\alpha_m \xi) - \cos(\alpha_m \xi)) \quad (5.2.1)$$

In this form, the function for large value of m leads to numerical instability because of the difference between large values of the hyperbolic functions. As a consequence, the following

asymptotic approximation proposed by Dowell [30] will be used for higher modes in order to avoid numerical error:

$$W_m(\xi) = \sin(\alpha_m \xi) - \cos(\alpha_m \xi) + e^{-\alpha_m} + (-1)^{m+1} e^{-\alpha_m(1-\xi)} + O[\varepsilon] \quad (5.2.2)$$

The order of error with this formulation can be expressed as $\varepsilon = e^{-\alpha_m}$, and it can be neglected for $m \geq 5$.

This approach is also proved by Yamada et al. [31].

5.3 Numerical results

5.3.1 Exact solution

Plane $x - y$

Considering a cantilever beam in $x - y$ plane, the plot of the characteristic equation is:

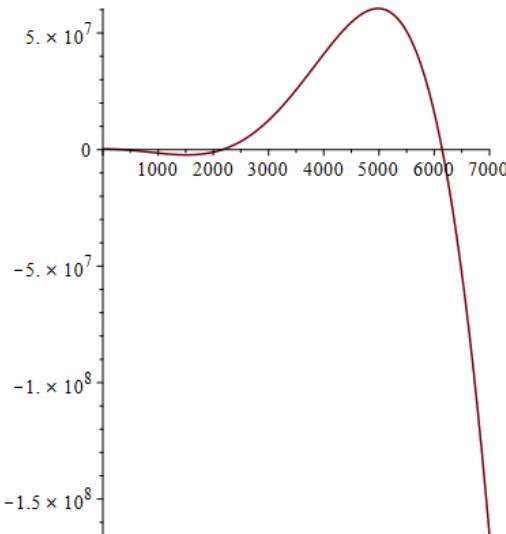


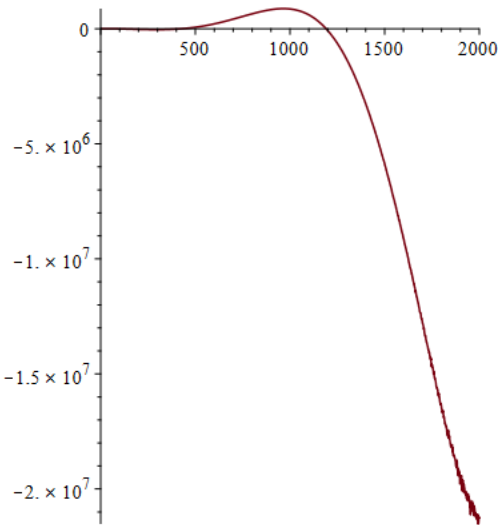
Figure 5.3: Characteristic equation for cantilever beam in $x - y$ plane

The first three roots are:

$$\begin{aligned} \omega_1 &= 342.4121 \text{ rad/s} \\ \omega_2 &= 2166.4943 \text{ rad/s} \\ \omega_3 &= 6143.9243 \text{ rad/s} \end{aligned} \quad (5.3.1)$$

Plane $x - z$

Considering a cantilever beam in $x - z$ plane, the plot of the characteristic equation is:

Figure 5.4: Characteristic equation for cantilever beam in $x - z$ plane

The first three roots are:

$$\begin{aligned}\omega_1 &= 67.5133 \text{ rad/s} \\ \omega_2 &= 423.9471 \text{ rad/s} \\ \omega_3 &= 1191.0450 \text{ rad/s}\end{aligned}\tag{5.3.2}$$

Exact solution [rad/s]		
Mode	$x - y$ Plane	$x - z$ Plane
1	342.4121	67.5133
2	2166.4943	423.9471
3	6143.9243	1191.0450

Table 5.3: Exact solution for the cantilever beam object of study

5.3.2 Naïve Galerkin method

Naïve Galerkin method with 100 terms leads us to the following results:

Plane $x - y$

Mode	Naïve Galerkin method							
	$x - y$ Plane							
	Frequencies [rad/s]							
Mode	1 Term	2 Terms	3 Terms	25 Terms	50 Terms	75 Terms	100 Terms	
1	531.0601	530.9327	530.7799	462.7421	427.8476	420.8202	419.3807	
2		3 335.5952	3 334.2992	2 884.2579	2 697.5635	2 652.9731	2 645.0811	
3			9 357.7550	8 163.1046	7 594.1873	7 490.8281	7 450.9256	

Table 5.4: Frequencies obtained with naïve Galerkin method in $x - y$ plane

We evaluate the relative error between the obtained natural frequencies and the exact solution with the following formula:

$$\varepsilon = \frac{\omega_{Galerkin} - \omega_{exact}}{\omega_{exact}} \times 100 \quad (5.3.3)$$

Mode	Naïve Galerkin method							
	$x - y$ Plane							
	Relative error [%]							
Mode	1 Term	2 Terms	3 Terms	25 Terms	50 Terms	75 Terms	100 Terms	
1	55.09%	55.06%	55.01%	35.14%	24.95%	22.90%	22.48%	
2		53.96%	53.90%	33.13%	24.51%	22.45%	22.09%	
3			52.31%	32.86%	23.60%	21.92%	21.27%	

Table 5.5: Relative error between naïve Galerkin method and theoretical results in $x - y$ plane

Plane $x - z$

Mode	Naïve Galerkin method							
	$x - z$ Plane							
	Frequencies [rad/s]							
Mode	1 Term	2 Terms	3 Terms	25 Terms	50 Terms	75 Terms	100 Terms	
1	71.5207	71.5207	71.5207	71.5207	71.5207	71.5207	71.5207	
2		448.2448	448.2448	448.2448	448.2448	448.2448	448.2448	
3			1 255.2248	1 255.2248	1 255.2248	1 255.2248	1 255.2248	

Table 5.6: Frequencies obtained with naïve Galerkin method in $x - z$ plane

Mode	Naïve Galerkin method							
	$x - z$ Plane							
	Relative error [%]							
Mode	1 Term	2 Terms	3 Terms	25 Terms	50 Terms	75 Terms	100 Terms	
1	5.94%	5.94%	5.94%	5.94%	5.94%	5.94%	5.94%	
2		5.73%	5.73%	5.73%	5.73%	5.73%	5.73%	
3			5.39%	5.39%	5.39%	5.39%	5.39%	

Table 5.7: Relative error between naïve Galerkin method and theoretical results in $x - z$ plane

5.3.3 Rigorous Galerkin method

Rigorous Galerkin method with 100 terms leads us to the following results:

Plane $x - y$

Rigorous Galerkin method

$x - y$ Plane

Frequencies [rad/s]

Mode	1 Term	2 Term	3 Term	25 Terms	50 Terms	75 Terms	100 Terms
1	532.3005	525.2584	525.2059	385.5929	362.8573	353.8210	352.2366
2		3 303.9364	3 302.5800	2 590.9190	2 296.1458	2 238.5734	2 229.1627
3			9 288.0450	7 360.6548	6 511.9947	6 377.2805	6 322.6071

Table 5.8: Frequencies obtained with rigorous Galerkin method in $x - y$ plane

Rigorous Galerkin method

$x - y$ Plane

Relative error [%]

Mode	1 Term	2 Term	3 Term	25 Terms	50 Terms	75 Terms	100 Terms
1	53.41%	53.40%	53.38%	12.61%	5.97%	3.33%	2.87%
2		52.50%	52.44%	19.59%	5.98%	3.33%	2.89%
3			51.17%	19.80%	5.99%	3.80%	2.91%

Table 5.9: Relative error between rigorous Galerkin method and theoretical results in $x - y$ plane

Plane $x - z$

Mode	Rigorous Galerkin method						
	$x - z$ Plane						
	Frequencies [rad/s]						
Mode	1 Term	2 Terms	3 Term	25 Terms	50 Terms	75 Terms	100 Terms
1	71.1399	71.1379	71.1364	68.1456	67.9620	67.7800	67.7035
2		446.1477	446.0782	427.7656	426.7094	425.6417	425.1656
3			1 250.6176	1 208.3126	1 199.1534	1 195.9843	1 194.5526

Table 5.10: Frequencies obtained with rigorous Galerkin method in $x - z$ plane

Mode	Rigorous Galerkin method						
	$x - z$ Plane						
	Relative error [%]						
Mode	1 Term	2 Terms	3 Terms	25 Terms	50 Terms	75 Terms	100 Terms
1	5.37%	5.37%	5.37%	0.94%	0.66%	0.39%	0.28%
2		5.24%	5.22%	0.90%	0.65%	0.40%	0.29%
3			5.00%	1.45%	0.68%	0.41%	0.29%

Table 5.11: Relative error between rigorous Galerkin method and theoretical results in $x - z$ plane

5.3.4 Comparison of results

In their paper, Jaworsky and Dowell studied many different approaches. However, to compare our results, we choose the Rayleigh-Ritz method which is an approximate method for solving differential equations starting from energetic considerations. We select this method because there are many similarities between the Galerkin method and the Rayleigh-Ritz method, as demonstrated by several studies in literature (for example Ref. [32]).

Resuming in a table our obtained frequencies converted in Hertz and the results obtained by Jaworsky and Dowell through the Rayleigh-Ritz method, we have:

Plane	Mode	Frequencies [Hz]				Reference
		Exact solution	Naïve Galerkin method	Rigorous Galerkin method		
$x - y$	ω_1	54.4964	56.0601	66.7434	54.795	
$x - z$	ω_1	10.7451	10.7753	11.3828	10.752	
	ω_2	67.4731	67.6670	71.3402	67.429	

Table 5.12: Comparison of results in Hertz

The relative error between these approaches, evaluated with the following formula, is:

$$\varepsilon = \frac{\omega - \omega_{reference}}{\omega_{reference}} \times 100 \quad (5.3.4)$$

Plane	Mode	Relative error [%]		
		Exact solution	Naïve Galerkin method	Rigorous Galerkin method
$x - y$	ω_1	-0.54%	21.81%	2.31%
$x - z$	ω_1	-0.06%	5.87%	0.22%
	ω_2	0.07%	5.80%	0.35%

Table 5.13: Relative error between our approaches and the reference solution

The above tables show that the rigorous Galerkin method can reach the exact analytical solution. This aspect is also sustained by Fig. 5.5 which illustrates that the error decreases when increasing the number of terms. On the other hand, the naïve Galerkin method does not converge (Fig. 5.6). We compare our results with those provided in Ref. [29]. The Rayleigh-Ritz frequencies are close to what we obtain through the analytical approach and rigorous Galerkin method but not through the naïve implementation.

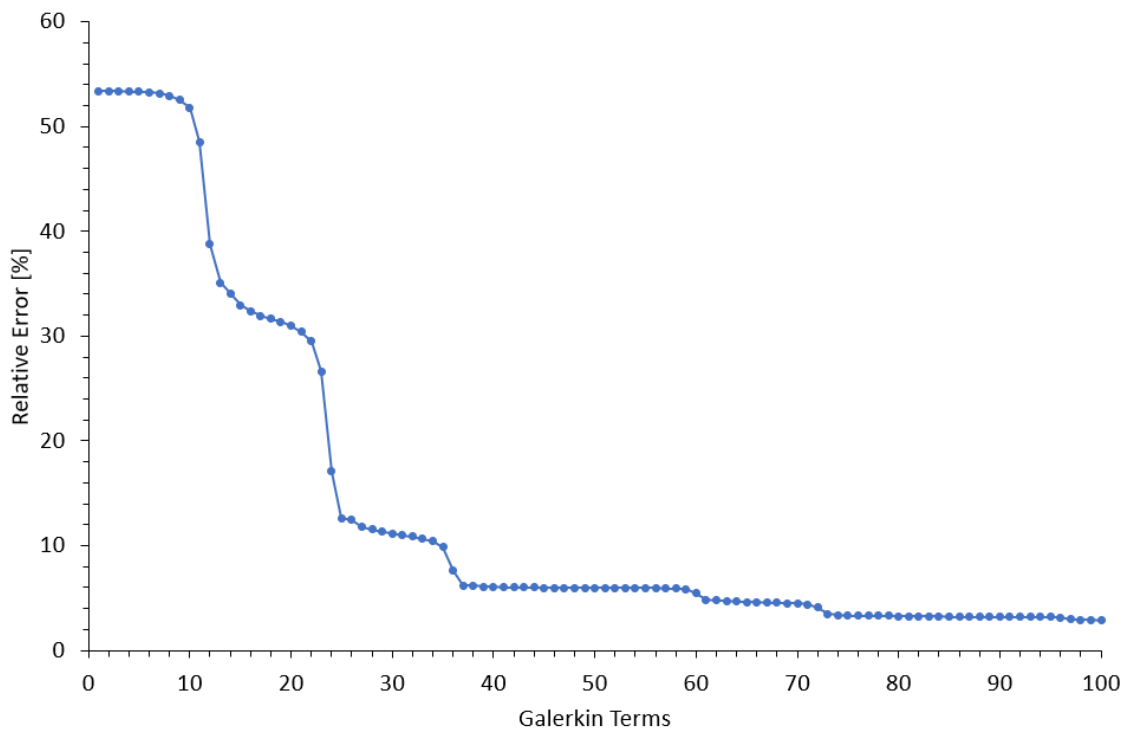


Figure 5.5: Trend of relative error of first natural frequency obtained with rigorous Galerkin method in clamped-free boundary condition for vibrations into $x - y$ plane

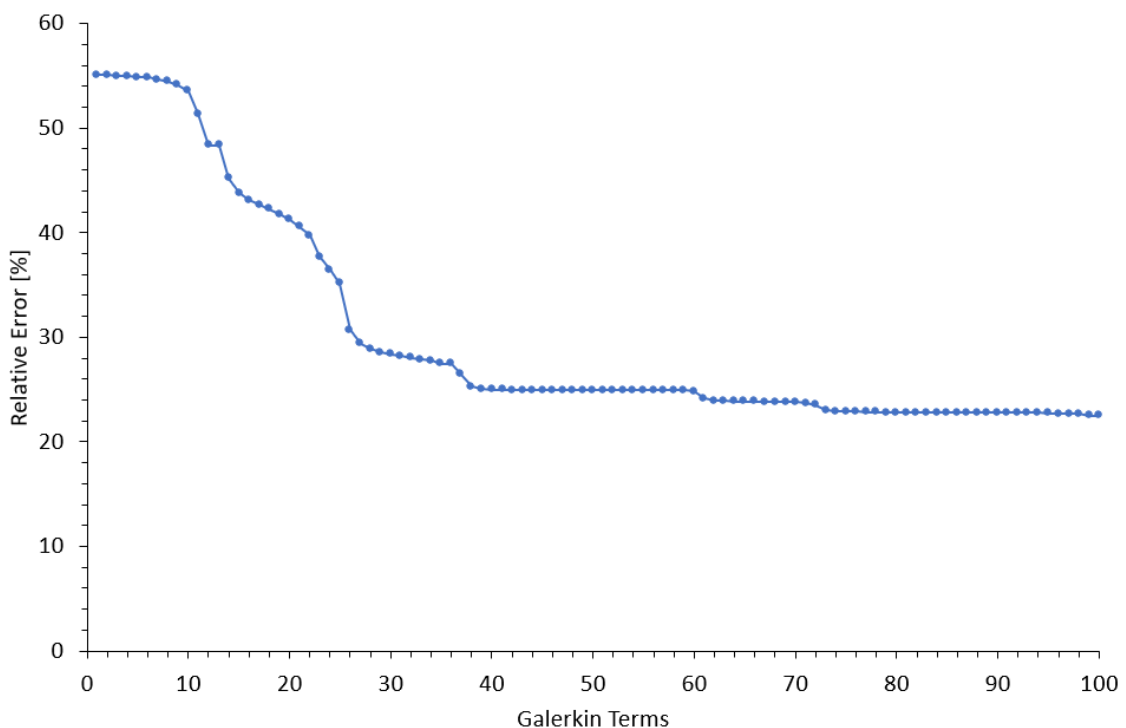


Figure 5.6: Trend of relative error of first natural frequency obtained with naïve Galerkin method in clamped-free boundary condition for vibrations into $x - y$ plane

5.4 Conclusion

In this study, we analyze the free vibration of a homogeneous and non-uniform beam. We compare two different implementations of Galerkin method: the rigorous version and the straightforward one. The study shows that the rigorous implementation reaches the convergence. On the other hand, the naïve version does not.

In addition, this study demonstrates that with an appropriate choice of the comparison function also the cantilever beam can reach convergence avoiding any noise and any numerical instability.

Moreover, the results of this study are supported by Ref. [29] which solves the problem in different ways, and besides it has the experimental results.

6. Plate

In this chapter, we analyze the bending free vibration of stepped plates, which is mathematically characterized by two-dimension fourth order differential equation. We investigate a homogeneous and non-uniform plate simply supported on all edges.

We study this object in different ratio of its characteristic dimensions, i.e. length, depth and thickness. We compare the frequencies obtained through four different approaches: exact solution derived by Kirchhoff-Love thin plate theory, naïve Galerkin method, rigorous Galerkin method and an FEM commercial code Strand7.

In order to support our results, we compare them with those found in literature in Xiang Y. and Wang C.M. paper (see Ref. [33]).

6.1 Basic Equations

We are interested in finding the natural frequencies of the structure represented in Fig. 6.1: a stepped plate.

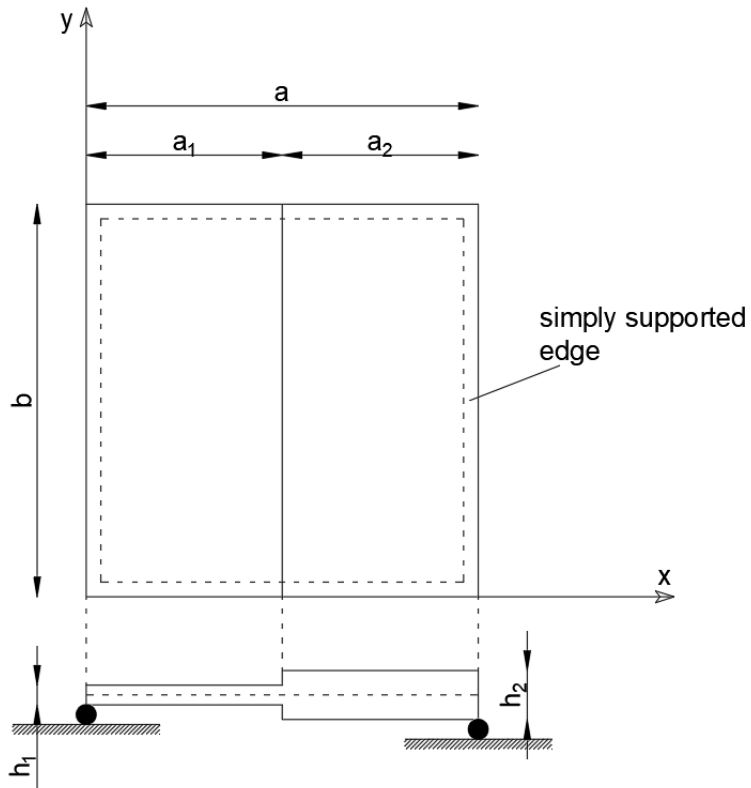


Figure 6.1: Simply-supported and stepped plate under study

We deal with a stepped plate simply supported on all edges. This plate has a as a side-length in x -direction and b as a side-length in y -direction. The first step has a_1 as length in x -direction and b as length in y -direction. The first step has h_1 as thickness, E_1 as elastic modulus, ν_1 as Poisson's coefficient and ρ_1 as mass density. The second step has a_2 as length in x -direction and b as length in y -direction. The second step has h_2 as thickness, E_2 as elastic modulus, ν_2 as Poisson's ratio and ρ_2 as mass density. We study the variation of natural frequencies for different ratio of h_2/h_1 , a_1/a and a/b .

We derive the governing differential equation of homogeneous and non-uniform Kirchhoff-Love plate starting from dynamic equilibrium on a differential element of Kirchhoff-Love plate, as shown in Fig. 6.2.

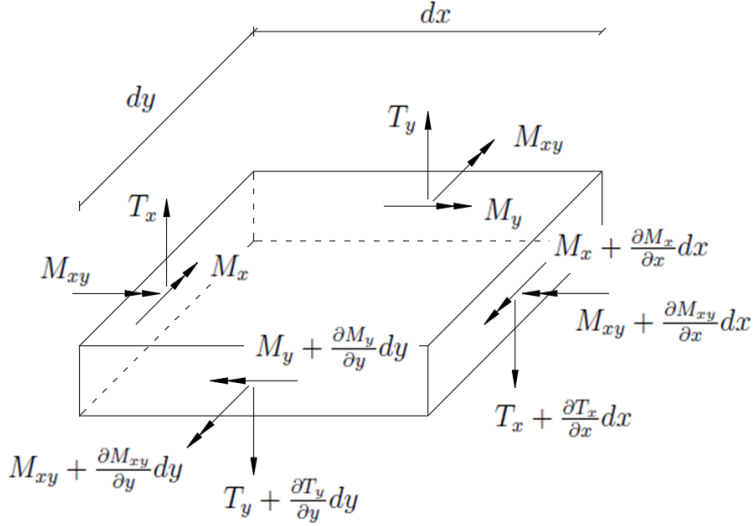


Figure 6.2: A differential element of plate

The equilibrium in vertical direction leads us to:

$$\frac{\partial T_x}{\partial x} + \frac{\partial T_y}{\partial y} = \rho(x)h(x)\frac{\partial^2 w}{\partial t^2} \quad (6.1.1)$$

The equilibrium of bending moment yields:

$$\frac{\partial M_x}{\partial x} + \frac{\partial M_{xy}}{\partial y} = T_x \quad (6.1.2)$$

$$\frac{\partial M_y}{\partial y} + \frac{\partial M_{xy}}{\partial x} = T_y \quad (6.1.3)$$

Remembering that:

$$M_x(x) = -D(x) \left(\frac{\partial^2 w}{\partial x^2} + \nu \frac{\partial^2 w}{\partial y^2} \right) \quad (6.1.4)$$

$$M_y(x) = -D(x) \left(\frac{\partial^2 w}{\partial y^2} + \nu \frac{\partial^2 w}{\partial x^2} \right) \quad (6.1.5)$$

$$M_{xy}(x) = -D(x)(1 - \nu) \left(\frac{\partial^2 w}{\partial x \partial y} \right) \quad (6.1.6)$$

Finally, assembling (6.1.4), (6.1.5), (6.1.6), (6.1.2), (6.1.3) and (6.1.1), we obtain:

$$\begin{aligned} & \frac{\partial^2}{\partial x^2} \left[D(x) \left(\frac{\partial^2 w}{\partial x^2} + \nu \frac{\partial^2 w}{\partial y^2} \right) \right] + 2 \frac{\partial^2}{\partial x \partial y} \left[D(x)(1 - \nu) \left(\frac{\partial^2 w}{\partial x \partial y} \right) \right] \\ & + \frac{\partial^2}{\partial y^2} \left[D(x) \left(\frac{\partial^2 w}{\partial y^2} + \nu \frac{\partial^2 w}{\partial x^2} \right) \right] + \rho(x)h(x)\frac{\partial^2 w}{\partial t^2} = 0 \end{aligned} \quad (6.1.7)$$

where $w(x, y, t)$ is the transverse displacement, x and y the coordinates and t is the time.

$D(x)$ represents the flexural stiffness of the plate as follows:

$$D(x) = \frac{E(x)h(x)^3}{12(1 - \nu(x)^2)} \quad (6.1.8)$$

Specifically, for each component, with piecewise constants D , ρ and h , we can write:

$$D_1 \nabla^4 w_1 + \rho_1 h_1 \frac{\partial^2 w_1}{\partial t^2} = 0 \quad 0 \leq x \leq a_1 \quad (6.1.9a)$$

$$D_2 \nabla^4 w_2 + \rho_2 h_2 \frac{\partial^2 w_2}{\partial t^2} = 0 \quad a_1 \leq x \leq a \quad (6.1.9b)$$

If we divide Eq. (6.1.9a) by D_1 and (6.1.9b) by D_2 , we obtain:

$$\nabla^4 w_1 + \frac{\rho_1 h_1}{D_1} \frac{\partial^2 w_1}{\partial t^2} = 0 \quad 0 \leq x \leq a_1 \quad (6.1.10a)$$

$$\nabla^4 w_2 + \frac{\rho_2 h_2}{D_2} \frac{\partial^2 w_2}{\partial t^2} = 0 \quad a_1 \leq x \leq a \quad (6.1.10b)$$

Now we separate the variable of the function $w_i(x, y, t)$ as follows:

$$w_i(x, y, t) = W_i(x, y) \sin(\omega t) \quad (6.1.11)$$

If we insert Eq. (6.1.11) in Eq. (6.1.10a) and (6.1.10b), we obtain:

$$\left(\nabla^4 W_1 - \frac{\rho_1 h_1}{D_1} \omega^2 W_1(x, y) \right) \sin(\omega t) = 0 \quad 0 \leq x \leq a_1 \quad (6.1.12a)$$

$$\left(\nabla^4 W_2 - \frac{\rho_2 h_2}{D_2} \omega^2 W_2(x, y) \right) \sin(\omega t) = 0 \quad a_1 \leq x \leq a \quad (6.1.12b)$$

We are interested in a solution which is true for any value of time, so we can divide by $\sin(\omega t)$:

$$\nabla^4 W_1 - k_1^4 W_1(x, y) = 0 \quad 0 \leq x \leq a_1 \quad (6.1.13a)$$

$$\nabla^4 W_2 - k_2^4 W_2(x, y) = 0 \quad a_1 \leq x \leq a \quad (6.1.13b)$$

where k_i^4 is defined as follows:

$$k_i^4 = \frac{\rho_i h_i}{D_i} \omega^2 \quad (6.1.14)$$

Voigt (1893) [34] and Lévy (1899) [35] independently propose to define the function $W_i(x, y)$ which describes two opposite supported edges as follows:

$$W_i(x, y) = \sum_{n=1}^{\infty} X_n(x) \sin\left(\frac{n\pi y}{b}\right) \quad (6.1.15)$$

Eq. (6.1.15), written in this form, specifies that the supported edges are $y = 0$ and $y = b$. This formulation does not provide any information about the edges $x = 0$ and $x = a$.

If we substitute Eq. (6.1.15) into Eq. (6.1.13a) and (6.1.13b) and explicit the Laplacian operator, we obtain:

$$\sum_{n=1}^{\infty} \left(\frac{d^4}{dx^4} X_{n,1}(x) - 2 \frac{n^2 \pi^2}{b^2} \frac{d^2}{dx^2} X_{n,1}(x) + \frac{n^4 \pi^4}{b^4} X_{n,1}(x) - k_1^4 X_{n,1}(x) \right) \sin\left(\frac{n\pi y}{b}\right) = 0 \quad 0 \leq x \leq a_1 \quad (6.1.16a)$$

$$\sum_{n=1}^{\infty} \left(\frac{d^4}{dx^4} X_{n,2}(x) - 2 \frac{n^2 \pi^2}{b^2} \frac{d^2}{dx^2} X_{n,2}(x) + \frac{n^4 \pi^4}{b^4} X_{n,2}(x) - k_2^4 X_{n,2}(x) \right) \sin\left(\frac{n\pi y}{b}\right) = 0 \quad a_1 \leq x \leq a \quad (6.1.16b)$$

For a non-trivial solution, we investigate the terms between parenthesis, i.e.:

$$\frac{d^4}{dx^4} X_{n,1}(x) - 2 \frac{n^2 \pi^2}{b^2} \frac{d^2}{dx^2} X_{n,1}(x) + \frac{n^4 \pi^4}{b^4} X_{n,1}(x) - k_1^4 X_{n,1}(x) = 0 \quad 0 \leq x \leq a_1 \quad (6.1.17a)$$

$$\frac{d^4}{dx^4} X_{n,2}(x) - 2 \frac{n^2 \pi^2}{b^2} \frac{d^2}{dx^2} X_{n,2}(x) + \frac{n^4 \pi^4}{b^4} X_{n,2}(x) - k_2^4 X_{n,2}(x) = 0 \quad a_1 \leq x \leq a \quad (6.1.17b)$$

We can find a solution for (6.1.17a) and (6.1.17b) supposing $X_n(x)$ in the following form:

$$X_n(x) = A e^{rx} \quad (6.1.18)$$

where r is the characteristic exponent which have to satisfy the equation:

$$r^4 - 2 \frac{n^2 \pi^2}{b^2} r^2 + \frac{n^4 \pi^4}{b^4} - k^4 = 0 \quad (6.1.19)$$

Solving first for r^2 , we have:

$$r_{1,2}^2 = \frac{n^2 \pi^2}{b^2} \pm k^2 \quad (6.1.20)$$

The four roots of (6.1.19) are obtained as:

$$r_{1,2} = \pm R_n^+ = \pm \sqrt{\frac{n^2 \pi^2}{b^2} + k^2} \quad (6.1.21a)$$

$$r_{3,4} = \pm R_n^- = \pm \sqrt{\frac{n^2 \pi^2}{b^2} - k^2} \quad \text{for } k^2 < \frac{n^2 \pi^2}{b^2} \quad (6.1.21b)$$

$$r_{3,4} = \pm i Q_n = \pm i \sqrt{k^2 - \frac{n^2 \pi^2}{b^2}} \quad \text{for } k^2 > \frac{n^2 \pi^2}{b^2} \quad (6.1.21c)$$

The solution for Eq. (6.1.17a) and (6.1.17b) may then be constructed as follows:

$$X_n(x) = A_1 \sinh(R_n^- x) + A_2 \cosh(R_n^- x) + A_3 \sinh(R_n^+ x) + A_4 \cosh(R_n^+ x) \quad (6.1.22a)$$

for $k^2 < \frac{n^2\pi^2}{b^2}$

$$X_n(x) = A_1 \sin(Q_n x) + A_2 \cos(Q_n x) + A_3 \sinh(R_n^+ x) + A_4 \cosh(R_n^+ x) \quad (6.1.22b)$$

for $k^2 > \frac{n^2\pi^2}{b^2}$

where A_i are unknown constants.

6.2 Exact solution

In our problem, we have eight unknowns in total: four for the first step and four for the second step.

In this analysis, we are interested in finding the natural frequencies. For this reason, we suppose to know the geometry and the material of our plate so that we can define the inequality in terms of the natural frequencies. This leads us to:

$$\omega < \frac{n^2\pi^2}{b^2} \sqrt{\frac{E_1 h_1^2}{12(1 - \nu_1^2)\rho_1}} \quad (6.2.1a)$$

$$\omega > \frac{n^2\pi^2}{b^2} \sqrt{\frac{E_2 h_2^2}{12(1 - \nu_2^2)\rho_2}} \quad (6.2.1b)$$

The boundary conditions, for plate simply supported on all edges, require that the vertical displacement and the bending moment are equal to zero. These are written as:

$$W_1(x = 0) = 0 \quad (6.2.2a)$$

$$M_x(x = 0) = D_1 \left[\frac{\partial^2 W_1}{\partial x^2} + \nu \frac{\partial^2 W_1}{\partial y^2} \right]_{x=0} = 0 \quad (6.2.2b)$$

$$W_2(x = a) = 0 \quad (6.2.2c)$$

$$M_x(x = a) = D_2 \left[\frac{\partial^2 W_2}{\partial x^2} + \nu \frac{\partial^2 W_2}{\partial y^2} \right]_{x=a} = 0 \quad (6.2.2d)$$

The continuity conditions between the two steps require that the vertical displacement, the slope, the bending moment and the shear force are equal along all the interface. These are

written as:

$$W_1(x = a_1) = W_2(x = a_1) \quad (6.2.3a)$$

$$W'_1(x = a_1) = W'_2(x = a_1) \quad (6.2.3b)$$

$$M_x(x = a_1) = D_1 \left[\frac{\partial^2 W_1}{\partial x^2} + \nu \frac{\partial^2 W_1}{\partial y^2} \right]_{x=a_1} = D_2 \left[\frac{\partial^2 W_2}{\partial x^2} + \nu \frac{\partial^2 W_2}{\partial y^2} \right]_{x=a_1} = M_x(x = a_1) \quad (6.2.3c)$$

$$T_x(x = a_1) = D_1 \left[\frac{\partial^3 W_1}{\partial x^3} + (2 - \nu) \frac{\partial^3 W_1}{\partial x \partial y^2} \right]_{x=a_1} = D_2 \left[\frac{\partial^3 W_2}{\partial x^3} + (2 - \nu) \frac{\partial^3 W_2}{\partial x \partial y^2} \right]_{x=a_1} = T_x(x = a_1) \quad (6.2.3d)$$

The above expressions of boundary conditions and compatibility conditions are correct in contrast with those in Ref. [36] and [37]. In fact, they do not consider the bi-dimensional effect, they treat the plate as a Bernoulli-Euler beam. Specifically, they write:

$$W_1(x = a_1) = W_2(x = a_1) \quad (6.2.4a)$$

$$W'_1(x = a_1) = W'_2(x = a_1) \quad (6.2.4b)$$

$$M_x(x = a_1) = W''_1(x = a_1) = W''_2(x = a_1) = M_x(x = a_1) \quad (6.2.4c)$$

$$T_x(x = a_1) = W'''_1(x = a_1) = W'''_2(x = a_1) = T_x(x = a_1) \quad (6.2.4d)$$

Now we create a system of eight equations in eight unknowns where the equations are boundary and continuity conditions (eight equations) and the unknowns are the coefficients of the vertical displacement, the A_i . We have four A_i for the first step and four A_i for the second step.

In this way, we obtain a homogeneous system which has non-trivial solution only when the coefficient matrix has determinant equal to zero. Now our problem is to find the value of ω which leads to the vanishing determinant.

6.3 Naïve Galerkin method

We start from the governing differential equation below, which is the expansion of Laplacian in Eq. (6.1.13a) and (6.1.13b):

$$\frac{\partial^4}{\partial x^4} W(x, y) + 2 \frac{\partial^4}{\partial x^2 \partial y^2} W(x, y) + \frac{\partial^4}{\partial y^4} W(x, y) - k_j^4 W_1(x, y) = 0 \quad x_{j-1} \leq x \leq x_j \quad (6.3.1)$$

Now we express the function $W(x, y)$ in series as follows:

$$W(x, y) = \sum_{m=1}^{\infty} \sum_{n=1}^{\infty} p_{mn} \psi_{mn}(x, y) \quad (6.3.2)$$

Where $\psi_{mn}(x, y)$ is a comparison function that has to respect all the boundary conditions. We also suppose to separate the variables as follows:

$$W(x, y) = \sum_{m=1}^{\infty} \sum_{n=1}^{\infty} p_{mn} \psi_{mn}(x, y) = \sum_{m=1}^{\infty} \sum_{n=1}^{\infty} p_{mn} \psi_m(x) \psi_n(y) \quad (6.3.3)$$

Substituting these in Eq. (6.3.1), we get:

$$\sum_{m=1}^{\infty} \sum_{n=1}^{\infty} [\psi_m'''(x)\psi_n(y) + 2\psi_m''(x)\psi_n''(y) + \psi_m(x)\psi_n'''(y) - k_j^4\psi_m(x)\psi_n(y)] p_{mn} = \varepsilon(x, y)$$

$$x_{j-1} \leq x \leq x_j \quad (6.3.4)$$

where $\varepsilon(x, y)$ is the residual or error. Now we multiply by the comparison functions and we integrate over the plate's domain as follows:

$$\begin{aligned} & \sum_{m=1}^{\infty} \sum_{n=1}^{\infty} \left(\int_0^a \int_0^b \psi_m'''(x)\psi_n(y)\psi_q(x)\psi_n(y) dx dy \right. \\ & + \int_0^a \int_0^b 2\psi_m''(x)\psi_n''(y)\psi_q(x)\psi_n(y) dx dy + \int_0^a \int_0^b \psi_m(x)\psi_n'''(y)\psi_q(x)\psi_n(y) dx dy \\ & \quad \left. + \int_0^a \int_0^b -k_1^4\psi_m(x)\psi_n(y)\psi_q(x)\psi_n(y) dx dy \right. \\ & \quad \left. + \int_0^a \int_0^b -k_2^4\psi_m(x)\psi_n(y)\psi_q(x)\psi_n(y) dx dy \right) p_{mn} = 0 \end{aligned} \quad (6.3.5)$$

Introducing the following notation:

$$A_{mnq} = \int_0^a \int_0^b \psi_m'''(x)\psi_n(y)\psi_q(x)\psi_n(y) dx dy \quad (6.3.6a)$$

$$B_{mnq} = \int_0^a \int_0^b 2\psi_m''(x)\psi_n''(y)\psi_q(x)\psi_n(y) dx dy \quad (6.3.6b)$$

$$C_{mnq} = \int_0^a \int_0^b \psi_m(x)\psi_n'''(y)\psi_q(x)\psi_n(y) dx dy \quad (6.3.6c)$$

$$\begin{aligned} M_{mnq} = & \int_0^{a_1} \int_0^b -\frac{\rho_1 h_1}{D_1} \psi_m(x)\psi_n(y)\psi_q(x)\psi_n(y) dx dy \\ & + \int_{a_1}^a \int_0^b -\frac{\rho_2 h_2}{D_2} \psi_m(x)\psi_n(y)\psi_q(x)\psi_n(y) dx dy \end{aligned} \quad (6.3.6d)$$

In this form, we obtain the following equation:

$$\sum_{m=1}^{\infty} \sum_{n=1}^{\infty} (A_{mnq} + B_{mnq} + C_{mnq} + \omega^2 M_{mnq}) p_{mn} = 0 \quad (6.3.7)$$

For a specific value of n , we can rewrite Eq. (6.3.7) in a matrix form as follows:

$$(\mathbf{A} + \mathbf{B} + \mathbf{C} + \omega^2 \mathbf{M}) \mathbf{p} = \mathbf{0} \quad (6.3.8)$$

Denoting:

$$\mathbf{K} = \mathbf{A} + \mathbf{B} + \mathbf{C} \quad (6.3.9)$$

We obtain:

$$(\mathbf{K} + \omega^2 \mathbf{M}) \mathbf{p} = \mathbf{0} \quad (6.3.10)$$

Non-trivial solution of the problem is achieved when the determinant of the expression between parenthesis vanishes:

$$\det (\mathbf{K} + \omega^2 \mathbf{M}) = 0 \quad (6.3.11)$$

6.4 Rigorous Galerkin method

Remembering Eq. (6.1.7) and applying consideration (6.1.11) on it, we obtain:

$$\begin{aligned} & \frac{\partial^2}{\partial x^2} \left[D(x) \left(\frac{\partial^2 W}{\partial x^2} + \nu \frac{\partial^2 W}{\partial y^2} \right) \right] + 2 \frac{\partial^2}{\partial x \partial y} \left[D(x)(1-\nu) \left(\frac{\partial^2 W}{\partial x \partial y} \right) \right] \\ & + \frac{\partial^2}{\partial y^2} \left[D(x) \left(\frac{\partial^2 W}{\partial y^2} + \nu \frac{\partial^2 W}{\partial x^2} \right) \right] - \rho(x)h(x)\omega^2W = 0 \end{aligned} \quad (6.4.1)$$

Denoting $\rho(x)h(x)$ as $M(x)$, we obtain:

$$\begin{aligned} & \frac{\partial^2}{\partial x^2} \left[D(x) \left(\frac{\partial^2 W}{\partial x^2} + \nu \frac{\partial^2 W}{\partial y^2} \right) \right] + 2 \frac{\partial^2}{\partial x \partial y} \left[D(x)(1-\nu) \left(\frac{\partial^2 W}{\partial x \partial y} \right) \right] \\ & + \frac{\partial^2}{\partial y^2} \left[D(x) \left(\frac{\partial^2 W}{\partial y^2} + \nu \frac{\partial^2 W}{\partial x^2} \right) \right] - M(x)\omega^2W = 0 \end{aligned} \quad (6.4.2)$$

In order to implement the rigorous Galerkin method, we represent the flexural rigidity and the mass of the system as a generalized function:

$$D(x) = D_1 H(x) + (D_2 - D_1) H(x - a_1) \quad (6.4.3)$$

$$M(x) = M_1 H(x) + (M_2 - M_1) H(x - a_1) \quad (6.4.4)$$

where $H(x)$ is the unit step function or Heaviside function which has the following properties:

$$H(x - \alpha) = \begin{cases} 1, & \text{if } x > \alpha \\ 0, & \text{otherwise} \end{cases} \quad (6.4.5)$$

$$\frac{d}{dx} H(x - \alpha) = \delta(x - \alpha) \quad (6.4.6)$$

$$\frac{d}{dx} \delta(x - \alpha) = \delta'(x - \alpha) \quad (6.4.7)$$

where $\delta(x)$ is the Dirac delta function and $\delta'(x)$ is the doublet function.

Using these functions, we obtain:

$$\begin{aligned} & \frac{\partial^2 D(x)}{\partial x^2} \left(\frac{\partial^2 W(x, y)}{\partial x^2} + \nu \frac{\partial^2 W(x, y)}{\partial y^2} \right) + 2 \frac{\partial D(x)}{\partial x} \left(\frac{\partial^3 W(x, y)}{\partial x^3} + \nu \frac{\partial^3 W(x, y)}{\partial x \partial y^2} \right) \\ & + D(x) \left(\frac{\partial^4 W(x, y)}{\partial x^4} + \nu \frac{\partial^4 W(x, y)}{\partial x^2 \partial y^2} \right) \\ & + 2(1-\nu) \left(\frac{\partial D(x)}{\partial x} \frac{\partial^3 W(x, y)}{\partial x \partial y^2} + D(x) \frac{\partial^4 W(x, y)}{\partial x^2 \partial y^2} \right) \\ & + D(x) \left(\frac{\partial^4 W(x, y)}{\partial y^4} + \nu \frac{\partial^4 W(x, y)}{\partial x^2 \partial y^2} \right) - M(x)\omega^2W(x, y) = 0 \end{aligned} \quad (6.4.8)$$

Now we express the function $W(x, y)$ in series as follows:

$$W(x, y) = \sum_{m=1}^{\infty} \sum_{n=1}^{\infty} p_{mn} \psi_{mn}(x, y) \quad (6.4.9)$$

where $\psi_{mn}(x, y)$ is a comparison function that has to respect all the boundary conditions. We also suppose to separate the variables as follows:

$$W(x, y) = \sum_{m=1}^{\infty} \sum_{n=1}^{\infty} p_{mn} \psi_{mn}(x, y) = \sum_{m=1}^{\infty} \sum_{n=1}^{\infty} p_{mn} \psi_m(x) \psi_n(y) \quad (6.4.10)$$

Substituting these in Eq. (6.4.8), we get:

$$\begin{aligned} & \sum_{m=1}^{\infty} \sum_{n=1}^{\infty} \left[\frac{\partial^2 D(x)}{\partial x^2} \left(\frac{\partial^2 \psi_m(x)}{\partial x^2} \psi_n(y) + \nu \psi_m(x) \frac{\partial^2 \psi_n(y)}{\partial y^2} \right) \right. \\ & \quad + 2 \frac{\partial D(x)}{\partial x} \left(\frac{\partial^3 \psi_m(x)}{\partial x^3} \psi_n(y) + \nu \frac{\partial \psi_m(x)}{\partial x} \frac{\partial^2 \psi_n(y)}{\partial y^2} \right) \\ & \quad + D(x) \left(\frac{\partial^4 \psi_m(x)}{\partial x^4} \psi_n(y) + \nu \frac{\partial^2 \psi_m(x)}{\partial x^2} \frac{\partial^2 \psi_n(y)}{\partial y^2} \right) \quad (6.4.11) \\ & \quad + 2(1 - \nu) \left(\frac{\partial D(x)}{\partial x} \frac{\partial \psi_m(x)}{\partial x} \frac{\partial^2 \psi_n(y)}{\partial y^2} + D(x) \frac{\partial^2 \psi_m(x)}{\partial x^2} \frac{\partial^2 \psi_n(y)}{\partial y^2} \right) \\ & \quad + D(x) \left(\frac{\partial^4 \psi_n(y)}{\partial y^4} \psi_m(x) + \nu \frac{\partial^2 \psi_m(x)}{\partial x^2} \frac{\partial^2 \psi_n(y)}{\partial y^2} \right) \\ & \quad \left. - M(x) \omega^2 \psi_m(x) \psi_n(y) \right] p_{mn} = \varepsilon(x, y) \end{aligned}$$

or:

$$\begin{aligned} & \sum_{m=1}^{\infty} \sum_{n=1}^{\infty} \left[D''(x) \psi_m''(x) \psi_n(y) + \nu D''(x) \psi_m(x) \psi_n''(y) + 2D'(x) \psi_m'''(x) \psi_n(y) \right. \\ & \quad + D(x) \psi_m'''(x) \psi_n(y) + 2D'(x) \psi_m'(x) \psi_n''(y) + 2D(x) \psi_m''(x) \psi_n''(y) \\ & \quad \left. + D(x) \psi_m(x) \psi_n'''(y) - \omega^2 M(x) \psi_m(x) \psi_n(y) \right] p_{mn} = \varepsilon(x, y) \quad (6.4.12) \end{aligned}$$

Now we multiply by the comparison functions and we integrate in both x and y directions as follows:

$$\begin{aligned}
& \sum_{m=1}^{\infty} \sum_{n=1}^{\infty} \left[\int_0^a \int_0^b D''(x) \psi_m''(x) \psi_n(y) \psi_q(x) \psi_n(y) dx dy \right. \\
& \quad + \int_0^a \int_0^b \nu D''(x) \psi_m(x) \psi_n''(y) \psi_q(x) \psi_n(y) dx dy \\
& \quad + \int_0^a \int_0^b 2D'(x) \psi_m'''(x) \psi_n(y) \psi_q(x) \psi_n(y) dx dy \\
& \quad + \int_0^a \int_0^b D(x) \psi_m''''(x) \psi_n(y) \psi_q(x) \psi_n(y) dx dy \quad (6.4.13) \\
& \quad + \int_0^a \int_0^b 2D'(x) \psi_m'(x) \psi_n''(y) \psi_q(x) \psi_n(y) dx dy \\
& \quad + \int_0^a \int_0^b 2D(x) \psi_m''(x) \psi_n''(y) \psi_q(x) \psi_n(y) dx dy \\
& \quad + \int_0^a \int_0^b D(x) \psi_m(x) \psi_n'''(y) \psi_q(x) \psi_n(y) dx dy \\
& \quad \left. + \int_0^a \int_0^b -\omega^2 M(x) \psi_m(x) \psi_n(y) \psi_q(x) \psi_n(y) dx dy \right] p_{mn} = 0
\end{aligned}$$

Introducing the following notation:

$$A_{mnq} = \int_0^a \int_0^b D''(x) \psi_m''(x) \psi_n(y) \psi_q(x) \psi_n(y) dx dy \quad (6.4.14a)$$

$$B_{mnq} = \int_0^a \int_0^b \nu D''(x) \psi_m(x) \psi_n''(y) \psi_q(x) \psi_n(y) dx dy \quad (6.4.14b)$$

$$C_{mnq} = \int_0^a \int_0^b 2D'(x) \psi_m'''(x) \psi_n(y) \psi_q(x) \psi_n(y) dx dy \quad (6.4.14c)$$

$$D_{mnq} = \int_0^a \int_0^b D(x) \psi_m''''(x) \psi_n(y) \psi_q(x) \psi_n(y) dx dy \quad (6.4.14d)$$

$$E_{mnq} = \int_0^a \int_0^b 2D'(x) \psi_m'(x) \psi_n''(y) \psi_q(x) \psi_n(y) dx dy \quad (6.4.14e)$$

$$F_{mnq} = \int_0^a \int_0^b 2D(x) \psi_m''(x) \psi_n''(y) \psi_q(x) \psi_n(y) dx dy \quad (6.4.14f)$$

$$G_{mnq} = \int_0^a \int_0^b D(x) \psi_m(x) \psi_n'''(y) \psi_q(x) \psi_n(y) dx dy \quad (6.4.14g)$$

$$M_{mnq} = \int_0^a \int_0^b -M(x) \psi_m(x) \psi_n(y) \psi_q(x) \psi_n(y) dx dy \quad (6.4.14h)$$

In this form, we obtain the following equation:

$$\sum_{m=1}^{\infty} \sum_{n=1}^{\infty} [A_{mnq} + B_{mnq} + C_{mnq} + D_{mnq} + E_{mnq} + F_{mnq} + G_{mnq} + \omega^2 M_{mnq}] p_{mn} = 0 \quad (6.4.15)$$

For a specific value of n , we can rewrite Eq. (6.4.15) in a matrix form as follows:

$$(\mathbf{A} + \mathbf{B} + \mathbf{C} + \mathbf{D} + \mathbf{E} + \mathbf{F} + \mathbf{G} + \omega^2 \mathbf{M}) \mathbf{p} = \mathbf{0} \quad (6.4.16)$$

Denoting:

$$\mathbf{K} = \mathbf{A} + \mathbf{B} + \mathbf{C} + \mathbf{D} + \mathbf{E} + \mathbf{F} + \mathbf{G} \quad (6.4.17)$$

We obtain:

$$(\mathbf{K} + \omega^2 \mathbf{M}) \mathbf{p} = \mathbf{0} \quad (6.4.18)$$

Non-trivial solution of the problem is achieved when the determinant of the expression between parenthesis vanishes:

$$\det(\mathbf{K} + \omega^2 \mathbf{M}) = 0 \quad (6.4.19)$$

6.5 Comparison functions for Galerkin method

As stated before, a comparison function for Galerkin method is a function which is required to approximate the differential equation object of study and which must satisfy all the boundary conditions.

For our plate simply supported on all edges, the preferable comparison function is the product of two sinusoidal functions. This reads as follows:

$$\psi_{mn}(x, y) = \psi_m(x)\psi_n(y) = \sin\left(\frac{m\pi x}{a}\right) \sin\left(\frac{n\pi y}{b}\right) \quad (6.5.1)$$

6.6 Numerical example

We study a simply supported on all edges stepped plate made of only one material, i.e. steel, with the following parameters:

Steel	
E	$207 \cdot 10^9$ Pa
ν	0.3
ρ	7800 kg/m ³

Table 6.1: Material's parameters

We study the stepped plate in three different ratios of a/b , three different ratios of a_1/a and two different ratios of h_1/h_2 . We combine these values obtaining ten different cases, listed in the following table:

	Cases							
	a	b	a_1	h_1	h_2	h_1/h_2	a_1/a	a/b
Case 1	1.0 m	1.0 m	0.3 m	0.001 m	0.0015 m	0.67	0.30	1
Case 2	1.0 m	1.0 m	0.5 m	0.001 m	0.0015 m	0.67	0.50	1
Case 3	1.0 m	1.0 m	0.7 m	0.001 m	0.0015 m	0.67	0.70	1
Case 4	1.0 m	1.0 m	0.3 m	0.001 m	0.002 m	0.5	0.30	1
Case 5	1.0 m	1.0 m	0.5 m	0.001 m	0.002 m	0.5	0.50	1
Case 6	1.0 m	1.0 m	0.7 m	0.001 m	0.002 m	0.5	0.70	1
Case 7	1.0 m	2.0 m	0.5 m	0.001 m	0.0015 m	0.67	0.50	0.5
Case 8	1.0 m	2.0 m	0.5 m	0.001 m	0.002 m	0.5	0.50	0.5
Case 9	2.0 m	1.0 m	0.1 m	0.001 m	0.0015 m	0.67	0.50	2
Case 10	2.0 m	1.0 m	0.1 m	0.001 m	0.002 m	0.5	0.50	2

Table 6.2: Geometrical parameters for each of the ten studied cases

6.6.1 Exact solution

We report the exact solution in Tables 6.3 - 6.12. We assign a separate table to each case described in Table 6.2. In each entry, we report the mode as a progressive number, the number of half-waves associated with each mode in both directions: x and y , the natural frequencies of that mode. In each table, there is also a reference solution provided by Ref. [33] and the relative error between our solution and the referenced one.

The solutions reported in Ref. [33] are non-dimensional since frequencies are multiplied by the following coefficient:

$$\gamma = \left(\frac{b}{\pi} \right)^2 \sqrt{\frac{\rho h_1}{D_1}} \quad (6.6.1)$$

The relative error is evaluated with the following formula:

$$\varepsilon = \frac{\omega_{evaluated} - \omega_{reference}}{\omega_{reference}} \times 100 \quad (6.6.2)$$

Case 1						
Mode	Half-waves in x direction	Half-waves in y direction	Frequencies [rad/s]	Frequencies [dimensionless]	Reference frequencies [dimensionless]	Relative error [%]
1	1	1	40.4486	2.6289	2.6289	0.0003%
2	2	1	100.5934	6.5379	6.5380	-0.0009%
3	1	2	104.0137	6.7602	6.7603	-0.0009%
4	2	2	164.9920	10.7234	10.7240	-0.0051%
5	3	1	206.6667	13.4320	13.4320	0.0003%
6	1	3	207.7331	13.5013	13.5010	0.0026%

Table 6.3: Exact solution of Case 1

Case 2						
Mode	Half-waves in x direction	Half-waves in y direction	Frequencies [rad/s]	Frequencies [dimensionless]	Reference frequencies [dimensionless]	Relative error [%]
1	1	1	37.6505	2.4470	2.4471	-0.0021%
2	1	2	94.3753	6.1338	6.1338	0.0001%
3	2	1	95.7461	6.2229	6.2229	0.0000%
4	2	2	151.6692	9.8575	9.8576	-0.0005%
5	1	3	181.5737	11.8012	11.8010	0.0013%
6	3	1	183.8369	11.9482	11.9480	0.0021%

Table 6.4: Exact solution of Case 2

Case 3						
Mode	Half-waves in x direction	Half-waves in y direction	Frequencies [rad/s]	Frequencies [dimensionless]	Reference frequencies [dimensionless]	Relative error [%]
1	1	1	35.5534	2.3107	2.3108	-0.0022%
2	2	1	85.0714	5.5291	5.5291	0.0002%
3	1	2	85.6058	5.5638	5.5639	-0.0010%
4	2	2	138.9492	9.0308	9.0309	-0.0008%
5	1	3	164.8776	10.7160	10.7160	0.0001%
6	3	1	174.8403	11.3635	11.3640	-0.0041%

Table 6.5: Exact solution of Case 3

Case 4						
Mode	Half-waves in x direction	Half-waves in y direction	Frequencies [rad/s]	Frequencies [dimensionless]	Reference frequencies [dimensionless]	Relative error [%]
1	1	1	48.3914	3.1451	3.1452	-0.0019%
2	2	1	124.4603	8.0891	8.0892	-0.0007%
3	1	2	129.6047	8.4235	8.4235	0.0000%
4	2	2	207.9360	13.5145	13.5150	-0.0034%
5	1	3	254.0414	16.5111	16.5110	0.0006%
6	3	1	254.4169	16.5355	16.5360	-0.0030%

Table 6.6: Exact solution of Case 4

Case 5						
Mode	Half-waves in x direction	Half-waves in y direction	Frequencies [rad/s]	Frequencies [dimensionless]	Reference frequencies [dimensionless]	Relative error [%]
1	1	1	44.6428	2.9015	2.9015	0.0001%
2	2	1	109.4810	7.1156	7.1156	-0.0003%
3	1	2	110.5175	7.1829	7.1830	-0.0007%
4	2	2	173.1523	11.2538	11.2540	-0.0016%
5	1	3	197.9323	12.8644	12.8640	0.0028%
6	3	1	212.0934	13.7847	13.7850	-0.0018%

Table 6.7: Exact solution of Case 5

Case 6						
Mode	Half-waves in x direction	Half-waves in y direction	Frequencies [rad/s]	Frequencies [dimensionless]	Reference frequencies [dimensionless]	Relative error [%]
1	1	1	41.0941	2.6709	2.6709	-0.0015%
2	2	1	89.9274	5.8447	5.8447	0.0003%
3	1	2	92.4917	6.0114	6.0116	-0.0036%
4	2	2	155.1220	10.0820	10.0820	-0.0004%
5	1	3	170.5992	11.0879	11.0880	-0.0010%
6	3	1	185.1245	12.0319	12.0320	-0.0005%

Table 6.8: Exact solution of Case 6

From the above tables, we can see that the error between our calculation and the provided solution is in the order of $\pm 0.0010\%$, so we conclude that our derivation is correct.

In addition, we provide four more cases. In these cases the plates are rectangular. We do not have a reference solution for these, so the layout of the tables is the same as before, except for the last two columns.

Case 7				
Mode	Half-waves in x direction	Half-waves in y direction	Frequencies [rad/s]	Frequencies [dimensionless]
1	1	1	22.5869	5.8720
2	1	2	37.6505	9.7882
3	1	3	61.7983	16.0660
4	2	1	82.0344	21.3269
5	1	4	94.3753	24.5352
6	2	2	95.7461	24.8916

Table 6.9: Exact solution of Case 7

Case 8				
Mode	Half-waves in x direction	Half-waves in y direction	Frequencies [rad/s]	Frequencies [dimensionless]
1	1	1	24.9198	6.4785
2	1	2	44.6428	11.6060
3	1	3	74.0080	19.2402
4	2	1	95.1208	24.7290
5	2	2	109.4810	28.4623
6	1	4	110.5173	28.7317

Table 6.10: Exact solution of Case 8

Case 9				
Mode	Half-waves in x direction	Half-waves in y direction	Frequencies [rad/s]	Frequencies [dimensionless]
1	1	1	23.5938	1.5334
2	2	1	37.9173	2.4644
3	3	1	60.9814	3.9634
4	1	2	73.9007	4.8031
5	4	1	94.0520	6.1128
6	2	2	97.2059	6.3178

Table 6.11: Exact solution of Case 9

Case 10				
Mode	Half-waves in x direction	Half-waves in y direction	Frequencies [rad/s]	Frequencies [dimensionless]
1	1	1	27.6293	1.7957
2	2	1	43.2881	2.8135
3	3	1	72.0259	4.6812
4	1	2	77.1459	5.0140
5	4	1	104.6939	6.8045
6	2	2	112.8011	7.3314

Table 6.12: Exact solution of Case 10

6.6.2 Naïve Galerkin method

We report the result of Galerkin method up to 10 terms. For each case, we report a table with the frequency value, then a table with the relative error using the following formula:

$$\varepsilon = \frac{\omega_{\text{Galerkin}} - \omega_{\text{exact}}}{\omega_{\text{exact}}} \times 100 \quad (6.6.3)$$

And, in conclusion, a chart of the relative error in function of the number of terms.

Mode	Naïve Galerkin method					
	Frequencies [rad/s]					
	Case 1					
Mode	1 Term	2 Terms	3 Terms	4 Terms	5 Terms	10 Terms
1	42.3880	42.1571	42.1142	42.1106	42.1105	42.1098
2		99.2403	98.3092	98.2014	98.1995	98.1945
3	105.9700	103.9772	103.4244	103.3628	103.3628	103.3524
4		160.9462	158.7705	158.4516	158.4403	158.4293
5			206.4340	204.9155	204.6357	204.6014
6	211.9401	203.1052	199.6772	199.1581	199.1564	199.0877

Table 6.13: Frequencies obtained with naïve Galerkin method for Case 1

Mode	Naïve Galerkin method					
	Relative error [%]					
	Case 1					
Mode	1 Term	2 Terms	3 Terms	4 Terms	5 Terms	10 Terms
1	4.7948%	4.2240%	4.1178%	4.1088%	4.1088%	4.1071%
2		-1.3451%	-2.2707%	-2.3779%	-2.3798%	-2.3847%
3	1.8808%	-0.0351%	-0.5666%	-0.6258%	-0.6258%	-0.6358%
4		-2.4521%	-3.7708%	-3.9641%	-3.9709%	-3.9776%
5			-0.1126%	-0.8473%	-0.9828%	-0.9994%
6	2.0252%	-2.2278%	-3.8780%	-4.1279%	-4.1287%	-4.1618%

Table 6.14: Relative error between naïve Galerkin method and exact solution for Case 1

Mode	Naïve Galerkin method					
	Frequencies [rad/s]					
	Case 2					
Mode	1 Term	2 Terms	3 Terms	4 Terms	5 Terms	10 Terms
1	36.2094	35.8555	35.8554	35.8514	35.8514	35.8510
2	90.5234	87.8408	87.8323	87.7930	87.7929	87.7880
3		96.7161	95.9182	95.8902	95.8858	95.8833
4		157.9133	155.4271	155.2271	155.2145	155.1979
5	181.0468	171.1117	170.9888	170.8331	170.8307	170.8072
6			186.6043	182.9962	182.9637	182.8884

Table 6.15: Frequencies obtained with naïve Galerkin method for Case 2

Mode	Naïve Galerkin method					
	Relative error [%]					
	Case 2					
Mode	1 Term	2 Terms	3 Terms	4 Terms	5 Terms	10 Terms
1	-3.8277%	-4.7674%	-4.7677%	-4.7784%	-4.7784%	-4.7795%
2	-4.0815%	-6.9240%	-6.9330%	-6.9746%	-6.9747%	-6.9799%
3		1.0130%	0.1798%	0.1506%	0.1459%	0.1433%
4		4.1169%	2.4777%	2.3458%	2.3375%	2.3266%
5	-0.2902%	-5.7619%	-5.8295%	-5.9153%	-5.9166%	-5.9295%
6			1.5054%	-0.4573%	-0.4750%	-0.5159%

Table 6.16: Relative error between naïve Galerkin method and exact solution for Case 2

Mode	Naïve Galerkin method					
	Frequencies [rad/s]					
	Case 3					
Mode	1 Term	2 Terms	3 Terms	4 Terms	5 Terms	10 Terms
1	32.1271	32.0720	32.0633	32.0626	32.0626	32.0625
2		86.6821	85.8238	85.7645	85.7645	85.7585
3	80.3176	79.8857	79.8141	79.8085	79.8083	79.8066
4		139.2024	136.6401	136.4862	136.4861	136.4648
5	160.6353	158.9073	158.6610	158.6432	158.6417	158.6327
6			178.8368	176.2053	176.1467	176.1158

Table 6.17: Frequencies obtained with naïve Galerkin method for Case 3

Mode	Naïve Galerkin method					
	Relative error [%]					
	Case 3					
Mode	1 Term	2 Terms	3 Terms	4 Terms	5 Terms	10 Terms
1	-9.6372%	-9.7920%	-9.8165%	-9.8183%	-9.8184%	-9.8188%
2		1.8933%	0.8845%	0.8147%	0.8147%	0.8076%
3	-6.1773%	-6.6820%	-6.7655%	-6.7721%	-6.7723%	-6.7743%
4		0.1823%	-1.6618%	-1.7726%	-1.7726%	-1.7880%
5	-2.5730%	-3.6211%	-3.7704%	-3.7813%	-3.7821%	-3.7876%
6			2.2858%	0.7807%	0.7472%	0.7295%

Table 6.18: Relative error between naïve Galerkin method and exact solution for Case 3

Mode	Naïve Galerkin method					
	Frequencies [rad/s]					
	Case 4					
Mode	1 Term	2 Terms	3 Terms	4 Terms	5 Terms	10 Terms
1	51.1819	50.1257	49.9222	49.9043	49.9043	49.9012
2		119.5823	117.1217	116.7886	116.7749	116.7671
3	127.9548	119.6618	117.3159	117.0319	117.0317	116.9942
4		200.3695	195.8356	194.9783	194.8910	194.8839
5	255.9096	225.7072	215.1582	213.4685	213.4473	213.2822
6			259.6424	254.4361	252.7522	252.3003

Table 6.19: Frequencies obtained with naïve Galerkin method for Case 4

Mode	Naïve Galerkin method					
	Relative error [%]					
	Case 4					
Mode	1 Term	2 Terms	3 Terms	4 Terms	5 Terms	10 Terms
1	5.7666%	3.5839%	3.1635%	3.1264%	3.1263%	3.1199%
2		-3.9193%	-5.8963%	-6.1639%	-6.1750%	-6.1812%
3	-1.2730%	-7.6717%	-9.4817%	-9.7009%	-9.7010%	-9.7299%
4		-3.6389%	-5.8193%	-6.2316%	-6.2736%	-6.2770%
5	0.7354%	-11.1534%	-15.3058%	-15.9710%	-15.9793%	-16.0443%
6			2.0539%	0.0076%	-0.6543%	-0.8319%

Table 6.20: Relative error between naïve Galerkin method and exact solution for Case 4

Mode	Naïve Galerkin method					
	Frequencies [rad/s]					
	Case 5					
Mode	1 Term	2 Terms	3 Terms	4 Terms	5 Terms	10 Terms
1	38.9239	38.0439	38.0433	38.033	38.0338	38.0328
2		115.6887	112.2373	111.9515	111.9377	111.9165
3	97.3097	91.3015	91.2675	91.1901	91.1896	91.1799
4		192.8224	181.5735	179.7126	179.6943	179.5708
5	194.6195	174.9413	174.5900	174.3389	174.3317	174.2918
6			214.5904	205.3066	205.0335	204.9166

Table 6.21: Frequencies obtained with naïve Galerkin method for Case 5

Mode	Naïve Galerkin method					
	Relative error [%]					
	Case 5					
Mode	1 Term	2 Terms	3 Terms	4 Terms	5 Terms	10 Terms
1	-12.8104%	-14.7816%	-14.7828%	-14.8042%	-14.8042%	-14.8065%
2		5.6701%	2.5176%	2.2565%	2.2439%	2.2246%
3	-11.9508%	-17.3873%	-17.4180%	-17.4881%	-17.4886%	-17.4973%
4		11.3600%	4.8634%	3.7888%	3.7782%	3.7069%
5	-1.6737%	-11.6156%	-11.7931%	-11.9200%	-11.9236%	-11.9437%
6			1.1773%	-3.1999%	-3.3287%	-3.3838%

Table 6.22: Relative error between naïve Galerkin method and exact solution for Case 5

Mode	Naïve Galerkin method					
	Frequencies [rad/s]					
	Case 6					
Mode	1 Term	2 Terms	3 Terms	4 Terms	5 Terms	10 Terms
1	32.6454	32.5383	32.5219	32.5206	32.5206	32.5203
2		91.7324	89.6315	89.5095	89.5095	89.4955
3	81.6134	80.8004	80.6783	80.6691	80.6688	80.6657
4		147.7625	141.6828	141.4154	141.4141	141.3681
5	163.2269	160.1357	159.7693	159.7459	159.7428	159.7281
6			199.3632	189.9891	189.9140	189.7765

Table 6.23: Frequencies obtained with naïve Galerkin method for Case 6

Mode	Naïve Galerkin method					
	Relative error [%]					
	Case 6					
Mode	1 Term	2 Terms	3 Terms	4 Terms	5 Terms	10 Terms
1	-20.5595%	-20.8200%	-20.8600%	-20.8630%	-20.8630%	-20.8637%
2		2.0072%	-0.3290%	-0.4647%	-0.4647%	-0.4802%
3	-11.7613%	-12.6404%	-12.7724%	-12.7823%	-12.7827%	-12.7861%
4		-4.7443%	-8.6636%	-8.8360%	-8.8368%	-8.8665%
5	-4.3214%	-6.1334%	-6.3481%	-6.3619%	-6.3637%	-6.3723%
6			7.6914%	2.6278%	2.5872%	2.5129%

Table 6.24: Relative error between naïve Galerkin method and exact solution for Case 6

Mode	Naïve Galerkin method					
	Frequencies [rad/s]					
	Case 7					
Mode	1 Term	2 Terms	3 Terms	4 Terms	5 Terms	10 Terms
1	22.6309	22.5187	22.5187	22.5176	22.5176	22.5175
1	36.2094	35.8555	35.8554	35.8514	35.8514	35.8510
1	58.8402	57.7652	57.7640	57.7499	57.7499	57.7482
1		81.8107	81.2752	81.2607	81.2577	81.2564
1	90.5234	87.8408	87.8323	87.7930	87.7929	87.7880
1		96.7161	95.9182	95.8902	95.8858	95.8833

Table 6.25: Frequencies obtained with naïve Galerkin method for Case 7

Mode	Naïve Galerkin method					
	Relative error [%]					
	Case 7					
Mode	1 Term	2 Terms	3 Terms	4 Terms	5 Terms	10 Terms
1	0.1946%	-0.3019%	-0.3019%	-0.3068%	-0.3068%	-0.3073%
2	-3.8277%	-4.7674%	-4.7677%	-4.7784%	-4.7784%	-4.7795%
3	-4.7867%	-6.5263%	-6.5282%	-6.5510%	-6.5511%	-6.5537%
4		-0.2727%	-0.9255%	-0.9432%	-0.9468%	-0.9484%
5	-4.0815%	-6.9240%	-6.9330%	-6.9746%	-6.9747%	-6.9799%
6		1.0130%	0.1798%	0.1506%	0.1459%	0.1433%

Table 6.26: Relative error between naïve Galerkin method and exact solution for Case 7

Mode	Naïve Galerkin method					
	Frequencies [rad/s]					
	Case 8					
Mode	1 Term	2 Terms	3 Terms	4 Terms	5 Terms	10 Terms
1	24.3274	24.0414	24.0414	24.0386	24.0386	24.0383
2	38.9239	38.0439	38.0433	38.0338	38.0338	38.0328
3	63.2513	60.6954	60.6898	60.6589	60.6588	60.6553
4		97.2556	94.9773	94.8279	94.8180	94.8066
5		115.6887	112.2373	111.9515	111.9377	111.9165
6	97.3097	91.3015	91.2675	91.1901	91.1896	91.1799

Table 6.27: Frequencies obtained with naïve Galerkin method for Case 8

Mode	Naïve Galerkin method					
	Relative error [%]					
	Case 8					
Mode	1 Term	2 Terms	3 Terms	4 Terms	5 Terms	10 Terms
1	-2.3771%	-3.5249%	-3.5250%	-3.5361%	-3.5361%	-3.5372%
2	-12.8104%	-14.7816%	-14.7828%	-14.8042%	-14.8042%	-14.8065%
3	-14.5345%	-17.9881%	-17.9956%	-18.0374%	-18.0375%	-18.0423%
4		2.2443%	-0.1509%	-0.3079%	-0.3183%	-0.3303%
5		5.6701%	2.5176%	2.2565%	2.2439%	2.2246%
6	-11.9507%	-17.3871%	-17.4179%	-17.4880%	-17.4884%	-17.4972%

Table 6.28: Relative error between naïve Galerkin method and exact solution for Case 8

Mode	Naïve Galerkin method					
	Frequencies [rad/s]					
	Case 9					
Mode	1 Term	2 Terms	3 Terms	4 Terms	5 Terms	10 Terms
1	22.6309	21.9602	21.9581	21.9483	21.9482	21.9470
2		39.4783	38.8568	38.8068	38.8036	38.7995
3			61.1140	59.5858	59.5598	59.5293
4	76.9449	71.0899	70.9366	70.8518	70.8479	70.8317
5				97.7947	95.2334	94.9320
6		103.6588	98.4448	96.6539	96.6535	96.5343

Table 6.29: Frequencies obtained with naïve Galerkin method for Case 9

Mode	Naïve Galerkin method					
	Relative error [%]					
	Case 9					
Mode	1 Term	2 Terms	3 Terms	4 Terms	5 Terms	10 Terms
1	-4.0814%	-6.9239%	-6.9329%	-6.9745%	-6.9746%	-6.9798%
2		4.1169%	2.4777%	2.3458%	2.3375%	2.3266%
3			0.2174%	-2.2885%	-2.3312%	-2.3812%
4	4.1193%	-3.8035%	-4.0109%	-4.1257%	-4.1310%	-4.1529%
5				3.9794%	1.2561%	0.9357%
6		6.6384%	1.2745%	-0.5679%	-0.5683%	-0.6909%

Table 6.30: Relative error between naïve Galerkin method and exact solution for Case 9

Mode	Naïve Galerkin method					
	Frequencies [rad/s]					
	Case 10					
Mode	1 Term	2 Terms	3 Terms	4 Terms	5 Terms	10 Terms
1	24.3274	22.8254	22.8169	22.7975	22.7974	22.7950
2		48.2056	45.3934	44.9282	44.9236	44.8927
3			71.8788	68.3137	68.0910	68.0642
4	82.7133	72.1063	71.7571	71.6400	71.6306	71.6058
5				118.2536	108.7166	106.6804
6		129.7064	109.4210	102.5927	102.5171	102.2219

Table 6.31: Frequencies obtained with naïve Galerkin method for Case 10

Mode	Naïve Galerkin method					
	Relative error [%]					
	Case 10					
1 Term	2 Terms	3 Terms	4 Terms	5 Terms	10 Terms	
1	-11.9506%	-17.3871%	-17.4178%	-17.4879%	-17.4883%	-17.4971%
2		11.3600%	4.8634%	3.7887%	3.7781%	3.7068%
3			-0.2042%	-5.1539%	-5.4632%	-5.5004%
4	7.2167%	-6.5326%	-6.9852%	-7.1370%	-7.1492%	-7.1814%
5				12.9518%	3.8423%	1.8975%
6		14.9868%	-2.9965%	-9.0499%	-9.1169%	-9.3787%

Table 6.32: Relative error between naïve Galerkin method and exact solution for Case 10

In all these cases, we observe that the frequency has a decreasing trend in function of the Galerkin approximation terms.

The exact solution can be lower or higher than the frequency obtained by the naïve Galerkin method but anyway, through this approach, increasing the number of terms the value of the frequency decreases.

We have obtained three patterns in total: in the first pattern we obtain a frequency that in the beginning is higher than the exact one and after a decreasing behavior, it ends anyway higher than the exact one (e.g. the first natural frequency of Case 1), in the second pattern the frequency starts higher but ends lower (e.g. the fourth natural frequency of Case 9) and in conclusion in the third pattern the frequency starts lower and ends more lower (e.g. the second natural frequency of Case 2).

We show the plot of the second pattern, i.e. the fourth natural frequency of Case 9. In this way, we see the behavior of the error in function of the number of Galerkin terms.

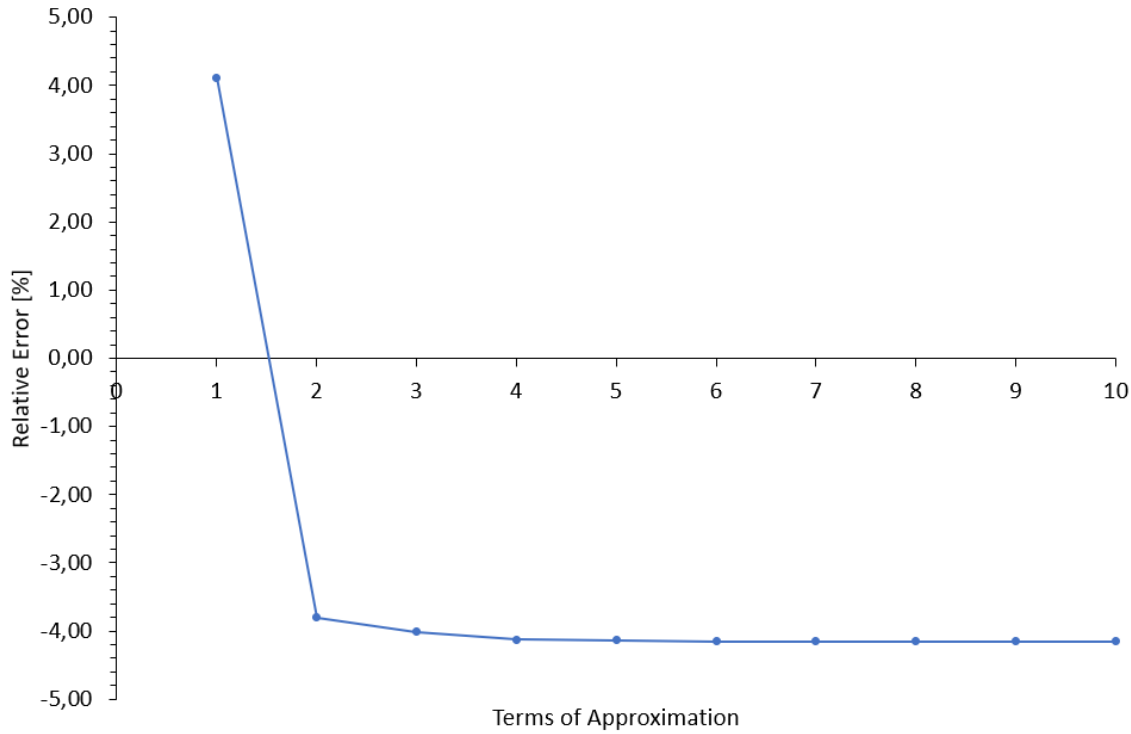


Figure 6.3: Trend of relative error of fourth natural frequency obtained with naïve Galerkin method for Case 9

6.6.3 Rigorous Galerkin method

We report the result of Galerkin method up 10 terms. For each case we report a table with the frequency value, after that a table with the relative error using the following formula:

$$\varepsilon = \frac{\omega_{\text{Galerkin}} - \omega_{\text{exact}}}{\omega_{\text{exact}}} \times 100 \quad (6.6.4)$$

And, in conclusion, a chart of the relative error in function of the number of terms.

Rigorous Galerkin method						
Mode	Frequencies [rad/s]					
	Case 1					
1	42.8955	42.1596	41.4168	41.0100	40.9660	40.7270
2		107.7234	104.4985	102.1641	101.5716	101.0984
3	108.9781	107.0490	105.5209	104.7518	104.6483	104.3427
4		173.5322	169.5910	166.6639	165.6704	165.2734
5			215.3084	210.8741	208.3348	206.9733
6	220.6238	215.8230	211.6194	209.1886	208.6383	208.1606

Table 6.33: Frequencies obtained with rigorous Galerkin method for Case 1

Mode	Rigorous Galerkin method					
	Relative error [%]					
	Case 1					
Mode	1 Term	2 Terms	3 Terms	4 Terms	5 Terms	10 Terms
1	6.0495%	4.2301%	2.3937%	1.3880%	1.2792%	0.6883%
2		7.0879%	3.8821%	1.5614%	0.9724%	0.5020%
3	4.7728%	2.9181%	1.4491%	0.7096%	0.6101%	0.3163%
4		5.1761%	2.7874%	1.0133%	0.4112%	0.1706%
5			4.1815%	2.0358%	0.8071%	0.1483%
6	6.2054%	3.8944%	1.8708%	0.7007%	0.4358%	0.2058%

Table 6.34: Relative error between rigorous Galerkin method and exact solution for Case 1

Mode	Rigorous Galerkin method					
	Frequencies [rad/s]					
	Case 2					
Mode	1 Term	2 Terms	3 Terms	4 Terms	5 Terms	10 Terms
1	40.7076	38.4596	38.1918	38.0360	37.9551	37.8009
2	101.7690	95.9307	94.8487	94.7618	94.5832	94.4621
3		101.8046	97.5942	96.6099	96.5804	96.0993
4		163.2580	155.3114	153.1887	153.1635	152.2871
5	203.5379	186.4942	182.2839	182.2717	181.8099	181.6324
6			203.8280	189.7660	187.3467	185.2831

Table 6.35: Frequencies obtained with rigorous Galerkin method for Case 2

Mode	Rigorous Galerkin method					
	Relative error [%]					
	Case 2					
Mode	1 Term	2 Terms	3 Terms	4 Terms	5 Terms	10 Terms
1	8.1196%	2.1489%	1.4376%	1.0239%	0.8090%	0.3995%
2	7.8343%	1.6481%	0.5016%	0.4096%	0.2203%	0.0919%
3		6.3277%	1.9303%	0.9021%	0.8714%	0.3689%
4		7.6408%	2.4014%	1.0019%	0.9852%	0.4074%
5	12.0966%	2.7099%	0.3912%	0.3844%	0.1301%	0.0323%
6			10.8744%	3.2252%	1.9092%	0.7866%

Table 6.36: Relative error between rigorous Galerkin method and exact solution for Case 2

Mode	Rigorous Galerkin method					
	Frequencies [rad/s]					
	Case 3					
Mode	1 Term	2 Terms	3 Terms	4 Terms	5 Terms	10 Terms
1	37.6080	35.7939	35.6745	35.6674	35.6196	35.5792
2		94.6280	87.5117	87.1568	86.8965	85.8492
3	91.3275	85.9100	85.8320	85.7414	85.6497	85.6161
4		151.3072	140.9828	140.8134	140.4308	139.5353
5	178.3542	165.4650	165.3866	165.1555	164.9774	164.9063
6			190.1972	178.1963	178.1727	176.1503

Table 6.37: Frequencies obtained with rigorous Galerkin method for Case 3

Mode	Rigorous Galerkin method					
	Relative error [%]					
	Case 3					
Mode	1 Term	2 Terms	3 Terms	4 Terms	5 Terms	10 Terms
1	5.7790%	0.6765%	0.3407%	0.3206%	0.1862%	0.0726%
2		11.2336%	2.8685%	2.4513%	2.1454%	0.9143%
3	6.6838%	0.3553%	0.2642%	0.1584%	0.0513%	0.0121%
4		8.8939%	1.4635%	1.3417%	1.0663%	0.4218%
5	8.1737%	0.3563%	0.3087%	0.1686%	0.0605%	0.0174%
6			8.7834%	1.9194%	1.9059%	0.7493%

Table 6.38: Relative error between rigorous Galerkin method and exact solution for Case 3

Mode	Rigorous Galerkin method					
	Frequencies [rad/s]					
	Case 4					
Mode	1 Term	2 Terms	3 Terms	4 Terms	5 Terms	10 Terms
1	56.3937	54.7846	52.5630	50.6011	49.9811	49.3204
2		143.1332	136.0003	129.0339	126.0312	124.9824
3	143.9796	140.0831	135.8552	132.3525	131.0046	130.2839
4		230.7939	222.7310	214.5993	210.0490	208.1373
5	292.5338	283.4800	272.5929	262.2175	256.5512	254.3917
6			286.2703	276.7141	269.4116	259.7112

Table 6.39: Frequencies obtained with rigorous Galerkin method for Case 4

Mode	Rigorous Galerkin method					
	Relative error [%]					
	Case 4					
Mode	1 Term	2 Terms	3 Terms	4 Terms	5 Terms	10 Terms
1	16.5367%	13.2115%	8.6205%	4.5664%	3.2850%	1.9198%
2		15.0031%	9.2720%	3.6747%	1.2622%	0.4195%
3	11.0914%	8.0849%	4.8228%	2.1201%	1.0802%	0.5240%
4		10.9928%	7.1152%	3.2045%	1.0162%	0.0968%
5	15.1520%	11.5881%	7.3025%	3.2184%	0.9880%	0.1379%
6			12.5202%	8.7640%	5.8937%	2.0810%

Table 6.40: Relative error between rigorous Galerkin method and exact solution for Case 4

Mode	Rigorous Galerkin method					
	Frequencies [rad/s]					
	Case 5					
Mode	1 Term	2 Terms	3 Terms	4 Terms	5 Terms	10 Terms
1	53.2987	47.2508	45.4493	45.4041	45.0611	44.8523
2		133.7036	122.4214	115.5079	114.9329	112.2456
3	133.2468	118.3599	111.5564	111.2504	110.8841	110.5979
4		213.5049	193.9276	181.5420	180.0448	176.4892
5	266.4937	224.6408	202.6623	200.3225	199.8622	198.6413
6			266.8265	231.0350	216.5384	213.5624

Table 6.41: Frequencies obtained with rigorous Galerkin method for Case 5

Mode	Rigorous Galerkin method					
	Relative error [%]					
	Case 5					
Mode	1 Term	2 Terms	3 Terms	4 Terms	5 Terms	10 Terms
1	19.3893%	5.8420%	1.8066%	1.7054%	0.9371%	0.4693%
2		22.1249%	11.8198%	5.5049%	4.9797%	2.5252%
3	20.5663%	7.0961%	0.9401%	0.6632%	0.3317%	0.0727%
4		23.3047%	11.9983%	4.8453%	3.9806%	1.9271%
5	34.6388%	13.4938%	2.3897%	1.2076%	0.9751%	0.3582%
6			25.8061%	8.9308%	2.0958%	0.6926%

Table 6.42: Relative error between rigorous Galerkin method and exact solution for Case 5

Mode	Rigorous Galerkin method					
	Frequencies [rad/s]					
	Case 6					
Mode	1 Term	2 Terms	3 Terms	4 Terms	5 Terms	10 Terms
1	47.8910	41.3673	41.3660	41.1838	41.1395	41.1070
2		120.1310	95.7548	95.7540	93.8713	91.7910
3	113.8374	94.2389	93.8193	93.0996	93.0811	92.7696
4		192.8263	159.6190	158.7629	156.7139	155.7087
5	218.0728	173.8212	172.9385	171.6423	171.5879	171.0498
6			243.0750	201.5275	198.7658	190.7107

Table 6.43: Frequencies obtained with rigorous Galerkin method for Case 6

Mode	Rigorous Galerkin method					
	Relative error [%]					
	Case 6					
Mode	1 Term	2 Terms	3 Terms	4 Terms	5 Terms	10 Terms
1	16.5399%	0.6649%	0.6617%	0.2183%	0.1104%	0.0313%
2		33.5866%	6.4802%	6.4792%	4.3856%	2.0724%
3	23.0785%	1.8891%	1.4353%	0.6573%	0.6372%	0.3004%
4		24.3062%	2.8990%	2.3471%	1.0262%	0.3782%
5	27.8276%	1.8886%	1.3712%	0.6114%	0.5795%	0.2641%
6			31.3035%	8.8606%	7.3687%	3.0176%

Table 6.44: Relative error between rigorous Galerkin method and exact solution for Case 6

Mode	Rigorous Galerkin method					
	Frequencies [rad/s]					
	Case 7					
Mode	1 Term	2 Terms	3 Terms	4 Terms	5 Terms	10 Terms
1	25.4422	23.4563	23.2566	23.0557	22.9783	22.7835
2	40.7076	38.4596	38.1918	38.0360	37.9551	37.8009
3	66.1498	62.7791	62.2770	62.1550	62.0447	61.9144
4		86.6126	83.4384	82.7033	82.6808	82.3103
5	101.7690	95.9307	94.8487	94.7618	94.5832	94.4621
6		101.8046	97.5942	96.6099	96.5804	96.0993

Table 6.45: Frequencies obtained with rigorous Galerkin method for Case 7

Mode	Rigorous Galerkin method					
	Relative error [%]					
	Case 7					
Mode	1 Term	2 Terms	3 Terms	4 Terms	5 Terms	10 Terms
1	12.6416%	3.8491%	2.9649%	2.0757%	1.7328%	0.8704%
2	8.1196%	2.1489%	1.4376%	1.0239%	0.8090%	0.3995%
3	7.0415%	1.5871%	0.7746%	0.5773%	0.3987%	0.1879%
4		5.5808%	1.7115%	0.8154%	0.7879%	0.3364%
5	7.8343%	1.6481%	0.5016%	0.4096%	0.2203%	0.0919%
6		6.3277%	1.9303%	0.9021%	0.8714%	0.3689%

Table 6.46: Relative error between rigorous Galerkin method and exact solution for Case 7

Mode	Rigorous Galerkin method					
	Frequencies [rad/s]					
	Case 8					
Mode	1 Term	2 Terms	3 Terms	4 Terms	5 Terms	10 Terms
1	33.3117	27.7291	26.3069	26.1381	25.7229	25.3618
2	53.2987	47.2508	45.4493	45.4041	45.0611	44.8523
3	86.6104	77.8334	74.5509	74.5414	74.2025	74.0585
4		114.0204	105.4640	100.1451	99.6998	97.4761
5		133.7036	122.4214	115.5079	114.9329	112.2456
6	133.2468	118.3599	111.5564	111.2504	110.8841	110.5979

Table 6.47: Frequencies obtained with rigorous Galerkin method for Case 8

Mode	Rigorous Galerkin method					
	Relative error [%]					
	Case 8					
Mode	1 Term	2 Terms	3 Terms	4 Terms	5 Terms	10 Terms
1	33.6757%	11.2732%	5.5663%	4.8889%	3.2229%	1.7737%
2	19.3893%	5.8420%	1.8066%	1.7054%	0.9371%	0.4693%
3	17.0285%	5.1688%	0.7336%	0.7207%	0.2628%	0.0682%
4		19.8691%	10.8737%	5.2820%	4.8139%	2.4761%
5		22.1249%	11.8198%	5.5049%	4.9797%	2.5252%
6	20.5665%	7.0963%	0.9402%	0.6634%	0.3319%	0.0729%

Table 6.48: Relative error between rigorous Galerkin method and exact solution for Case 8

Mode	Rigorous Galerkin method					
	Frequencies [rad/s]					
	Case 9					
Mode	1 Term	2 Terms	3 Terms	4 Terms	5 Terms	10 Terms
1	25.4422	23.9827	23.7122	23.6905	23.6458	23.6155
2		40.8145	38.8279	38.2972	38.2909	38.0718
3			66.5754	62.5401	61.6302	61.2217
4	86.5036	76.8252	74.2320	74.2282	74.0127	73.9258
5				102.5554	97.2838	94.7905
6		105.7783	101.1889	98.2457	98.0064	97.4907

Table 6.49: Frequencies obtained with rigorous Galerkin method for Case 9

Mode	Rigorous Galerkin method					
	Relative error [%]					
	Case 9					
Mode	1 Term	2 Terms	3 Terms	4 Terms	5 Terms	10 Terms
1	7.8344%	1.6482%	0.5017%	0.4097%	0.2204%	0.0920%
2		7.6408%	2.4014%	1.0019%	0.9852%	0.4074%
3			9.1732%	2.5561%	1.0640%	0.3941%
4	17.0538%	3.9574%	0.4484%	0.4432%	0.1516%	0.0340%
5				9.0411%	3.4362%	0.7852%
6		8.8188%	4.0974%	1.0697%	0.8235%	0.2930%

Table 6.50: Relative error between rigorous Galerkin method and exact solution for Case 9

Mode	Rigorous Galerkin method					
	Frequencies [rad/s]					
	Case 10					
Mode	1 Term	2 Terms	3 Terms	4 Terms	5 Terms	10 Terms
1	33.3117	29.5900	27.8891	27.8126	27.7210	27.6495
1		53.3762	48.4819	45.3855	45.0112	44.1223
1			87.3747	77.9031	72.9811	72.1427
1	113.2598	90.4901	79.3196	78.1232	77.9641	77.4380
1				134.6683	122.4002	108.3460
1		139.7581	131.0958	120.4313	114.2840	113.0691

Table 6.51: Frequencies obtained with rigorous Galerkin method for Case 10

Rigorous Galerkin method						
	Relative error [%]					
	Case 10					
Mode	1 Term	2 Terms	3 Terms	4 Terms	5 Terms	10 Terms
1	20.5666%	7.0964%	0.9403%	0.6634%	0.3319%	0.0730%
1		23.3046%	11.9982%	4.8452%	3.9805%	1.9271%
1			21.3101%	8.1598%	1.3262%	0.1622%
1	46.8125%	17.2973%	2.8177%	1.2668%	1.0606%	0.3786%
1				28.6305%	16.9125%	3.4883%
1		23.8978%	16.2185%	6.7643%	1.3146%	0.2376%

Table 6.52: Relative error between rigorous Galerkin method and exact solution for Case 10

In all these cases, we see that the relative error tends to convergence. It starts from a specific value and, increasing the number of terms of approximation, the error decreases. In general, it is less than 1%. Only in few cases, it is between the 2-3%. We provide a plot for one case so that we can graphically see the trend of the error. In this specific case, we have the relative error for the fourth natural frequency of Case 10 in function of the number of Galerkin terms of approximation.

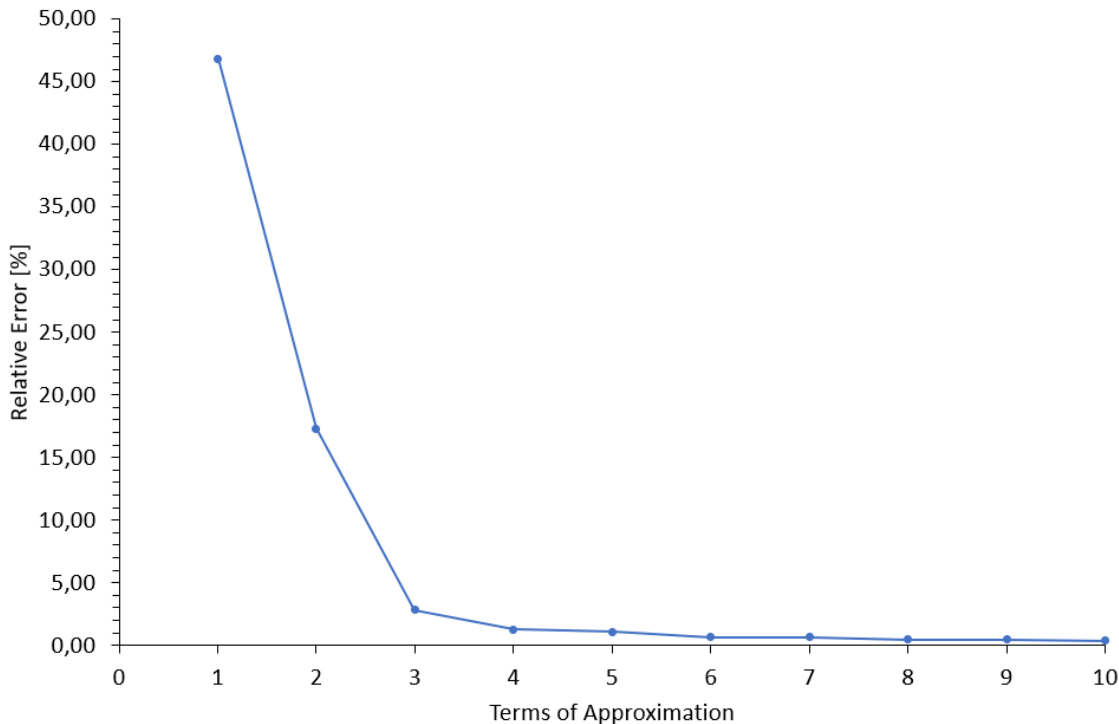


Figure 6.4: Trend of relative error of fourth natural frequency obtained with rigorous Galerkin method for Case 10

6.6.4 Finite Element Method solution

One more analysis has also been conducted with FEM. We use the FEM software Strand7. This code was developed by a group of academics from the University of Sydney and the University of New South Wales in 2000 (see Ref. [38]).

The mesh is made of Quad4 element of dimension $0,05m \times 0,05m$. According to [38], the Quad4 element implements the think plate theory: Kirchhoff-Love plate theory.

We report the results in the following tables in which the non-dimensional frequency, the relative error between the FEM analysis and the exact solution (evaluated with the formula (6.6.5)), the number of half-waves in x and y direction and a depiction of the mode shape are present.

$$\varepsilon = \frac{\omega_{exact} - \omega_{FEM}}{\omega_{exact}} \times 100 \quad (6.6.5)$$

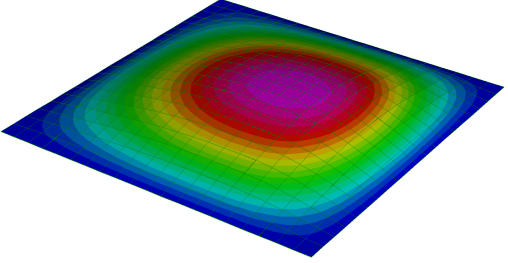
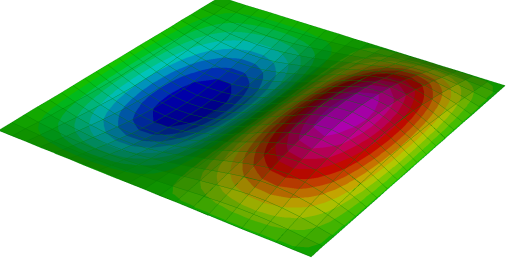
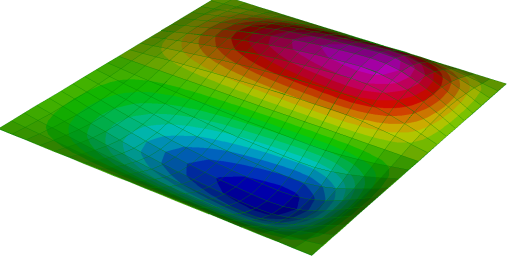
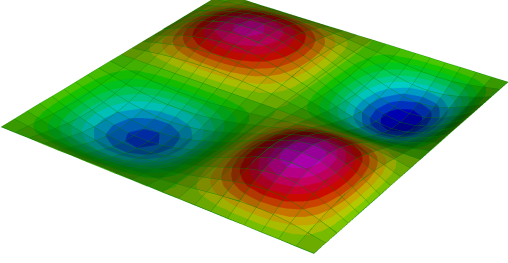
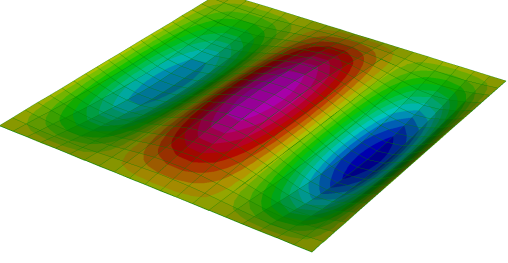
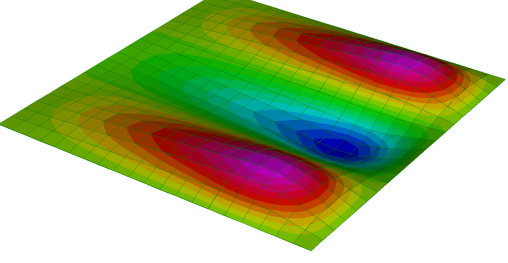
Case 1	
Mode 1 Natural Frequency: 2.6242 Relative Error: 0.1774% Number of half-waves in x direction: 1 Number of half-waves in y direction: 1	
Mode 2 Natural Frequency: 6.5145 Relative Error: 0.3585% Number of half-waves in x direction: 2 Number of half-waves in y direction: 1	
Mode 3 Natural Frequency: 6.7415 Relative Error: 0.2770% Number of half-waves in x direction: 1 Number of half-waves in y direction: 2	
Mode 4 Natural Frequency: 10.6414 Relative Error: 0.7656% Number of half-waves in x direction: 2 Number of half-waves in y direction: 2	
Mode 5 Natural Frequency: 13.3849 Relative Error: 0.3513% Number of half-waves in x direction: 3 Number of half-waves in y direction: 1	
Mode 6 Natural Frequency: 13.4475 Relative Error: 0.3986% Number of half-waves in x direction: 1 Number of half-waves in y direction: 3	

Table 6.53: Results obtained with FEM software Strand7 for Case 1

Case 2	
Mode 1 Natural Frequency: 2.4471 Relative Error: 0.1877% Number of half-waves in x direction: 1 Number of half-waves in y direction: 1	
Mode 2 Natural Frequency: 6.1142 Relative Error: 0.3200% Number of half-waves in x direction: 1 Number of half-waves in y direction: 2	
Mode 3 Natural Frequency: 6.2050 Relative Error: 0.2870% Number of half-waves in x direction: 2 Number of half-waves in y direction: 1	
Mode 4 Natural Frequency: 9.7853 Relative Error: 0.7326% Number of half-waves in x direction: 2 Number of half-waves in y direction: 2	
Mode 5 Natural Frequency: 11.7398 Relative Error: 0.5200% Number of half-waves in x direction: 1 Number of half-waves in y direction: 3	
Mode 6 Natural Frequency: 11.8971 Relative Error: 0.4279% Number of half-waves in x direction: 3 Number of half-waves in y direction: 1	

Table 6.54: Results obtained with FEM software Strand7 for Case 2

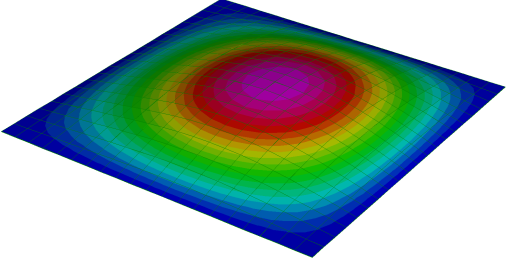
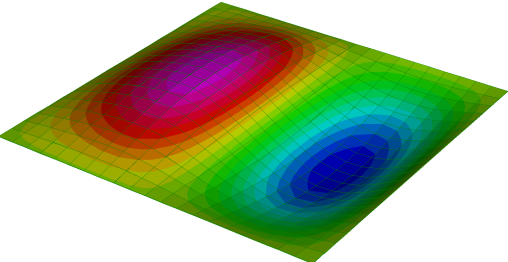
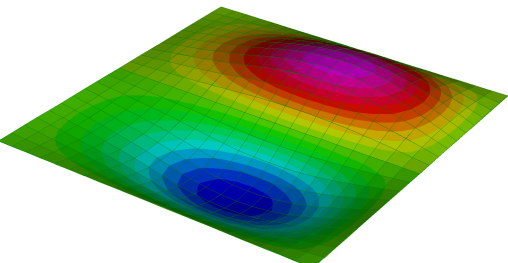
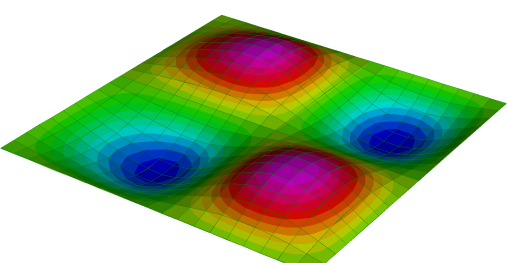
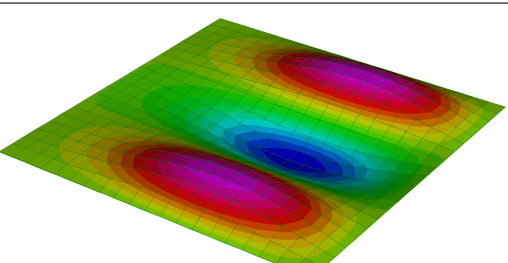
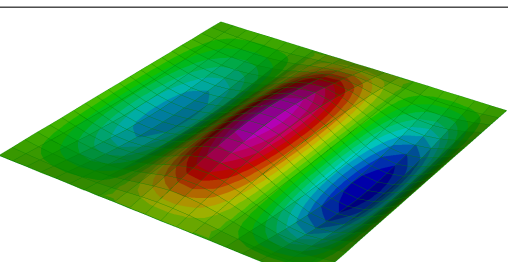
Case 3	
Mode 1 Natural Frequency: 2.3062 Relative Error: 0.1968% Number of half-waves in x direction: 1 Number of half-waves in y direction: 1	
Mode 2 Natural Frequency: 5.5119 Relative Error: 0.3117% Number of half-waves in x direction: 2 Number of half-waves in y direction: 1	
Mode 3 Natural Frequency: 5.5446 Relative Error: 0.3461% Number of half-waves in x direction: 1 Number of half-waves in y direction: 2	
Mode 4 Natural Frequency: 8.9648 Relative Error: 0.7317% Number of half-waves in x direction: 2 Number of half-waves in y direction: 2	
Mode 5 Natural Frequency: 10.6673 Relative Error: 0.4543% Number of half-waves in x direction: 1 Number of half-waves in y direction: 3	
Mode 6 Natural Frequency: 11.3293 Relative Error: 0.3013% Number of half-waves in x direction: 3 Number of half-waves in y direction: 1	

Table 6.55: Results obtained with FEM software Strand7 for Case 3

Case 4	
Mode 1 Natural Frequency: 3.1398 Relative Error: 0.1713% Number of half-waves in x direction: 1 Number of half-waves in y direction: 1	
Mode 2 Natural Frequency: 8.0557 Relative Error: 0.4136% Number of half-waves in x direction: 2 Number of half-waves in y direction: 1	
Mode 3 Natural Frequency: 8.4018 Relative Error: 0.2573% Number of half-waves in x direction: 1 Number of half-waves in y direction: 2	
Mode 4 Natural Frequency: 13.4084 Relative Error: 0.7855% Number of half-waves in x direction: 2 Number of half-waves in y direction: 2	
Mode 5 Natural Frequency: 16.4167 Relative Error: 0.5717% Number of half-waves in x direction: 1 Number of half-waves in y direction: 3	
Mode 6 Natural Frequency: 16.4835 Relative Error: 0.3147% Number of half-waves in x direction: 3 Number of half-waves in y direction: 1	

Table 6.56: Results obtained with FEM software Strand7 for Case 4

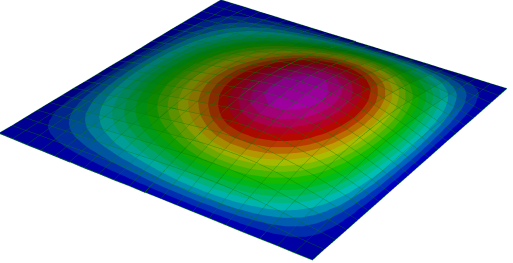
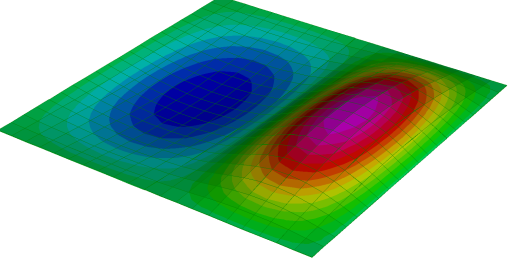
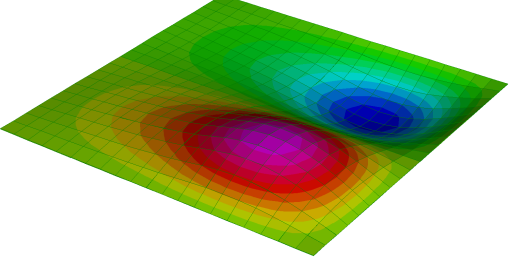
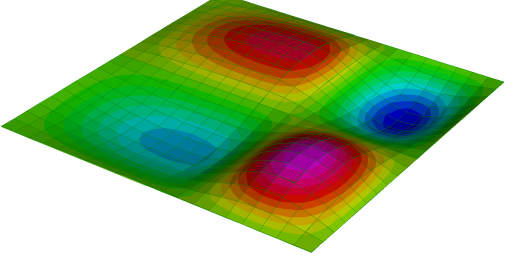
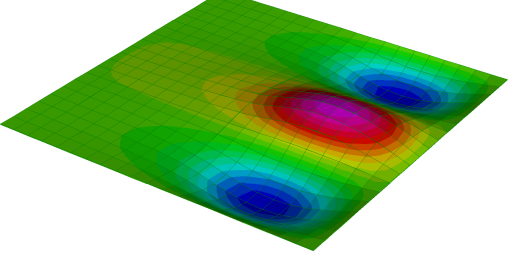
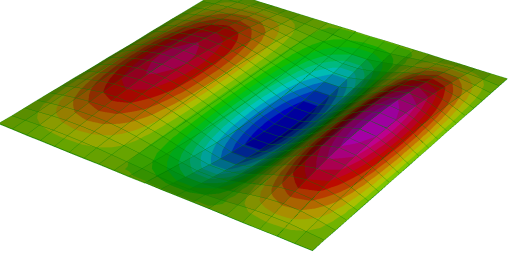
Case 5	
Mode 1 Natural Frequency: 2.8961 Relative Error: 0.1861% Number of half-waves in x direction: 1 Number of half-waves in y direction: 1	
Mode 2 Natural Frequency: 7.0957 Relative Error: 0.2789% Number of half-waves in x direction: 2 Number of half-waves in y direction: 1	
Mode 3 Natural Frequency: 7.1546 Relative Error: 0.3944% Number of half-waves in x direction: 1 Number of half-waves in y direction: 2	
Mode 4 Natural Frequency: 11.1758 Relative Error: 0.6934% Number of half-waves in x direction: 2 Number of half-waves in y direction: 2	
Mode 5 Natural Frequency: 12.7613 Relative Error: 0.8013% Number of half-waves in x direction: 1 Number of half-waves in y direction: 3	
Mode 6 Natural Frequency: 13.7122 Relative Error: 0.5259% Number of half-waves in x direction: 3 Number of half-waves in y direction: 1	

Table 6.57: Results obtained with FEM software Strand7 for Case 5

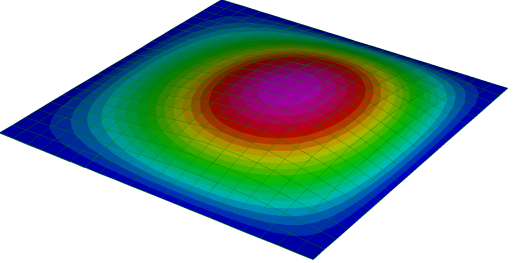
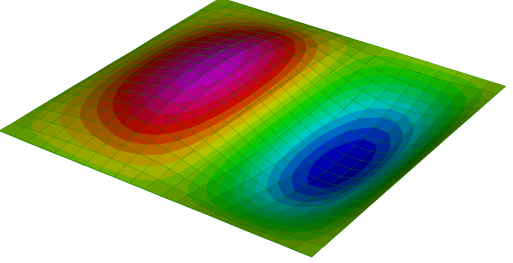
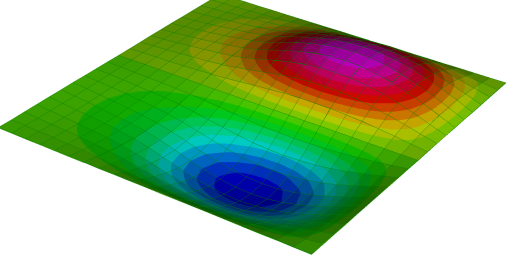
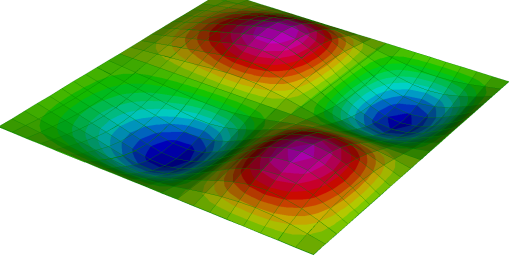
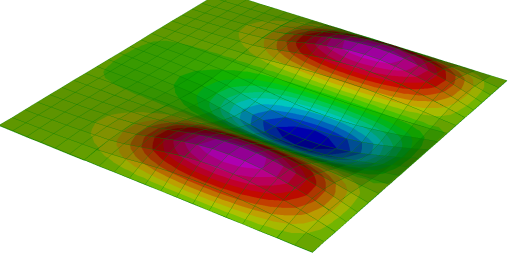
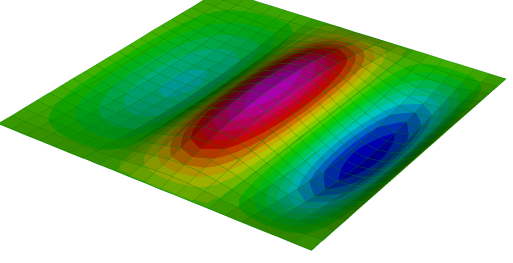
Case 6	
Mode 1 Natural Frequency: 2.6654 Relative Error: 0.2049% Number of half-waves in x direction: 1 Number of half-waves in y direction: 1	
Mode 2 Natural Frequency: 5.8246 Relative Error: 0.3435% Number of half-waves in x direction: 2 Number of half-waves in y direction: 1	
Mode 3 Natural Frequency: 5.9857 Relative Error: 0.4265% Number of half-waves in x direction: 1 Number of half-waves in y direction: 2	
Mode 4 Natural Frequency: 10.0109 Relative Error: 0.7051% Number of half-waves in x direction: 2 Number of half-waves in y direction: 2	
Mode 5 Natural Frequency: 11.0230 Relative Error: 0.5854% Number of half-waves in x direction: 1 Number of half-waves in y direction: 3	
Mode 6 Natural Frequency: 11.9939 Relative Error: 0.3160% Number of half-waves in x direction: 3 Number of half-waves in y direction: 1	

Table 6.58: Results obtained with FEM software Strand7 for Case 6

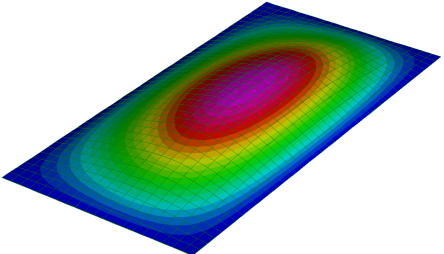
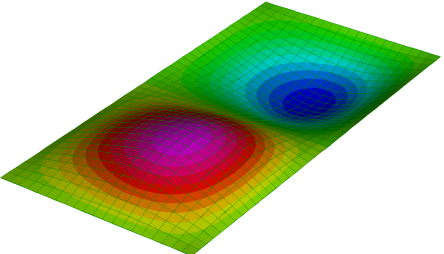
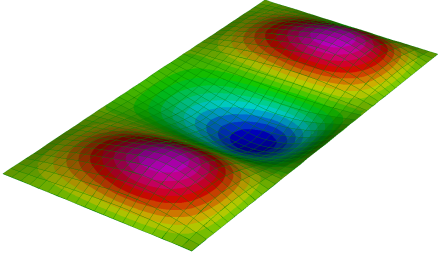
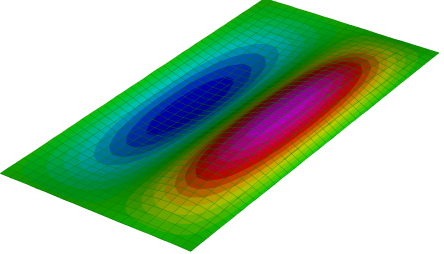
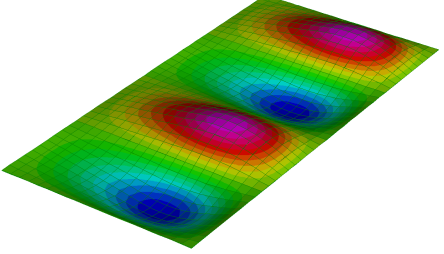
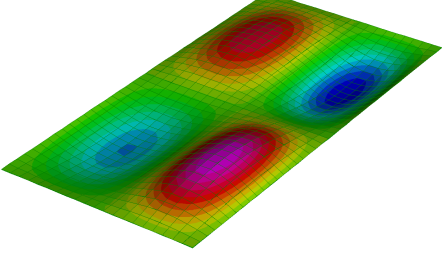
Case 7	
Mode 1 Natural Frequency: 5.8668 Relative Error: 0.0893% Number of half-waves in x direction: 1 Number of half-waves in y direction: 1	
Mode 2 Natural Frequency: 9.7698 Relative Error: 0.1877% Number of half-waves in x direction: 1 Number of half-waves in y direction: 2	
Mode 3 Natural Frequency: 16.0248 Relative Error: 0.2562% Number of half-waves in x direction: 1 Number of half-waves in y direction: 3	
Mode 4 Natural Frequency: 21.3106 Relative Error: 0.0762% Number of half-waves in x direction: 2 Number of half-waves in y direction: 1	
Mode 5 Natural Frequency: 24.4567 Relative Error: 0.3200% Number of half-waves in x direction: 1 Number of half-waves in y direction: 4	
Mode 6 Natural Frequency: 24.8202 Relative Error: 0.2870% Number of half-waves in x direction: 2 Number of half-waves in y direction: 2	

Table 6.59: Results obtained with FEM software Strand7 for Case 7

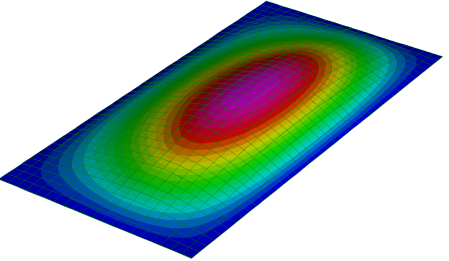
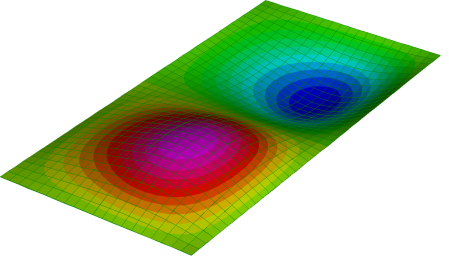
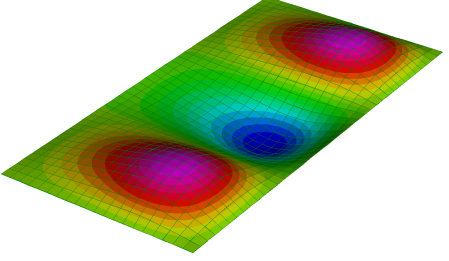
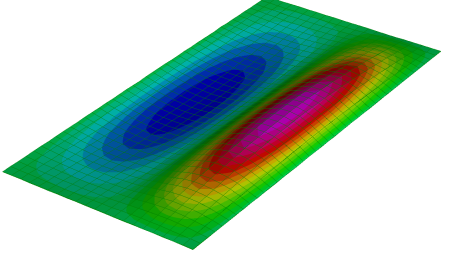
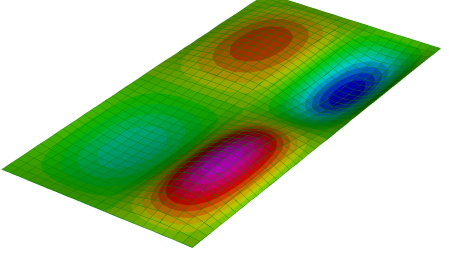
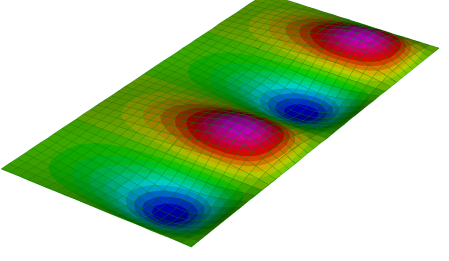
Case 8	
Mode 1 Natural Frequency: 6.4715 Relative Error: 0.1087% Number of half-waves in x direction: 1 Number of half-waves in y direction: 1	
Mode 2 Natural Frequency: 11.5844 Relative Error: 0.1861% Number of half-waves in x direction: 1 Number of half-waves in y direction: 2	
Mode 3 Natural Frequency: 19.1899 Relative Error: 0.2616% Number of half-waves in x direction: 1 Number of half-waves in y direction: 3	
Mode 4 Natural Frequency: 24.7138 Relative Error: 0.0615% Number of half-waves in x direction: 2 Number of half-waves in y direction: 1	
Mode 5 Natural Frequency: 28.3829 Relative Error: 0.2789% Number of half-waves in x direction: 2 Number of half-waves in y direction: 2	
Mode 6 Natural Frequency: 28.6185 Relative Error: 0.3942% Number of half-waves in x direction: 1 Number of half-waves in y direction: 4	

Table 6.60: Results obtained with FEM software Strand7 for Case 8

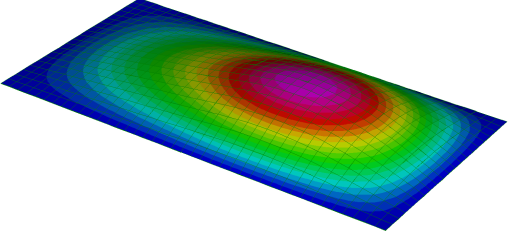
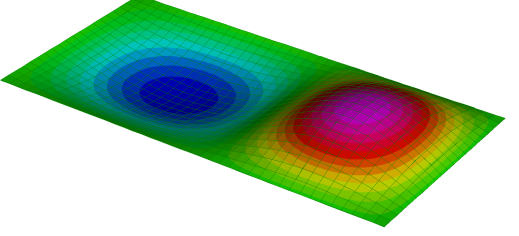
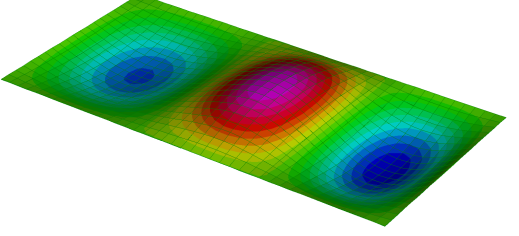
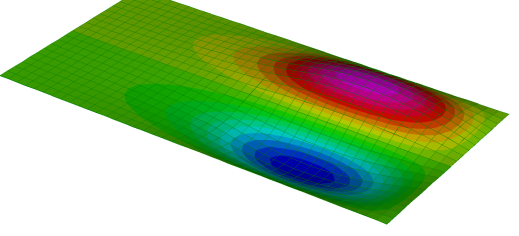
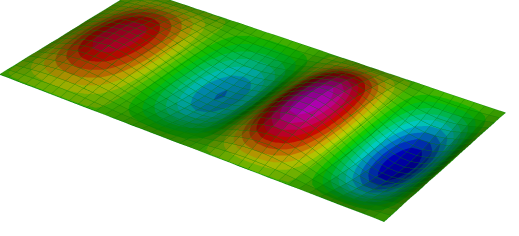
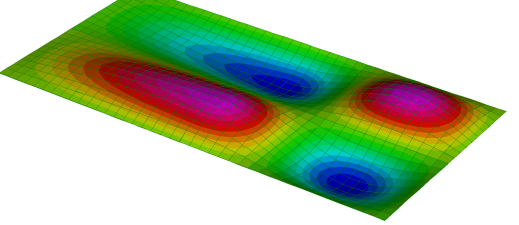
Case 9	
Mode 1 Natural Frequency: 1.5322 Relative Error: 0.0797% Number of half-waves in x direction: 1 Number of half-waves in y direction: 1	
Mode 2 Natural Frequency: 2.4599 Relative Error: 0.1833% Number of half-waves in x direction: 2 Number of half-waves in y direction: 1	
Mode 3 Natural Frequency: 3.9526 Relative Error: 0.2724% Number of half-waves in x direction: 3 Number of half-waves in y direction: 1	
Mode 4 Natural Frequency: 4.7940 Relative Error: 0.1882% Number of half-waves in x direction: 1 Number of half-waves in y direction: 2	
Mode 5 Natural Frequency: 6.0952 Relative Error: 0.2880% Number of half-waves in x direction: 4 Number of half-waves in y direction: 1	
Mode 6 Natural Frequency: 6.2997 Relative Error: 0.2855% Number of half-waves in x direction: 2 Number of half-waves in y direction: 2	

Table 6.61: Results obtained with FEM software Strand7 for Case 9

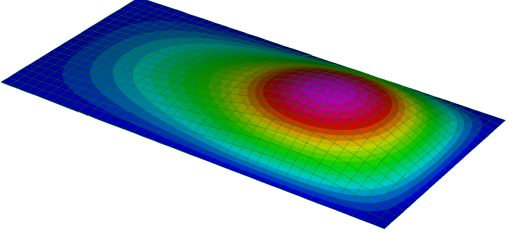
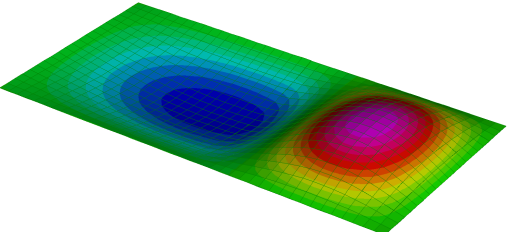
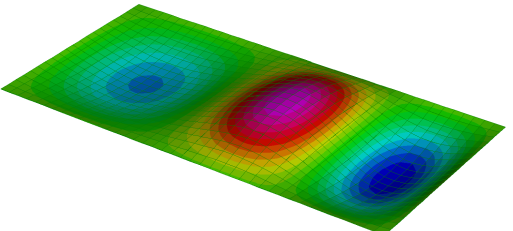
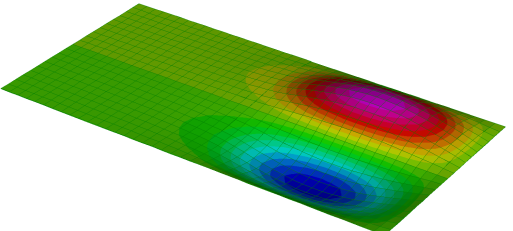
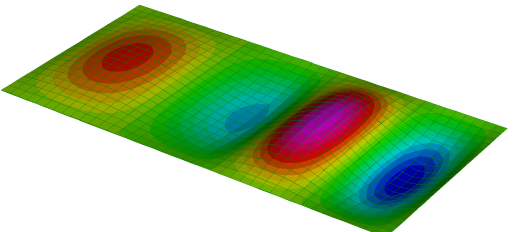
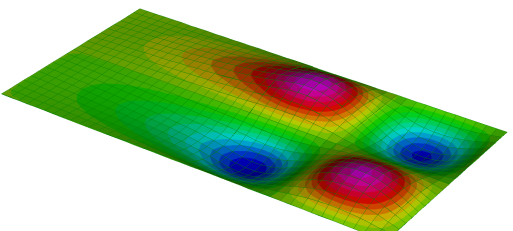
Case 10	
Mode 1 Natural Frequency: 1.7940 Relative Error: 0.0982% Number of half-waves in x direction: 1 Number of half-waves in y direction: 1	
Mode 2 Natural Frequency: 2.8086 Relative Error: 0.1737% Number of half-waves in x direction: 2 Number of half-waves in y direction: 1	
Mode 3 Natural Frequency: 4.6682 Relative Error: 0.2787% Number of half-waves in x direction: 3 Number of half-waves in y direction: 1	
Mode 4 Natural Frequency: 5.0004 Relative Error: 0.2706% Number of half-waves in x direction: 1 Number of half-waves in y direction: 2	
Mode 5 Natural Frequency: 6.7838 Relative Error: 0.3038% Number of half-waves in x direction: 4 Number of half-waves in y direction: 1	
Mode 6 Natural Frequency: 7.3020 Relative Error: 0.4000% Number of half-waves in x direction: 2 Number of half-waves in y direction: 2	

Table 6.62: Results obtained with FEM software Strand7 for Case 10

In all these cases we can clearly see that the relative error is less than 1%. This means that the chosen mesh is correct. Moreover, it is hereby confirmed that the Quad4 element implements the Kirchhoff-Love theory for thin plate.

6.7 Conclusion

In this study, we provide a derivation for both the exact and approximate solutions and we compare our results with the results of Ref. [33]. From the comparison, we remark that the relative error between our exact solution and the one provided by Ref. [33] turns out to be of the order of $\pm 0.0010\%$.

The rigorous version of Galerkin method demonstrates the convergent trend in all the evaluated frequencies in each case study. In general, it leads to an error lesser than 1%. Only in few cases, the error is between 2 – 3%. An important finding of this study is that the conventionally used naïve version of Galerkin method does not tend to the exact solution.

In addition, the conducted FEM analysis shows that the Quad4 element of the package Strand7 implements the Kirchhoff-Love thin plate theory with the chosen mesh leading to an error which is less than 1%, in each frequency for all considered cases. As a conclusion, we argue that the naïve Galerkin method for stepped structures should be replaced with the rigorous version.

7. Flutter of a Bernoulli-Euler beam

In this chapter, we analyze the dynamic stability of beams subject to a supersonic gas flow. The aerodynamic load is modeled with the piston theory. The beam object of study is simply supported at both ends. Considering two materials, which one has greater mechanical parameters compared to the other one, we investigate simply supported beam in three different material patterns. The first pattern is a homogeneous beam made of strong material, the second is a homogeneous beam made of weak material and the third is a multi-component beam made of strong, weak and again strong material in equal portion.

In the analysis, firstly, we evaluate the natural frequencies of the three different material patterns of the beam.

After the evaluation of natural frequencies, we investigate the dynamic stability of these patterns.

All these studies are conducted through the same approaches, namely exact solution, naïve and rigorous version of Galerkin method. In particular, since the evaluation of exact solution in dynamic stability is difficult to obtain, only in this case we take as reference solution a FEM code written by ourselves.

7.1 Free vibrations

We are interested in solving the problem shown in Fig. 7.1: a multi-component beam composed of three different elements.

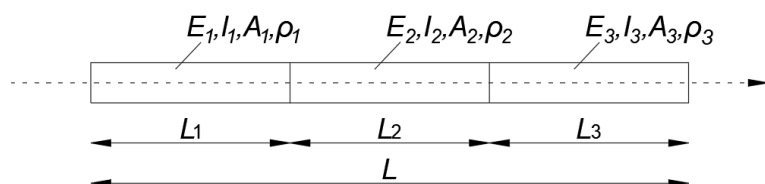


Figure 7.1: A multi-component beam of length L

In Fig. 7.1, E_1 , E_2 and E_3 denote the elastic modulus of the related element; I_1 , I_2 and I_3 denote the associated moments of inertia of the cross section; A_1 , A_2 and A_3 denote the cross-sectional areas of the span; ρ_1 , ρ_2 and ρ_3 denote the mass density of the span material and L_1 , L_2 and L_3 denote the lengths of the relevant portion.

In our case, we deal with a multi-component beam. In this way, the cross section remains the same and the result is that $I_1 = I_2 = I_3$ and $A_1 = A_2 = A_3$.

We derive the exact solution, naïve Galerkin method and rigorous Galerkin method through the same procedures, previously illustrated in Chapter 4.

7.1.1 Numerical example

In this subchapter, we study three different cases. We consider two materials, one of which has greater mechanical parameters than the other one. The case studies differ depending on the material configuration of the beam. The first case is a multi-component beam with the pattern S-W-S, which stands for strong material - weak material - strong material; the second case is a homogeneous beam made only of strong material, namely with the pattern S-S-S and finally the third case is a homogeneous beam made of weak material, i.e. with the pattern W-W-W. In particular, we are interested in studying the effects of the multi-component material pattern on free vibrations of beams.

The beam is in simply supported at both ends constrain condition.

We choose the geometrical and material parameters as follows:

Strong: Naval brass		Weak: Acrylic	
E	$100 \cdot 10^9 \text{ Pa}$	E	$3.2 \cdot 10^9 \text{ Pa}$
ρ	8553 kg/m^3	ρ	1180 kg/m^3
b	0.1 m	b	0.1 m
h	0.1 m	h	0.1 m
A	0.01 m^2	A	0.01 m^2
I	$8.33 \cdot 10^{-6} \text{ m}^4$	I	$8.33 \cdot 10^{-6} \text{ m}^4$

Table 7.1: Parameters of each segment

Exact solution

Considering the S-W-S pattern, the plot of the characteristic equation is:

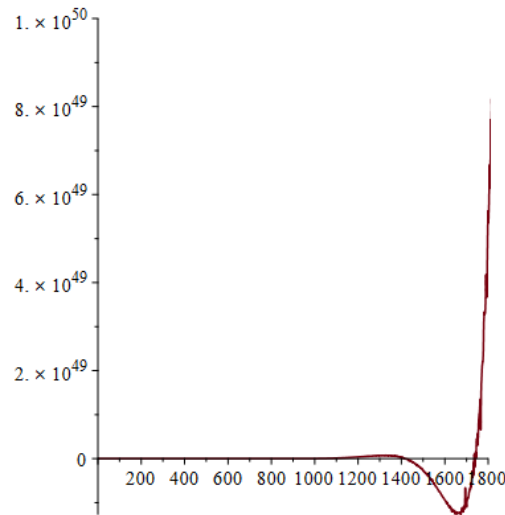
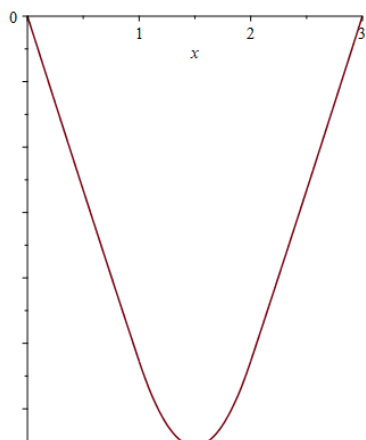


Figure 7.2: Characteristic equation for S-W-S case

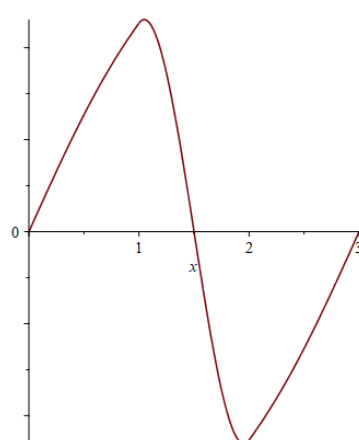
The first five roots are:

$$\begin{aligned}\omega_1 &= 37.6747 \text{ rad/s} \\ \omega_2 &= 197.5394 \text{ rad/s} \\ \omega_3 &= 922.3063 \text{ rad/s} \\ \omega_4 &= 1471.3729 \text{ rad/s} \\ \omega_5 &= 1735.9609 \text{ rad/s}\end{aligned}\tag{7.1.1}$$

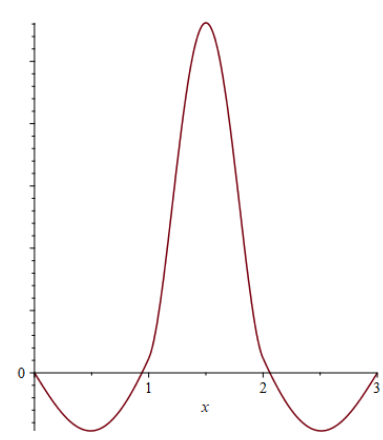
The related mode shapes are depicted in Fig. 7.3:



(a) Mode 1



(b) Mode 2



(c) Mode 3

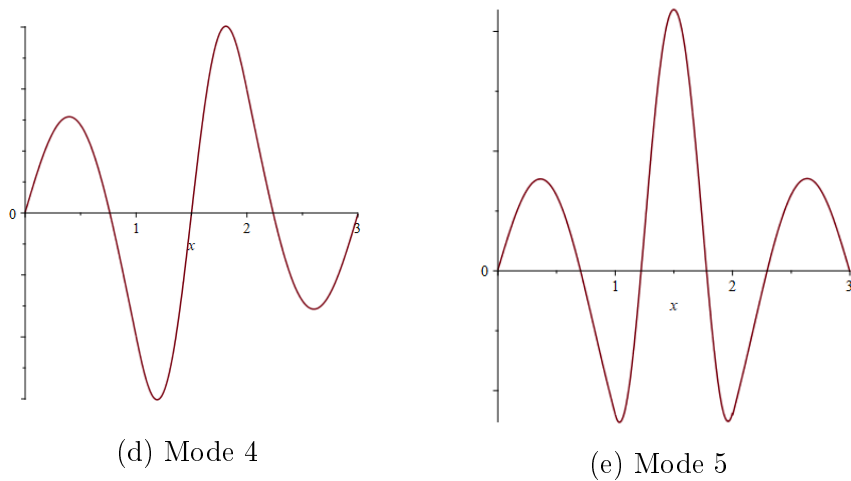


Figure 7.3: Mode shapes for strong - weak - strong material pattern

Considering the S-S-S pattern, the plot of the characteristic equation is:

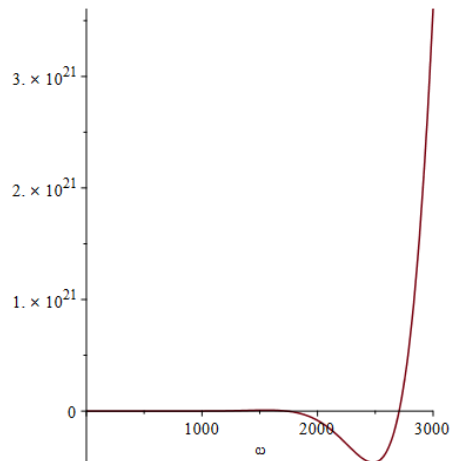


Figure 7.4: Characteristic equation for S-S-S case

The first five roots are:

$$\begin{aligned}\omega_1 &= 108.2449 \text{ rad/s} \\ \omega_2 &= 432.9795 \text{ rad/s} \\ \omega_3 &= 974.2039 \text{ rad/s} \\ \omega_4 &= 1731.9181 \text{ rad/s} \\ \omega_5 &= 2706.1221 \text{ rad/s}\end{aligned}\quad (7.1.2)$$

The related mode shapes are depicted in Fig. 7.5:

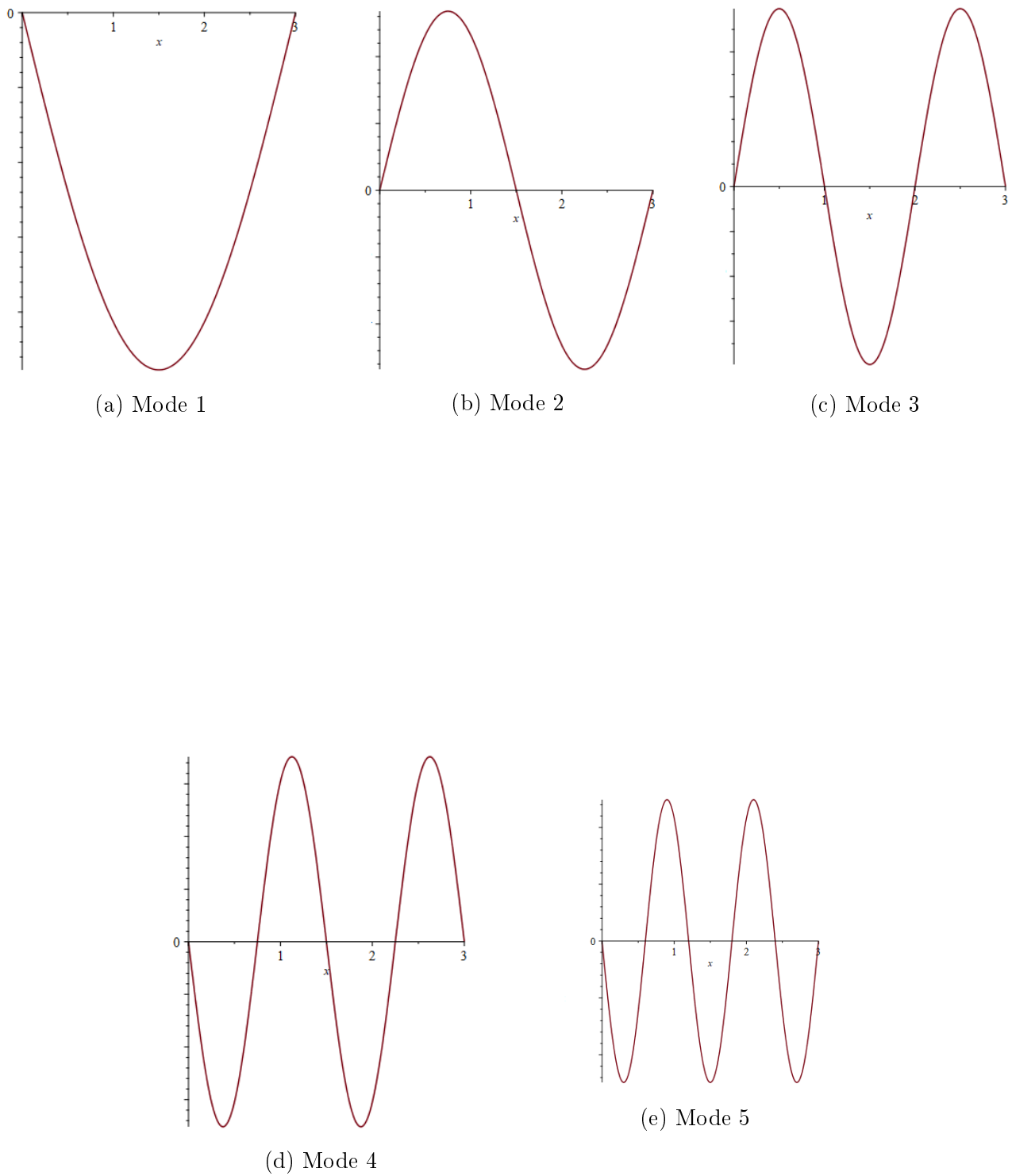


Figure 7.5: Mode shapes for strong - strong - strong material pattern

Considering the W-W-W pattern, the plot of the characteristic equation is:

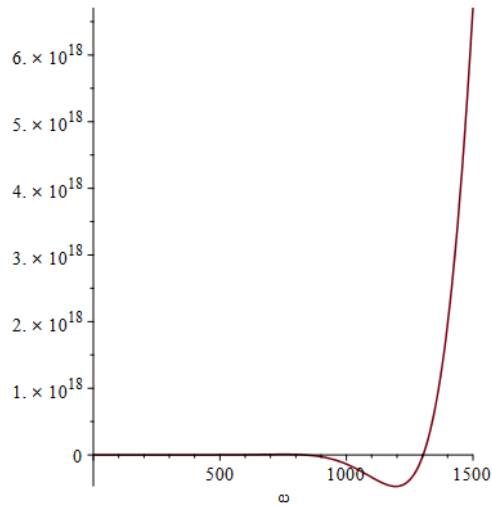
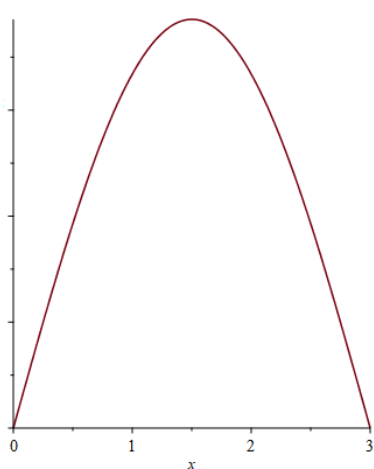


Figure 7.6: Characteristic equation for W-W-W case

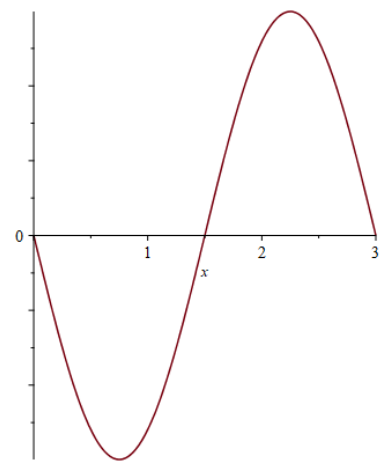
The first five roots are:

$$\begin{aligned}
 \omega_1 &= 52.1315 \text{ rad/s} \\
 \omega_2 &= 208.5262 \text{ rad/s} \\
 \omega_3 &= 469.1839 \text{ rad/s} \\
 \omega_4 &= 834.1047 \text{ rad/s} \\
 \omega_5 &= 1303.2886 \text{ rad/s}
 \end{aligned} \tag{7.1.3}$$

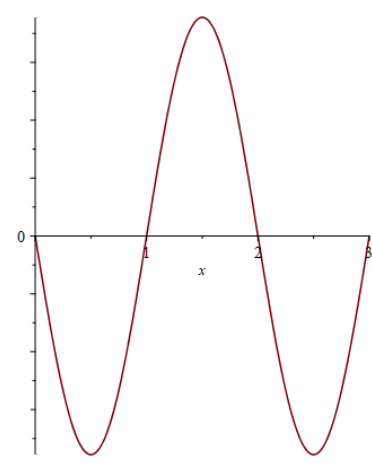
The related mode shapes are depicted in Fig. 7.7:



(a) Mode 1



(b) Mode 2



(c) Mode 3

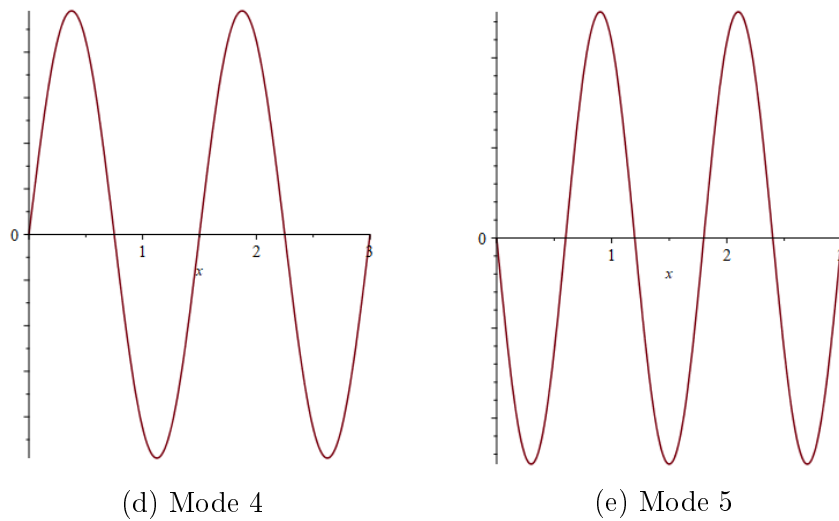


Figure 7.7: Mode shapes for weak - weak - weak material pattern

Collecting these results into a table, we get:

Exact solution [rad/s]			
Mode	S-W-S	S-S-S	W-W-W
1	37.6747	108.2449	52.1315
2	197.5394	432.9795	208.5262
3	922.3063	974.2039	469.1839
4	1471.3729	1731.9181	834.1047
5	1735.9609	2706.1221	1303.2886

Table 7.2: Exact solution for the multi-component beam under consideration in three different material pattern conditions

Naïve Galerkin method

Naïve Galerkin method with 300 terms leads us to the following results:

Mode	Naïve Galerkin method					
	Frequencies [rad/s]					
	S-W-S					
Mode	1 Term	2 Terms	3 Terms	4 Terms	5 Terms	300 Terms
1	100.6241	100.6241	87.7711	87.7711	71.8365	62.3607
2		427.5517	427.5517	422.8396	422.8396	334.7218
3			896.8162	896.8162	843.6827	794.5409
4				1 655.0303	1 655.0303	1 271.6062
5					2 581.3917	2 005.0889

Table 7.3: Frequencies obtained with naïve Galerkin method for S-W-S material pattern

We evaluate the relative error between the obtained natural frequencies and the exact solution with the following formula:

$$\varepsilon = \frac{\omega_{Galerkin} - \omega_{exact}}{\omega_{exact}} \times 100 \quad (7.1.4)$$

Mode	Naïve Galerkin method					
	Relative error [%]					
	S-W-S					
Mode	1 Term	2 Terms	3 Terms	4 Terms	5 Terms	300 Terms
1	167.09%	167.09%	132.97%	132.97%	90.68%	65.52%
2		116.44%	116.44%	114.05%	114.05%	69.45%
3			-2.76%	-2.76%	-8.52%	-13.85%
4				16.77%	16.77%	-10.28%
5					48.70%	15.50%

Table 7.4: Relative error between naïve Galerkin method and exact solution for S-W-S material pattern

Mode	Naïve Galerkin method					
	Frequencies [rad/s]					
	S-S-S					
Mode	1 Term	2 Terms	3 Terms	4 Terms	5 Terms	300 Terms
1	108.2449	108.2449	108.2449	108.2449	108.2449	108.2449
2		432.9795	432.9795	432.9795	432.9795	432.9795
3			974.2040	974.2040	974.2040	974.2040
4				1 731.9181	1 731.9181	1 731.9181
5					2 706.1221	2 706.1221

Table 7.5: Frequencies obtained with naïve Galerkin method for S-S-S material pattern

Mode	Naïve Galerkin method					
	Relative error [%]					
	S-S-S					
Mode	1 Term	2 Terms	3 Terms	4 Terms	5 Terms	300 Terms
1	$-1.53 \cdot 10^{-5}\%$					
2		$7.75 \cdot 10^{-6}\%$				
3			$5.18 \cdot 10^{-6}\%$	$5.18 \cdot 10^{-6}\%$	$5.18 \cdot 10^{-6}\%$	$5.18 \cdot 10^{-6}\%$
4				$1.98 \cdot 10^{-6}\%$	$1.98 \cdot 10^{-6}\%$	$1.98 \cdot 10^{-6}\%$
5					$-5.64 \cdot 10^{-7}\%$	$-5.64 \cdot 10^{-7}\%$

Table 7.6: Relative error between naïve Galerkin method and exact solution for S-S-S material pattern

Mode	Naïve Galerkin method					
	Frequencies [rad/s]					
	W-W-W					
Mode	1 Term	2 Terms	3 Terms	4 Terms	5 Terms	300 Terms
1	52.1315	52.1315	52.1315	52.1315	52.1315	52.1315
2		208.5262	208.5262	208.5262	208.5262	208.5262
3			469.1839	469.1839	469.1839	469.1839
4				834.1047	834.1047	834.1047
5					1 303.2886	1 303.2886

Table 7.7: Frequencies obtained with naïve Galerkin method for W-W-W material pattern

Mode	Naïve Galerkin method					
	Relative error [%]					
	W-W-W					
Mode	1 Term	2 Terms	3 Terms	4 Terms	5 Terms	300 Terms
1	$8.69 \cdot 10^{-5}\%$	$8.69 \cdot 10^{-5}\%$	$8.69 \cdot 10^{-5}\%$	$8.69 \cdot 10^{-5}\%$	$8.69 \cdot 10^{-5}\%$	$8.69 \cdot 10^{-5}\%$
2		$-9.06 \cdot 10^{-6}\%$				
3			$1.06 \cdot 10^{-6}\%$	$1.06 \cdot 10^{-6}\%$	$1.06 \cdot 10^{-6}\%$	$1.06 \cdot 10^{-6}\%$
4				$2.93 \cdot 10^{-6}\%$	$2.93 \cdot 10^{-6}\%$	$2.93 \cdot 10^{-6}\%$
5					$2.45 \cdot 10^{-6}\%$	$2.45 \cdot 10^{-6}\%$

Table 7.8: Relative error between naïve Galerkin method and exact solution for W-W-W material pattern

From the table above, in the S-W-S case, we see that the relative error does not respect any law. In general, the frequencies have a decreasing behavior without tending to the exact solution.

In the S-S-S and W-W-W cases, the frequencies do not change increasing the number of Galerkin terms and the relative error is less than $10^{-4}\%$. The result we obtain is the exact one because the comparison function adopted is the exact solution for the differential equation in homogeneous cases.

In the figure below, we depict the trend of the relative error in function of the number of Galerkin terms.

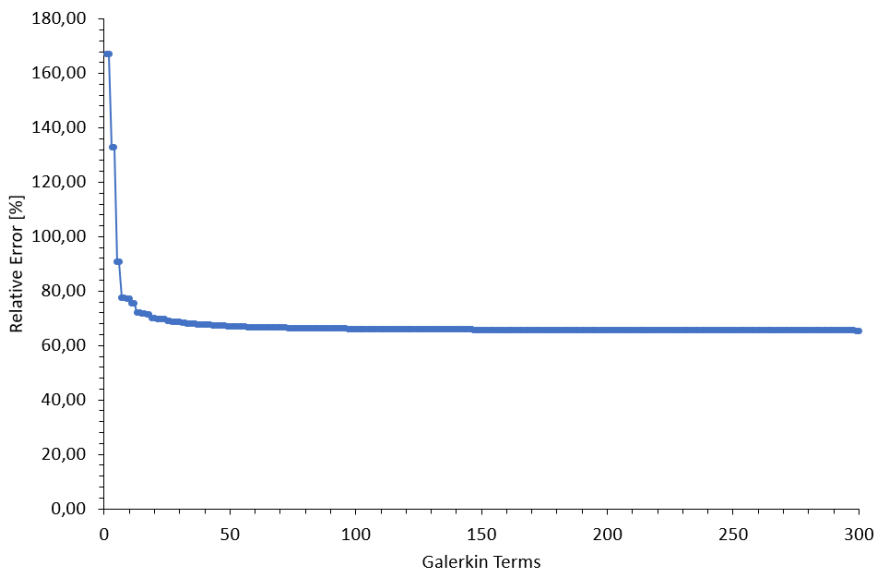


Figure 7.8: Trend of relative error of first natural frequency obtained with naïve Galerkin method for S-W-S material pattern

Rigorous Galerkin method

Rigorous Galerkin method with 300 terms leads us to the following results:

Mode	Rigorous Galerkin method					
	Frequencies [rad/s]					
	S-W-S					
Mode	1 Term	2 Terms	3 Terms	4 Terms	5 Terms	300 Terms
1	100.6241	100.6241	68.6895	68.6895	47.1132	37.7909
2		427.5517	427.5517	405.8657	405.8657	199.1888
3			1 145.947	1 145.9474	1 135.1799	928.0672
4				1 724.2458	1 724.2458	1 419.1213
5					2 925.3048	1 745.9967

Table 7.9: Frequencies obtained with rigorous Galerkin method for S-W-S material pattern

We evaluate the relative error between the obtained natural frequencies and the exact solution with the following formula:

$$\varepsilon = \frac{\omega_{Galerkin} - \omega_{exact}}{\omega_{exact}} \times 100 \quad (7.1.5)$$

Mode	Rigorous Galerkin method					
	Relative error [%]					
	S-W-S					
Mode	1 Term	2 Terms	3 Terms	4 Terms	5 Terms	300 Terms
1	167.0867%	167.0867%	82.3225%	82.3225%	25.0525%	0.3085%
2		116.4387%	116.4387%	105.4607%	105.4607%	0.8350%
3			24.2480%	24.2480%	23.0806%	0.6246%
4				21.6508%	21.6508%	0.1234%
5					68.5121%	0.5781%

Table 7.10: Relative error between rigorous Galerkin method and exact solution for S-W-S material pattern

Mode	Rigorous Galerkin method					
	Frequencies [rad/s]					
	S-S-S					
Mode	1 Term	2 Terms	3 Terms	4 Terms	5 Terms	300 Terms
1	108.2449	108.2449	108.2449	108.2449	108.2449	108.2449
2		432.9795	432.9795	432.9795	432.9795	432.9795
3			974.2040	974.2040	974.2040	974.2040
4				1 731.9181	1 731.9181	1 731.9181
5					2 706.1221	2 706.1221

Table 7.11: Frequencies obtained with rigorous Galerkin method for S-S-S material pattern

Mode	Rigorous Galerkin method					
	Relative error [%]					
	S-S-S					
Mode	1 Term	2 Terms	3 Terms	4 Terms	5 Terms	300 Terms
1	$-1.53 \cdot 10^{-5}\%$	$-1.53 \cdot 10^{-5}\%$	$-1.53 \cdot 10^{-5}\%$	$-1.53 \cdot 10^{-5}\%$	$-1.53 \cdot 10^{-5}\%$	$-1.53 \cdot 10^{-5}\%$
2		$7.75 \cdot 10^{-6}\%$				
3			$5.18 \cdot 10^{-6}\%$	$5.18 \cdot 10^{-6}\%$	$5.18 \cdot 10^{-6}\%$	$5.18 \cdot 10^{-6}\%$
4				$1.98 \cdot 10^{-6}\%$	$1.98 \cdot 10^{-6}\%$	$1.98 \cdot 10^{-6}\%$
5					$-5.64 \cdot 10^{-7}\%$	$-5.64 \cdot 10^{-7}\%$

Table 7.12: Relative error between rigorous Galerkin method and exact solution for S-S-S material pattern

Mode	Rigorous Galerkin method					
	Frequencies [rad/s]					
	W-W-W					
Mode	1 Term	2 Terms	3 Terms	4 Terms	5 Terms	300 Terms
1	52.1315	52.1315	52.1315	52.1315	52.1315	52.1315
2		208.5262	208.5262	208.5262	208.5262	208.5262
3			469.1839	469.1839	469.1839	469.1839
4				834.1047	834.1047	834.1047
5					1 303.2886	1 303.2886

Table 7.13: Frequencies obtained with rigorous Galerkin method for W-W-W material pattern

Mode	Rigorous Galerkin method					
	Relative error [%]					
	W-W-W					
Mode	1 Term	2 Terms	3 Terms	4 Terms	5 Terms	300 Terms
1	$8.69 \cdot 10^{-5}\%$	$8.69 \cdot 10^{-5}\%$	$8.69 \cdot 10^{-5}\%$	$8.69 \cdot 10^{-5}\%$	$8.69 \cdot 10^{-5}\%$	$8.69 \cdot 10^{-5}\%$
2		$-9.06 \cdot 10^{-6}\%$				
3			$1.06 \cdot 10^{-6}\%$	$1.06 \cdot 10^{-6}\%$	$1.06 \cdot 10^{-6}\%$	$1.06 \cdot 10^{-6}\%$
4				$2.93 \cdot 10^{-6}\%$	$2.93 \cdot 10^{-6}\%$	$2.93 \cdot 10^{-6}\%$
5					$2.45 \cdot 10^{-6}\%$	$2.45 \cdot 10^{-6}\%$

Table 7.14: Relative error between rigorous Galerkin method and exact solution for W-W-W material pattern

From the table above, in the S-W-S case, we see that the relative error decreases, increasing the number of Galerkin terms and reaching 300 terms the error is less than 1%. This means that the method converges.

In the S-S-S and W-W-W cases the frequencies do not change increasing the number of Galerkin terms and the relative error is less than $10^{-4}\%$. The result we obtain is the exact one because the comparison function adopted is the exact solution for the differential equation in homogeneous cases.

In the figure below, we depict the trend of the relative error in function of the number of Galerkin terms.

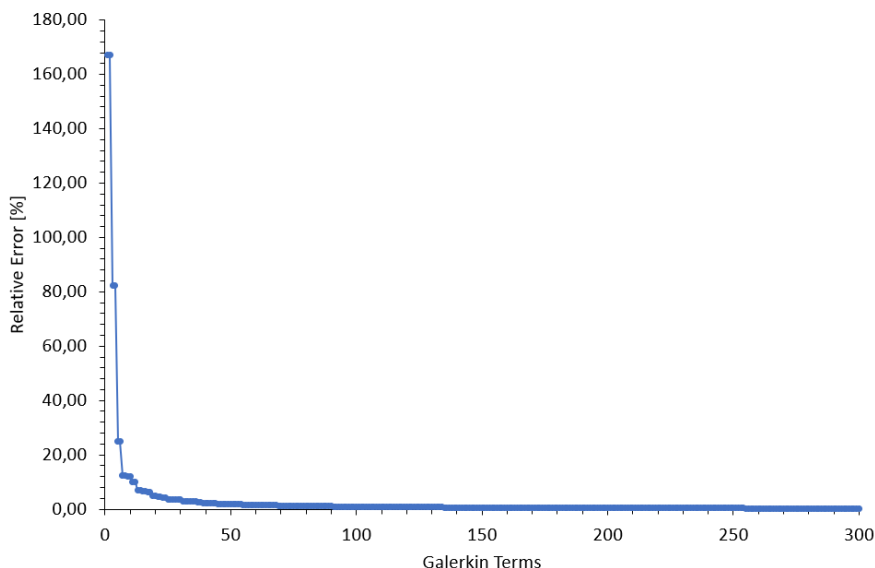


Figure 7.9: Trend of relative error of first natural frequency obtained with rigorous Galerkin method for S-W-S material pattern

7.2 Dynamic stability

7.2.1 Piston theory

The stability problem of elastic bodies in a gas flow hardly finds a solution due to the complicated formulation of the non-stationary forces in a distributed flow. Fortunately, when the supersonic velocity is high enough, the aerodynamic aspect of the problem can be greatly simplified. Besides, high values of supersonic velocity is what nowadays attracts the interest of many researchers.

If we consider the steady motion of a thin beam into a supersonic gas flow, in contrast with the subsonic case, the disturbance is transmitted only in the perpendicular direction. We note that as the velocity of the flow increases, the pressure assumes more local effects, whereas, when the velocity is supersonic, the load is perpendicular to the gas flow.

On the basis of this assumption, we can say that the aerodynamic load on a body can be expressed in the same way as the pressure on a piston moving in a cylinder (see Ref. [39]):

$$P = \frac{\kappa p_\infty}{c_\infty} \left(\frac{\partial w}{\partial t} + U \frac{\partial w}{\partial x} \right) \quad (7.2.1)$$

where κ is the polytropy index of the gas; p_∞ is the pressure in the undisturbed gas; c_∞ is the velocity of sound in undisturbed gas; U is the velocity of gas flow.

If we analyze this formula from a dimensional point of view, we can see that P has a dimension of pressure. We can convert this load to the distributed load $q(x, t)$ by easily multiplying the pressure by the width of section b :

$$q(x, t) = Pb = \frac{\kappa p_\infty b}{c_\infty} \left(\frac{\partial w}{\partial t} + U \frac{\partial w}{\partial x} \right) \quad (7.2.2)$$

7.2.2 Governing differential equation

Governing differential equation of flutter problem reads as follows:

$$\frac{\partial^2}{\partial x^2} \left(E(x) I(x) \frac{\partial^2 w}{\partial x^2} \right) + \rho(x) A(x) \frac{\partial^2 w}{\partial t^2} + q(x, t) = 0 \quad (7.2.3)$$

where $q(x, t)$ represents the load from piston theory of gas flow.

Piston theory load is analyzed in the following formula, as shown in the previous section:

$$q(x, t) = \frac{\kappa p_\infty b}{c_\infty} \left(\frac{\partial w}{\partial t} + U \frac{\partial w}{\partial x} \right) \quad (7.2.4)$$

where κ is the polytropy index of the gas; p_∞ is the pressure in the undisturbed gas; c_∞ is the velocity of sound in undisturbed gas; U is the velocity of gas flow.

Inserting Eq. (7.2.4) into (7.2.3), we obtain:

$$\frac{\partial^2}{\partial x^2} \left(E(x) I(x) \frac{\partial^2 w}{\partial x^2} \right) + \rho(x) A(x) \frac{\partial^2 w}{\partial t^2} + \frac{\kappa p_\infty b}{c_\infty} \left(\frac{\partial w}{\partial t} + U \frac{\partial w}{\partial x} \right) = 0 \quad (7.2.5)$$

or:

$$\frac{\partial^2}{\partial x^2} \left(E(x)I(x) \frac{\partial^2 w}{\partial x^2} \right) + \rho(x)A(x) \frac{\partial^2 w}{\partial t^2} + \frac{\kappa p_\infty b}{c_\infty} \frac{\partial w}{\partial t} + \frac{\kappa p_\infty bU}{c_\infty} \frac{\partial w}{\partial x} = 0 \quad (7.2.6)$$

For each step:

$$E_i I_i \frac{\partial^4 w}{\partial x^4} + \rho_i A_i \frac{\partial^2 w}{\partial t^2} + \frac{\kappa p_\infty b}{c_\infty} \frac{\partial w}{\partial t} + \frac{\kappa p_\infty bU}{c_\infty} \frac{\partial w}{\partial x} = 0 \quad (7.2.7)$$

7.2.3 Exact solution

The exact solution for homogeneous and uniform structures in a gas flow was proposed by Movchan (1959) [40]. We extend his idea to our case of uniform but non-homogeneous beam.

Considering $w(x, t)$ as:

$$w(x, t) = e^{rx} e^{\Omega t} \quad (7.2.8)$$

where r is a characteristic exponent and Ω is a complex eigenfrequency, we obtain:

$$E_i I_i r^4 + \rho_i A_i \Omega^2 + \frac{\kappa p_\infty b}{c_\infty} \Omega + \frac{\kappa p_\infty bU}{c_\infty} r = 0 \quad (7.2.9)$$

or:

$$E_i I_i r^4 + \frac{\kappa p_\infty bU}{c_\infty} r - \lambda_i = 0 \quad (7.2.10)$$

where λ_i is defined as follows:

$$\lambda_i = - \left(\rho_i A_i \Omega^2 + \frac{\kappa p_\infty b}{c_\infty} \Omega \right) \quad (7.2.11)$$

Considering the first two roots of Eq. (7.2.9) as:

$$r_{1,2} = \mu \pm i\beta \quad (7.2.12)$$

we can divide Eq. (7.2.9) by:

$$(r - r_1)(r - r_2) \quad (7.2.13)$$

Or we substitute the meaning of Eq. (7.2.12):

$$r^2 - 2\mu r + \mu^2 + \beta^2 \quad (7.2.14)$$

in order to define $r_{3,4}$.

The ratio of Eq. (7.2.9) by (7.2.14) reads as follows:

$E_i I_i r^4$	$-2E_i I_i \mu r^3$	$E_i I_i (\mu^2 + \beta^2) r^2$	$\frac{\kappa p_\infty bU}{c_\infty} r$	$-\lambda_i$
$//$	$2E_i I_i \mu r^3$	$E_i I_i (-\mu^2 - \beta^2) r^2$	$\frac{\kappa p_\infty bU}{c_\infty} r$	
$2E_i I_i \mu r^3$	$-4E_i I_i \mu^2 r^2$	$2E_i I_i \mu (\mu^2 + \beta^2) r$	$\frac{\kappa p_\infty bU}{c_\infty} r$	
$//$	$E_i I_i (3\mu^2 - \beta^2) r^2$	$\left(\frac{\kappa p_\infty bU}{c_\infty} - 2E_i I_i \mu^3 - 2E_i I_i \mu \beta^2 \right) r$	$-\lambda_i$	
$E_i I_i (3\mu^2 - \beta^2) r^2$	$-2E_i I_i \mu (3\mu^2 - \beta^2) r$	$E_i I_i (\mu^2 + \beta^2) (3\mu^2 - \beta^2)$	$//$	$\left(\frac{\kappa p_\infty bU}{c_\infty} + 4E_i I_i \mu^3 - 4E_i I_i \mu \beta^2 \right) r$
		$-\lambda_i - E_i I_i (\mu^2 + \beta^2) (3\mu^2 - \beta^2)$		

In order to be a divisor, the remainder must vanish. This leads us to the following system:

$$\begin{cases} \frac{\kappa p_\infty bU}{c_\infty} + 4E_i I_i \mu^3 - 4E_i I_i \mu \beta^2 = 0 \\ -\lambda_i - E_i I_i (\mu^2 + \beta^2) (3\mu^2 - \beta^2) = 0 \end{cases} \quad (7.2.15)$$

From this system, we can define $\frac{\kappa p_\infty bU}{c_\infty}$ and λ_i :

$$\begin{cases} \frac{\kappa p_\infty bU}{c_\infty} = 4E_i I_i \mu (\beta^2 - \mu^2) \\ \lambda_i = E_i I_i (\mu^2 + \beta^2) (\beta^2 - 3\mu^2) \end{cases} \quad (7.2.16)$$

The last two roots of Eq. (7.2.9), namely r_3 and r_4 , are the roots of the ratio. We can obtain them as follows:

$$E_i I_i r^2 + 2E_i I_i \mu r + E_i I_i (3\mu^2 - \beta^2) = 0 \quad (7.2.17a)$$

$$r^2 + 2\mu r + 3\mu^2 - \beta^2 = 0 \quad (7.2.17b)$$

$$r_{3,4} = \frac{-2\mu \pm \sqrt{-8\mu^2 + 4\beta^2}}{2} \quad (7.2.17c)$$

$$r_{3,4} = -\mu \pm \sqrt{-2\mu^2 + \beta^2} \quad (7.2.17d)$$

We assume that $w(x, t) = W(x)T(t)$, where the spatial part is e^{rx} . Moreover, we find out that we have four values for the characteristic exponent. As a conclusion:

$$W_i(x) = e^{r_{1,i}x} + e^{r_{2,i}x} + e^{r_{3,i}x} + e^{r_{4,i}x} \quad (7.2.18)$$

With the obtained roots, we can define the system of equations which determines the problem:

$$W_1(0) = 0 \quad (7.2.19a)$$

$$W_1''(0) = 0 \quad (7.2.19b)$$

$$W_1(x_1) = W_2(x_1) \quad (7.2.19c)$$

$$W_1'(x_1) = W_2'(x_1) \quad (7.2.19d)$$

$$E_1 I_1 W_1''(x_1) = E_2 I_2 W_2''(x_1) \quad (7.2.19e)$$

$$E_1 I_1 W_1'''(x_1) = E_2 I_2 W_2'''(x_1) \quad (7.2.19f)$$

$$W_2(x_2) = W_3(x_2) \quad (7.2.19g)$$

$$W_2'(x_2) = W_3'(x_2) \quad (7.2.19h)$$

$$E_2 I_2 W_2''(x_2) = E_3 I_3 W_3''(x_2) \quad (7.2.19i)$$

$$E_2 I_2 W_2'''(x_2) = E_3 I_3 W_3'''(x_2) \quad (7.2.19j)$$

$$W_3(L) = 0 \quad (7.2.19k)$$

$$W_3''(L) = 0 \quad (7.2.19l)$$

We can rewrite this system of equation in a matrix form (defined matrix \mathbf{P}), after that we substitute the meaning of the four roots. This is a homogeneous system and it has non-trivial solution only when the determinant of \mathbf{P} is equal to zero. This determinant is in function of

the parameters μ_i, β_i for each portion of beam. As a result, the final system which allows us to solve the flutter problem reads:

$$\det(\mathbf{P}(\mu_1, \beta_1, \mu_2, \beta_2, \mu_3, \beta_3)) = 0 \quad (7.2.20a)$$

$$\frac{\kappa p_\infty b_1 U}{c_\infty} = 4E_1 I_1 \mu_1 (\beta_1^2 - \mu_1^2) \quad (7.2.20b)$$

$$\frac{\kappa p_\infty b_2 U}{c_\infty} = 4E_2 I_2 \mu_2 (\beta_2^2 - \mu_2^2) \quad (7.2.20c)$$

$$\frac{\kappa p_\infty b_3 U}{c_\infty} = 4E_3 I_3 \mu_3 (\beta_3^2 - \mu_3^2) \quad (7.2.20d)$$

$$\lambda_1 = E_1 I_1 (\mu_1^2 + \beta_1^2) (\beta_1^2 - 3\mu_1^2) \quad (7.2.20e)$$

$$\lambda_2 = E_2 I_2 (\mu_2^2 + \beta_2^2) (\beta_2^2 - 3\mu_2^2) \quad (7.2.20f)$$

$$\lambda_3 = E_3 I_3 (\mu_3^2 + \beta_3^2) (\beta_3^2 - 3\mu_3^2) \quad (7.2.20g)$$

We suppose to know all the parameters related to the beam and to the gas flow. Considering this assumption, we obtain seven unknowns for seven equations: the non-linear system is solvable. The unknowns are the six parameters related to the three characteristic exponents $\mu_1, \beta_1, \mu_2, \beta_2, \mu_3, \beta_3$ and the eigenfrequency Ω which are inside λ_i .

The non-linear system composed by Eq. (7.2.20a) - (7.2.20g) is too big to be analytically solved, so we need a different solution for the stepped beam. On the other hand, if our beam is homogeneous and uniform the solution can be obtained because we do not need compatibility conditions (Eq. (7.2.19c) - (7.2.19j)). Therefore, the system is in the following heavier form:

$$\det(\mathbf{P}(\mu_1, \beta_1)) = 0 \quad (7.2.21a)$$

$$\frac{\kappa p_\infty b_1 U}{c_\infty} = 4E_1 I_1 \mu_1 (\beta_1^2 - \mu_1^2) \quad (7.2.21b)$$

$$\lambda_1 = E_1 I_1 (\mu_1^2 + \beta_1^2) (\beta_1^2 - 3\mu_1^2) \quad (7.2.21c)$$

7.2.4 Finite Element Method

In order to obtain a reference solution for the two different implementations of Galerkin method, we implement our finite element method code.

Finite element method applied on structures subject to gas flow is not a new method. In fact, it was already used for example by Marzani et al. (2012) [41], Olson and Jamison (1997) [42], Kock and Olson (1991) [43], Pramila et al. (1991) [44], Ryu et al. (2002) [45].

According to the mentioned works, the use of variational approach starting on Hamilton's principle reads:

$$\int_{t_1}^{t_2} \delta(T - \Pi) dt + \int_{t_1}^{t_2} \delta W_{nc} dt = 0 \quad (7.2.22)$$

denoting Π , the potential total energy of the system, as:

$$\Pi = \Phi + H \quad (7.2.23)$$

where Φ is the elastic deformation energy of the system, H is the potential of the conservative forces, T is the kinetic energy of the system and W_{nc} is the virtual work of non-conservative forces. According to Hamilton's principle, and for one-dimensional system under study, we can say that the difference between the variation of kinetic energy T and potential energy Π added to variation of virtual work of non-conservative forces into any time interval $[t_1-t_2]$ must be equal to zero. Due to a configuration change, the energetical terms and the work terms take the following form:

- Elastic potential energy of the beam:

$$\Phi = \frac{1}{2} \int_0^L EI \left(\frac{\partial^2 w}{\partial x^2} \right)^2 dx \quad (7.2.24)$$

- Kinetic energy:

$$T = \frac{1}{2} \int_0^L \rho A \left(\frac{\partial w}{\partial t} \right)^2 dx \quad (7.2.25)$$

- Virtual work of non-conservative forces:

$$\delta W_{nc} = - \int_0^L q(x, t) \delta w dx \quad (7.2.26)$$

Substituting in (7.2.26) the meaning of piston theory non-conservative forces (7.2.4), we obtain:

$$\delta W_{nc} = - \int_0^L \frac{\kappa p_\infty b}{c_\infty} \left(\frac{\partial w}{\partial t} + U \frac{\partial w}{\partial x} \right) \delta w dx \quad (7.2.27)$$

or:

$$\delta W_{nc} = - \int_0^L \frac{\kappa p_\infty b}{c_\infty} \frac{\partial w}{\partial t} \delta w dx - \int_0^L \frac{\kappa p_\infty b U}{c_\infty} \frac{\partial w}{\partial x} \delta w dx \quad (7.2.28)$$

Now we evaluate the variations of quantities (7.2.24) and (7.2.25):

$$\delta \Phi = \int_0^L EI \frac{\partial^2 w}{\partial x^2} \delta \left(\frac{\partial^2 w}{\partial x^2} \right) dx \quad (7.2.29)$$

$$\delta T = \int_0^L \rho A \frac{\partial w}{\partial t} \delta \left(\frac{\partial w}{\partial t} \right) dx \quad (7.2.30)$$

Substituting (7.2.29), (7.2.30) and (7.2.28) into (7.2.23) and in conclusion into (7.2.22), we obtain:

$$\begin{aligned} & \int_{t_1}^{t_2} \left[\int_0^L \rho A \frac{\partial w}{\partial t} \delta \left(\frac{\partial w}{\partial t} \right) dx \right] dt - \int_{t_1}^{t_2} \left[\int_0^L EI \frac{\partial^2 w}{\partial x^2} \delta \left(\frac{\partial^2 w}{\partial x^2} \right) dx \right] dt \\ & - \int_{t_1}^{t_2} \left[\int_0^L \frac{\kappa p_\infty b}{c_\infty} \frac{\partial w}{\partial t} \delta w dx + \int_0^L \frac{\kappa p_\infty b U}{c_\infty} \frac{\partial w}{\partial x} \delta w dx \right] dt = 0 \end{aligned} \quad (7.2.31)$$

Integration by part of first term leads us to:

$$\int_0^L \left[\int_{t_1}^{t_2} \rho A \frac{\partial w}{\partial t} \delta \left(\frac{\partial w}{\partial t} \right) dt \right] dx = \int_0^L \left[\rho A \frac{\partial w}{\partial t} \delta w \right]_{t_1}^{t_2} dx - \int_0^L \left\{ \int_{t_1}^{t_2} \left[\rho A \frac{\partial^2 w}{\partial t^2} \delta w \right] dt \right\} dx \quad (7.2.32)$$

We can switch the integration order because the length of the system does not change over time.

Since we rely on the assumption of *synchronous varied motions*, we have $\delta w(x, t_1) = \delta w(x, t_2) = 0$. As a conclusion, (7.2.32) becomes:

$$\int_0^L \left[\int_{t_1}^{t_2} \rho A \frac{\partial w}{\partial t} \delta \left(\frac{\partial w}{\partial t} \right) dt \right] dx = - \int_0^L \left\{ \int_{t_1}^{t_2} \left[\rho A \frac{\partial^2 w}{\partial t^2} \delta w \right] dt \right\} dx \quad (7.2.33)$$

The request of a variational formulation valid for each time interval $[t_1 - t_2]$ demands that the integrand of (7.2.31) vanishes. In addition, the use of (7.2.33) leads Hamilton's principle to:

$$\int_0^L \rho A \frac{\partial^2 w}{\partial t^2} \delta w dx + \int_0^L EI \frac{\partial^2 w}{\partial x^2} \delta \left(\frac{\partial^2 w}{\partial x^2} \right) dx + \int_0^L \frac{\kappa p_\infty b}{c_\infty} \frac{\partial w}{\partial t} \delta w dx + \int_0^L \frac{\kappa p_\infty b U}{c_\infty} \frac{\partial w}{\partial x} \delta w dx = 0 \quad (7.2.34)$$

Now subdividing the whole domain in n elements, the length of each element becomes:

$$L_e = \frac{L}{n} \quad (7.2.35)$$

The local coordinate \bar{x} of each element, in particular for the i^{th} element reads as follows:

$$\bar{x} = x - (i-1)L_e \quad (7.2.36)$$

In view of considerations (7.2.36) and (7.2.35), we can rewrite (7.2.34) as follows:

$$\sum_{i=1}^n \left[\int_0^{L_e} \rho A \frac{\partial^2 w}{\partial t^2} \delta w d\bar{x} + \int_0^{L_e} EI \frac{\partial^2 w}{\partial \bar{x}^2} \delta \left(\frac{\partial^2 w}{\partial \bar{x}^2} \right) d\bar{x} + \int_0^{L_e} \frac{\kappa p_\infty b}{c_\infty} \frac{\partial w}{\partial t} \delta w d\bar{x} + \int_0^{L_e} \frac{\kappa p_\infty b U}{c_\infty} \frac{\partial w}{\partial \bar{x}} \delta w d\bar{x} \right] = 0 \quad (7.2.37)$$

We can also introduce the following dimensionless coordinate in order to reduce the analytical complexity:

$$v = \frac{w}{L_e} \rightarrow w = v L_e \quad (7.2.38a)$$

$$\xi = \frac{\bar{x}}{L_e} \rightarrow \bar{x} = \xi L_e \quad (7.2.38b)$$

Eq. (7.2.37) with considerations (7.2.38a) and (7.2.38b) becomes:

$$\sum_{i=1}^n \left[\int_0^1 \rho A L_e^3 \frac{\partial^2 v}{\partial t^2} \delta v d\xi + \int_0^1 \frac{EI}{L_e} \frac{\partial^2 v}{\partial \xi^2} \delta \left(\frac{\partial^2 v}{\partial \xi^2} \right) d\xi + \int_0^1 \frac{\kappa p_\infty b}{c_\infty} L_e^3 \frac{\partial v}{\partial t} \delta v d\xi + \int_0^1 \frac{\kappa p_\infty b U}{c_\infty} L_e^2 \frac{\partial v}{\partial \xi} \delta v d\xi \right] = 0 \quad (7.2.39)$$

The displacement field of a Bernoulli-Euler finite element is described in four components: two for each extremity. In particular, these movements are two translations $w_1 = w_1(t)$ and $w_2 = w_2(t)$ and two rotations $\varphi_1 = \varphi_1(t)$ and $\varphi_2 = \varphi_2(t)$.

Given these assumptions, the displacement field is defined as follows:

$$w(\bar{x}, t) = N_1(\bar{x})w_1(t) + N_2(\bar{x})\varphi_1(t) + N_3(\bar{x})w_2(t) + N_4(\bar{x})\varphi_2(t) \quad (7.2.40)$$

Eq. (7.2.40) is the linear combination of shape functions $N_i(\bar{x})(i = 1, 2, 3, 4)$ with the displacement fields $w_1(t)$, $\varphi_1(t)$, $w_2(t)$ and $\varphi_2(t)$.

Differential equation (7.2.7) shows that the function $w(\bar{x}, t)$ must be differentiable until four times. This requires polynomial shape functions of third order as follows:

$$N_1 = N_1(\bar{x}) = 1 - 3\frac{\bar{x}^2}{L_e^2} + 2\frac{\bar{x}^3}{L_e^3} \quad (7.2.41a)$$

$$N_2 = N_2(\bar{x}) = -\bar{x} + 2\frac{\bar{x}^2}{L_e} - \frac{\bar{x}^3}{L_e^3} \quad (7.2.41b)$$

$$N_3 = N_3(\bar{x}) = 3\frac{\bar{x}^2}{L_e^2} - 2\frac{\bar{x}^3}{L_e^3} \quad (7.2.41c)$$

$$N_4 = N_4(\bar{x}) = \frac{\bar{x}^2}{L_e} - \frac{\bar{x}^3}{L_e^2} \quad (7.2.41d)$$

Eq. (7.2.41a) - (7.2.41d) with consideration (7.2.38b) take the following form:

$$N_1 = N_1(\xi) = 1 - 3\xi^2 + 2\xi^3 \quad (7.2.42a)$$

$$N_2 = N_2(\xi) = L_e(-\xi + 2\xi^2 - \xi^3) \quad (7.2.42b)$$

$$N_3 = N_3(\xi) = 3\xi^2 - 2\xi^3 \quad (7.2.42c)$$

$$N_4 = N_4(\xi) = L_e(\xi^2 - \xi^3) \quad (7.2.42d)$$

Thanks to Eq. (7.2.42a) - (7.2.42d), the variable $w(\xi, t)$ takes the following form:

$$w(\xi, t) = N_1(\xi)w_1(t) + N_2(\xi)\varphi_1(t) + N_3(\xi)w_2(t) + N_4(\xi)\varphi_2(t) \quad (7.2.43)$$

The dimensionless variable $v = v(\xi, t)$, with considerations (7.2.43) and (7.2.38a), can be expressed in the following form:

$$v(\xi, t) = \frac{w(\xi, t)}{L_e} = \frac{1}{L_e}N_1(\xi)w_1(t) + \frac{1}{L_e}N_2(\xi)\varphi_1(t) + \frac{1}{L_e}N_3(\xi)w_2(t) + \frac{1}{L_e}N_4(\xi)\varphi_2(t) \quad (7.2.44)$$

Introducing the following notations:

$$\bar{N}_1 = \frac{1}{L_e}N_1(\xi) = \frac{1}{L_e}(1 - 3\xi^2 + 2\xi^3) \quad (7.2.45a)$$

$$\bar{N}_2 = \frac{1}{L_e}N_2(\xi) = -\xi + 2\xi^2 - \xi^3 \quad (7.2.45b)$$

$$\bar{N}_3 = \frac{1}{L_e}N_3(\xi) = \frac{1}{L_e}(3\xi^2 - 2\xi^3) \quad (7.2.45c)$$

$$\bar{N}_4 = \frac{1}{L_e}N_4(\xi) = \xi^2 - \xi^3 \quad (7.2.45d)$$

Defining with \mathbf{N} the shape functions vector and with \mathbf{u} the nodal displacements vector, we have:

$$\mathbf{N} = \mathbf{N}(\xi) = [\bar{N}_1(\xi) \quad \bar{N}_2(\xi) \quad \bar{N}_3(\xi) \quad \bar{N}_4(\xi)]^T \quad (7.2.46)$$

$$\mathbf{u} = \mathbf{u}(t) = [w_1(t) \quad \varphi_1(t) \quad w_2(t) \quad \varphi_2(t)]^T \quad (7.2.47)$$

Keeping considerations (7.2.46) and (7.2.47) in mind, Eq. (7.2.44) takes the following form:

$$v(\xi, t) = \mathbf{N}^T(\xi) \mathbf{u}(t) = \mathbf{u}^T(t) \mathbf{N}(\xi) \quad (7.2.48)$$

Into Eq. (7.2.39), we have the first and second derivative of variable $v(\xi, t)$ with respect to the dimensionless coordinate ξ .

The first derivative can be written as follows:

$$v'(\xi, t) = \frac{\partial v(\xi, t)}{\partial \xi} = \bar{N}'_1(\xi)w_1(t) + \bar{N}'_2(\xi)\varphi_1(t) + \bar{N}'_3(\xi)w_2(t) + \bar{N}'_4(\xi)\varphi_2(t) \quad (7.2.49)$$

with:

$$\bar{N}'_1(\xi) = \frac{d\bar{N}_1(\xi)}{d\xi} = \frac{1}{L_e}(-6\xi + 6\xi^2) \quad (7.2.50a)$$

$$\bar{N}'_2(\xi) = \frac{d\bar{N}_2(\xi)}{d\xi} = -1 + 4\xi - 3\xi^2 \quad (7.2.50b)$$

$$\bar{N}'_3(\xi) = \frac{d\bar{N}_3(\xi)}{d\xi} = \frac{1}{L_e}(6\xi - 6\xi^2) \quad (7.2.50c)$$

$$\bar{N}'_4(\xi) = \frac{d\bar{N}_4(\xi)}{d\xi} = 2\xi - 3\xi^2 \quad (7.2.50d)$$

Denoting with \mathbf{D} the vector of first derivative of shape functions, we have:

$$\mathbf{D} = \frac{d}{d\xi} [\bar{N}_1(\xi) \quad \bar{N}_2(\xi) \quad \bar{N}_3(\xi) \quad \bar{N}_4(\xi)]^T = [\bar{N}'_1(\xi) \quad \bar{N}'_2(\xi) \quad \bar{N}'_3(\xi) \quad \bar{N}'_4(\xi)]^T = \frac{d}{d\xi} \mathbf{N}(\xi) \quad (7.2.51)$$

Eq. (7.2.49) becomes:

$$v'(\xi, t) = \mathbf{D}^T(\xi) \mathbf{u}(t) = \mathbf{u}^T(t) \mathbf{D}(\xi) \quad (7.2.52)$$

Analogously, we can define the second derivative:

$$v''(\xi, t) = \frac{\partial^2 v(\xi, t)}{\partial \xi^2} = \bar{N}''_1(\xi)w_1(t) + \bar{N}''_2(\xi)\varphi_1(t) + \bar{N}''_3(\xi)w_2(t) + \bar{N}''_4(\xi)\varphi_2(t) \quad (7.2.53)$$

with:

$$\bar{N}_1''(\xi) = \frac{d^2\bar{N}_1(\xi)}{d\xi^2} = \frac{1}{L_e}(-6 + 6\xi) \quad (7.2.54a)$$

$$\bar{N}_2''(\xi) = \frac{d^2\bar{N}_2(\xi)}{d\xi^2} = 4 - 6\xi \quad (7.2.54b)$$

$$\bar{N}_3''(\xi) = \frac{d^2\bar{N}_3(\xi)}{d\xi^2} = \frac{1}{L_e}(6 - 12\xi) \quad (7.2.54c)$$

$$\bar{N}_4''(\xi) = \frac{d^2\bar{N}_4(\xi)}{d\xi^2} = 2 - 6\xi \quad (7.2.54d)$$

Denoting with \mathbf{B} the vector of second derivative of shape functions, we have:

$$\mathbf{B} = \frac{d^2}{d\xi^2} [\bar{N}_1(\xi) \quad \bar{N}_2(\xi) \quad \bar{N}_3(\xi) \quad \bar{N}_4(\xi)]^T = [\bar{N}_1''(\xi) \quad \bar{N}_2''(\xi) \quad \bar{N}_3''(\xi) \quad \bar{N}_4''(\xi)]^T = \frac{d^2}{d\xi^2} \mathbf{N}(\xi) \quad (7.2.55)$$

Eq. (7.2.53) becomes:

$$v''(\xi, t) = \mathbf{B}^T(\xi) \mathbf{u}(t) = \mathbf{u}^T(t) \mathbf{B}(\xi) \quad (7.2.56)$$

In Eq. (7.2.39), we also have the second derivative with respect to the time of variable $v(\xi, t)$. This derivative can be written as follows:

$$\ddot{v}(\xi, t) = \frac{\partial^2 v(\xi, t)}{\partial t^2} = \bar{N}_1(\xi)\ddot{w}_1(t) + \bar{N}_2(\xi)\ddot{\varphi}_1(t) + \bar{N}_3(\xi)\ddot{w}_2(t) + \bar{N}_4(\xi)\ddot{\varphi}_2(t) \quad (7.2.57)$$

or:

$$\ddot{v}(\xi, t) = \mathbf{N}^T(\xi) \ddot{\mathbf{u}}(t) = \ddot{\mathbf{u}}^T(t) \mathbf{N}(\xi) \quad (7.2.58)$$

Introducing Eq. (7.2.48), (7.2.52), (7.2.56) and (7.2.58) into Eq. (7.2.39), we obtain:

$$\begin{aligned} & \sum_{i=1}^n \left[\int_0^1 \delta(\mathbf{u}^T \mathbf{N}) \rho A L_e^3 \mathbf{N}^T \dot{\mathbf{u}} d\xi + \int_0^1 \delta(\mathbf{u}^T \mathbf{B}) \frac{EI}{L_e} \mathbf{B}^T \mathbf{u} d\xi \right. \\ & \left. + \int_0^1 \delta(\mathbf{u}^T \mathbf{N}) \frac{\kappa p_\infty b}{c_\infty} L_e^3 \mathbf{N}^T \dot{\mathbf{u}} d\xi + \int_0^1 \delta(\mathbf{u}^T \mathbf{N}) \frac{\kappa p_\infty b U}{c_\infty} L_e^2 \mathbf{D}^T \mathbf{u} d\xi \right] = \mathbf{0} \end{aligned} \quad (7.2.59)$$

Since vector \mathbf{u} is function only of the time, we can remove it from the integral sign:

$$\begin{aligned} & \sum_{i=1}^n \delta(\mathbf{u}^T) \left[\int_0^1 \mathbf{N} \rho A L_e^3 \mathbf{N}^T d\xi \ddot{\mathbf{u}} + \int_0^1 \mathbf{B} \frac{EI}{L_e} \mathbf{B}^T d\xi \mathbf{u} + \int_0^1 \mathbf{N} \frac{\kappa p_\infty b}{c_\infty} L_e^3 \mathbf{N}^T d\xi \dot{\mathbf{u}} \right. \\ & \left. + \int_0^1 \mathbf{N} \frac{\kappa p_\infty b U}{c_\infty} L_e^2 \mathbf{D}^T d\xi \mathbf{u} \right] = \mathbf{0} \end{aligned} \quad (7.2.60)$$

Denoting:

- Element mass matrix $\mathbf{m} = m_{ij}$ as follows:

$$\mathbf{m} = \int_0^1 \mathbf{N} \rho A L_e^3 \mathbf{N}^T d\xi \quad (7.2.61)$$

or:

$$m_{ij} = \int_0^1 N_i \rho A L_e^3 N_j d\xi \quad (7.2.62)$$

- Element stiffness matrix $\mathbf{k} = k_{ij}$ as follows:

$$\mathbf{k} = \int_0^1 \mathbf{B} \frac{EI}{L_e} \mathbf{B}^T d\xi \quad (7.2.63)$$

or:

$$k_{ij} = \int_0^1 B_i \frac{EI}{L_e} B_j d\xi \quad (7.2.64)$$

- Aerodynamic damping matrix $\mathbf{q}_1 = q_{1ij}$ as follows:

$$\mathbf{q}_1 = \int_0^1 \mathbf{N} \frac{\kappa p_\infty b}{c_\infty} L_e^3 \mathbf{N}^T d\xi \quad (7.2.65)$$

or:

$$q_{1ij} = \int_0^1 N_i \frac{\kappa p_\infty b}{c_\infty} L_e^3 N_j d\xi \quad (7.2.66)$$

- Velocity load matrix $\mathbf{q}_2 = q_{2ij}$ as follows:

$$\mathbf{q}_2 = \int_0^1 \mathbf{N} \frac{\kappa p_\infty b U}{c_\infty} L_e^2 \mathbf{D}^T d\xi \quad (7.2.67)$$

or:

$$q_{2ij} = \int_0^1 N_i \frac{\kappa p_\infty b U}{c_\infty} L_e^2 D_j d\xi \quad (7.2.68)$$

Eq. (7.2.60) becomes:

$$\sum_{i=1}^n \delta(\mathbf{u}^T) [\mathbf{m} \ddot{\mathbf{u}} + \mathbf{k} \mathbf{u} + \mathbf{q}_1 \dot{\mathbf{u}} + \mathbf{q}_2 \mathbf{u}] = \mathbf{0} \quad (7.2.69)$$

After a standard assembly procedure, we obtain:

$$\delta \mathbf{v}^T (\mathbf{M} \ddot{\mathbf{v}} + \mathbf{K} \mathbf{v} + \mathbf{Q}_1 \dot{\mathbf{v}} + \mathbf{Q}_2 \mathbf{v}) = \mathbf{0} \quad (7.2.70)$$

where \mathbf{M} is the global mass matrix of the system, \mathbf{K} is the global stiffness matrix of the system, \mathbf{Q}_1 is the global aerodynamic damping matrix of the system, \mathbf{Q}_2 is the global velocity load matrix of the system, and \mathbf{v} is the global nodal displacements vector of the system.

Adding the terms which multiply \mathbf{v} , we obtain:

$$\delta \mathbf{v}^T (\mathbf{M} \ddot{\mathbf{v}} + \mathbf{Q}_1 \dot{\mathbf{v}} + \mathbf{Z} \mathbf{v}) = \mathbf{0} \quad (7.2.71)$$

where:

$$\mathbf{Z} = \mathbf{K} + \mathbf{Q}_2 \quad (7.2.72)$$

In order to obtain a solution which is valid for each variation $\delta \mathbf{v}^T$, the term into parenthesis in (7.2.71) must vanish:

$$\mathbf{M} \ddot{\mathbf{v}} + \mathbf{Q}_1 \dot{\mathbf{v}} + \mathbf{Z} \mathbf{v} = \mathbf{0} \quad (7.2.73)$$

Defining now $\mathbf{v}(t)$ as follows:

$$\mathbf{v}(t) = \mathbf{V} e^{\Omega t} \quad (7.2.74)$$

We obtain:

$$\Omega^2 \mathbf{M} \mathbf{v} + \Omega \mathbf{Q}_1 \mathbf{v} + \mathbf{Z} \mathbf{v} = \mathbf{0} \quad (7.2.75)$$

Collecting $\mathbf{v}(t)$:

$$(\Omega^2 \mathbf{M} + \Omega \mathbf{Q}_1 + \mathbf{Z}) \mathbf{v} = \mathbf{0} \quad (7.2.76)$$

Eq. (7.2.76) is a homogeneous linear system in the parameter Ω . This system has non-trivial solution only when the determinant of coefficient matrix (the term into parenthesis) is equal to zero. Now the problem is to find the value of Ω which leads the determinant equal to zero:

$$\det (\Omega^2 \mathbf{M} + \Omega \mathbf{Q}_1 + \mathbf{Z}) = 0 \quad (7.2.77)$$

7.2.5 Naïve Galerkin method

Differential equation (7.2.7) can be solved with the well-known weighted residual method proposed by Galerkin in 1915. In order to apply the Galerkin procedure, we express the variable $w(x, t)$ by a series as follows:

$$w(x, t) = \sum_{k=1}^n Q_k \psi_k(x) f_k(t) \quad (7.2.78)$$

where $\psi_k(x)$ is a function of axial coordinate and $f_k(t)$ of time t .

We consider the following variation of the function $f_k(t)$ in time:

$$f_k(t) = e^{\Omega t} \quad (7.2.79)$$

We multiply the expression resulting from substitution of Eq. (7.2.79) into Eq. (7.2.7) by $\psi_j(x)$ and we integrate from zero to total length with respect to x :

$$\int_0^L \sum_{i=1}^3 \left(\sum_{k=1}^n Q_k \left(E_i I_i \frac{d^4 \psi_k(x)}{dx^4} \psi_j(x) + \frac{\kappa p_\infty b U}{c_\infty} \frac{d \psi_k(x)}{dx} \psi_j(x) + \Omega^2 \rho_i A_i \psi_k(x) \psi_j(x) + \Omega \frac{\kappa p_\infty b}{c_\infty} \psi_k(x) \psi_j(x) \right) \right) dx = 0 \quad (7.2.80)$$

After some algebra:

$$\begin{aligned} & \sum_{k=1}^n Q_k \left(\sum_{i=1}^3 \left[E_i I_i \int_{x_i}^{x_{i+1}} \frac{d^4 \psi_k(x)}{dx^4} \psi_j(x) dx \right] + \frac{\kappa p_\infty b U}{c_\infty} \sum_{i=1}^3 \left[\int_{x_i}^{x_{i+1}} \frac{d \psi_k(x)}{dx} \psi_j(x) dx \right] \right. \\ & \left. + \Omega^2 \sum_{i=1}^3 \left[\rho_i A_i \int_{x_i}^{x_{i+1}} \psi_k(x) \psi_j(x) dx \right] + \Omega \frac{\kappa p_\infty b}{c_\infty} \sum_{i=1}^3 \left[\int_{x_i}^{x_{i+1}} \psi_k(x) \psi_j(x) dx \right] \right) = 0 \end{aligned} \quad (7.2.81)$$

We introduce the following notations:

$$A_{kj} = \sum_{i=1}^3 \left[E_i I_i \int_{x_i}^{x_{i+1}} \frac{d^4 \psi_k(x)}{dx^4} \psi_j(x) dx \right] \quad (7.2.82a)$$

$$B_{kj} = \sum_{i=1}^3 \left[\int_{x_i}^{x_{i+1}} \frac{d \psi_k(x)}{dx} \psi_j(x) dx \right] \quad (7.2.82b)$$

$$C_{kj} = \sum_{i=1}^3 \left[\rho_i A_i \int_{x_i}^{x_{i+1}} \psi_k(x) \psi_j(x) dx \right] \quad (7.2.82c)$$

$$D_{kj} = \sum_{i=1}^3 \left[\int_{x_i}^{x_{i+1}} \psi_k(x) \psi_j(x) dx \right] \quad (7.2.82d)$$

The problem takes the following form:

$$\sum_{k=1}^n Q_k \left(A_{kj} + \frac{\kappa p_\infty b U}{c_\infty} B_{kj} + \Omega^2 C_{kj} + \Omega \frac{\kappa p_\infty b}{c_\infty} D_{kj} \right) = 0 \quad (7.2.83)$$

In matrix representation:

$$\left(\mathbf{A} + \frac{\kappa p_\infty b U}{c_\infty} \mathbf{B} + \Omega^2 \mathbf{C} + \Omega \frac{\kappa p_\infty b}{c_\infty} \mathbf{D} \right) \mathbf{Q} = \mathbf{0} \quad (7.2.84)$$

This system has non-trivial solution only if the following determinant vanishes:

$$\det \left(\mathbf{A} + \frac{\kappa p_\infty b U}{c_\infty} \mathbf{B} + \Omega^2 \mathbf{C} + \Omega \frac{\kappa p_\infty b}{c_\infty} \mathbf{D} \right) = 0 \quad (7.2.85)$$

In order to study the dynamic stability, we fix parameters related to the beam. Therefore, the only variable of the system is the parameter related to the load: the velocity U . The unknown of the problem is the complex eigenfrequency Ω .

7.2.6 Rigorous Galerkin method

We consider:

$$w(x, t) = W(x)e^{\Omega t} \quad (7.2.86)$$

Starting from Eq. (7.2.6) and using consideration (7.2.86), we obtain:

$$\frac{d^2}{dx^2} \left(E(x)I(x) \frac{d^2W}{dx^2} \right) + \frac{\kappa p_\infty bU}{c_\infty} \frac{dW}{dx} + \rho(x)A(x)\Omega^2W(x) + \frac{\kappa p_\infty b}{c_\infty}\Omega W(x) = 0 \quad (7.2.87)$$

In order to implement the rigorous Galerkin method, we represent the flexural rigidity and the mass of the system as a generalized function:

$$D(x) = E(x)I(x) = D_1H(x) + \sum_{j=1}^2 [(D_{j+1} - D_j)H(x - x_j)] \quad (7.2.88)$$

$$M(x) = \rho(x)A(x) = M_1H(x) + \sum_{j=1}^2 [(M_{j+1} - M_j)H(x - x_j)] \quad (7.2.89)$$

where $H(x)$ is the unit step function or Heaviside function which has the following properties:

$$H(x - \alpha) = \begin{cases} 1, & \text{if } x > \alpha \\ 0, & \text{otherwise} \end{cases} \quad (7.2.90)$$

$$\frac{d}{dx}H(x - \alpha) = \delta(x - \alpha) \quad (7.2.91)$$

$$\frac{d}{dx}\delta(x - \alpha) = \delta'(x - \alpha) \quad (7.2.92)$$

where $\delta(x)$ is the Dirac delta function and $\delta'(x)$ is the doublet function.

Now rewriting Eq. (7.2.87) with these considerations, we obtain:

$$\frac{d^2}{dx^2} \left(D(x) \frac{d^2W}{dx^2} \right) + \frac{\kappa p_\infty bU}{c_\infty} \frac{dW}{dx} + M(x)\Omega^2W(x) + \frac{\kappa p_\infty b}{c_\infty}\Omega W(x) = 0 \quad (7.2.93)$$

We evaluate the derivatives to get:

$$D(x) \frac{d^4W}{dx^4} + 2 \frac{d}{dx}D(x) \frac{d^3W}{dx^3} + \frac{d^2}{dx^2}D(x) \frac{d^2W}{dx^2} + \frac{\kappa p_\infty bU}{c_\infty} \frac{dW}{dx} + M(x)\Omega^2W(x) + \frac{\kappa p_\infty b}{c_\infty}\Omega W(x) = 0 \quad (7.2.94)$$

We substitute the approximation in series of $W(x)$ as:

$$W(x) = \sum_{k=1}^n Q_k \psi_k(x) \quad (7.2.95)$$

Obtaining:

$$\sum_{k=1}^n \left[D(x) \frac{d^4 \psi_k}{dx^4} + 2 \frac{d}{dx} D(x) \frac{d^3 \psi_k}{dx^3} + \frac{d^2}{dx^2} D(x) \frac{d^2 \psi_k}{dx^2} + \frac{\kappa p_\infty b U}{c_\infty} \frac{d \psi_k}{dx} + \Omega^2 M(x) \psi_k(x) + \frac{\kappa p_\infty b}{c_\infty} \Omega \psi_k(x) \right] Q_k = 0 \quad (7.2.96)$$

We multiply the differential equation by $\psi_j(x)$ and we integrate it from zero to the total length, to get:

$$\begin{aligned} \sum_{k=1}^n & \left[\int_0^L D(x) \frac{d^4 \psi_k}{dx^4} \psi_j(x) dx + 2 \int_0^L \frac{d}{dx} D(x) \frac{d^3 \psi_k}{dx^3} \psi_j(x) dx \right. \\ & + \int_0^L \frac{d^2}{dx^2} D(x) \frac{d^2 \psi_k}{dx^2} \psi_j(x) dx + \frac{\kappa p_\infty b U}{c_\infty} \int_0^L \frac{d \psi_k}{dx} \psi_j(x) dx \\ & \left. + \Omega^2 \int_0^L M(x) \psi_k(x) \psi_j(x) dx + \frac{\kappa p_\infty b}{c_\infty} \Omega \int_0^L \psi_k(x) \psi_j(x) dx \right] Q_k = 0 \end{aligned} \quad (7.2.97)$$

Defining:

$$A'_{kj} = \int_0^L D(x) \frac{d^4 \psi_k}{dx^4} \psi_j(x) dx \quad (7.2.98a)$$

$$A''_{kj} = \int_0^L \frac{d}{dx} D(x) \frac{d^3 \psi_k}{dx^3} \psi_j(x) dx \quad (7.2.98b)$$

$$A'''_{kj} = \int_0^L \frac{d^2}{dx^2} D(x) \frac{d^2 \psi_k}{dx^2} \psi_j(x) dx \quad (7.2.98c)$$

$$B_{kj} = \int_0^L \frac{d \psi_k}{dx} \psi_j(x) dx \quad (7.2.98d)$$

$$C_{kj} = \int_0^L M(x) \psi_k(x) \psi_j(x) dx \quad (7.2.98e)$$

$$D_{kj} = \int_0^L \psi_k(x) \psi_j(x) dx \quad (7.2.98f)$$

We obtain:

$$\sum_{k=1}^n \left(A'_{kj} + 2A''_{kj} + A'''_{kj} + \frac{\kappa p_\infty b U}{c_\infty} B_{kj} + \Omega^2 C_{kj} + \frac{\kappa p_\infty b}{c_\infty} \Omega D_{kj} \right) Q_k = 0 \quad (7.2.99)$$

Using matrix expression:

$$\left(\mathbf{A}' + 2\mathbf{A}'' + \mathbf{A}''' + \frac{\kappa p_\infty b U}{c_\infty} \mathbf{B} + \Omega^2 \mathbf{C} + \frac{\kappa p_\infty b}{c_\infty} \Omega \mathbf{D} \right) \mathbf{Q} = \mathbf{0} \quad (7.2.100)$$

This is a homogeneous system and has non-trivial solution only if the determinant of the coefficient matrix is equal to zero:

$$\det \left(\mathbf{A}' + 2\mathbf{A}'' + \mathbf{A}''' + \frac{\kappa p_\infty b U}{c_\infty} \mathbf{B} + \Omega^2 \mathbf{C} + \frac{\kappa p_\infty b}{c_\infty} \Omega \mathbf{D} \right) = 0 \quad (7.2.101)$$

We observe that the rigorous implementation of Galerkin method leads us to a more detailed stiffness matrix, which is composed of three sub-matrixes \mathbf{A}' , \mathbf{A}'' , \mathbf{A}''' . We also note that \mathbf{A}' is exactly \mathbf{A} for the naïve implementation so \mathbf{A}'' , \mathbf{A}''' represent the additional terms which give more precision to the method.

7.2.7 Numerical example

In order to study the dynamic stability of a beam into a gas flow, we need to know the parameter of the beam and gas. We take the following data:

Strong: Naval brass		Weak: Acrylic	
E	$100 \cdot 10^9 \text{ Pa}$	E	$3.2 \cdot 10^9 \text{ Pa}$
ρ	8553 kg/m^3	ρ	1180 kg/m^3
b	0.1 m	b	0.1 m
h	0.1 m	h	0.1 m
A	0.01 m^2	A	0.01 m^2
I	$8.33 \cdot 10^{-6} \text{ m}^4$	I	$8.33 \cdot 10^{-6} \text{ m}^4$

Table 7.15: Parameters of each segment

We also set $L_1 = 1\text{m}$, $L_2 = 1\text{m}$, $L_3 = 1\text{m}$ so $L = 3\text{m}$.

The gas parameters are:

Air	
κ	1.4
c_∞	340 m/s
p_∞	$101 \cdot 10^3 \text{ Pa}$

Table 7.16: Gas parameters

We discretize the velocity U into 100 points in the interval $U_1 = 0$ and $U_{100} = U_{max}$ (which is different for each material pattern) and we solve the problem for any speed value in the interval.

Strong - Weak - Strong material pattern

In Fig. 7.10, we have the trend of the imaginary part of the complex frequency Ω in function of the velocity of gas flow U . In this chart, we see that when the speed is equal to zero the two frequencies coincide with the natural frequencies ω_1 and ω_2 evaluated in the previous section. Increasing the velocity of the flow, instead the two frequencies tend to get closer, up to reaching the coalescence. The velocity in which the coalescence appears is called “critical velocity” U_{cr} and at that velocity we have the dynamic instability.

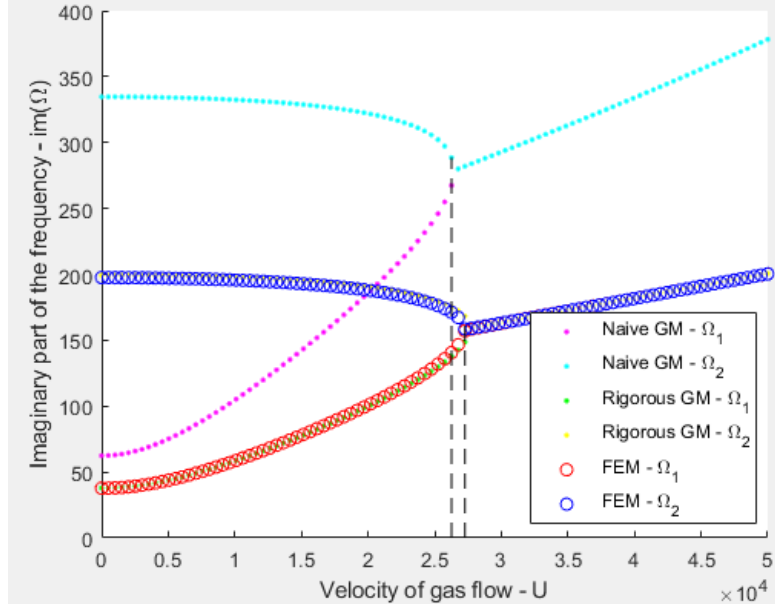


Figure 7.10: Imaginary part of the frequency vs velocity of gas flow for S-W-S material pattern

In Fig. 7.11, we have the trend of the real part of the complex frequency Ω in function of the velocity of gas flow U . In this plot, we see that for low value of gas velocity the real part of Ω_1 and Ω_2 is the same, the two lines are overlapped. When the speed reaches the value of U_{cr} , the two real parts of the frequencies differentiate and we have the instability.

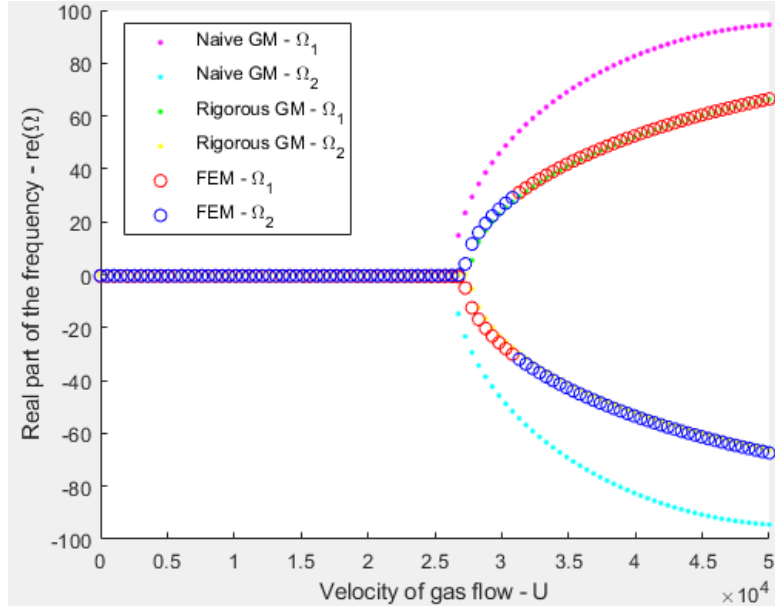


Figure 7.11: Real part of the frequency vs velocity of gas flow for S-W-S material pattern

In Fig. 7.12, we see how complex frequencies evolve with increasing gas flow velocity U . In this plot, the trend is that when the speed is equal to zero, the imaginary part of the frequencies is the same obtained in the natural frequencies and the real part is equal to zero. Increasing the velocity, the two frequencies start getting closer: the imaginary part of Ω_1 increases whereas the imaginary part of Ω_2 decreases and the real part of both is equal to zero. They reach

the coalescence at $U = U_{cr}$. Increasing again the velocity, the two frequencies diverge: the imaginary part of both increases and the real part of Ω_1 becomes greater than zero while the real part of Ω_2 becomes lower than zero.

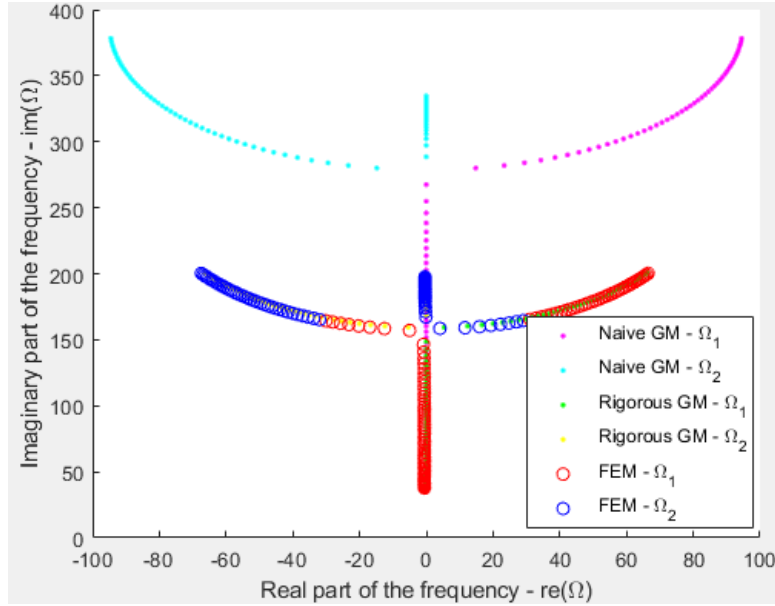


Figure 7.12: Imaginary part of the frequency vs real part of the frequency for S-W-S material pattern

As we can see from Figures 7.10 - 7.12, the trend of the methods is not the same. In particular, rigorous Galerkin method tends to FEM's solution. Instead, naïve Galerkin method does not tend to the exact solution: it is indeed far from FEM's results everywhere in the plot.

In this case, we use the Galerkin method up to three hundred terms and three finite elements for each step: nine finite elements in total.

Here, we report the critical velocities obtained with different methods:

Critical velocity U_{cr} [m/s]	
Naïve Galerkin method	$2.6263 \cdot 10^4$ m/s
Rigorous Galerkin method	$2.7273 \cdot 10^4$ m/s
Finite Element method	$2.7273 \cdot 10^4$ m/s

Table 7.17: Critical velocities obtained with different approaches for S-W-S material pattern

The relative error between the critical velocity obtained with both Galerkin methods and the FEM approach is evaluated with the following formula:

$$\varepsilon = \frac{\omega_{Galerkin} - \omega_{FEM}}{\omega_{FEM}} \times 100 \quad (7.2.102)$$

And it leads us to the following results:

Relative error [%]	
Naïve Galerkin method vs FEM	-3.70%
Rigorous Galerkin method vs FEM	0.00%

Table 7.18: Relative error between Galerkin methods and Finite Element method for S-W-S material pattern

Strong - Strong - Strong material pattern

As shown for S-W-S material pattern, we report the plots of the solution.

In Fig. 7.13, we show the trend of the imaginary part of complex frequency Ω in function of the velocity of gas flow U . When the speed is zero, we have the natural frequencies and the critical velocity is represented by the coalescence of the frequencies.

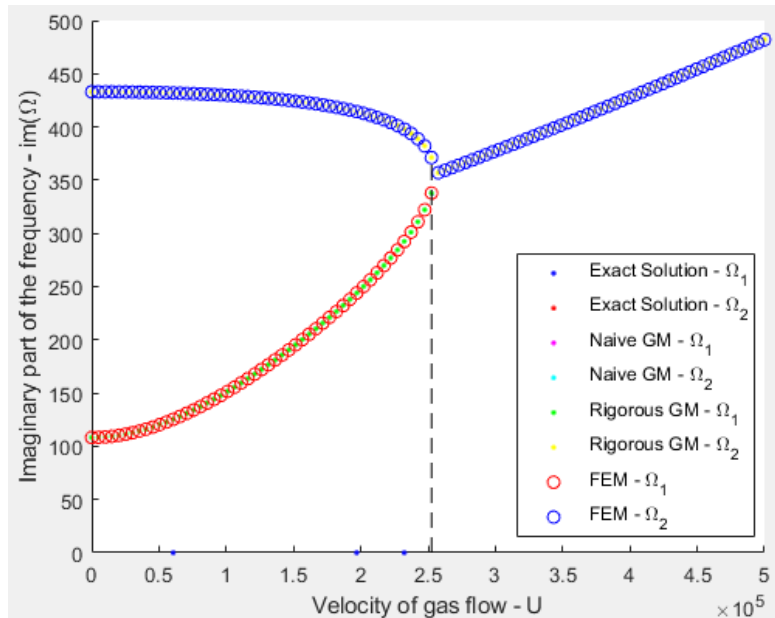


Figure 7.13: Imaginary part of the frequency vs velocity of gas flow for S-S-S material pattern

In Fig. 7.14, we have the trend of the real part of complex frequency Ω in function of the velocity of gas flow U . This plot is characterized by the coincidence of the frequencies for low value of speed and the instability is reached when the frequencies differ.

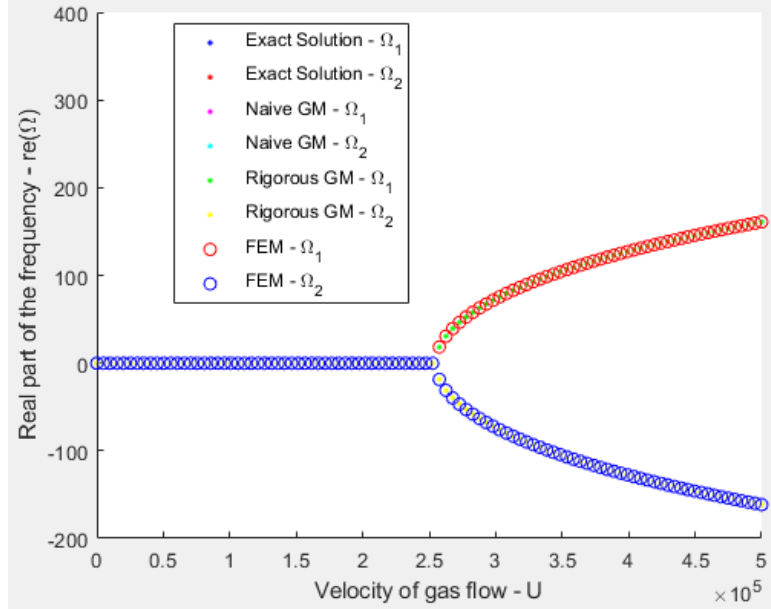


Figure 7.14: Real part of the frequency vs velocity of gas flow for S-S-S material pattern

In Fig. 7.15, we see how complex frequencies evolve with increasing gas flow velocity U . When speed is zero, the imaginary part of the frequencies is the natural frequency. Increasing in velocity flow brings imaginary part closer and the beam becomes unstable when critical velocity is reached: here we have the divergence of the frequencies.

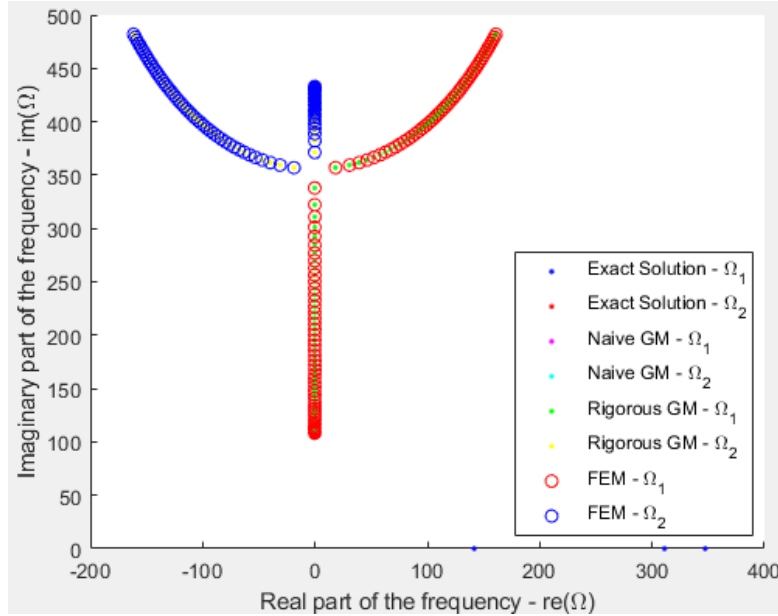


Figure 7.15: Imaginary part of the frequency vs real part of the frequency for S-S-S material pattern

As we can see from Figures 7.13 - 7.15, all the approaches used lead us to the same critical velocity and all the methods in each plot are perfectly overlapped. In particular, the two different implementations of Galerkin method yield to the same results because the beam is homogeneous and uniform. Besides, Eq. (7.2.101) becomes equal to Eq. (7.2.85) because the

two additional terms are equal to zero since there are no steps in this beam. In this case, we use the Galerkin method up to ten terms and three finite elements for each step: nine finite elements in total.

Here, we report the critical velocities obtained with different methods:

Critical velocity U_{cr} [m/s]	
Exact solution	$2.5253 \cdot 10^5$ m/s
Naïve Galerkin method	$2.5253 \cdot 10^5$ m/s
Rigorous Galerkin method	$2.5253 \cdot 10^5$ m/s
Finite Element method	$2.5253 \cdot 10^5$ m/s

Table 7.19: Critical velocities obtained with different approaches for S-S-S material pattern

The relative error between the critical velocity obtained with both Galerkin methods and with the FEM approach compared with the exact solution is evaluated with the following formula:

$$\varepsilon = \frac{\omega - \omega_{exact}}{\omega_{exact}} \times 100 \quad (7.2.103)$$

And it leads us to the following results:

Relative error [%]	
Naïve Galerkin method vs Exact solution	0.00%
Rigorous Galerkin method vs Exact solution	0.00%
Finite Element method vs Exact solution	0.00%

Table 7.20: Relative error between Galerkin methods, Finite Element method and exact solution for S-S-S material pattern

Weak - Weak - Weak material pattern

Following the same approach of S-W-S and S-S-S material patterns, we show the solution plots.

In Fig. 7.16, we have the trend of the imaginary part of complex frequency Ω in function of the velocity of gas flow U .

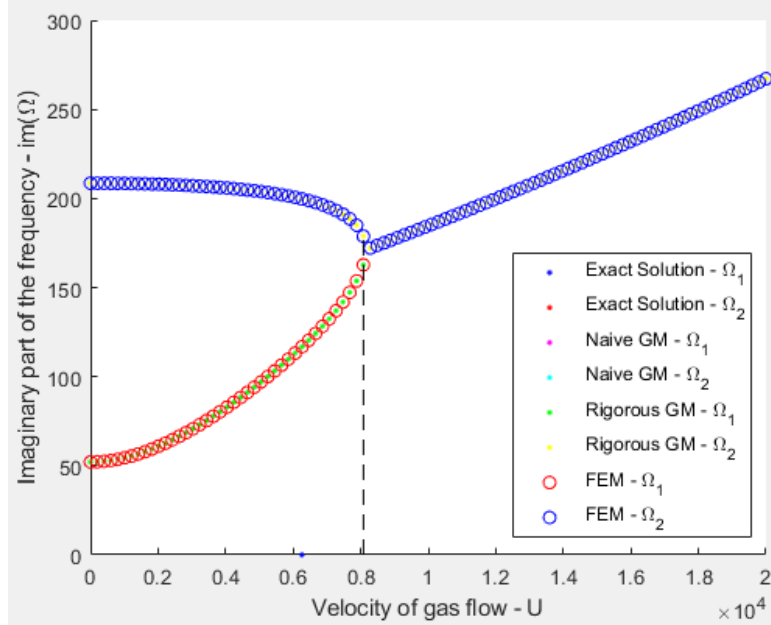


Figure 7.16: Imaginary part of the frequency vs velocity of gas flow for W-W-W material pattern

In Fig. 7.17, we have the trend of the real part of complex frequency Ω in function of the velocity of gas flow U .

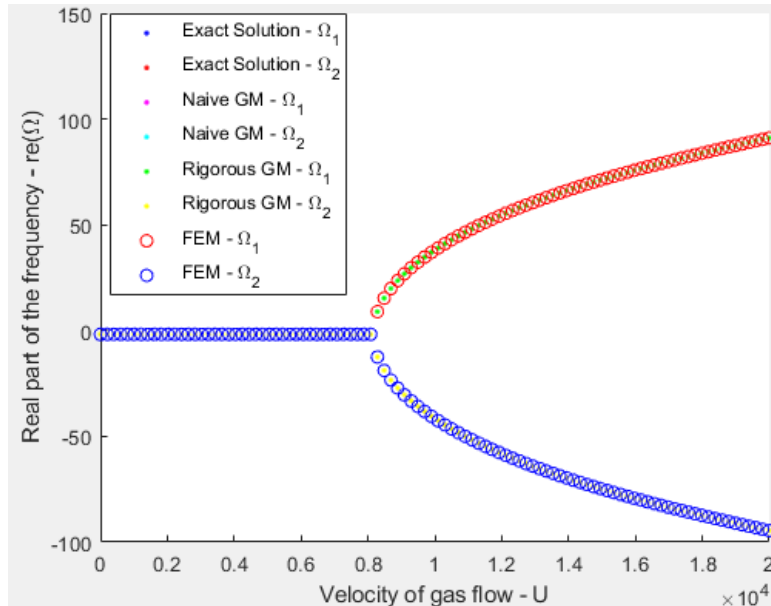


Figure 7.17: Real part of the frequency vs velocity of gas flow for W-W-W material pattern

In Fig. 7.18, we see how complex frequencies evolve with increasing gas flow velocity U .

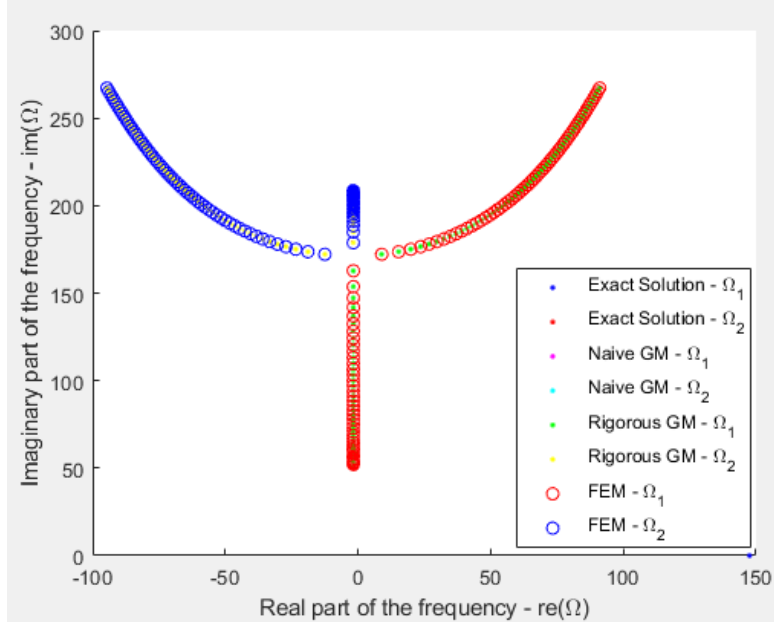


Figure 7.18: Imaginary part of the frequency vs real part of the frequency for W-W-W material pattern

The Figures 7.16 - 7.18 lead us to the following considerations: all the approaches used bring us to the same critical velocity. According to the S-S-S case, for homogeneous and uniform beam, there are no differences between rigorous and naïve Galerkin method implementations.

Here, we report the critical velocities obtained with different methods:

Critical velocity U_{cr} [m/s]	
Exact solution	$8.0808 \cdot 10^3$ m/s
Naïve Galerkin method	$8.0808 \cdot 10^3$ m/s
Rigorous Galerkin method	$8.0808 \cdot 10^3$ m/s
Finite Element method	$8.0808 \cdot 10^3$ m/s

Table 7.21: Critical velocities obtained with different approaches for W-W-W material pattern

The relative error between the critical velocity obtained with both Galerkin methods and with the FEM approach compared with the exact solution is evaluated with the following formula:

$$\varepsilon = \frac{\omega - \omega_{exact}}{\omega_{exact}} \times 100 \quad (7.2.104)$$

And it leads us to the following results:

Relative error [%]	
Naïve Galerkin method vs Exact solution	0.00%
Rigorous Galerkin method vs Exact solution	0.00%
Finite Element method vs Exact solution	0.00%

Table 7.22: Relative error between Galerkin methods, Finite Element method and exact solution for W-W-W material pattern

7.3 Conclusion

In the first section, we analyze free vibrations of three different combinations of material, keeping the geometric features of the beam as constant. Through this analysis, we reach the following interesting conclusions. First of all, rigorous Galerkin method tends to the exact solution for the in-homogeneous case whereas the naïve implementation does not. Secondly, rigorous and naïve Galerkin methods tend to the same solution in the homogeneous case, and in addition, increasing the number of terms, rigorous and naïve Galerkin methods in the homogeneous case do not improve the results. This because we immediately get the exact solution since the comparison function we choose is exactly the solution of the differential equation in the homogeneous case. Thirdly and finally, the frequencies obtained in the in-homogeneous case are smaller than the ones related to both homogeneous cases, i.e. with strong and weak material.

In the second section, we investigate the dynamic stability of three different combinations of material, keeping the geometric features of the beam as constant. We obtain then the following conclusions. Firstly, rigorous Galerkin method tends to the finite element solution for the in-homogeneous case in contrast with the naïve implementation which does not. Secondly, rigorous and naïve Galerkin methods tend to the same solution in the homogeneous case. Thirdly, rigorous and naïve Galerkin methods in the homogeneous case require much lesser terms (10) than rigorous Galerkin method in the in-homogeneous case (300) in order to represent the problem with an acceptable error.

8. Conclusion

In this thesis, we have investigated the vibrational problem of stepped structures, providing two versions of Galerkin method. The first one, named *naïve* or *straightforward*, consists in the integration along each step where the rigidity and the mass remain constant. The second version, named *rigorous*, consists in the representation of the rigidity and the mass as a generalized functions. This implementation utilizes unit step functions, as well as the Dirac delta function and its derivative: the doublet function.

We have applied these methods for free vibration problem on stepped bars, beams and plates. In order to prove the robustness of the method, we have conducted different analyses. In the third chapter regarding bars, we have investigated three different constrain conditions with two strategies of comparison functions. In the fourth and fifth chapters concerning beams, we have applied all the methods to five-span beams in four different constrain conditions and to a thirteen-span cantilever beam. In the sixth chapter related to plates, we have analyzed ten geometrically different one-stepped plates simply supported on all edges.

All these mentioned studies lead us to the same and expected conclusion: only the rigorous implementation of Galerkin method reaches the exact solution.

We have obtained the same results also applying the above mentioned methods in dynamic stability of simply supported beam into gas flow. Only the rigorous version of Galerkin method converges to the exact critical velocity.

In conclusion, this thesis demonstrates that great attention is required when implementing the Galerkin method for stepped structures because only the rigorous implementation converges.

Appendices

A. Flutter of a Timoshenko-Ehrenfest beam

In this appendix, we show a particular vibration problem: the flutter. We investigate this problem applied on a homogeneous and uniform beam. The beam under study is a thick beam, as a result we apply the Timoshenko-Ehrenfest theory. Moreover, we show that in such a theory the full expression is not required: we compare the result of the original formulation with a consistent one which does not include the fourth order derivative of the vertical displacement with respect to time.

We conduct the study analyzing first the free vibration with theoretical approach and with the Finite Element commercial software Strand7. After that, we study the dynamic stability in the flutter analysis. We apply the piston theory in order to find the critical velocity. We conduct this study with the Galerkin method. Since the beam is homogeneous and uniform, there are no differences between naïve and rigorous implementation.

A.1 Introduction

Timoshenko and Ehrenfest cooperated in the development of the beam theory which incorporates the effects of rotary inertia and shear deformation, as detailed in the recent monograph by Elishakoff [46]. This theory, referred hereinafter as Timoshenko-Ehrenfest beam theory, was first presented in the book by Timoshenko [47] in 1916, in the Russian language. In this book, Stephen Prokofievich Timoshenko (1878-1972) mentioned that the theory was the result of his cooperation with Paul Ehrenfest (1880-1933), the famous Austrian-born Dutch physicist. Later on, Timoshenko published the same results twice again, both in English, namely, in 1920 [48] and in 1921 [49]. Usually, this latter publication is referenced in the overwhelming majority of papers and books. Later on, Timoshenko [50] introduced the same material into his textbook on vibration, almost without any modification.

In 1985, Elishakoff and Lubliner [51] suggested to drop the last term in the original Timoshenko-Ehrenfest equation, namely the fourth order derivative with respect to time, altogether, since it alters natural frequencies insignificantly. In Ref. [52], it was shown that this equation can be obtained by making relevant kinematic assumptions. Ref. [53] demonstrated that the original Timoshenko-Ehrenfest equations were asymptotically inconsistent. It turned out that the simplest consistent equation was the Timoshenko-Ehrenfest equation without the fourth-order derivative with respect to time, as suggested by Elishakoff and Lubliner [51]. Ref. [54] discusses in some detail the question of priority associated with incorporating the effects of shear deformation and rotary inertia (see also Ref. [55]). We first study free vibrations of beams incorporating the effects of shear deformation and rotary inertia, and with knowledge of natural frequencies and normal modes, we proceed to evaluate flutter velocities when beam is in the supersonic flow.

A.2 Free vibrations

A.2.1 Governing differential equation for original theory

The classical Bernoulli-Euler equation for free vibration of uniform beams, as we derived in (4.1.5), reads:

$$\frac{\partial^2}{\partial x^2} \left(E(x)I(x) \frac{\partial^2 w}{\partial x^2} \right) + \rho(x)A(x) \frac{\partial^2}{\partial t^2} = 0 \quad (\text{A.2.1})$$

where E is the modulus of elasticity, I is the moment of inertia of the cross-section, A is the cross-sectional area, ρ is the mass density of the beam material, $w(x, t)$ is the deflection, x is the axial coordinate, t is time.

Rayleigh [56] modifies it introducing rotary movements of the beam elements in addition to the translatory ones. Following Rayleigh's idea, we define the angle of rotation ζ equal to the slope of the deflection curve as follows:

$$\zeta = \frac{\partial w}{\partial x} \quad (\text{A.2.2})$$

The angular acceleration of the above quantity reads:

$$\ddot{\zeta} = \frac{\partial^3 w}{\partial x \partial t^2} dx \quad (\text{A.2.3})$$

As a consequence, the inertia moment of the element about an axis through its center of mass is expressed by:

$$Z = \rho I \frac{\partial^3 w}{\partial x \partial t^2} dx \quad (\text{A.2.4})$$

Inclusion of Eq. (A.2.4) into bending moment equilibrium leads us to the following equation:

$$-V + \frac{\partial M}{\partial x} - \rho I \frac{\partial^3 w}{\partial x \partial t^2} = 0 \quad (\text{A.2.5})$$

where V is the shearing force.

Now we substitute the meaning of V obtained by Eq. (A.2.5) into the equation of dynamic equilibrium in vertical direction:

$$\frac{\partial V}{\partial x} = \frac{\partial}{\partial x} \left(\frac{\partial M}{\partial x} - \rho I \frac{\partial^3 w}{\partial x \partial t^2} \right) = -\rho A \frac{\partial^2 w}{\partial t^2} \quad (\text{A.2.6})$$

As a result, the final governing equation reads as follows:

$$EI \frac{\partial^4 w}{\partial x^4} + \rho(x)A(x) \frac{\partial^2}{\partial t^2} - \rho I \frac{\partial^4 w}{\partial x^2 \partial t^2} = 0 \quad (\text{A.2.7})$$

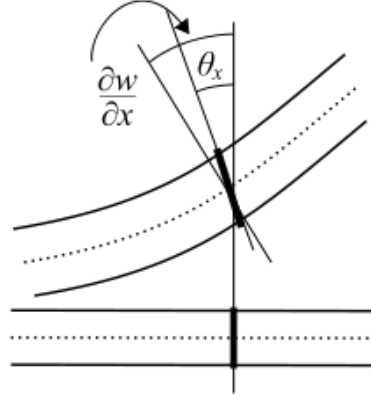


Figure A.1: Representation of shear deformation

Timoshenko [49] improved Rayleigh Eq. (A.2.7) including the shear deformation as shown in Fig. (A.1). Timoshenko defined the slope of a beam by two terms, namely:

$$\frac{\partial w}{\partial x} = \theta + \beta \quad (\text{A.2.8})$$

where θ represents the rotation of the cross-sections with shear deformation neglected, and β is the angle associated with the shear deformation.

Remembering that:

$$M = EI \frac{\partial \theta}{\partial x} \quad (\text{A.2.9})$$

$$V = -k' \beta AG = -k' AG \left(\frac{\partial w}{\partial x} - \theta \right) \quad (\text{A.2.10})$$

where k' is the shear coefficient, G is the shear modulus.

Considering these equations, we update Eq. (A.2.5) resulting in:

$$-V + \frac{\partial M}{\partial x} - \rho I \frac{\partial^2 \theta}{\partial t^2} = 0 \quad (\text{A.2.11})$$

Now we insert Eq. (A.2.9) and (A.2.10) into Eq. (A.2.11) obtaining:

$$EI \frac{\partial^2 \theta}{\partial x^2} + k' AG \left(\frac{\partial w}{\partial x} - \theta \right) - \rho I \frac{\partial^2 \theta}{\partial t^2} = 0 \quad (\text{A.2.12})$$

Substituting Eq. (A.2.10) into (A.2.6), we have:

$$k' AG \left(\frac{\partial^2 w}{\partial x^2} - \frac{\partial \theta}{\partial x} \right) - \rho A \frac{\partial^2 w}{\partial t^2} = 0 \quad (\text{A.2.13})$$

Defining from Eq. (A.2.13) $\frac{\partial \theta}{\partial x}$:

$$\frac{\partial \theta}{\partial x} = \frac{\partial^2 w}{\partial x^2} - \frac{\rho}{k' G} \frac{\partial^2 w}{\partial t^2} \quad (\text{A.2.14})$$

Now we differentiate Eq. (A.2.12) with respect to x and this leads to:

$$EI \frac{\partial^3 \theta}{\partial x^3} + k' AG \frac{\partial^2 w}{\partial x^2} - k' AG \frac{\partial \theta}{\partial x} - \rho I \frac{\partial^3 \theta}{\partial x \partial t^2} = 0 \quad (\text{A.2.15})$$

Then we introduce Eq. (A.2.14) into Eq.(A.2.15), resulting in:

$$EI \frac{\partial^4 w}{\partial x^4} + \rho A \frac{\partial^2 w}{\partial t^2} - \rho I \left(1 + \frac{E}{k'G}\right) \frac{\partial^4 w}{\partial x^2 \partial t^2} + \frac{\rho^2 I}{k'G} \frac{\partial^4 w}{\partial t^4} = 0 \quad (\text{A.2.16})$$

A.2.2 Governing differential equation for consistent theory

Timoshenko [48], [49] concluded that the fourth term in Eq. (A.2.16) produces a small effect in the characteristic equation. On the basis of this affirmation, we recapitulate the derivation of consistent Timoshenko-Ehrenfest theory which does not contain the last term.

Looking at the third term in Eq. (A.2.11), i.e. $\rho I \frac{\partial^2 \theta}{\partial t^2}$, we see that it replaces the last term in Eq. (A.2.5) due to rotary inertia. The consistent set of equations is obtained by not performing this substitution as follows:

$$k' AG \left(\frac{\partial^2 w}{\partial x^2} - \frac{\partial \theta}{\partial x} \right) - \rho A \frac{\partial^2 w}{\partial t^2} = 0 \quad (\text{A.2.17a})$$

$$EI \frac{\partial^2 \theta}{\partial x^2} + k' AG \left(\frac{\partial w}{\partial x} - \theta \right) - \rho I \frac{\partial^3 w}{\partial x \partial t^2} = 0 \quad (\text{A.2.17b})$$

In this way, we clearly see that Eq. (A.2.17a) coincides with Eq. (A.2.13) while Eq. (A.2.17b) is derived by substitution of Eq. (A.2.9) and (A.2.10) into Eq. (A.2.5).

Now from the first one, we can define $\frac{\partial \theta}{\partial x}$:

$$\frac{\partial \theta}{\partial x} = \frac{\partial^2 w}{\partial x^2} - \frac{\rho}{k'G} \frac{\partial^2 w}{\partial t^2} \quad (\text{A.2.18})$$

The differentiation of the second equation with respect to x leads to:

$$EI \frac{\partial^3 \theta}{\partial x^3} + k' AG \frac{\partial^2 w}{\partial x^2} - k' AG \frac{\partial \theta}{\partial x} - \rho I \frac{\partial^4 w}{\partial x^2 \partial t^2} = 0 \quad (\text{A.2.19})$$

Now we substitute the value of $\frac{\partial \theta}{\partial x}$ from Eq. (A.2.18) in the last equation, to result in:

$$EI \frac{\partial^4 w}{\partial x^4} + \rho A \frac{\partial^2 w}{\partial t^2} - \rho I \left(1 + \frac{E}{k'G}\right) \frac{\partial^4 w}{\partial x^2 \partial t^2} = 0 \quad (\text{A.2.20})$$

Actually, we put the governing differential equation in the following generic form:

$$EI \frac{\partial^4 w}{\partial x^4} + \rho A \frac{\partial^2 w}{\partial t^2} + \varepsilon \left[-\rho I \left(1 + \frac{E}{k'G}\right) \frac{\partial^4 w}{\partial x^2 \partial t^2} + \delta \frac{\rho^2 I}{k'G} \frac{\partial^4 w}{\partial t^4} \right] = 0 \quad (\text{A.2.21})$$

When $\varepsilon = 0$, the equation results in the Bernoulli-Euler's beam theory. When $\varepsilon = 1$, we obtain two different Timoshenko-Ehrenfest beam's theories which are identified by a control parameter δ . When $\delta = 1$, we derive the original theory otherwise for $\delta = 0$, we obtain the consistent theory.

A.2.3 Exact solution for original theory

We think $w(x, t)$ as a product of two functions: one in time and one in the axial coordinate x :

$$w(x, t) = W(x)T(t) \quad (\text{A.2.22})$$

More specifically, we think:

$$w(x, t) = e^{\beta x} e^{i\omega t} \quad (\text{A.2.23})$$

where ω is the frequency of the beam's vibration.

With this substitution and dividing by EI , we obtain the following 4th order equation:

$$\beta^4 + \frac{k'G\rho\omega^2 + \rho E\omega^2}{k'GE}\beta^2 + \frac{\rho^2 I\omega^4 - \rho A\omega^2 k'G}{k'GEI} = 0 \quad (\text{A.2.24})$$

Denoting:

$$d = \frac{k'G\rho\omega^2 + \rho E\omega^2}{k'GE} \quad (\text{A.2.25})$$

$$e = \frac{\rho^2 I\omega^4 - \rho A\omega^2 k'G}{k'GEI} \quad (\text{A.2.26})$$

We obtain:

$$\beta^4 + d\beta^2 + e = 0 \quad (\text{A.2.27})$$

Defining now:

$$\beta^2 = z \quad (\text{A.2.28})$$

We obtain:

$$z^2 + dz + e = 0 \quad (\text{A.2.29})$$

Solutions of this equation are:

$$z_{1,2} = \frac{1}{2} \left(-d \pm \sqrt{(\Delta)} \right) \quad (\text{A.2.30})$$

$$z_1 = \frac{1}{2} \left(-d + \sqrt{(\Delta)} \right) \quad (\text{A.2.31a})$$

$$z_2 = \frac{1}{2} \left(-d - \sqrt{(\Delta)} \right) \quad (\text{A.2.31b})$$

where:

$$\Delta = d^2 - 4e = \left(\frac{\omega^2 \rho}{E} - \frac{\omega^2 \rho}{k'G} \right)^2 + \frac{4\omega^2 \rho A}{EI} \quad (\text{A.2.32})$$

It is easy to see that this part is positive for any value of ω .

Now we study the sign of z_1 and z_2 :

- $z_2 < 0$ for any value of ω
- $z_1 > 0 \Leftrightarrow -d + \sqrt{d^2 - 4e} \Leftrightarrow \sqrt{d^2 - 4e} > d \Leftrightarrow e < 0$

$e < 0$ means

$$\omega^2 < \frac{k'AG}{\rho I} \quad (\text{A.2.33})$$

We define $\omega = \sqrt{\frac{k'AG}{\rho I}} = \omega_{lim}$.

Note that $z_1 < 0$ implies that $\omega^2 > \omega_{lim}^2$.

Now we define the quantities β_1 , β_2 , β_3 and β_4 as follows:

$$\beta_3 = i\sqrt{|z_2|} \quad (\text{A.2.34a})$$

$$\beta_4 = -i\sqrt{|z_2|} \quad (\text{A.2.34b})$$

If $\omega < \omega_{lim}$,

$$\beta_1 = \sqrt{z_1} \quad (\text{A.2.35a})$$

$$\beta_2 = -\sqrt{z_1} \quad (\text{A.2.35b})$$

If $\omega > \omega_{lim}$,

$$\beta_1 = i\sqrt{|z_1|} \quad (\text{A.2.36a})$$

$$\beta_2 = -i\sqrt{|z_1|} \quad (\text{A.2.36b})$$

In general, we can write the spatial part of Eq. (A.2.22) in the following form:

$$W(x) = C_1 e^{\beta_1 x} + C_2 e^{\beta_2 x} + C_3 e^{\beta_3 x} + C_4 e^{\beta_4 x} \quad (\text{A.2.37})$$

In the specific case $\omega < \omega_{lim}$, we have:

$$W(x) = C_1 e^{\sqrt{z_1}x} + C_2 e^{-\sqrt{z_1}x} + C_3 e^{i\sqrt{|z_2|}x} + C_4 e^{-i\sqrt{|z_2|}x} \quad (\text{A.2.38})$$

Bearing Euler's formula in mind, we obtain:

$$W(x) = P_1 \cosh(\lambda_1 x) + P_2 \sinh(\lambda_1 x) + P_3 \cosh(\lambda_2 x) + P_4 \sin(\lambda_2 x) \quad (\text{A.2.39})$$

where:

$$\lambda_1 = \sqrt{\frac{-d + \sqrt{\Delta}}{2}} \quad (\text{A.2.40})$$

$$\lambda_2 = \sqrt{\frac{d + \sqrt{\Delta}}{2}} \quad (\text{A.2.41})$$

If we substitute Eq. (A.2.39) in the integral with respect to x of Eq. (A.2.14), we obtain (see Ref. [57]):

$$\theta(x, t) = \left[\left(\lambda_1 + \frac{\rho\omega^2}{k'G\lambda_1} \right) P_1 \sinh(\lambda_1 x) + \left(\lambda_1 + \frac{\rho\omega^2}{k'G\lambda_1} \right) P_2 \cosh(\lambda_1 x) \right. \\ \left. + \left(-\lambda_2 + \frac{\rho\omega^2}{k'G\lambda_2} \right) P_3 \sin(\lambda_2 x) + \left(\lambda_2 - \frac{\rho\omega^2}{k'G\lambda_2} \right) P_4 \cos(\lambda_2 x) \right] e^{i\omega t} \quad (\text{A.2.42})$$

If $\omega > \omega_{lim}$,

$$W(x) = C_1 e^{i\sqrt{|z_1|}x} + C_2 e^{-i\sqrt{|z_1|}x} + C_3 e^{i\sqrt{|z_2|}x} + C_4 e^{-i\sqrt{|z_2|}x} \quad (\text{A.2.43})$$

Considering Euler's formula, we obtain:

$$W(x) = Q_1 \cosh(\lambda_1 x) + Q_2 \sinh(\lambda_1 x) + Q_3 \cosh(\lambda_2 x) + Q_4 \sin(\lambda_2 x) \quad (\text{A.2.44})$$

where:

$$\lambda_1 = \sqrt{\frac{d - \sqrt{\Delta}}{2}} \quad (\text{A.2.45})$$

$$\lambda_2 = \sqrt{\frac{d + \sqrt{\Delta}}{2}} \quad (\text{A.2.46})$$

If we substitute Eq. (A.2.44) in the integral with respect to x of Eq. (A.2.14), we get:

$$\theta(x, t) = \left[\left(-\lambda_1 + \frac{\rho\omega^2}{k'G\lambda_1} \right) Q_1 \sin(\lambda_1 x) + \left(\lambda_1 - \frac{\rho\omega^2}{k'G\lambda_1} \right) Q_2 \cos(\lambda_1 x) \right. \\ \left. + \left(-\lambda_2 + \frac{\rho\omega^2}{k'G\lambda_2} \right) Q_3 \sin(\lambda_2 x) + \left(\lambda_2 - \frac{\rho\omega^2}{k'G\lambda_2} \right) Q_4 \cos(\lambda_2 x) \right] e^{i\omega t} \quad (\text{A.2.47})$$

In order to find the four coefficients P_1 , P_2 , P_3 , and P_4 or Q_1 , Q_2 , Q_3 and Q_4 in the Eq. (A.2.39) or (A.2.44), we have to satisfy the boundary conditions. For the clamped-free beam under consideration, we demand vertical displacement and rotation angle equal to zero in the left end and bending moment and shear force equal to zero in the right end.

For $x = 0$:

$$w(0) = 0 \quad (\text{A.2.48a})$$

$$\theta(0) = 0 \quad (\text{A.2.48b})$$

- If $\omega < \omega_{lim}$,

$$P_1 + P_3 = 0 \quad (\text{A.2.49a})$$

$$\left(\lambda_1 + \frac{\rho\omega^2}{k'G\lambda_1} \right) P_2 + \left(\lambda_2 - \frac{\rho\omega^2}{k'G\lambda_2} \right) P_4 = 0 \quad (\text{A.2.49b})$$

- If $\omega > \omega_{lim}$,

$$Q_1 + Q_3 = 0 \quad (\text{A.2.50a})$$

$$\left(\lambda_1 - \frac{\rho\omega^2}{k'G\lambda_1} \right) Q_2 + \left(\lambda_2 - \frac{\rho\omega^2}{k'G\lambda_2} \right) Q_4 = 0 \quad (\text{A.2.50b})$$

For $x = L$:

$$w'(L) - \theta(L) = 0 \quad (\text{A.2.51a})$$

$$\theta'(L) = 0 \quad (\text{A.2.51b})$$

- If $\omega < \omega_{lim}$,

$$-\frac{\rho\omega^2 P_1}{k'G\lambda_1} \sinh(\lambda_1 L) - \frac{\rho\omega^2 P_2}{k'G\lambda_1} \cosh(\lambda_1 L) - \frac{\rho\omega^2 P_3}{k'G\lambda_2} \sin(\lambda_2 L) + \frac{\rho\omega^2 P_4}{k'G\lambda_2} \cos(\lambda_2 L) = 0 \quad (\text{A.2.52a})$$

$$\begin{aligned} & \left(\lambda_1 + \frac{\rho\omega^2}{k'G\lambda_1} \right) \lambda_1 P_1 \cosh(\lambda_1 L) + \left(\lambda_1 + \frac{\rho\omega^2}{k'G\lambda_1} \right) \lambda_1 P_2 \sinh(\lambda_1 L) \\ & + \left(\lambda_2 - \frac{\rho\omega^2}{k'G\lambda_2} \right) \lambda_2 P_3 \cos(\lambda_2 L) - \left(\lambda_2 - \frac{\rho\omega^2}{k'G\lambda_2} \right) \lambda_2 P_4 \sin(\lambda_2 L) = 0 \end{aligned} \quad (\text{A.2.52b})$$

- If $\omega > \omega_{lim}$,

$$-\frac{\rho\omega^2 Q_1}{k'G\lambda_1} \sin(\lambda_1 L) + \frac{\rho\omega^2 Q_2}{k'G\lambda_1} \cos(\lambda_1 L) - \frac{\rho\omega^2 Q_3}{k'G\lambda_2} \sin(\lambda_2 L) + \frac{\rho\omega^2 Q_4}{k'G\lambda_2} \cos(\lambda_2 L) = 0 \quad (\text{A.2.53a})$$

$$\begin{aligned} & \left(-\lambda_1 + \frac{\rho\omega^2}{k'G\lambda_1} \right) \lambda_1 Q_1 \cos(\lambda_1 L) - \left(\lambda_1 - \frac{\rho\omega^2}{k'G\lambda_1} \right) \lambda_1 Q_2 \sin(\lambda_1 L) \\ & + \left(-\lambda_2 + \frac{\rho\omega^2}{k'G\lambda_2} \right) \lambda_2 Q_3 \cos(\lambda_2 L) - \left(\lambda_2 - \frac{\rho\omega^2}{k'G\lambda_2} \right) \lambda_2 Q_4 \sin(\lambda_2 L) = 0 \end{aligned} \quad (\text{A.2.53b})$$

In this way, we obtain four equations for four unknowns. For a non-trivial solution, we demand that the determinant of the matrix coefficient is equal to zero. This demand leads to a function in the single variable in terms of ω . When the function crosses the x -axis, we find the value of ω that makes the determinant equal to zero.

- If $\omega < \omega_{lim}$, the frequency determinant becomes:

$$\det \begin{bmatrix} 1 & 0 & 1 & 0 \\ 0 & \lambda_1 + \frac{\rho\omega^2}{k'G\lambda_1} & 0 & \lambda_2 - \frac{\rho\omega^2}{k'G\lambda_2} \\ -\frac{\rho\omega^2}{k'G\lambda_1} \sinh(\lambda_1 L) & -\frac{\rho\omega^2}{k'G\lambda_1} \cosh(\lambda_1 L) & -\frac{\rho\omega^2}{k'G\lambda_2} \sin(\lambda_2 L) & \frac{\rho\omega^2}{k'G\lambda_2} \cos(\lambda_2 L) \\ \left(\lambda_1 + \frac{\rho\omega^2}{k'G\lambda_1} \right) \lambda_1 \cosh(\lambda_1 L) & \left(\lambda_1 + \frac{\rho\omega^2}{k'G\lambda_1} \right) \lambda_1 \sinh(\lambda_1 L) & \left(\lambda_2 - \frac{\rho\omega^2}{k'G\lambda_2} \right) \lambda_2 \sin(\lambda_2 L) & \left(\lambda_2 - \frac{\rho\omega^2}{k'G\lambda_2} \right) \lambda_2 \cos(\lambda_2 L) \end{bmatrix} = 0 \quad (\text{A.2.54})$$

- If $\omega > \omega_{lim}$, the frequency determinant reads:

$$\det \begin{bmatrix} 1 & 0 & 1 & 0 \\ 0 & \lambda_1 - \frac{\rho\omega^2}{k'G\lambda_1} & 0 & \lambda_2 - \frac{\rho\omega^2}{k'G\lambda_2} \\ -\frac{\rho\omega^2}{k'G\lambda_1^2} \sin(\lambda_1 L) & \frac{\rho\omega^2}{k'G\lambda_1} \cos(\lambda_1 L) & -\frac{\rho\omega^2}{k'G\lambda_2^2} \sin(\lambda_2 L) & \frac{\rho\omega^2}{k'G\lambda_2} \cos(\lambda_2 L) \\ \left(-\lambda_1 + \frac{\rho\omega^2}{k'G\lambda_1}\right) \lambda_1 \cos(\lambda_1 L) & \left(-\lambda_1 + \frac{\rho\omega^2}{k'G\lambda_1}\right) \lambda_1 \sin(\lambda_1 L) & \left(-\lambda_2 + \frac{\rho\omega^2}{k'G\lambda_2}\right) \lambda_2 \sin(\lambda_2 L) & \left(-\lambda_2 + \frac{\rho\omega^2}{k'G\lambda_2}\right) \lambda_2 \cos(\lambda_2 L) \end{bmatrix} = 0 \quad (\text{A.2.55})$$

A.2.4 Exact solution for consistent theory

We represent the displacement in the multiplicative form:

$$w(x, t) = W(x)T(t) \quad (\text{A.2.56})$$

We suppose:

$$w(x, t) = e^{\beta x} e^{i\omega t} \quad (\text{A.2.57})$$

where ω is the frequency of the beam's vibration.

Operating this substitution and dividing by term EI , we obtain the following 4th order polynomial equation in terms of β :

$$\beta^4 + \frac{k'G\rho\omega^2 + \rho E\omega^2}{k'GE} \beta^2 - \frac{\rho A\omega^2}{EI} = 0 \quad (\text{A.2.58})$$

Denoting:

$$d = \frac{k'G\rho\omega^2 + \rho E\omega^2}{k'GE} \quad (\text{A.2.59})$$

$$e = -\frac{\rho A\omega^2}{EI} \quad (\text{A.2.60})$$

We obtain:

$$\beta^4 + d\beta^2 + e = 0 \quad (\text{A.2.61})$$

We introduce the following notation:

$$\beta^2 = z \quad (\text{A.2.62})$$

We obtain:

$$z^2 + dz + e = 0 \quad (\text{A.2.63})$$

The solutions of the equation above are:

$$z_{1,2} = \frac{1}{2} \left(-d \pm \sqrt{(\Delta)} \right) \quad (\text{A.2.64})$$

$$z_1 = \frac{1}{2} \left(-d + \sqrt{(\Delta)} \right) \quad (\text{A.2.65a})$$

$$z_2 = \frac{1}{2} \left(-d - \sqrt{(\Delta)} \right) \quad (\text{A.2.65b})$$

where:

$$\Delta = d^2 - 4e = \left(\frac{\omega^2 \rho}{E} + \frac{\omega^2 \rho}{k' G} \right)^2 + \frac{4\omega^2 \rho A}{EI} \quad (\text{A.2.66})$$

It is easy to see that this part is positive for any value of ω .

Now we study the sign of z_1 and z_2 :

- $z_2 < 0$ for any value of ω
 - $z_1 > 0 \Leftrightarrow -d + \sqrt{d^2 - 4e} \Leftrightarrow \sqrt{d^2 - 4e} > d \Leftrightarrow e < 0$
- $e < 0$ for any value of ω

It is interesting to see that for the consistent version of Timoshenko-Ehrenfest theory, the term ω_{lim} does not appear.

Defining the quantities $\beta_1, \beta_2, \beta_3$ and β_4 :

$$\beta_1 = \sqrt{z_1} \quad (\text{A.2.67a})$$

$$\beta_2 = -\sqrt{z_1} \quad (\text{A.2.67b})$$

$$\beta_3 = i\sqrt{|z_2|} \quad (\text{A.2.67c})$$

$$\beta_4 = -i\sqrt{|z_2|} \quad (\text{A.2.67d})$$

We write the spatial part of Eq. (A.2.56) in the following form:

$$W(x) = C_1 e^{\beta_1 x} + C_2 e^{\beta_2 x} + C_3 e^{\beta_3 x} + C_4 e^{\beta_4 x} \quad (\text{A.2.68})$$

In our case, we have:

$$W(x) = C_1 e^{\sqrt{z_1} x} + C_2 e^{-\sqrt{z_1} x} + C_3 e^{i\sqrt{|z_2|} x} + C_4 e^{-i\sqrt{|z_2|} x} \quad (\text{A.2.69})$$

With Euler's transformation, we obtain:

$$W(x) = P_1 \cosh(\lambda_1 x) + P_2 \sinh(\lambda_1 x) + P_3 \cosh(\lambda_2 x) + P_4 \sin(\lambda_2 x) \quad (\text{A.2.70})$$

where:

$$\lambda_1 = \sqrt{\frac{-d + \sqrt{\Delta}}{2}} \quad (\text{A.2.71})$$

$$\lambda_2 = \sqrt{\frac{d + \sqrt{\Delta}}{2}} \quad (\text{A.2.72})$$

Substitution of Eq. (A.2.70) in the result of integration of Eq. (A.2.18) with respect to x leads to:

$$\theta(x, t) = \left[\left(\lambda_1 + \frac{\rho\omega^2}{k'G\lambda_1} \right) P_1 \sinh(\lambda_1 x) + \left(\lambda_1 + \frac{\rho\omega^2}{k'G\lambda_1} \right) P_2 \cosh(\lambda_1 x) + \left(-\lambda_2 + \frac{\rho\omega^2}{k'G\lambda_2} \right) P_3 \sin(\lambda_2 x) + \left(\lambda_2 - \frac{\rho\omega^2}{k'G\lambda_2} \right) P_4 \cos(\lambda_2 x) \right] e^{i\omega t} \quad (\text{A.2.73})$$

To find the four coefficients, we have to satisfy the boundary conditions.

Specifically for $x = 0$, we have:

$$w(0) = 0 \quad (\text{A.2.74a})$$

$$\theta(0) = 0 \quad (\text{A.2.74b})$$

This implies that:

$$P_1 + P_3 = 0 \quad (\text{A.2.75a})$$

$$\left(\lambda_1 + \frac{\rho\omega^2}{k'G\lambda_1} \right) P_2 + \left(\lambda_2 - \frac{\rho\omega^2}{k'G\lambda_2} \right) P_4 = 0 \quad (\text{A.2.75b})$$

When $x = L$:

$$w'(L) - \theta(L) = 0 \quad (\text{A.2.76a})$$

$$\theta'(L) = 0 \quad (\text{A.2.76b})$$

This means:

$$-\frac{\rho\omega^2 P_1}{k'G\lambda_1} \sinh(\lambda_1 L) - \frac{\rho\omega^2 P_2}{k'G\lambda_1} \cosh(\lambda_1 L) - \frac{\rho\omega^2 P_3}{k'G\lambda_2} \sin(\lambda_2 L) + \frac{\rho\omega^2 P_4}{k'G\lambda_2} \cos(\lambda_2 L) = 0 \quad (\text{A.2.77a})$$

$$\begin{aligned} & \left(\lambda_1 + \frac{\rho\omega^2}{k'G\lambda_1} \right) \lambda_1 P_1 \cosh(\lambda_1 L) + \left(\lambda_1 + \frac{\rho\omega^2}{k'G\lambda_1} \right) \lambda_1 P_2 \sinh(\lambda_1 L) \\ & + \left(\lambda_2 - \frac{\rho\omega^2}{k'G\lambda_2} \right) \lambda_2 P_3 \cos(\lambda_2 L) - \left(\lambda_2 - \frac{\rho\omega^2}{k'G\lambda_2} \right) \lambda_2 P_4 \sin(\lambda_2 L) = 0 \end{aligned} \quad (\text{A.2.77b})$$

The problem is in the form of:

$$\det \begin{bmatrix} 1 & 0 & 1 & 0 \\ 0 & \lambda_1 + \frac{\rho\omega^2}{k'G\lambda_1} & 0 & \lambda_2 - \frac{\rho\omega^2}{k'G\lambda_2} \\ -\frac{\rho\omega^2}{k'G\lambda_1} \sinh(\lambda_1 L) & -\frac{\rho\omega^2}{k'G\lambda_1} \cosh(\lambda_1 L) & -\frac{\rho\omega^2}{k'G\lambda_2} \sin(\lambda_2 L) & \frac{\rho\omega^2}{k'G\lambda_2} \cos(\lambda_2 L) \\ \left(\lambda_1 + \frac{\rho\omega^2}{k'G\lambda_1} \right) \lambda_1 \cosh(\lambda_1 L) & \left(\lambda_1 + \frac{\rho\omega^2}{k'G\lambda_1} \right) \lambda_1 \sinh(\lambda_1 L) & \left(\lambda_2 - \frac{\rho\omega^2}{k'G\lambda_2} \right) \lambda_2 \sin(\lambda_2 L) & \left(\lambda_2 - \frac{\rho\omega^2}{k'G\lambda_2} \right) \lambda_2 \cos(\lambda_2 L) \end{bmatrix} = 0 \quad (\text{A.2.78})$$

A.2.5 Numerical example

We deal with a cantilever beam with the following data:

Steel	
E	$2.1 \cdot 10^{11}$ Pa
G	$6.3 \cdot 10^{10}$ Pa
ρ	7860 kg/m^3
ν	0.2
L	1 m
b	0.02 m
h	0.10 m

Table A.1: Beam's parameters

Normally, for a rectangular section, the shear coefficient k' is taken as follows:

$$k' = \frac{10(1 + \nu)}{12 + 11\nu} \quad (\text{A.2.79})$$

FEM solution

In order to validate the theoretical results, we use the FEM software Strand7 (see Ref. [38]) which uses shear-deformable elements. The mesh with 51 nodes leads us to the following ten natural frequencies:

FEM - Strand7		
Mode	Frequencies [Hz]	Frequencies [rad/s]
1	82.8435	520.5223
2	496.737	3 121.0979
3	1305.48	8 202.5919
4	2361.47	14 837.5883
5	3577.09	22 475.5719
6	4883.81	30 685.9550
7	6236.89	39 187.6272
8	7607.79	47 801.2661
9	8978.98	56 416.7271
10	10340.00	64 968.2880

Table A.2: Frequencies obtained with FEM software Strand7

Original Timoshenko-Ehrenfest results

With the beam's data, the value of ω_{lim} is:

$$\omega_{lim} = \sqrt{\frac{k'AG}{\rho I}} = 89\ 528.0245 \frac{rad}{s} \quad (\text{A.2.80})$$

It turns out that this value exceeds the value of the natural frequency ω_{10} obtained with FEM analysis, so we concentrate on the first case relating to $\omega < \omega_{lim}$.

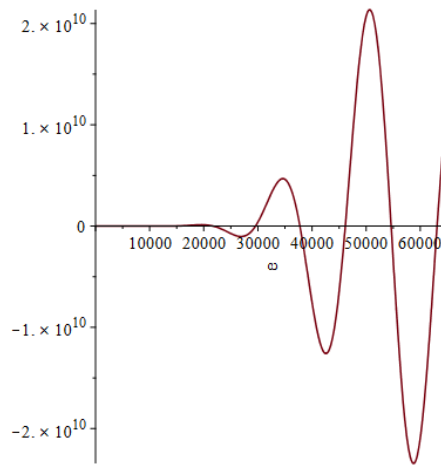


Figure A.2: Plot of characteristic equation by original Timoshenko-Ehrenfest theory

And the first ten roots are:

Original Timoshenko-Ehrenfest theory	
Mode	Frequencies [rad/s]
1	519.6399
2	3 086.8280
3	8 031.3652
4	14 402.9084
5	21 700.9585
6	29 560.5088
7	37 755.5844
8	46 139.6594
9	54 614.3405
10	63 106.0902

Table A.3: Frequencies obtained with original Timoshenko-Ehrenfest theory

Consistent Timoshenko-Ehrenfest results

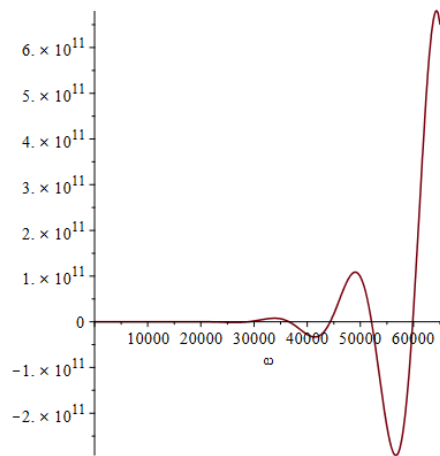


Figure A.3: Plot of characteristic equation by consistent Timoshenko-Ehrenfest theory

The first ten roots are:

Consistent Timoshenko-Ehrenfest theory	
Mode	Frequencies [rad/s]
1	519.6313
2	3 085.2128
3	8 006.8717
4	14 285.3683
5	21 369.5008
6	28 870.1051
7	36 564.7675
8	44 330.5689
9	52 102.8447
10	59 851.0564

Table A.4: Frequencies obtained with consistent Timoshenko-Ehrenfest theory

In Table A.5, we list the values of the first ten natural frequencies obtained with three different approaches:

Solutions obtained with different approaches			
Mode	FEM [rad/s]	Original T-E theory [rad/s]	Consistent T-E theory [rad/s]
1	520.5223	519.6399	519.6313
2	3 121.0979	3 086.8280	3 085.2128
3	8 202.5919	8 031.3652	8 006.8717
4	14 837.5883	14 402.9084	14 285.3683
5	22 475.5719	21 700.9585	21 369.5008
6	30 685.9550	29 560.5088	28 870.1051
7	39 187.6272	37 755.5844	36 564.7675
8	47 801.2661	46 139.6594	44 330.5689
9	56 416.7271	54 614.3405	52 102.8447
10	64 968.2880	63 106.0902	59 851.0564

Table A.5: Solutions obtained with different approaches

In Table A.6, we list the value of the relative error in percentual for the first ten natural

frequencies among all the three different approaches using the following expressions:

$$\varepsilon_1 = \frac{\omega_{FEM} - \omega_{original}}{\omega_{original}} \times 100 \quad (A.2.81a)$$

$$\varepsilon_2 = \frac{\omega_{FEM} - \omega_{consistent}}{\omega_{consistent}} \times 100 \quad (A.2.81b)$$

$$\varepsilon_3 = \frac{\omega_{original} - \omega_{consistent}}{\omega_{consistent}} \times 100 \quad (A.2.81c)$$

Mode	Relative error between different approaches		
	FEM vs Original T-E theory [%]	FEM vs Consistent T-E theory [%]	Original vs Consistent T-E theory [%]
1	0.1698%	0.1715%	0.0017%
2	1.1102%	1.1631%	0.0524%
3	2.1320%	2.4444%	0.3059%
4	3.0180%	3.8656%	0.8228%
5	3.5695%	5.1759%	1.5511%
6	3.8073%	6.2897%	2.3914%
7	3.7929%	7.1732%	3.2567%
8	3.6013%	7.8291%	4.0809%
9	3.3002%	8.2796%	4.8203%
10	2.9509%	8.5499%	5.4386%

Table A.6: Relative error between different approaches

Examination of Tables A.5 - A.6 shows that these three different approaches yield similar results. In particular, the two theoretical ways, namely original and consistent versions of Timoshenko-Ehrenfest equation, produce very close results. Thus, we verify that we can safely neglect the 4th derivative of time in the original Timoshenko-Ehrenfest equations.

A.3 Dynamic Stability

A.3.1 Governing differential equation for original Timoshenko-Ehrenfest beam in gas flow

The governing differential equations for Timoshenko-Ehrenfest beam are two: one for the vertical displacement $w(x, t)$ and one for the rotation angle of the cross section $\theta(x, t)$

$$\rho A \frac{\partial^2 w}{\partial t^2} = k' AG \left(\frac{\partial^2 w}{\partial t^2} - \frac{\partial \theta}{\partial x} \right) - q(x, t) \quad (\text{A.3.1a})$$

$$\rho I \frac{\partial^2 \theta}{\partial t^2} = EI \frac{\partial^2 \theta}{\partial x^2} + k' AG \left(\frac{\partial w}{\partial x} - \theta \right) \quad (\text{A.3.1b})$$

where E is the elastic modulus, G is the shear modulus, A is the area of the cross section, ρ is the mass density, I is the inertia moment of the cross section, k' is the shear coefficient and q the load.

Substituting into Eq. (A.3.1a) the expression of piston theory load as shown in Eq. (7.2.2), we obtain:

$$\rho A \frac{\partial^2 w}{\partial t^2} = k' AG \left(\frac{\partial^2 w}{\partial t^2} - \frac{\partial \theta}{\partial x} \right) - \frac{\kappa p_\infty b}{c_\infty} \left(\frac{\partial w}{\partial t} + U \frac{\partial w}{\partial x} \right) \quad (\text{A.3.2a})$$

$$\rho I \frac{\partial^2 \theta}{\partial t^2} = EI \frac{\partial^2 \theta}{\partial x^2} + k' AG \left(\frac{\partial w}{\partial x} - \theta \right) \quad (\text{A.3.2b})$$

Now we introduce the dimensionless parameters as follows:

$$\xi = \frac{x}{L} \rightarrow x = \xi L \quad (\text{A.3.3a})$$

$$v = \frac{w}{L} \rightarrow w = vL \quad (\text{A.3.3b})$$

$$\tau = t \sqrt{\frac{Gk'}{\rho L^2}} \rightarrow t = \tau \sqrt{\frac{\rho L^2}{Gk'}} \quad (\text{A.3.3c})$$

$$\mu = \frac{k' G}{E} \quad (\text{A.3.3d})$$

$$\eta = \frac{AL^2}{I} = \frac{L^2}{r^2} \quad (\text{A.3.3e})$$

$$\gamma = \frac{\kappa p_\infty b U L}{k' A G c_\infty} \quad (\text{A.3.3f})$$

$$\alpha = \frac{\kappa p_\infty b L}{A c_\infty \sqrt{k' G \rho}} \quad (\text{A.3.3g})$$

where ξ is the non-dimensional axial coordinate, v is the non-dimensional transversal displacement, τ is the non-dimensional time, μ is a non-dimensional mechanical parameter related to the shear deformation, η is a non-dimensional geometrical parameter related to the squared length L over radius of inertia, $r = \sqrt{\frac{I}{A}}$, γ is a non-dimensional parameter related to the gas

velocity and α is the non-dimensional damping caused by supersonic velocity.

Substituting the above parameters into (A.3.2a and A.3.2b) and dividing the first equation by $k'AG$ and the second by EA , the system becomes:

$$\frac{1}{L} \frac{\partial^2 v}{\partial \tau^2} = \frac{1}{L} \frac{\partial^2 v}{\partial \xi^2} - \frac{1}{L} \frac{\partial \theta}{\partial \xi} - \frac{\kappa p_\infty b}{Ac_\infty \sqrt{\rho G k'}} \frac{\partial v}{\partial \tau} - \frac{\kappa p_\infty b U}{k' AG c_\infty} \frac{\partial v}{\partial \xi} \quad (\text{A.3.4a})$$

$$\frac{IGk'}{EAL^2} \frac{\partial^2 \theta}{\partial \tau^2} = \frac{I}{AL^2} \frac{\partial^2 \theta}{\partial \xi^2} + \frac{k'G}{E} \left(\frac{\partial v}{\partial \xi} - \theta \right) \quad (\text{A.3.4b})$$

This means:

$$\frac{1}{L} \frac{\partial^2 v}{\partial \tau^2} = \frac{1}{L} \frac{\partial^2 v}{\partial \xi^2} - \frac{1}{L} \frac{\partial \theta}{\partial \xi} - \frac{\kappa p_\infty b}{Ac_\infty \sqrt{\rho G k'}} \frac{\partial v}{\partial \tau} - \frac{\kappa p_\infty b U}{k' AG c_\infty} \frac{\partial v}{\partial \xi} \quad (\text{A.3.5a})$$

$$\frac{\mu}{\eta} \frac{\partial^2 \theta}{\partial \tau^2} = \frac{1}{\eta} \frac{\partial^2 \theta}{\partial \xi^2} + \mu \left(\frac{\partial v}{\partial \xi} - \theta \right) \quad (\text{A.3.5b})$$

Now we multiply the first equation by L and the second by $\frac{\eta}{\mu}$ to obtain:

$$\frac{\partial^2 v}{\partial \tau^2} = \frac{\partial^2 v}{\partial \xi^2} - \frac{\partial \theta}{\partial \xi} - \gamma \frac{\partial v}{\partial \tau} - \alpha \frac{\partial v}{\partial \xi} \quad (\text{A.3.6a})$$

$$\frac{\partial^2 \theta}{\partial \tau^2} = \frac{1}{\mu} \frac{\partial^2 \theta}{\partial \xi^2} + \eta \left(\frac{\partial v}{\partial \xi} - \theta \right) \quad (\text{A.3.6b})$$

Now we perform some algebraic manipulations in order to reduce these two equations in a single one.

From the first one, we express $\frac{\partial \theta}{\partial \xi}$ as follows:

$$\frac{\partial \theta}{\partial \xi} = \frac{\partial^2 v}{\partial \xi^2} - \frac{\partial^2 v}{\partial \tau^2} - \gamma \frac{\partial v}{\partial \tau} - \alpha \frac{\partial v}{\partial \xi} \quad (\text{A.3.7})$$

Now we differentiate the second equation with respect to ξ :

$$\frac{\partial^3 \theta}{\partial \tau^2 \partial \xi} = \frac{1}{\mu} \frac{\partial^3 \theta}{\partial \xi^3} + \eta \left(\frac{\partial^2 v}{\partial \xi^2} - \frac{\partial \theta}{\partial \xi} \right) \quad (\text{A.3.8})$$

We substitute the value of $\frac{\partial \theta}{\partial \xi}$ in the last equation, obtaining:

$$\begin{aligned} & \frac{\partial^2}{\partial \tau^2} \left(\frac{\partial^2 v}{\partial \xi^2} - \frac{\partial^2 v}{\partial \tau^2} - \gamma \frac{\partial v}{\partial \xi} - \alpha \frac{\partial v}{\partial \tau} \right) - \frac{1}{\mu} \frac{\partial^2}{\partial \xi^2} \left(\frac{\partial^2 v}{\partial \xi^2} - \frac{\partial^2 v}{\partial \tau^2} - \gamma \frac{\partial v}{\partial \xi} - \alpha \frac{\partial v}{\partial \tau} \right) \\ & - \eta \left(\frac{\partial^2 v}{\partial \xi^2} - \frac{\partial^2 v}{\partial \xi^2} + \frac{\partial^2 v}{\partial \tau^2} + \gamma \frac{\partial v}{\partial \xi} + \alpha \frac{\partial v}{\partial \tau} \right) = 0 \end{aligned} \quad (\text{A.3.9})$$

or:

$$\begin{aligned} & \frac{1}{\mu} \frac{\partial^4 v}{\partial \xi^4} + \frac{\partial^4 v}{\partial \tau^4} - \left(1 + \frac{1}{\mu} \right) \frac{\partial^4 v}{\partial \tau^2 \partial \xi^2} - \frac{\gamma}{\mu} \frac{\partial^3 v}{\partial \xi^3} + \alpha \frac{\partial^3 v}{\partial \tau^3} \\ & + \gamma \frac{\partial^3 v}{\partial \tau^2 \partial \xi} - \frac{\alpha}{\mu} \frac{\partial^3 v}{\partial \tau \partial \xi^2} + \eta \frac{\partial^2 v}{\partial \tau^2} + \eta \gamma \frac{\partial v}{\partial \xi} + \eta \alpha \frac{\partial v}{\partial \tau} = 0 \end{aligned} \quad (\text{A.3.10})$$

The problem consists in fixing geometric and material parameters to specific values in order to evaluate the critical velocity U_{cr} of the gas flow.

A.3.2 Governing differential equation for consistent Timoshenko-Ehrenfest beam in gas flow

Similarly to the original theory, also the consistent theory is represented by two equations: one for the vertical displacement $w(x, t)$ and one for the rotation angle of the cross section $\theta(x, t)$

$$\rho A \frac{\partial^2 w}{\partial t^2} = k' AG \left(\frac{\partial^2 w}{\partial t^2} - \frac{\partial \theta}{\partial x} \right) - q(x, t) \quad (\text{A.3.11a})$$

$$\rho I \frac{\partial^3 w}{\partial x \partial t^2} = EI \frac{\partial^2 \theta}{\partial x^2} + k' AG \left(\frac{\partial w}{\partial x} - \theta \right) \quad (\text{A.3.11b})$$

where E is the elastic modulus, G is the shear modulus, A is the area of the cross section, ρ is the mass density, I is the inertia moment of the cross section, k' is the shear coefficient and q the load.

Substituting into Eq. (A.3.11a) the expression of piston theory load as shown in Eq. (7.2.2), we obtain:

$$\rho A \frac{\partial^2 w}{\partial t^2} = k' AG \left(\frac{\partial^2 w}{\partial t^2} - \frac{\partial \theta}{\partial x} \right) - \frac{\kappa p_\infty b}{c_\infty} \left(\frac{\partial w}{\partial t} + U \frac{\partial w}{\partial x} \right) \quad (\text{A.3.12a})$$

$$\rho I \frac{\partial^3 w}{\partial x \partial t^2} = EI \frac{\partial^2 \theta}{\partial x^2} + k' AG \left(\frac{\partial w}{\partial x} - \theta \right) \quad (\text{A.3.12b})$$

We introduce the same non-dimensional parameters shown before, i.e.:

$$\xi = \frac{x}{L} \rightarrow x = \xi L \quad (\text{A.3.13a})$$

$$v = \frac{w}{L} \rightarrow w = vL \quad (\text{A.3.13b})$$

$$\tau = t \sqrt{\frac{Gk'}{\rho L^2}} \rightarrow t = \tau \sqrt{\frac{\rho L^2}{Gk'}} \quad (\text{A.3.13c})$$

$$\mu = \frac{k' G}{E} \quad (\text{A.3.13d})$$

$$\eta = \frac{AL^2}{I} = \frac{L^2}{r^2} \quad (\text{A.3.13e})$$

$$\gamma = \frac{\kappa p_\infty b U L}{k' A G c_\infty} \quad (\text{A.3.13f})$$

$$\alpha = \frac{\kappa p_\infty b L}{A c_\infty \sqrt{k' G \rho}} \quad (\text{A.3.13g})$$

where ξ relates to the axial coordinate, v to the transversal displacement, τ is the non-dimensional time, μ is a non-dimensional mechanical parameter related to the shear deformation, η is associated to the squared length L over radius of inertia $r = \sqrt{\frac{I}{A}}$, γ is a non-dimensional parameter related to the gas velocity and α is the non-dimensional damping caused by supersonic velocity.

If we substitute the above parameters into (A.3.12a and A.3.12b) and divide the first equation by $k'AG$ and the second by EA , we obtain:

$$\frac{1}{L} \frac{\partial^2 v}{\partial \tau^2} = \frac{1}{L} \frac{\partial^2 v}{\partial \xi^2} - \frac{1}{L} \frac{\partial \theta}{\partial \xi} - \frac{\kappa p_\infty b}{Ac_\infty \sqrt{\rho G k'}} \frac{\partial v}{\partial \tau} - \frac{\kappa p_\infty b U}{k' AG c_\infty} \frac{\partial v}{\partial \xi} \quad (\text{A.3.14a})$$

$$\frac{IGk'}{EAL^2} \frac{\partial^3 v}{\partial \xi \partial \tau^2} = \frac{I}{AL^2} \frac{\partial^2 \theta}{\partial \xi^2} + \frac{k' G}{E} \left(\frac{\partial v}{\partial \xi} - \theta \right) \quad (\text{A.3.14b})$$

Or, alternatively:

$$\frac{1}{L} \frac{\partial^2 v}{\partial \tau^2} = \frac{1}{L} \frac{\partial^2 v}{\partial \xi^2} - \frac{1}{L} \frac{\partial \theta}{\partial \xi} - \frac{\kappa p_\infty b}{Ac_\infty \sqrt{\rho G k'}} \frac{\partial v}{\partial \tau} - \frac{\kappa p_\infty b U}{k' AG c_\infty} \frac{\partial v}{\partial \xi} \quad (\text{A.3.15a})$$

$$\frac{\mu}{\eta} \frac{\partial^3 v}{\partial \xi \partial \tau^2} = \frac{1}{\eta} \frac{\partial^2 \theta}{\partial \xi^2} + \mu \left(\frac{\partial v}{\partial \xi} - \theta \right) \quad (\text{A.3.15b})$$

Now we multiply the first equation by L and the second by $\frac{\eta}{\mu}$ obtaining:

$$\frac{\partial^2 v}{\partial \tau^2} = \frac{\partial^2 v}{\partial \xi^2} - \frac{\partial \theta}{\partial \xi} - \gamma \frac{\partial v}{\partial \tau} - \alpha \frac{\partial v}{\partial \xi} \quad (\text{A.3.16a})$$

$$\frac{\partial^3 v}{\partial \xi \partial \tau^2} = \frac{1}{\mu} \frac{\partial^2 \theta}{\partial \xi^2} + \eta \left(\frac{\partial v}{\partial \xi} - \theta \right) \quad (\text{A.3.16b})$$

In order to get a single equation starting from the system above (Eq. (A.3.16a) and (A.3.16b)), we express $\frac{\partial \theta}{\partial \xi}$:

$$\frac{\partial \theta}{\partial \xi} = \frac{\partial^2 v}{\partial \xi^2} - \frac{\partial^2 v}{\partial \tau^2} - \gamma \frac{\partial v}{\partial \tau} - \alpha \frac{\partial v}{\partial \xi} \quad (\text{A.3.17})$$

Differentiating the second equation with respect to ξ :

$$\frac{\partial^4 \theta}{\partial \tau^2 \partial \xi^2} = \frac{1}{\mu} \frac{\partial^3 \theta}{\partial \xi^3} + \eta \left(\frac{\partial^2 v}{\partial \xi^2} - \frac{\partial \theta}{\partial \xi} \right) \quad (\text{A.3.18})$$

Substituting the value of $\frac{\partial \theta}{\partial \xi}$ in the last equation, we obtain:

$$\frac{\partial^4 v}{\partial \tau^2 \partial \xi^2} - \frac{1}{\mu} \frac{\partial^2}{\partial \xi^2} \left(\frac{\partial^2 v}{\partial \xi^2} - \frac{\partial^2 v}{\partial \tau^2} - \gamma \frac{\partial v}{\partial \tau} - \alpha \frac{\partial v}{\partial \xi} \right) - \eta \left(\frac{\partial^2 v}{\partial \xi^2} - \frac{\partial^2 v}{\partial \xi^2} + \frac{\partial^2 v}{\partial \tau^2} + \gamma \frac{\partial v}{\partial \tau} + \alpha \frac{\partial v}{\partial \xi} \right) = 0 \quad (\text{A.3.19})$$

or:

$$\frac{1}{\mu} \frac{\partial^4 v}{\partial \xi^4} - \left(1 + \frac{1}{\mu} \right) \frac{\partial^4 v}{\partial \tau^2 \partial \xi^2} - \frac{\gamma}{\mu} \frac{\partial^3 v}{\partial \xi^3} - \frac{\alpha}{\mu} \frac{\partial^3 v}{\partial \tau \partial \xi^2} + \eta \frac{\partial^2 v}{\partial \tau^2} + \eta \gamma \frac{\partial v}{\partial \xi} + \eta \alpha \frac{\partial v}{\partial \tau} = 0 \quad (\text{A.3.20})$$

Actually, we think the governing differential equation as:

$$\begin{aligned} & \frac{1}{\mu} \frac{\partial^4 v}{\partial \xi^4} + \eta \frac{\partial^2 v}{\partial \tau^2} + \eta \gamma \frac{\partial v}{\partial \xi} + \eta \alpha \frac{\partial v}{\partial \tau} \\ & + \varepsilon \left[- \left(1 + \frac{1}{\mu} \right) \frac{\partial^4 v}{\partial \tau^2 \partial \xi^2} - \frac{\gamma}{\mu} \frac{\partial^3 v}{\partial \xi^3} - \frac{\alpha}{\mu} \frac{\partial^3 v}{\partial \tau \partial \xi^2} + \delta \left(+ \frac{\partial^4 v}{\partial \tau^4} + \alpha \frac{\partial^3 v}{\partial \tau^3} + \gamma \frac{\partial^3 v}{\partial \tau^2 \partial \xi} \right) \right] = 0 \end{aligned} \quad (\text{A.3.21})$$

When $\varepsilon = 0$, Eq. (A.3.21) reduces to the Bernoulli-Euler's beam theory. When $\varepsilon = 1$, we obtain two different Timoshenko-Ehrenfest beam's theories which are identified by the artificial parameter δ . When $\delta = 1$, we have the original Timoshenko-Ehrenfest theory and when $\delta = 0$, we have the consistent theory.

A.3.3 Galerkin method

In order to apply the Galerkin procedure, first we have to approximate the variable $v(\xi, \tau)$ by a series expansion, following Bolotin ([39], p.248):

$$v(\xi, \tau) = \sum_{k=1}^n \psi_k(\xi) f_k(\tau) \quad (\text{A.3.22})$$

where $\psi_k(\xi)$ is a function of the non-dimensional axial coordinate and $f_k(\tau)$ of non-dimensional time τ .

We consider the following variation of the function $f_k(\tau)$ in non-dimensional time:

$$f_k(\tau) = Q_k e^{\Omega\tau} \quad (\text{A.3.23})$$

We multiply the expression resulting from substitution of Eq. (A.3.22) into Eq. (A.3.23) by $\psi_j(\xi)$ and integrate from zero to one with respect to ξ :

$$\begin{aligned} & \sum_{k=1}^n Q_k \left(\frac{1}{\mu} \int_0^1 \frac{d^4 \psi_k(\xi)}{d\xi^4} \psi_j(\xi) d\xi - \varepsilon \frac{\gamma}{\mu} \int_0^1 \frac{d^3 \psi_k(\xi)}{d\xi^3} \psi_j(\xi) d\xi \right. \\ & - \varepsilon \frac{\mu\Omega^2 + \Omega^2 + \alpha}{\mu} \int_0^1 \frac{d^2 \psi_k(\xi)}{d\xi^2} \psi_j(\xi) d\xi + \gamma(\varepsilon\delta\Omega^2 + \eta) \int_0^1 \frac{d\psi_k(\xi)}{d\xi} \psi_j(\xi) d\xi \\ & \left. + (\varepsilon\delta(\Omega^4 + \alpha\Omega^3) + \eta\Omega^2 + \eta\alpha\Omega) \int_0^1 \psi_k(\xi) \psi_j(\xi) d\xi \right) = 0 \end{aligned} \quad (\text{A.3.24})$$

We introduce the following notations:

$$A_{kj} = \int_0^1 \frac{d^4 \psi_k(\xi)}{d\xi^4} \psi_j(\xi) d\xi \quad (\text{A.3.25a})$$

$$B_{kj} = - \int_0^1 \frac{d^3 \psi_k(\xi)}{d\xi^3} \psi_j(\xi) d\xi \quad (\text{A.3.25b})$$

$$C_{kj} = - \int_0^1 \frac{d^2 \psi_k(\xi)}{d\xi^2} \psi_j(\xi) d\xi \quad (\text{A.3.25c})$$

$$D_{kj} = \int_0^1 \frac{d\psi_k(\xi)}{d\xi} \psi_j(\xi) d\xi \quad (\text{A.3.25d})$$

$$E_{kj} = \int_0^1 \psi_k(\xi) \psi_j(\xi) d\xi \quad (\text{A.3.25e})$$

The problem takes the following form:

$$\begin{aligned} & \sum_{k=1}^n Q_k \left(\frac{1}{\mu} A_{kj} + \varepsilon \frac{\gamma}{\mu} B_{kj} + \varepsilon \frac{\mu\Omega^2 + \Omega^2 + \alpha}{\mu} C_{kj} + \gamma(\varepsilon\delta\Omega^2 + \eta) D_{kj} \right. \\ & \left. + (\varepsilon\delta(\Omega^4 + \alpha\Omega^3) + \eta\Omega^2 + \eta\alpha\Omega) E_{kj} \right) = 0 \end{aligned} \quad (\text{A.3.26})$$

In matrix representation:

$$\left(\frac{1}{\mu} \mathbf{A} + \varepsilon \frac{\gamma}{\mu} \mathbf{B} + \varepsilon \frac{\mu\Omega^2 + \Omega^2 + \alpha}{\mu} \mathbf{C} + \gamma(\varepsilon\delta\Omega^2 + \eta) \mathbf{D} + (\varepsilon\delta(\Omega^4 + \alpha\Omega^3) + \eta\Omega^2 + \eta\alpha\Omega) \mathbf{E} \right) \mathbf{Q} = \mathbf{0} \quad (\text{A.3.27})$$

This system has non-trivial solution only if the following determinant vanishes:

$$\det \left(\frac{1}{\mu} \mathbf{A} + \varepsilon \frac{\gamma}{\mu} \mathbf{B} + \varepsilon \frac{\mu\Omega^2 + \Omega^2 + \alpha}{\mu} \mathbf{C} + \gamma(\varepsilon\delta\Omega^2 + \eta) \mathbf{D} + (\varepsilon\delta(\Omega^4 + \alpha\Omega^3) + \eta\Omega^2 + \eta\alpha\Omega) \mathbf{E} \right) = 0 \quad (\text{A.3.28})$$

In order to study the dynamic stability, we fix parameters related to the beam. Therefore, the variables of the system are the parameters related to the load: the velocity γ and the damping α . The unknown of the problem is the complex eigenfrequency Ω .

A.3.4 Numerical example

Galerkin results with Original Timoshenko-Ehrenfest equations

We are interested in knowing the relationship between critical velocity γ and damping α in order to find the boundary of the stability of the system. This boundary can be found via the Routh-Hurwitz criterion. This criterion leads us to the following plot where the upper side is unstable while the other one is stable.

We proceed numerically. We subdivide the interval of γ and α , both from 0 to 1, in 100 points and evaluate the determinant in Eq. (A.3.28) for each combination of the 100 points of γ and α . This means that we subdivide the γ, α plan in 10 000 points where we study the stability. The determinant by Eq. (A.3.28) evaluated for each point is a polynomial in the variable Ω . For each obtained polynomial, we apply the Routh-Hurwitz criteria to get stability boundary.

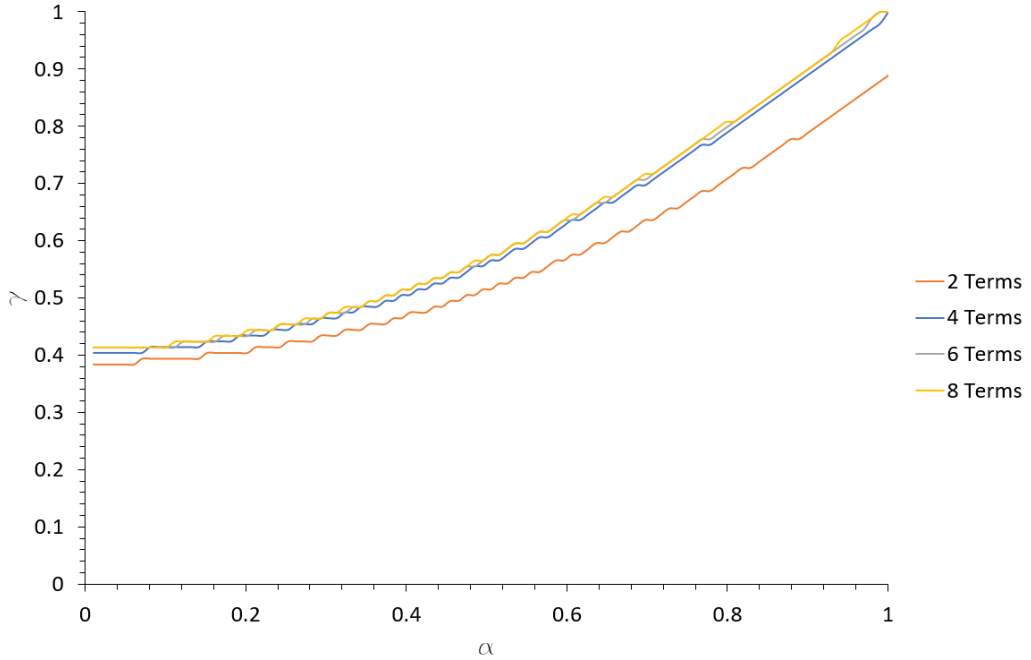


Figure A.4: Stability boundary for original Timoshenko-Ehrenfest theory

Fig. A.4 is the result of a numerical analysis. From this plot, we can see that increasing the number of terms in the approximated method, critical velocity increases in function of the damping. Instead, if we approximate the obtained point with a second order polynomial, we obtain the following chart:

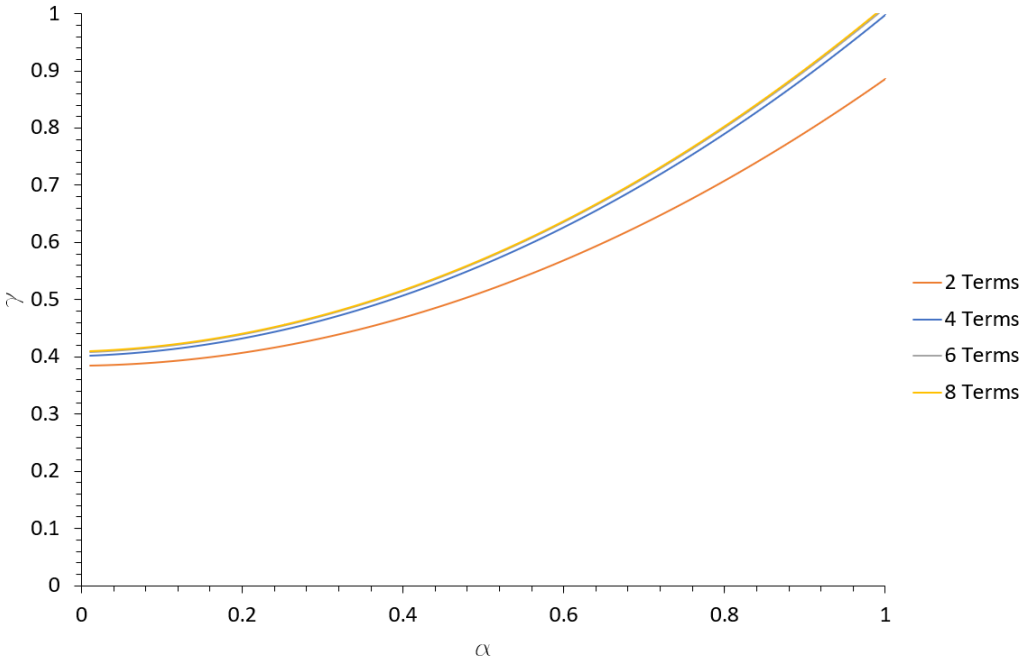


Figure A.5: Smoothing of stability boundary for original Timoshenko-Ehrenfest theory

We can see a great difference between the results obtained with 2 terms and those derived with 4, 6 or 8 terms. Indeed, for $\alpha = 0.07$, say, two-term approximation yields $\gamma_{cr} = 0.3939$, four-term analysis results in $\gamma_{cr} = 0.4040$, whereas six-term treatment leads to value $\gamma_{cr} = 0.4141$; finally, eight-term approximation results in $\gamma_{cr} = 0.4141$. The change observed between 6 and 8 terms results in a very small flutter velocity evaluation: the associated curves are almost overlapping. In conclusion, it appears that using 8 terms is sufficient to obtain an accurate stability boundary.

We illustrate the methodology as follows. Using 8th order Galerkin method and keeping the discretization for γ and just two points of α (0 and 0.5), we evaluate the determinant, which turns to be a polynomial in the variable Ω . Solution shows that Ω is complex, as expected.

To exemplify the Routh-Hurwitz criterion, we report the case for two-term approximation when $\gamma = 0.8$ and $\alpha = 0.2$. In this case, the determinant of Eq. (A.3.28) reads:

$$49.78\Omega^8 + 19.91\Omega^7 + 1.23 \cdot 10^5\Omega^6 + 4.85 \cdot 10^4\Omega^5 + 7.62 \cdot 10^7\Omega^4 + 2.96 \cdot 10^7\Omega^3 + 3.45 \cdot 10^8\Omega^2 + 6.78 \cdot 10^7\Omega + 5.25 \cdot 10^8 = 0 \quad (\text{A.3.29})$$

We study the stability using the Routh-Hurwitz stability criterion. This test is an efficient recursive algorithm proposed by Routh in 1877 [58] in order to analyze the sign of real part of all the roots of a linear system's characteristic polynomial. In 1895 [59] Hurwitz independently proposed to create a square matrix starting from the coefficients of the polynomial and demonstrated that the polynomial is stable only if the determinants of the principal sub-matrix are all

positive. These two procedures are equivalent. Both provide a way to determine if the equation of motion of a linear system has only stable solution without solving the system directly.

The Routh-Hurwitz criterion consists in building a table with the following structures:

a_n	a_{n-2}	a_{n-4}	a_{n-6}	\dots
a_{n-1}	a_{n-3}	a_{n-4}	\dots	
$k_{3,1}$	$k_{3,2}$	\dots		
$k_{4,1}$	$k_{4,2}$	\dots		
\dots	\dots			

When the table is completed, the number of sign changes in the first column shows the number of roots with non-negative real parts.

The table is built as follows, starting by a general polynomial in the form:

$$p(x) = a_n x^n + a_{n-1} x^{n-1} + a_{n-2} x^{n-2} + \dots + a_0 x^0 \quad (\text{A.3.30})$$

We set the first row of the table starting from the highest power coefficient (the first) and continuing with the odd order coefficient (third, fifth, etc.).

We set the second row with the even coefficient (second, fourth, etc.).

The first two rows read as follows:

a_n	a_{n-2}	a_{n-4}	a_{n-6}	\dots
a_{n-1}	a_{n-3}	a_{n-4}	\dots	

The other rows, when $i > 2$ and whose elements are called $k_{i,j}$, are evaluated starting from these two rows. These elements are obtained by creating the ratio between the determinant of the matrix built by the two upper rows. The first column of this under-matrix is the first column of the table and the second column is the next column with respect to the interested element. The denominator is the first element of the upper row with the sign changed. The expression of $k_{i,j}$ is:

$$k_{i,j} = \frac{\det \begin{bmatrix} k_{i-2,1} & k_{i-2,j+1} \\ k_{i-1,1} & k_{i-1,j+1} \end{bmatrix}}{-k_{i-1,j}} \quad (\text{A.3.31})$$

This process ends when we obtain a row full of zeros.

After completing the table, we read the first column. Each change (permanence) in the sign of the coefficient corresponds to the positive (negative) real part of the roots.

The Routh-Hurwitz table related to polynomial (A.3.29) is:

49.78	$1.23 \cdot 10^5$	$7.62 \cdot 10^7$	$3.45 \cdot 10^8$	$5.25 \cdot 10^8$
19.91	$4.85 \cdot 10^4$	$2.96 \cdot 10^7$	$6.78 \cdot 10^7$	
$1.78 \cdot 10^3$	$2.29 \cdot 10^6$	$1.76 \cdot 10^8$	$5.25 \cdot 10^8$	
$2.29 \cdot 10^4$	$2.76 \cdot 10^7$	$6.19 \cdot 10^7$		
$1.42 \cdot 10^5$	$1.71 \cdot 10^8$	$5.25 \cdot 10^8$		
$1.89 \cdot 10^4$	$-2.27 \cdot 10^7$			
$3.41 \cdot 10^8$	$5.25 \cdot 10^8$			
$-2.28 \cdot 10^7$				
$5.25 \cdot 10^8$				

The table above reports two changes of sign in the first column which means that the polynomial possesses the positive real part, inducting instability to the system for the above values.

Another example is reported for the case with two-term approximation when $\gamma = 0.1$ and $\alpha = 0.9$. In this case, the determinant of Eq. (A.3.28) reads:

$$49.78\Omega^8 + 89.61\Omega^7 + 1.23 \cdot 10^5\Omega^6 + 2.18 \cdot 10^5\Omega^5 + 7.60 \cdot 10^7\Omega^4 + 1.33 \cdot 10^8\Omega^3 + 2.20 \cdot 10^8\Omega^2 + 1.46 \cdot 10^8\Omega + 3.68 \cdot 10^7 = 0 \quad (\text{A.3.32})$$

49.78	$1.23 \cdot 10^5$	$7.60 \cdot 10^7$	$2.20 \cdot 10^8$	$3.68 \cdot 10^7$
89.61	$2.18 \cdot 10^5$	$1.33 \cdot 10^8$	$1.46 \cdot 10^8$	
$1.75 \cdot 10^3$	$2.23 \cdot 10^6$	$1.39 \cdot 10^8$	$3.68 \cdot 10^7$	
$1.04 \cdot 10^5$	$1.26 \cdot 10^8$	$1.44 \cdot 10^8$		
$1.14 \cdot 10^5$	$1.37 \cdot 10^8$	$3.68 \cdot 10^7$		
$3.02 \cdot 10^5$	$1.10 \cdot 10^8$			
$9.53 \cdot 10^7$	$3.68 \cdot 10^7$			
$1.10 \cdot 10^8$				
$3.68 \cdot 10^7$				

The table above reports no changes of sign in the first column. This means that the system is stable for adopted values of parameters.

Now we observe what happens if we depict the real part and the imaginary part of the frequencies versus the velocity γ , keeping the damping α constant first at zero and second at 0.5:

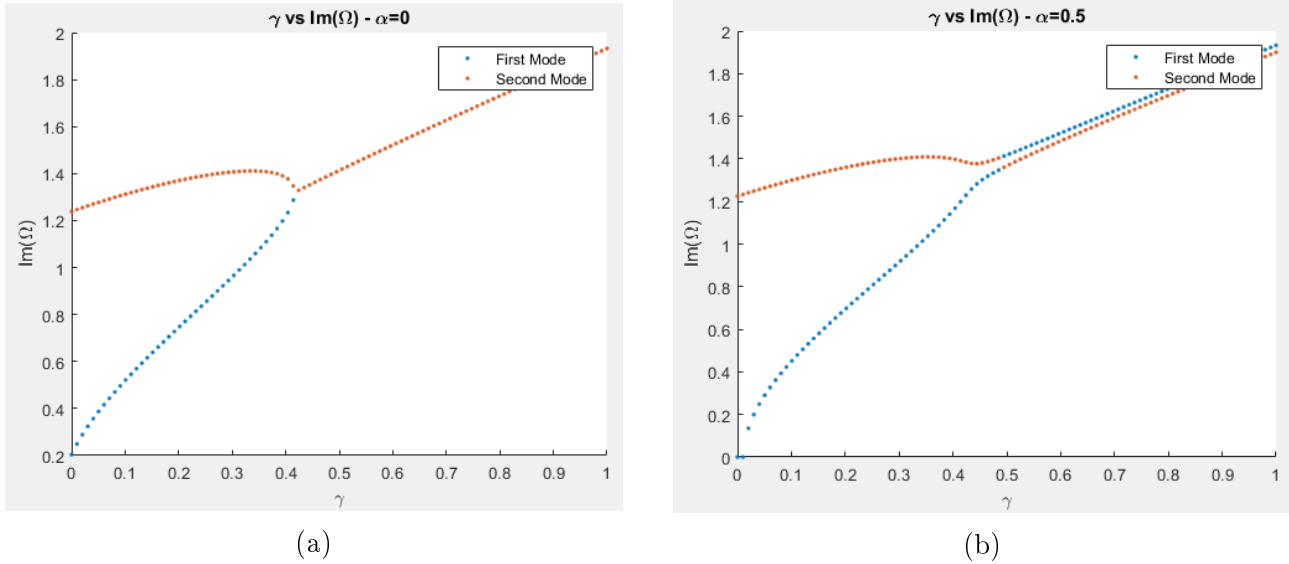


Figure A.6: Imaginary part of frequencies vs velocity for original Timoshenko-Ehrenfest theory

Fig. A.6a and A.6b are the representation of the imaginary part of the complex frequency Ω in function of the velocity γ . We observe that these frequencies get closer with the increasing of the velocity, until reaching the coalescence with a specific velocity called “critical velocity”.

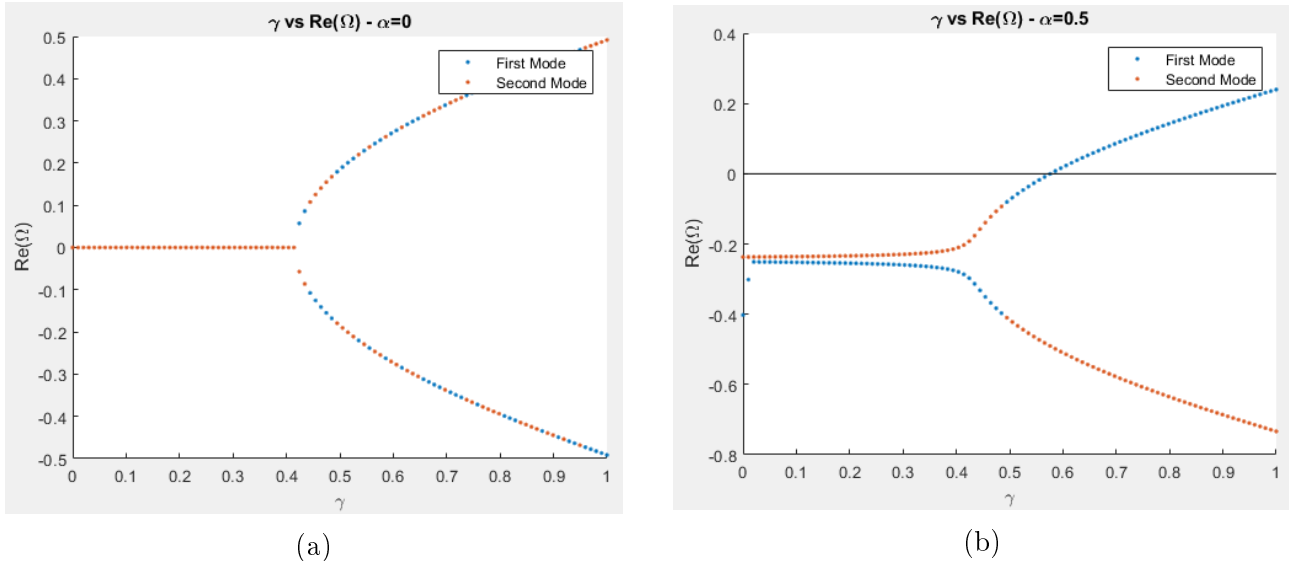


Figure A.7: Real part of frequencies vs velocity for original Timoshenko-Ehrenfest theory

Fig. A.7a and A.7b represent the real part of the complex frequency Ω in function of the velocity γ . We see that these frequencies are overlapped for low values of the velocity. When the velocity increases, we see a divergence in the frequencies. The real part of the frequencies becomes greater than zero for a specific velocity called “critical velocity”.

From these plots, we can see that in Fig. A.6 the stability condition is in the point of coalescence whereas in Fig. A.7, we have the stability condition when the real part is greater than zero. The velocity at which these phenomena occur is called “critical velocity”.

The critical velocity for each value of damping $\alpha = 0$ and $\alpha = 0.5$, which are the same in the reported pictures, is:

$$\gamma_{crit,\alpha=0} = 0.4141 \quad (\text{A.3.33a})$$

$$\gamma_{crit,\alpha=0.5} = 0.5657 \quad (\text{A.3.33b})$$

An interesting observation is that in the first plot (imaginary part vs γ , $\alpha = 0$), we can check our derivation because when γ is equal to zero, we expect to find the natural frequencies of our beam.

By 8th order Galerkin method, we have the following non-dimensional frequencies:

$$\omega_1 = 0.2034 \quad (\text{A.3.34a})$$

$$\omega_2 = 1.2387 \quad (\text{A.3.34b})$$

We convert the non-dimensional frequencies in dimensional frequencies dividing by $\sqrt{\frac{\rho L^2}{Gk'}}$:

$$\omega_1 = 525.5858 \frac{\text{rad}}{\text{s}} \quad (\text{A.3.35a})$$

$$\omega_2 = 3201.4080 \frac{\text{rad}}{\text{s}} \quad (\text{A.3.35b})$$

The relative error ε between Galerkin method and theoretical result is evaluated with the formula:

$$\varepsilon = \frac{\omega_{\text{Galerkin}} - \omega_{\text{theoretical}}}{\omega_{\text{theoretical}}} \times 100 \quad (\text{A.3.36})$$

leading to the following results:

$$\varepsilon_{\omega_1} = 1.1442\% \quad (\text{A.3.37a})$$

$$\varepsilon_{\omega_2} = 3.7119\% \quad (\text{A.3.37b})$$

Another interesting observation is that we have the same critical velocity for $\alpha = 0$ and $\alpha = 0.5$ in the first plot.

The last two plots are real part vs imaginary part for $\alpha = 0$ and $\alpha = 0.5$. In these plots, we see how complex frequencies evolve with the increasing of the load γ . It is possible to see in Fig. A.8a that for low values of the load the two frequencies are different. When the real part is zero, the imaginary parts are clearly distinguishable but for a specific value of the load, we have the coalescence of the imaginary part. It is possible to observe this behavior in the curved part of the plot where the dots are alternated in colors. This behavior is the same represented in Fig. A.6a. From Fig. A.8b, we see that when the real part becomes greater than zero, we have instability and the imaginary part associated with this real part results in the critical frequencies.

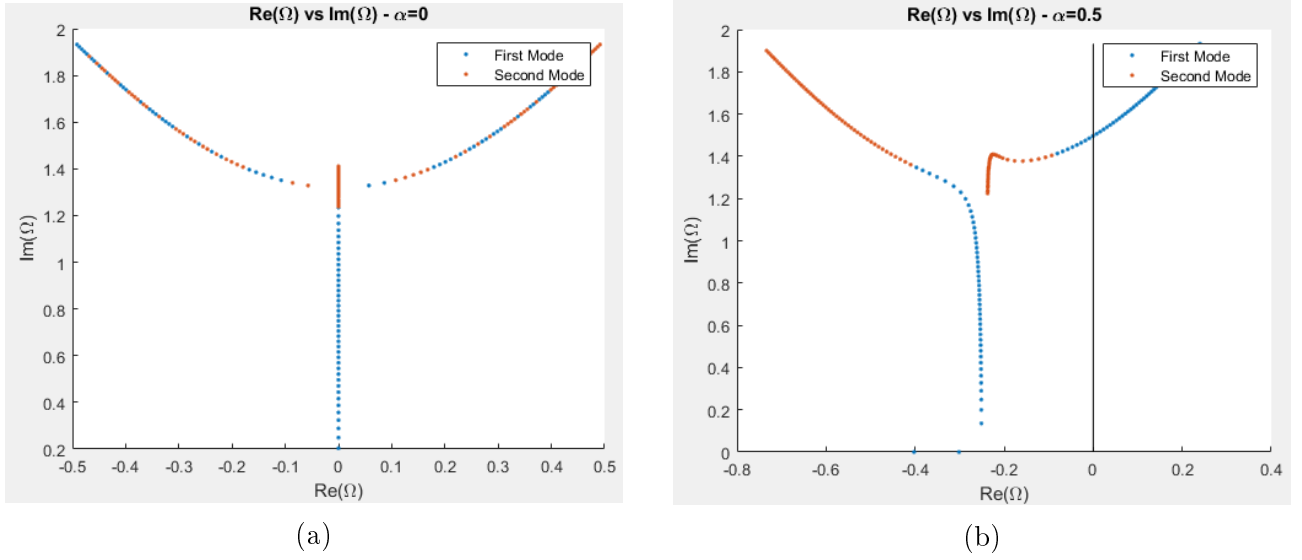


Figure A.8: Real vs imaginary part of frequencies for original Timoshenko-Ehrenfest theory

Galerkin results with Consistent Timoshenko-Ehrenfest model

For the consistent theory, we proceed analogously. Firstly, we find the stability diagram. In the same way described for the original formulation, we subdivide the interval of γ and α in 100 points and we evaluate the determinant in Eq. (A.3.28) for each combination of γ and α in the variable Ω . For each polynomial, we apply the Routh-Hurwitz criterion to obtain stability curve.

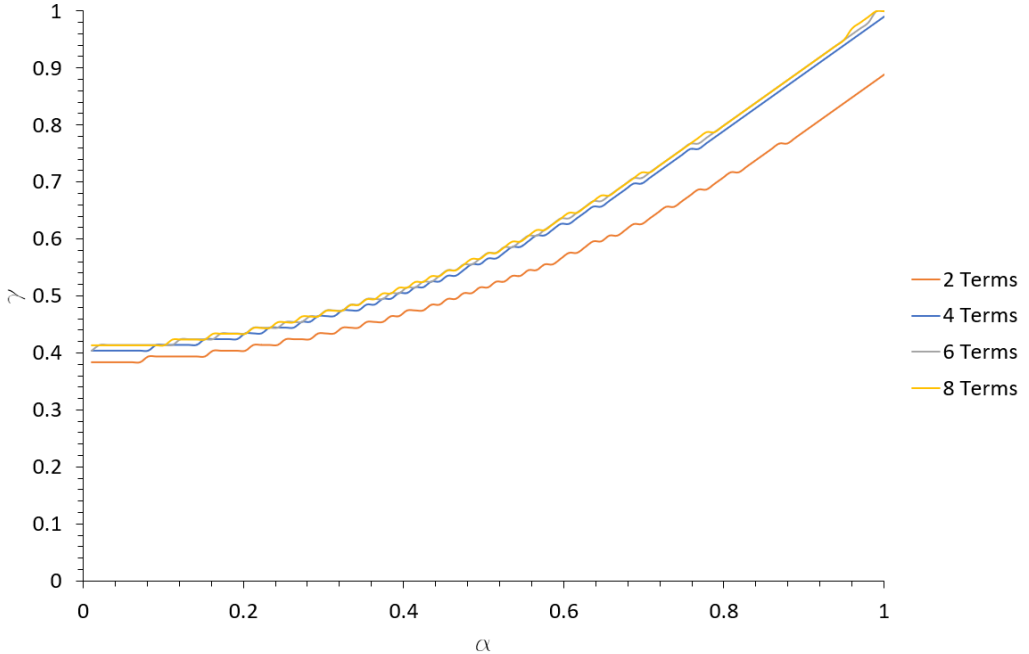


Figure A.9: Stability boundary for consistent Timoshenko-Ehrenfest theory

Smoothing the chart above, we get:

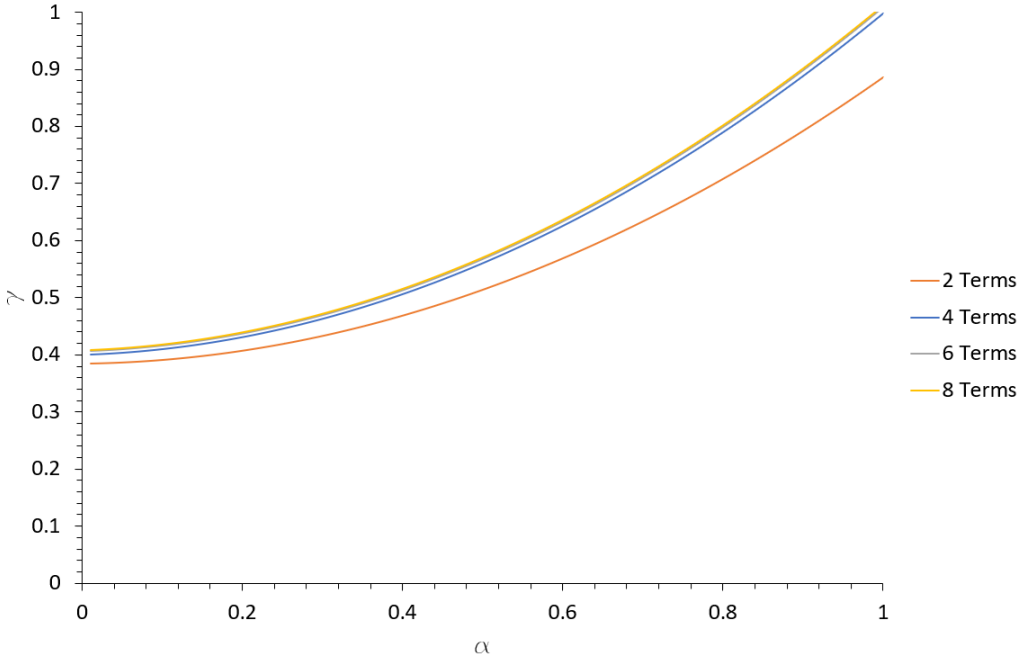


Figure A.10: Smoothing of stability boundary for consistent Timoshenko-Ehrenfest theory

From Fig. A.9, we can see that the change of the theory does not modify the trend of the chart. We still have the critical velocity which increases together with the damping value. Moreover, increasing the number of terms in the Galerkin method, we obtain higher value of critical velocity. However, when we move from 6 to 8 terms, the result is almost the same so we get a stable boundary.

According to the previous section, we use 8th order Galerkin method and we keep the discretization for γ and just two points of α (0 and 0.5). We evaluate the determinant which then generates the polynomial in the variable Ω . At this point, we solve the obtained polynomial for the above mentioned variable.

We depict the real part and the imaginary part of the frequencies versus the velocity γ keeping constant the damping α firstly set to zero and secondly to 0.5:

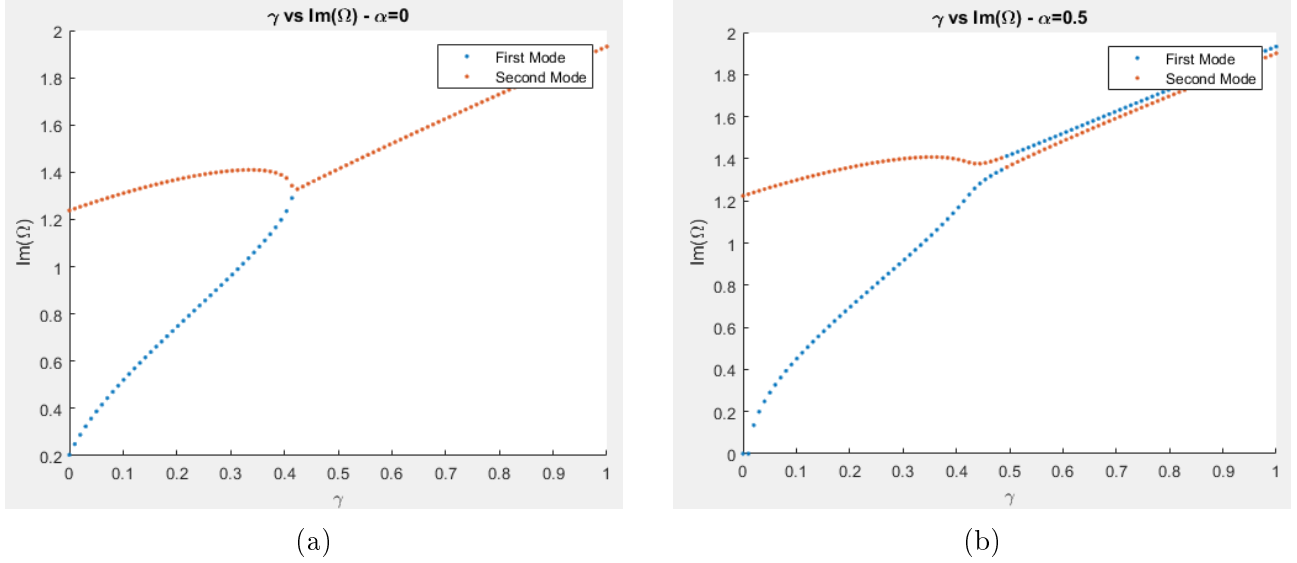


Figure A.11: Imaginary part of frequencies vs velocity for consistent Timoshenko-Ehrenfest theory

Fig. A.11a and A.11b are the representation of the imaginary part of the complex frequency Ω in function of the velocity γ . We see that these frequencies, related to the first two mode shapes, change their value together with the damping. Specifically, with the increase in the damping, these frequencies get closer.

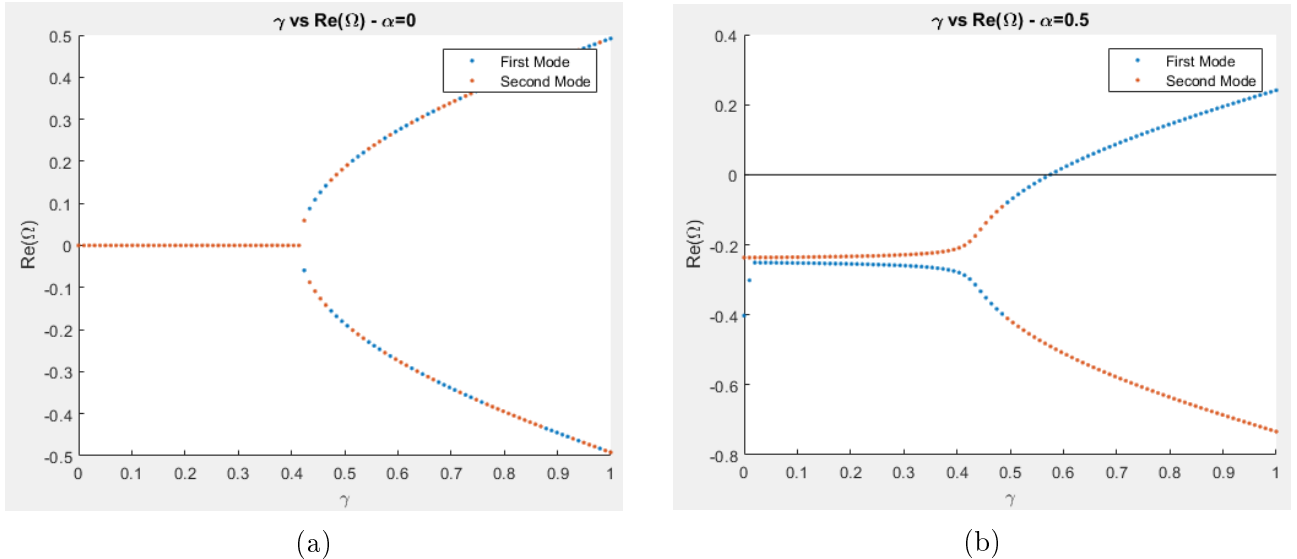


Figure A.12: Real part of frequencies vs velocity for original Timoshenko-Ehrenfest theory

Fig. A.12a and A.12b are the representation of the real part of the complex frequency Ω in function of the velocity γ . For low values of the velocity, we see that the real part of the frequency is less than zero. When the critical velocity is reached, we see that the real part becomes greater than zero and so the system flutters.

From the charts above, we see that in Fig. A.11 the stability condition is in the point of coalescence and in Fig. A.12 we have the stability condition when the real part is greater than

zero. This specific velocity is defined as “critical velocity”.

We report the critical velocity for each value of damping $\alpha = 0$ and $\alpha = 0.5$:

$$\gamma_{crit,\alpha=0} = 0.4141 \quad (\text{A.3.38a})$$

$$\gamma_{crit,\alpha=0.5} = 0.5657 \quad (\text{A.3.38b})$$

From the first plot (imaginary part vs γ , $\alpha = 0$), we can check the correctness of our derivation because when $\gamma = 0$ we have the natural frequency.

By applying the Galerkin method up to the 8th order, we obtain:

$$\omega_1 = 0.2034 \quad (\text{A.3.39a})$$

$$\omega_2 = 1.2380 \quad (\text{A.3.39b})$$

We convert the dimensionless frequencies in dimensional frequencies dividing by $\sqrt{\frac{\rho L^2}{Gk'}}$:

$$\omega_1 = 525.5767 \frac{\text{rad}}{\text{s}} \quad (\text{A.3.40a})$$

$$\omega_2 = 3199.4705 \frac{\text{rad}}{\text{s}} \quad (\text{A.3.40b})$$

The relative error ε between the two approaches is evaluated with the formula:

$$\varepsilon = \frac{\omega_{\text{Galerkin}} - \omega_{\text{theoretical}}}{\omega_{\text{theoretical}}} \times 100 \quad (\text{A.3.41})$$

Leading us to:

$$\varepsilon_{\omega_1} = 1.1442\% \quad (\text{A.3.42a})$$

$$\varepsilon_{\omega_2} = 3.7034\% \quad (\text{A.3.42b})$$

The last two plots are real part vs imaginary part for $\alpha = 0$ and $\alpha = 0.5$. In these charts, we see the evolving of complex frequencies in function of the load γ . In particular, when the level of the load is small, we can clearly distinguish the two frequencies. Instead, when the load increases, the frequencies get closer. When the real part is greater than zero, we achieve the phenomenon of the instability.

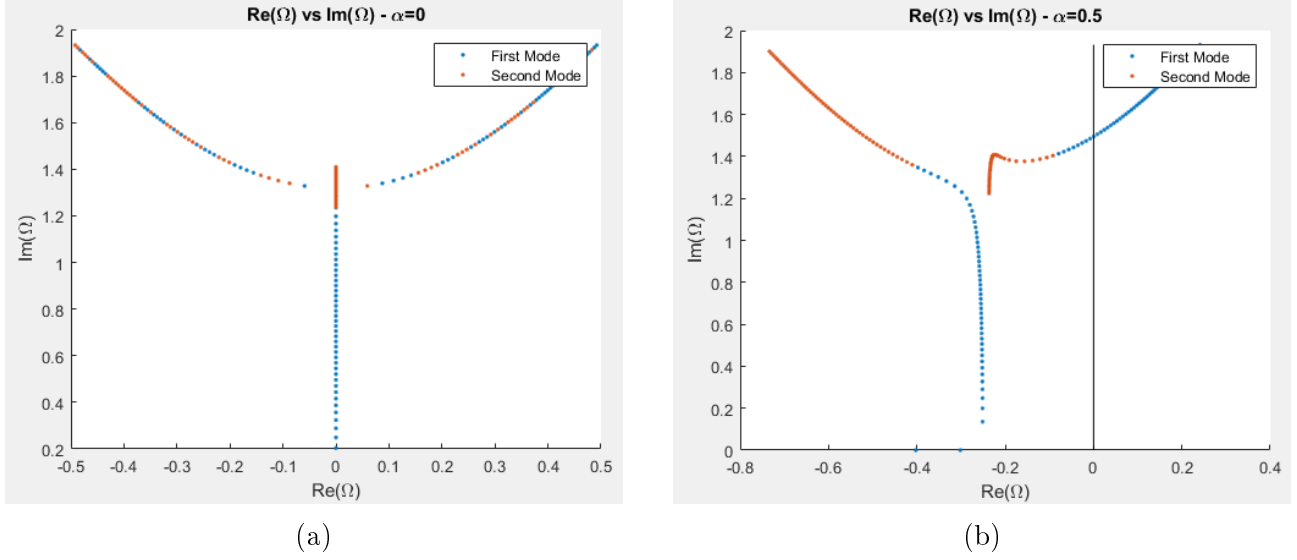


Figure A.13: Real vs imaginary part of frequencies for original Timoshenko-Ehrenfest theory

A.4 Conclusion

In this study, we have analyzed two Timoshenko-Ehrenfest beam theories in order to compare the differences in terms of results. We have applied these theories to the natural frequencies and flutter problems. In this way, we have observed that for the natural frequencies problem, the differences are negligible. On the contrary, analyzing the flutter problem, we have noted that the Galerkin method required at least the sixth term to obtain an acceptable result, reaching a better approximation with the increasing in the terms up to eight. Finally, comparing the critical velocities obtained by the two theories at the eighth order, we have remarked that they are the same.

As a conclusion, both versions of Timoshenko-Ehrenfest beam theory perform analogously even though the consistent version is much easier to implement.

Bibliography

- [1] N. S. Ottosen and H. Petersson, *Introduction to the Finite Element Method*. Prentice-Hall, 1992.
- [2] N. Taleb and E. Suppiger, “Vibration of stepped beams,” *Journal of the Aerospace Sciences*, vol. 28, no. 4, pp. 295–298, 1961.
- [3] F. Buckens, “Eigenfrequencies of nonuniform beams,” *AIAA Journal*, vol. 1, no. 1, pp. 121–127, 1963.
- [4] L. Klein, “Transverse vibrations of non-uniform beams,” *Journal of Sound and Vibration*, vol. 37, no. 4, pp. 491–505, 1974.
- [5] J. Yuan and S. Dickinson, “On the continuity conditions enforced when using artificial springs in the Rayleigh-Ritz method,” *Journal of Sound and Vibration*, vol. 161, no. 3, pp. 538–544, 1993.
- [6] M. Maurizi and P. Belles, “Natural frequencies of one-span beams with stepwise variable cross-section,” *Journal of Sound and Vibration*, vol. 168, no. 1, pp. 184–188, 1993.
- [7] M. Levinson, “Vibrations of stepped strings and beams,” *Journal of Sound and Vibration*, vol. 49, pp. 287–291, 1993.
- [8] S. Naguleswaran, “Natural frequencies, sensitivity and mode shape details of an Euler-Bernoulli beam with one-step change in cross-section and with ends on classical supports,” *Journal of Sound and Vibration*, vol. 252, no. 4, pp. 751–767, 2002.
- [9] G. Duan and X. Wang, “Free vibration analysis of multiple-stepped beams by the discrete singular convolution,” *Applied Mathematics and Computation*, vol. 219, no. 24, pp. 11 096–11 109, 2013.
- [10] Z. Lu, M. Huang, J. Liu, W. Chen, and W. Liao, “Vibration analysis of multiple-stepped beams with the composite element model,” *Journal of Sound and Vibration*, vol. 322, no. 4-5, pp. 1070–1080, 2009.
- [11] Q. Mao, “Free vibration analysis of multiple-stepped beams by using Adomian decomposition method,” *Mathematical and Computer Modelling*, vol. 54, no. 1-2, pp. 756–764, 2011.
- [12] X. Wang and Y. Wang, “Free vibration analysis of multiple-stepped beams by the differential quadrature element method,” *Applied Mathematics and Computation*, vol. 219, no. 11, pp. 5802–5810, 2013.
- [13] W. Wittrick and C. Ellen, “Buckling of tapered rectangular plates in compression,” *The Aeronautical Quarterly*, vol. 13, no. 4, pp. 308–326, 1962.
- [14] M. Ohga, T. Shigematsu, and K. Kawaguchi, “Buckling analysis of thin-walled members with variable thickness,” *Journal of Structural Engineering*, vol. 121, no. 6, pp. 919–924, 1995.

- [15] F. Ju, H. Lee, and K. Lee, “Free vibration of plates with stepped variations in thickness on non-homogeneous elastic foundations,” *Journal of Sound and Vibration*, vol. 183, no. 3, pp. 533–545, 1995.
- [16] Y. Cheung, F. Au, and D. Zheng, “Finite strip method for the free vibration and buckling analysis of plates with abrupt changes in thickness and complex support conditions,” *Thin-Walled Structures*, vol. 36, no. 2, pp. 89–110, 2000.
- [17] B. G. Galerkin, “Series solution of some problems of elastic equilibrium of rods and plates,” *Vestnik inzhenerov i tekhnikov*, vol. 19, no. 7, pp. 897–908, 1915.
- [18] H. Leipholz, “Use of Galerkin’s method for vibration problems,” *Shock and Vibration Digest*, vol. 8, pp. 3–18, 1976.
- [19] M. J. Gander and G. Wanner, “From Euler, Ritz, and Galerkin to modern computing,” *Siam Review*, vol. 54, no. 4, pp. 627–666, 2012.
- [20] S. Repin, “One Hundred Years of the Galerkin Method,” *Computational Methods in Applied Mathematics*, vol. 17, no. 3, pp. 351–357, 2017.
- [21] S. G. Mikhlin, *The numerical performance of variational methods*. Wolters-Noordhoff Publishing, 1971.
- [22] D. Chehil and R. Jategaonkar, “Determination of natural frequencies of a beam with varying section properties,” *Journal of Sound and Vibration*, vol. 115, no. 3, pp. 423–436, 1987.
- [23] C. Maurini, M. Porfiri, and J. Pouget, “Numerical methods for modal analysis of stepped piezoelectric beams,” *Journal of Sound and Vibration*, vol. 298, no. 4–5, pp. 918–933, 2006.
- [24] M. Soheylian and H. Ahmadian, “Dynamic stability of step beam carrying concentrated masses under follower force,” 2007.
- [25] S. M. Al-Said, “Crack detection in stepped beam carrying slowly moving mass,” *Journal of Vibration and Control*, vol. 14, no. 12, pp. 1903–1920, 2008.
- [26] S. R. Borneman, S. M. Hashemi, and H. Alighanbari, “Vibration Analysis of Cracked Stepped Laminated Composite Beams,” *International Journal of Vehicle Structures & Systems (IJVSS)*, vol. 1, 2009.
- [27] M. Pirmoradian, M. Keshmiri, and H. Karimpour, “On the parametric excitation of a Timoshenko beam due to intermittent passage of moving masses: Instability and resonance analysis,” *Acta Mechanica*, vol. 226, no. 4, pp. 1241–1253, 2015.
- [28] K. Graff, *Wave Motion in Elastic Solids*. 1975.
- [29] J. Jaworski and E. Dowell, “Free vibration of a cantilevered beam with multiple steps: Comparison of several theoretical methods with experiment,” *Journal of Sound and Vibration*, vol. 312, no. 4–5, pp. 713–725, 2008.
- [30] E. Dowell, “On asymptotic approximations to beam model shapes,” 1984.
- [31] G. Yamada, Y. Kobayashi, and T. Tomioka, “Vibration analysis of cantilever beam systems which consist of two segments by Ritz method with various combinations of the admissible functions,” *Journal of Sound and Vibration*, vol. 170, no. 2, pp. 280–288, 1994.
- [32] J. Singer, “On the equivalence of the Galerkin and Rayleigh-Ritz methods,” *The Aeronautical Journal*, vol. 66, no. 621, pp. 592–592, 1962.

- [33] Y. Xiang and C. Wang, "Exact buckling and vibration solutions for stepped rectangular plates," *Journal of Sound and Vibration*, vol. 250, no. 3, pp. 503–517, 2002.
- [34] W. Voigt, "Bemerkung zu dem Problem der transversalen Schwingungen rechteckiger Platten," *Nachrichten von der Königl. Gesellschaft der Wissenschaften und der Georg-Augusts-Universität zu Göttingen*, vol. 1893, pp. 225–230, 1893.
- [35] M. Levy, "Sur l'équilibre élastique d'une plaque rectangulaire," *Comptes Rendus Acad. Sci. Paris*, vol. 129, pp. 535–539, 1899.
- [36] I. Chopra, "Vibration of stepped thickness plates," *International Journal of Mechanical Sciences*, vol. 16, no. 6, pp. 337–344, 1974.
- [37] K. Lam and G. Amrutharaj, "Natural frequencies of rectangular stepped plates using polynomial beam functions with subsectioning," *Applied Acoustics*, vol. 44, no. 4, pp. 325–340, 1995.
- [38] Strand7, *Theoretical manual—theoretical background to the Strand7 finite element analysis system*, G+ D Computing Sydney, 2004.
- [39] V. V. Bolotin, *Nonconservative problems of the theory of elastic stability*. Macmillan, 1963.
- [40] A. Movchan, *On vibrations of a plate moving in a gas*. National Aeronautics and Space Administration, 1959.
- [41] A. Marzani, M. Mazzotti, E. Viola, P. Vittori, and I. Elishakoff, "FEM formulation for dynamic instability of fluid-conveying pipe on nonuniform elastic foundation," *Mechanics Based Design of Structures and Machines*, vol. 40, no. 1, pp. 83–95, 2012.
- [42] L. Olson and D. Jamison, "Application of a general purpose finite element method to elastic pipes conveying fluid," *Journal of Fluids and Structures*, vol. 11, no. 2, pp. 207–222, 1997.
- [43] E. Kock and L. Olson, "Fluid-structure interaction analysis by the finite element method—a variational approach," *International Journal for Numerical Methods in Engineering*, vol. 31, no. 3, pp. 463–491, 1991.
- [44] A. Pramila, J. Laukkanen, and S. Liukkonen, "Dynamics and stability of short fluid-conveying Timoshenko element pipes," *Journal of Sound and Vibration*, vol. 144, no. 3, pp. 421–425, 1991.
- [45] S.-U. Ryu, Y. Sugiyama, and B.-J. Ryu, "Eigenvalue branches and modes for flutter of cantilevered pipes conveying fluid," *Computers & structures*, vol. 80, no. 14-15, pp. 1231–1241, 2002.
- [46] I. Elishakoff, *Handbook on Timoshenko-Ehrenfest beam and Uflyand-Mindlin plate theories*. World Scientific, 2020.
- [47] S. Timoshenko, *A Course in Theory of Elasticity, Part II: Rods and Plates in Russian*. 1916.
- [48] ——, "On the differential equation for the flexural vibrations of prismatical rods," *Glas. Hrvat. Prirodosl. Drus., Zagreb*, vol. 32, no. 2, pp. 55–57, 1920.
- [49] ——, "On the correction for shear of the differential equation for transverse vibrations of prismatic bars," *Philosophical Magazine*, vol. 6, 1921.
- [50] W. Weaver Jr, S. P. Timoshenko, and D. H. Young, *Vibration problems in engineering*. John Wiley & Sons, 1990.

- [51] I. Elishakoff and E. Lubliner, “Random vibration of a structure via classical and nonclassical theories,” pp. 455–467, 1985.
- [52] I. Elishakoff, “An equation both more consistent and simpler than the Bresse-Timoshenko equation,” pp. 249–254, 2009.
- [53] I. Elishakoff, J. Kaplunov, and E. Nolde, “Celebrating the centenary of Timoshenko’s study of effects of shear deformation and rotary inertia,” *Applied Mechanics Reviews*, vol. 67, no. 6, 2015.
- [54] I. Elishakoff, “Who developed the so-called Timoshenko beam theory?” *Mathematics and Mechanics of Solids*, vol. 25, no. 1, pp. 97–116, 2020.
- [55] N. Challamel and I. Elishakoff, “A brief history of first-order shear-deformable beam and plate models,” *Mechanics Research Communications*, vol. 102, p. 103389, 2019.
- [56] J. W. S. B. Rayleigh, *The theory of sound*. Macmillan, 1896, vol. 2.
- [57] A. Pielorz, “Discrete-continuous models in the analysis of low structures subject to kinematic excitations caused by transversal waves,” *Journal of Theoretical and Applied Mechanics*, vol. 34, no. 3, pp. 547–566, 1996.
- [58] E. J. Routh, *A treatise on the stability of a given state of motion: particularly steady motion*. Macmillan and Company, 1877.
- [59] A. Hurwitz, “Ueber die Bedingungen, unter welchen eine Gleichung nur Wurzeln mit negativen reellen Theilen besitzt,” *Mathematische Annalen*, vol. 46, no. 2, pp. 273–284, 1895.